REPORT OF THE SPERT I DESTRUCTIVE TEST PROGRAM
# ON AN ALUMINUM, PLATE-TYPE, WATER-MODERATED REACTOR

R. W. Miller, Alain Sola and R. K. McCardell,

PRICE $2.75

AVAILABLE FROM THE
OFFICE OF TECHNICAL SERVICES
U. S. DEPARTMENT OF COMMERCE
WASHINGTON 25, D. C.

PRINTED IN USA

REPORT OF THE SPERT I DESTRUCTIVE TEST PROGRAM

ON AN ALUMINUM, PLATE-TYPE, WATER-MODERATED REACTOR

Reported By

R. W. Miller
Alain Sola (Euratom)
R. K. McCardell

ABSTRACT

In response to the need for an understanding of destructive mechanisms in aluminum plate-type cores, the Spert project conducted a series of reactor tests in which sudden insertions of excess reactivity were successively increased for each test until, in two such tests, melting temperatures had been experienced over small fractions of the core but with no other unusual behavior noted. In a final test which partially melted approximately 35 percent of the core, large pressures were suddenly produced after the power excursion. These pressures in combination with widespread melting were responsible for completely destroying the core, dispersing melted fuel, damaging other reactor hardware, and causing the release of about 0.7 percent of the fisside content of the core to the atmosphere. The explosion phenomenon was qualitatively absent in all previous tests and was in that sense not predictable. A chemical reaction between aluminum and water was detected and estimated to have released about 4 MW-sec of energy. However, results of the test indicate the existence of a triggering mechanism which dispersed the melted fractions of the core into fragments which were conducive to the chemical reaction. Conditions in the core were favorable for the initiation of a "steam explosion", and consequently this mechanism has been proposed both as a triggering device and as a contributor to the overall explosion.

SUMMARY

This report describes the results of a program of reactor testing conducted at Spert during the calendar year 1962 to demonstrate the behavior of an aluminum, plate-type, water-moderated, highly-enriched reactor when subjected to large reactivity insertions sufficient to induce very short-period power excursions. Previous test programs performed on reactors of this type had produced extensive data on reactor behavior characteristics but only at periods longer than about 8 msec, in which fuel temperatures remained well below melting. Tests in this period region were nondestructive, resulting in only minor fuel plate distortion, due to thermal stresses, in even the most severe cases. However, data had been obtained at a 2.6-msec period in the 1954 Borax I test in which an explosion was produced which completely destroyed the reactor. Thus, the period region between about 8 msec and 2.6 msec, which contained an abrupt transition from minor thermal distortion of core components (accompanied by small transient pressures) to violent destruction of the reactor, was relatively unexplored.

The Spert I destructive test program was, therefore, directed toward investigating this unexplored period region with the specific objective of studying the results of each test in search of evidence of a destructive threshold and relating, if possible, the onset of explosive pressures to the other measured or programmed test parameters. A sequence of transient tests was called for in which increasing insertions of reactivity were used to obtain successively shorter periods and greater energy releases. Portions of the core which might be destroyed or damaged beyond further use in each test were to be replaced in preparation for subsequent tests. Testing in this manner would continue to shorter periods until complete destruction of the core occurred in a single test.

The core was loaded in the Spert I facility in 1961, and by June of 1962 all calibrations, measurements, and nondestructive transients with periods ranging down to about 6 msec had been completed. Damage resulting from these tests was confined to thermal distortion and was not severe. Preparations were then made for shorter period tests which were predicted to yield more extensive damage to the core in the form of plate distortion and plate melting. Extrapolation of measured transient pressures to the shorter periods did not indicate expected pressures of destructive magnitude; however, it was recognized and anticipated that thresholds (in the sense of a change in pressure-producing phenomena) could occur either with the attainment of various degrees of fuel melting and subsequent dispersion of fuel in the water moderator or as a consequence of an aluminum-water reaction.

Two tests were conducted with periods of 5.0 msec and 4.6 msec, respectively, each of which resulted in both thermal distortion of the plates and in fuel plate melting. The combination of distortion with localized melting caused a few fuel plates to become permanently fused together. The transient pressures measured during both of these tests were in agreement with the extrapolations of pressure data from the longer period tests and there was no indication that the attainment of fuel plate melting, which had spread to about three percent of the core, constituted a threshold for the development of a new pressure source. Nor was there any indication that increasing the degree of melting in the core such as was expected in the next (3 msec) test would or would not provide such a threshold.

On November 5, 1962, the next test (which proved to be the final test) was conducted with a reactivity insertion of about 3.5 dollars producing a period of 3.2 msec. A typical self-limiting power excursion occurred, releasing about 31 MW-sec of nuclear energy. As the power excursion neared completion, approximately 15 msec following the peak of the power burst, a sharp pressure rise was recorded. The pressure pulse which occurred demolished the core, damaged most of the associated hardware and part of the control system, and bulged the earth-backed reactor vessel. Virtually no damage to the facility occurred outside the vessel.

Contamination of the facility and fisside release to the atmosphere was generally very slight since the fisside content of the core was small. Water was removed from the vessel for criticality control shortly after the test, and, even with this reduction in shielding protection, personnel were able to enter the area for observation of the reactor about four hours after the test.

It is estimated from radiological measurements taken in the area around the reactor building during the test that less than 0.7 percent of the fisside content of the core was released to the atmosphere. Radioiodines were not detected, but less than 0.01 percent of the iodines are calculated to have been released to the atmosphere.

Calculations indicate that the fuel plates at the core hot-spot reached a maximum temperature of approximately 1360°C and had probably cooled to about 1000°C at the time of the explosion. About 8 percent of the core was completely melted and about 35 percent of the core was partially melted prior to the explosion.

Since the explosion occurred at a time after the power excursion when the reactor was completely self-shutdown, it was possible to conclude from the power burst shape that thermal expansion and steam formation took place in a predictable mode and were effective as shutdown mechanisms and that, further, the explosion was not a consequence of either a failure or a change in the nature of these mechanisms.

A possible implication of this result is that the explosion which occurred during the Borax I test (but which could not, on the basis of the recorded data, be similarly separated from the power excursion) also was not due to failure of shutdown mechanisms. Both explosions appear to be the result of a process or reaction qualitatively absent in all other transient tests.

Analysis of residual solids collected from the Spert I vessel after the destructive test indicates that a chemical reaction between aluminum and water released about 4 MW-sec of energy. However, consideration of the metal temperatures attained during the test and the initially undivided state of the fuel has resulted in the conclusion that the chemical reaction likely was not responsible for initiation of the Spert I explosion. It is considered more likely that the chemical reaction took place only after being triggered by an initial disturbance in the core which dispersed hot fragments of the melted and semi-melted fuel plates into water, thereby producing an arrangement more favorable for the chemical reaction to proceed, and that the reaction in this way may have contributed to the overall severity of the explosion.

iv

It is known from the temperature data obtained that immediately prior to the destructive pressure pulse a significant fraction of the core was at melting temperature and could, therefore, have been dispersed into the water moderator as a result of any triggering mechanism which would produce a slight pressure surge. However, the available evidence does not permit a definitive description of the mode of initiation and propagation of the explosion and various mechanisms may be postulated as triggering devices. One of these mechanisms which appears likely is a steam explosion since it is consistent with the environment and has sufficient potential both in speed and magnitude to account for the results obtained. From a study of the fuel plate damage observed during longer period nondestructive tests it appears that conditions within the core just prior to the explosion were very favorable for the entrapment of water between the melting fuel plates. Conditions somewhat similar to this have been known to cause violent steam explosions, and this mechanism of super-heating and subsequent expansion of small quantities of water is suggested as a sufficient source for the dispersal of molten fuel in the water moderator of the Spert I core. It is further argued that once such a disturbance of the core has been initiated, further steam formation and pressure generation would be self-propagating as melted and otherwise weakened hot fuel plates become fragmented and come into intimate contact with water.

REPORT OF THE SPERT I DESTRUCTIVE TEST PROGRAM ON AN ALUMINUM, PLATE-TYPE, WATER-MODERATED REACTOR

CONTENTS

xi

FIGURES

TABLES

I. INTRODUCTION

In recognition of the need to obtain an understanding of reactor kinetic behavior and reactor accidents, the Atomic Energy Commission contracted Phillips Petroleum Company in 1954 to undertake a long range reactor safety program which included both nondestructive tests and integral core destructive tests.

The completion of a substantial portion of these investigations which could be performed in Spert I and the construction of the Spert II, III, and IV facilities to continue such studies, made it appropriate in 1962 to initiate a program of destructive tests. This phase of the program had been deferred in favor of extending the nondestructive studies on various core configurations in order to better understand and evaluate the reactivity compensating mechanisms.

The first extensive experimental kinetics studies of reactors prior to the Spert Program were the GODIVA tests [1] for fast systems, and the BORAX tests [2] for thermal systems. In the Borax-I tests, self-limiting power excursions were performed with exponential periods ranging between about 100 msec and 5 msec at boiling temperatures and between 100 msec and 13 msec at ambient temperatures. While only minor damage to the core occurred during these tests, the results indicated that shorter periods with larger energy releases could lead to extensive core damage. The Borax-I program was concluded with a test having a period of 2.6 msec at ambient temperature. This test yielded a maximum power of 19 GW and a burst energy of about 135 MW-sec, and resulted in nearly total destruction of the core and partial destruction of the facility.

Although the Borax destructive test constituted a major step forward in providing an understanding of accidental excursions, the nature of the explosion and factors influencing it could not be learned from the available data, and other damage effects such as plate distortion, channel blockage, and melting were concealed by the over-riding effects of the explosion.

The destructive program in Spert I, therefore, had as its objective a systematic exploration of the destructive region of reactivity insertions in order to describe damage effects encountered, to search for any explosive threshold, and finally to demonstrate a full-scale explosion in an effort to contribute to the understanding of these responses and consequences.

Since the results of the Spert I explosion tests are best understood in context with the entire testing program, this report presents the results of the preceding nondestructive and partially destructive tests but with particular emphasis on the destructive test which concluded the program. Briefly, the report is divided as follows: Section II contains a description of the reactor facility and the experimental methods used in the execution of this program; Section III presents data and analysis of all tests exclusive of the final destructive test; and Section IV and V present, respectively, a description of the destructive test and the results obtained from that test. Results of the entire program are finally discussed and analyzed in Section VI and some of the main conclusions are expressed in Section VII. In many cases where supporting information or peripheral studies are needed but are otherwise not pertinent to the main body of the report, this information has been included in the appendices. These appendices contain, for instance, details of transient instrumentation, representative data for various periods,

1

calculations of temperature, fisside release, etc, and results of metallurgical studies.

II. DESCRIPTION OF THE REACTOR FACILITY AND INSTRUMENTATION

In the following section, brief descriptions of the Spert I reactor facility including the building, the reactor, reactor control system, operational instrumentation, and auxiliary equipment are presented. A more detailed description of the reactor facility has been published [3].

1. REACTOR FACILITY

1.1 Reactor Site

The Spert I reactor is located at the National Reactor Testing Station in Idaho. The reactor is approximately one half mile from the reactor control room at the Spert control center building and approximately one half mile from the nearest other reactor facility. Spert I consists of the reactor building (shown in Figures 1 and 2) and an attached earth-shielded, instrumentation bunker containing electronic equipment for amplifying and sending instrumentation signals to the control center. A small service building located about 400 feet from the reactor building, houses the water-treatment equipment, air-compressor, and other auxiliary equipment. The reactor is operated remotely from a control console located in the control center building.
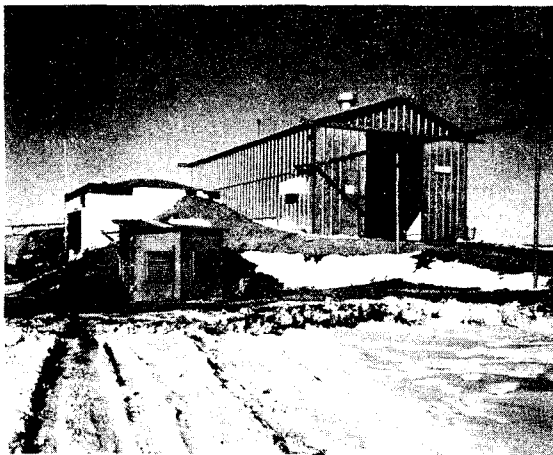
Fig. 1 Outside view of Spert I reactor building showing electronic bunker on left.
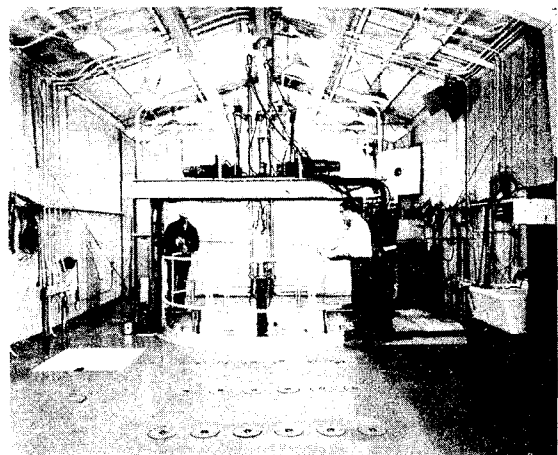
Fig. 2 Inside view of Spert I reactor building showing upper bridge with drive motors and top of vessel.

1.2 Reactor

Figure 3 is a cutaway view of the Spert I reactor. The reactor vessel is an open, unpressurized, 10-foot diameter by 16-foot deep, carbon-steel tank. The reactor which was moderated and cooled by light water had no provision for forced coolant circulation through the core. The water level in the reactor vessel was nominally 4.5 feet above the top of the fuel plates for the tests described here.

The test core was comprised of 25 fuel assemblies, mounted in a 5 x 5 rectangular grid structure as shown in Figure 4.
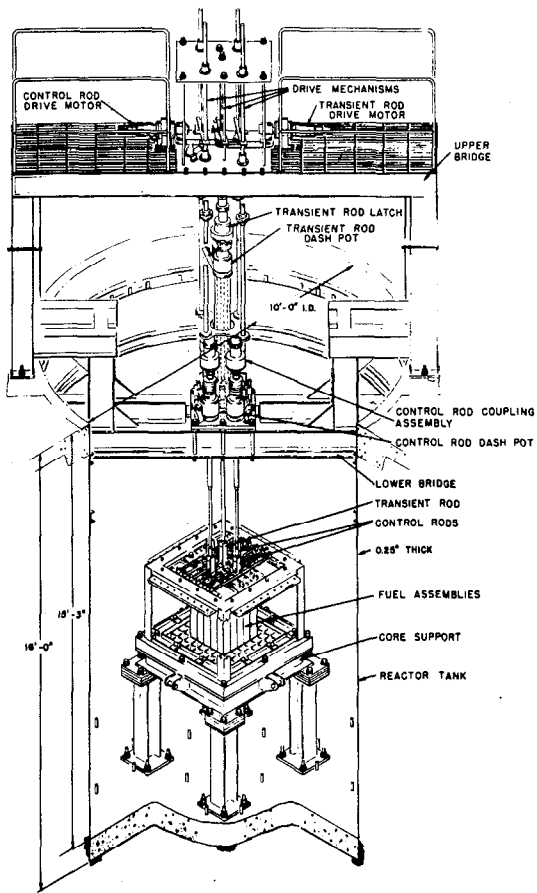
Fig. 3 Cutaway view of the Spert I reactor.

Fig. 5 Cutaway views of Spert I D-core fuel assemblies.

Fig. 4 Cross section of Spert I D-12/25 core showing positions of transient rod and control rods. (Each is identified by a letter and a number; ie, the fuel assembly in the central position with the transient rod is designated E-5.)

Four symmetrically-placed, gang-operated control rod assemblies, each consisting of a pair of seven weight percent boron–aluminum poison blades with aluminum followers provided reactor control. An additional, centrally-located "transient" rod assembly consisting of two aluminum blades with poison follower blades was used to initiate power transients.

The Spert I D-type fuel assembly is shown in Figure 5. It consisted of a square aluminum box, with two grooved aluminum side plates used for supporting removable fuel plates. The end-box section at the bottom of the fuel assembly fits into the lower core support grid structure, and a lifting bail at the top was used for handling. The standard assembly contained 12, highly enriched, U–Al alloy, aluminum-clad fuel plates, which could be removed from the fuel assembly box to permit fuel plate inspection, and installation and replacement of instrumentation. The four control-rod and one transient-rod fuel assemblies contained six fuel plates; the remaining six fuel plate positions were occupied by two blades and blade-guide channels. Fuel assembly design characteristics are included in Table I together with physical properties of the core.

4

TABLE I

PHYSICAL PROPERTIES OF SPERT I D-12/25 REACTOR

Reactor Type	Open Pool
Moderator-Reflector	H_2O
Vessel	10-ft ID x 16-ft High Right Cylinder
Vessel Material	Carbon Steel
Number of Fuel Assemblies	25
Standard (12-plate) Fuel Assemblies	20
Rod Bearing (6-plate) Fuel Assemblies	5
Approximate Fuel Assembly Size	3 x 3 x 25 in.
Total Number of Fuel Plates in Core	270
Fuel Plate Dimensions	0.060 x 2.704 x 25-1/8 in.
Clad Material	6061 Aluminum
Clad Thickness	0.020 in.
Meat Composition	93 percent enriched, U-Al Alloy (24 weight percent U-235)
Meat Dimensions	0.020 x 2.454 x 23-1/2 in.
U-235 Per Fuel Plate	14 g
Total U-235 in Core	3.8 kg
Coolant Channel Thickness	0.179 in.
Total Core Volume (inclusive of all materials and moderator)	5.3×10^3 in.^{3}
Moderator Volume	3.2×10^3 in.^{3}
Metal-to-Water Ratio	0.66
Heat Transfer Area	3.4×10^4 in.^{2}
Control Rods	4 double-bladed, gang-operated
Transient Rod	1 double-bladed
Control and Transient Rod Poison Material	Binal[a] (7 weight percent natural boron-Al alloy)

[a] Binal - Trademark for the Sintercast Corporation aluminum-boron powder-metallurgy process material.

2. OPERATIONAL INSTRUMENTATION

The Spert I operational instrumentation included neutron instrumentation, a reactor bulk water thermopile, a reactor water level indicator, and radiation-detection equipment.

Operational neutron instrumentation included several B^{10}-lined pulse chambers with amplifiers and counters, a B^{10}-lined gamma-compensated ion chamber connected through a linear electrometer to a 6-decade linear power recorder, and a B^{10}-lined uncompensated, ion chamber connected through a logarithmic electrometer to a 6-decade log-power recorder. The chambers and electronic amplifiers were located in the reactor building and instrument bunker, respectively, and the counters and recorders were located in the Spert I control room at the control center.

Bulk water temperature in the reactor was measured by a thermopile positioned near the tank wall and leads from the thermopile extended to a constant-temperature reference junction from which the signal was transmitted without amplification to a temperature recorder at the control center.

Gamma radiation levels directly over the reactor vessel and at other points in the reactor area were measured by gamma-sensitive ion chambers, the signals from which were transmitted to indicators in the Spert I control room and to a recorder in the health physics office at the control center.

3. TRANSIENT INSTRUMENTATION

This section contains a brief description of methods used to obtain data on the kinetic response of the reactor during transient tests. Structural details, locations, limitations, etc, of the instruments are discussed more extensively in Appendix B along with a description of the data system.

Reactor power was measured by neutron-sensitive ion chambers, which with the exception of one miniature chamber located inside of the core, were all located exterior to the core in the reflector where they detected leakage neutrons and, to a lesser extent, gammas.

Nuclear energy release was determined both by integration of the power data and in the case of the total energy, E_T, by activation of cobalt wires.

Fuel plate temperatures were measured by thermocouples attached either to the surface of the fuel plates or buried within the meat. Many locations in the core, especially in the region of the flux peak, were instrumented for each test in order to obtain measurements of the temperature distribution in the core. The flux peak occurred in the central fuel assembly, E5, (Figure 4) about three inches below the center-plane of the core.

Pressure measurements were obtained in the reflector at several positions surrounding the core by unbonded, strain-gage type, diaphragm transducers. The transducers were located close to the x, y, and z, core-centered axes of the reactor and at several radial distances from the core up to about four feet.

III. NONDESTRUCTIVE TEST RESULTS

1. INITIAL STATIC MEASUREMENTS

After the D-12/25 core (so designated because it contained 25 nominal 12-plate assemblies) had been loaded in Spert I, a series of tests was performed to measure characteristics of the core and to obtain various calibration information necessary for transient operation. These latter included primarily a calibration of the control rods by the reactor period method using both boric acid and the transient rod as poison shims. Integration of the control rod worth indicated that the total available excess reactivity was about 8.2$, and by inter-calibrating the transient rod against the control rods, it was determined that the transient rod was worth about 7$. Table II summarizes the nuclear characteristics of the core.

TABLE II

NUCLEAR CHARACTERISTICS OF THE SPERT I D-12/25 CORE

Total U-235	3.8 kg
Excess Reactivity	8.2$
M/W Ratio	0.66
H/U Ratio	360
Max/Ave Flux Ratio	2.4
Void Coefficient	
Average	-36¢/%
Average	-0.067¢/cm^3
Maximum	-0.16¢/cm^3
Temperature Coefficient, Isothermal	
@ 20°C	-2.1¢/°C
Reduced Prompt Neutron Generation	
Time, $\ell/\bar{\beta}$	8.16 ± 0.04 msec
nv/Watt (Average)	7.6 x 10^6

Detailed descriptions and results of most of the statics experiments are presented in Appendix A.

2. POWER EXCURSIONS

Measurements of the dynamic characteristics of the Spert I D-12/25 core were obtained from transient power excursions produced in the core by rapidly ejecting a poisonous "transient" rod from the core while the core was at very

low power levels (usually less than 10 watts). By this means, a step-wise increase of reactivity occurs in the reactor, with the amount of reactivity being predetermined by a measured displacement of the control rods above their normal critical position. The ensuing power excursion is initially exponential and finally self-limited and quenched by inherent "shutdown" mechanisms which cause a loss of reactivity.

The magnitudes of the measured variables during these self-limiting power excursions (power, fuel plate temperature, pressure generation, etc) and the relative times at which specific events occur during the course of an excursion are affected considerably by the initial excess reactivity insertion, Δk_0. In this section, some of these transient behavior characteristics of the test core are discussed briefly with respect to the variations taking place in each as Δk_0 is increased from about 1.0\$ to about 3.5\$. Nearly all aspects of the transient behavior of this core were qualitatively the same as those previously obtained at Spert with several other aluminum plate type cores. The results of these tests are presented here and discussed, especially to indicate the basis for predicting the results of the very short period tests.

2.1 General Behavior of Nondestructive Tests

In the region of relatively long periods, 50 msec and greater, (or $\Delta k_0 <$ 1.15\$) the initial power rise during the transients was found to gradually deviate from the exponential while still at low power levels, and then to slowly pass through a maximum. Maximum power was normally followed by a slow power decline with the rate of the decline again being small but increasing with shorter initial periods (Figures C-1, C-2, and C-3 on pages 90-91). Power levels always remained low during these excursions (ie, in the range of several megawatts) and there was, consequently, no appreciable peaking of the temperature in the meat portions of the fuel plate. Ordinary conductive heat transfer processes were adequate in these cases to nearly suppress temperature peaking in the fuel plate and distribute the heat in both the metal cladding of the fuel plate and in the water moderator. Boiling temperatures, if attained at all during the course of these long-period transients, always occured after the time of peak power and the compensation of reactivity before peak power was attributed principally to thermal expansion of metal and water[a].

When the initial reactivity insertion, Δk_0, was further increased to obtain shorter periods, more energy was required to compensate the increased reactivity and it was found that the maximum power attained during the tests increased approximately as the square of the initial asymptotic reciprocal period, α_0, (empirically, the exponent was found to be about 1.7). The reason for this (near) "square-law" dependence of peak power on α_0 arises from the two separate facts that the energy under an exponential power rise varies as the inverse of α_0, whereas the prompt reactivity increases directly as α_0 [b].

It is possible, at least in theory, for the thermal expansion mechanisms alone to compensate the prompt reactivity and to arrest the initial power rise of a power excursion provided enough energy is released. However, at some point,

---

[a] It should be noted however that attempts to make a quantitative computation of the reactivity compensation purely on the basis of thermal expansion of materials have not been successful (see Reference 4).

[b] See page 9 for footnote.

8

which for this core occurred at a period of about 50 msec, fuel plate temperatures were attained which allowed moderator boiling to commence and to contribute to the compensation of prompt reactivity by producing steam voids. Boiling void growth is extremely fast (often requiring less than 1 msec for the growth of a bubble) and the region over which boiling occurs generally spreads rapidly over the entire core, and as a consequence, peak power has never been observed to lag behind the onset of boiling by more than a few milliseconds regardless of the period. Although some reactivity is still compensated by thermal expansion, power behavior after the onset of boiling is primarily controlled by the dynamics of this single reactivity compensating mechanism, ie, production and condensation of steam.

The typical short-period transient is illustrated in Figure 6. As a result of the higher energy releases obtained in short-period excursions, boiling temperatures are eventually reached at nearly every point in the core, and voiding in all water channels is extensive. Reactivity compensation produced by steam voiding during short-period excursions has been found to greatly exceed the initial excess reactivity insertion and establish, as a consequence, a highly shutdown condition in the reactor. Due to this shutdown condition of the core the power will fall to a level approximately two to three decades below peak power and level off at this point. Further decline of the power is resisted by the release of delayed neutrons.
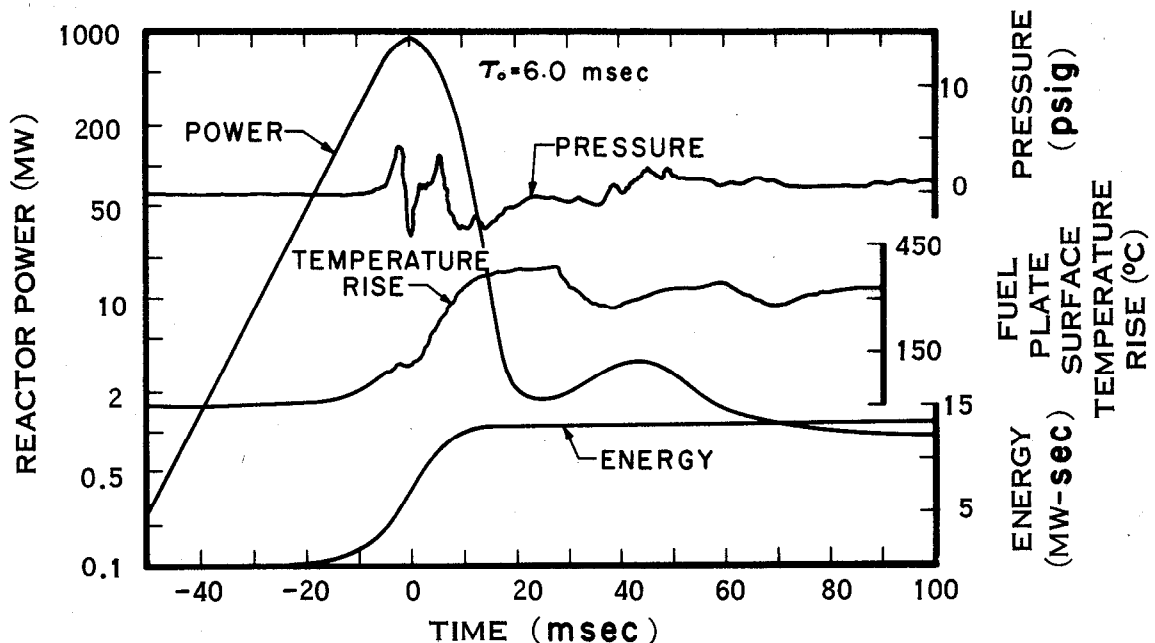
Fig. 6 General behavior of D-12/25 core during 6.0-msec power excursion.

[b] If the power, $\phi(t)$, varies as $e^{\alpha_o t}$ up to the time of peak power, t_m, then the energy release at time of peak power, $E(t_m)$, is equal to $\phi(t_m)/\alpha_o$. For short-period tests, the reactivity compensation at the time of peak power $k_c(t_m)$ is proportional to α_o [5]. If $k_c(t_m)$ also is assumed to be proportional to $E(t_m)$, then, it appears that $\phi(t_m)$ is proportional to α_o^2, a result which is only approximate since ordinary power excursions deviate from an exponential near peak power.

9

The ability of this reactor to self-limit itself during power excursions has been demonstrated for periods as short as 3.2 msec. Reactivity compensation (discussed in Section III-2.5) took place in a predictable manner for each test and demonstrated an ability to over-compensate the initial excess reactivity insertion by several dollars.

Nevertheless, the energy release resulting from these short-period tests was reaching to potentially damaging magnitudes. At periods around 5 msec and below, maximum temperatures of the fuel plates were expected to exceed the melting point of aluminum, a threshold which had been avoided in previous Spert testing on aluminum cores, and it was not known what new effects might arise as a result. Another consequence of these short-period tests was an increased temperature peaking within the fuel plates which produced thermal gradient stresses and consequent severe warping of the plates along with cracking of the clad. Permanent damage to fuel plates from thermal distortion first became significant in the 7- to 8-msec period region, and, although in these tests there was no apparent change in the effectiveness of reactivity compensation as a consequence of the damage produced, warping was often severe enough to completely block several water channels.

Finally, a pressure pulse arising from the initial super-heating of water prior to the onset of boiling was of concern. Although only small pressures were attributed to this mechanism (ie, about 6 psi at a 5-msec period), these pressures tended to increase with decreasing period. By extrapolation, it was expected that this pressure source could cause damage in tests with periods of less than about 2 msec.

2.2 Transient Data

In this section and in those following, specific results of the 54 transient tests conducted on the D-12/25 core are presented in the form of plotted relationships of several measured variables against the inverse period, α_o. Further summary of the data including illustration of the temporal relationship between these quantities, general behavior plots of the power, energy, temperature, and others are presented in Appendix C.

Peak power data as shown in Figure 7, were found to be nearly collinear (on a log-plot) for all tests. A least-squares fit to peak power data, $\phi(t_m)$, yields the form:

$$\phi(t_m) = 0.13 \, \alpha_o^{1.72} \ \text{MW}$$

over the range, $10 < \alpha_o < 300 \ \text{sec}^{-1}$. The regularity of the data made it possible to obtain accurate extrapolations of peak power during the entire test series.

As seen in Figure 8 the energy released at peak power, $E(t_m)$, and the total energy, E_T, vary linearly with reciprocal period, α_o, for α_o less than about 125 sec^{-1}. At shorter periods, however, both sets of data were observed to rise steeply. This change in slope (as shown below) appears to be a consequence of the boiling shutdown process and its effect upon the burst shape.

Figure 9 is a plot of peak fuel plate temperature data obtained during the test series as a function of the reciprocal period, α_o. The highest temperatures
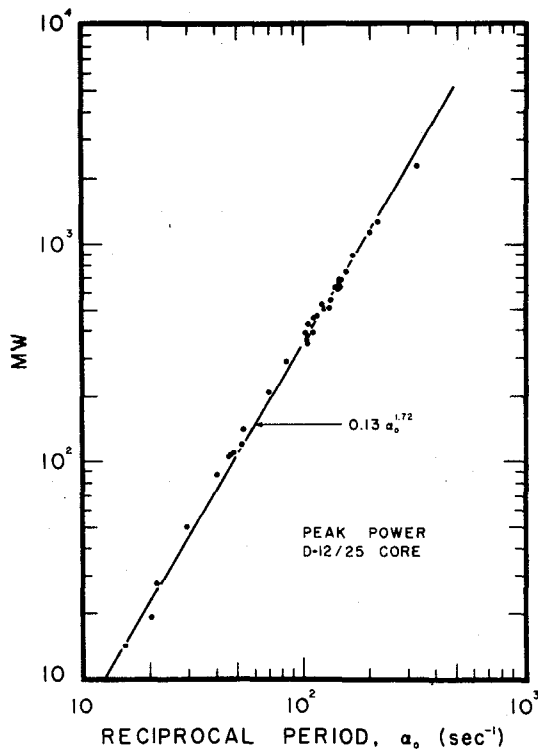
Fig. 7 Peak power vs reciprocal period.
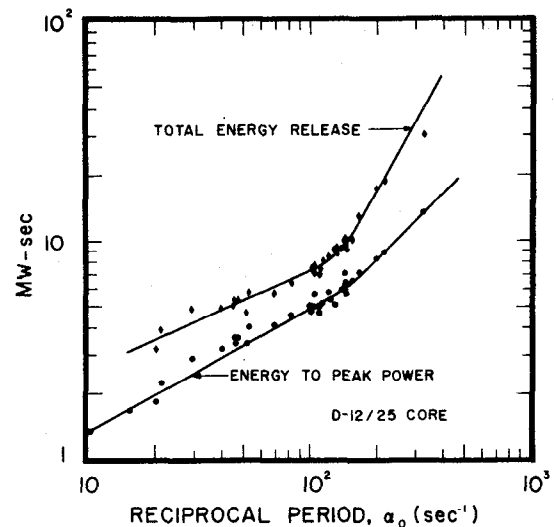
Fig. 8 Total energy release and energy release to time of peak power vs reciprocal period.
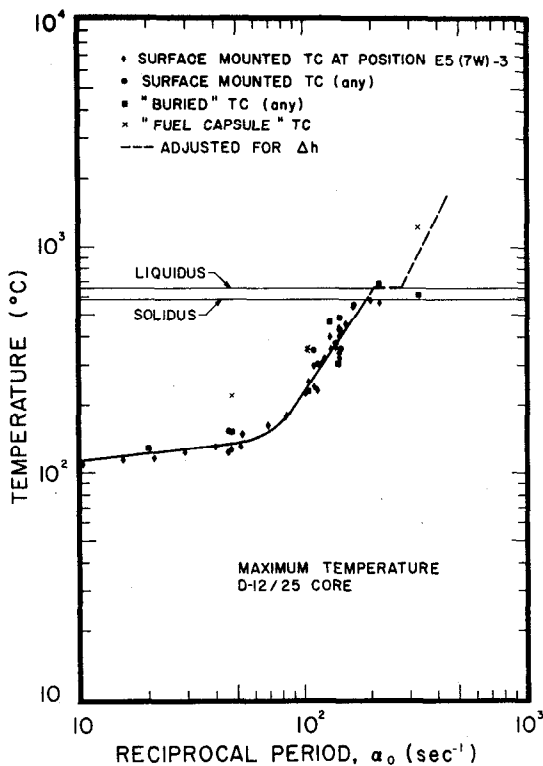
Fig. 9 Maximum fuel plate temperatures as a function of the reciprocal period. Δh is the heat of fusion of aluminum. The notation TC is an abbreviation for thermocouple.

were usually observed in the center of the central assembly of the core and about three inches below the midplane of the core. This position (denoted as position E5(7W)-3) was the nearest instrumented point to the flux peak. The solid line in Figure 9 has been faired through the data points and the dashed line is an extrapolation of these data adjusted at the melting point for the heat of fusion of aluminum, Δk.

The fact that temperature data are not exactly proportional to the energy data is interpreted as a consequence of the variation of heat capacity with temperature and of a variation in the fraction of the nuclear heat which is transferred from the fuel plate to the water. From an extrapolation of the temperature data, it was possible to predict closely the onset of melting, which occurred first at a period of 5 msec ($\alpha_0 = 200$ sec^{-1}).

The functional relationship of $\theta(t_m)$, the measured fuel plate temperature at the time of peak power, with α_0 in Figure 10 is explained as follows: In the longer period region, τ_0 greater than 50 msec, ($\alpha_0 < 20$ sec^{-1}), peak power occurs while surface temperatures of the fuel plates are still rising (but below 100°C). At about

11

$\alpha_0 = 50 \ \text{sec}^{-1}$, peak power occurs almost simultaneously with maximum temperature, $\theta(\text{max})$, so that $\theta(t_m) \approx \theta(\text{max})$. Energy which is released after peak power (in this range of periods) is apparently lost rapidly from the fuel plates to the moderator by boiling heat transfer so that higher fuel plate temperatures are never obtained. The rise in $\theta(t_m)$ between $\alpha_0 = 50 \ \text{sec}^{-1}$ and $\alpha_0 = 160 \ \text{sec}^{-1}$ reflects the fact that boiling heat transfer eventually becomes unable to offset the rapidly increasing power levels of the short-period excursions; and finally, the apparent jump of $\theta(t_m)$ at $\alpha_0 \approx 160 \ \text{sec}^{-1}$ indicates that film boiling also has occurred before peak power so that $\theta(t_m)$

Fig. 10 Fuel plate temperatures at the time of peak power as a function of reciprocal period.

Fig. 11 Plot of the maximum measured transient pressures at various positions outside the core. Location #'s indicated refer to Table B-II, Appendix B. Positions 4 and 4d are several inches below core; positions 8 and 8d are at the side of the core; and position 10 is near the vessel wall.

includes part of a nearly adiabatic temperature rise after vapor blanketing on the fuel plates [6].

The maximum transient pressures as measured in the reflector water at several positions around the core are shown in Figure 11. While the maximum pressures measured at any location demonstrate a fairly regular dependence upon the reciprocal period, both the period-dependence and the pressure magnitudes were found to vary considerably with the location of the pressure transducer [a]. The lines shown in Figure 11 are only faired-in to connect related data points. Pressure profiles differed greatly according to position and highest

[a] Reference 9 contains a summary of reactor dynamic pressure measurements made during previous transient testing programs at Spert. It constitutes a comprehensive source of information on the problems and interpretations of pressure measurements.

pressures were measured below the core. Position numbers shown in Figure 11 refer to locations as shown in Appendix B, Figure B-4. Actual coordinates of these positions are shown in Table B-II of Appendix B, page 77.

The pressure data in Figure 11 were recorded at times always immediately after the onset of boiling in the core and are, therefore, associated with the vapor pressure of superheated water on the fuel plate surfaces just prior to the initiation of boiling. The moderate superheats of water indicated by the data (for instance about 35°C for the destructive test) are probably less than actually achieved in the core since the pressures are measured external to the core after undergoing some attenuation.

2.3 Reactivity Compensation Characteristics

It has been shown that a super prompt critical power excursion may be temporarily terminated by compensation of only a part of the original reactivity insertion, Δk_0; [7, 8] the reason being that when the reactor power is greatly in excess of the delayed neutron equilibrium value, up to one dollar of reactivity is lost in the buildup of neutron precursors. The actual amount of reactivity compensated at the time of peak power, $k_c(t_m)$, therefore, is usually less than the initial excess reactivity by as much as one dollar, but may increase depending upon the rate of shutdown. Thus, if the initial reactivity compensation in a transient occurs very slowly (as in the case of extremely long period transients, ie, $\tau_0 > 1$ sec) then it is possible for delayed neutron precursors to approach equilibrium with the power, and a compensation of nearly all of the inserted excess reactivity is required to halt the power rise. On the other hand, it was found with this core as with many others, that in the case of short period transients, self-shutdown from both thermal expansion and from boiling occurred very rapidly and arrestment of the power rise occurred after a compensation of only the prompt reactivity, $\Delta k_p \approx (\Delta k_0 - 1)\$$. Figure 12 shows the empirical relationships of $k_c(t_m)$ to the prompt reactivity and to the total reactivity for the D-12/25 core. As with all other light-water moderated, highly-enriched cores studied at Spert, $k_c(t_m)$ departs from Δk_0 (for extremely long periods) and approaches the prompt reactivity in the region of $\alpha_0 \approx 10$ sec^{-1}.

2.4 Energy Coefficient

Since compensation of reactivity arises primarily from thermal processes taking place in response to the release of energy during a power excursion, the ratio, $b(t)$, of the compensated reactivity to the energy can be defined as an "energy coefficient" which is an indicator of the efficiency of the shutdown mechanisms in the arrestment of power excursions. In Figure 13, the energy coefficient evaluated at the time of peak power, $b(t_m)$, has been shown for most of the D-core power excursions. For excursions in which boiling did not occur before peak power (ie, $\alpha_0 \lesssim 20$ sec^{-1}), characteristically low values of $b(t_m)$ approximately 10¢/MW-sec are obtained. The slight decrease in $b(t_m)$ with increasing α_0 may be attributed to the change in energy partition between the fuel plate and the water moderator. That is, with shorter periods, a relatively greater amount of energy remains in the fuel plate which has a lower coefficient of thermal expansion than does water. The effect of boiling shutdown begins to appear at about $\alpha_0 = 30$ sec^{-1}, causing the reactivity coefficient to turn upward to larger values (ie, more efficient shutdown). Although very large volumes of steam can be produced by extracting only a small fraction of the heat from the plates, it takes a few milliseconds for boiling to spread over the core and the modest rate of increase of $b(t_m)$ for α_0 above 30 sec^{-1} (rather than a stepwise

13
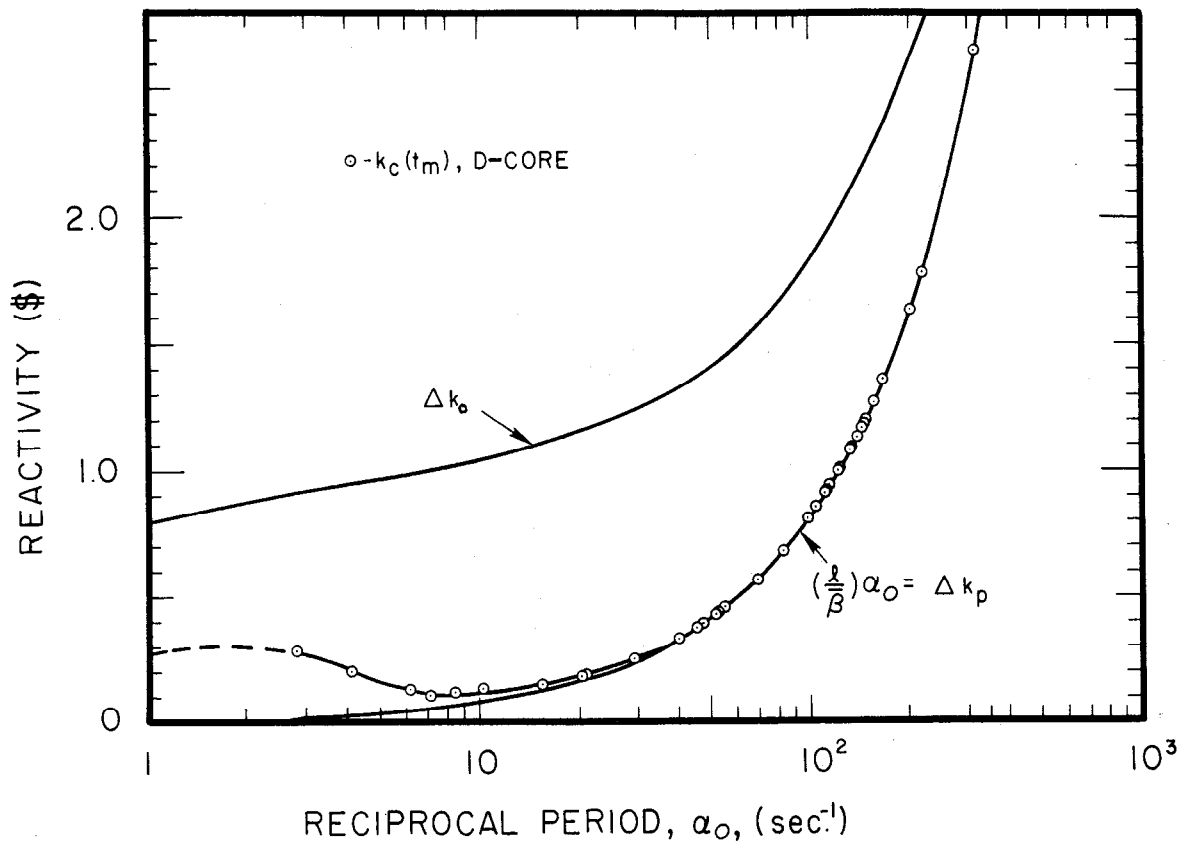
Fig. 12 $k_c(t_m)$, and Δk_o, vs reciprocal period α_o.
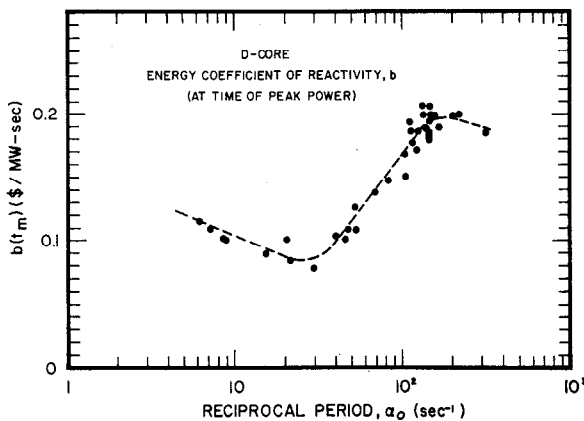
Fig. 13 Energy coefficient of the reactivity evaluated at the time of peak power as a function of the reciprocal period, α_o.

jump) reflects this fact since at the time of peak power, void growth from boiling is only partially complete. Above $\alpha_o = 100$ sec^{-1}, it appears that the energy coefficient reaches a maximum and begins to decline, probably because of the onset of film boiling and the resultant decrease in heat transfer rate to the water.

2.5 Time Dependent Reactivity Compensation

Information on the dynamic condition of the reactor as indicated by the compensated reactivity has been obtained from analysis of the power data for tests with periods less than 10 msec. Two aspects of the compensated reactivity behavior were carefully considered, viz, whether there was any evidence of the existence or proximity of, first, an upper limit to the amount of reactivity which could be compensated by boiling and, second, a significant change (specifically a reduction) in the rate at which self-compensation occurs. Possible failure of the existing shutdown mechanisms to terminate a power excursion for either reason might be anticipated by

computing the compensated reactivity for each test and extrapolating to the shorter periods.

The first step in this examination was to compare power burst shapes in order to observe any changes. The curves in Figure 14, drawn for this purpose, have been normalized at peak power both in magnitude and in time. For excursions with periods less than 9 msec $(\alpha_0 > 111\,\text{sec}^{-1})$, the power bursts were observed to become increasingly broad. That is, after passing through peak power, high power levels were sustained momentarily, prior to the fast decline which normally took place. At still shorter periods, this broadening began to occur before peak power. This effect resulted in excursions with greater relative energy releases and consequently increased the slopes of the energy versus reciprocal period curves as shown in Figure 8 for the region $\alpha_0 \gtrsim 125\,\text{sec}^{-1}$. Broadening of the power burst is indicative of less rapid rate of reactivity compensation occurring around the time of peak power. This effect also was noted in the decrease in the energy coefficient as shown in Figure 13.

A possible explanation of the burst shape can be made from what is known about moderator boiling in the core. As the period is shortened film boiling arises over larger portions of the core and is established earlier in the burst with respect to peak power. This film boiling can inhibit the formation of larger amounts of steam and retard the self-shutdown process, leading to the observed broadening of the power peak. The power decrease is equally delayed but, when a sufficient degree of superheat exists, it appears that instabilities in film
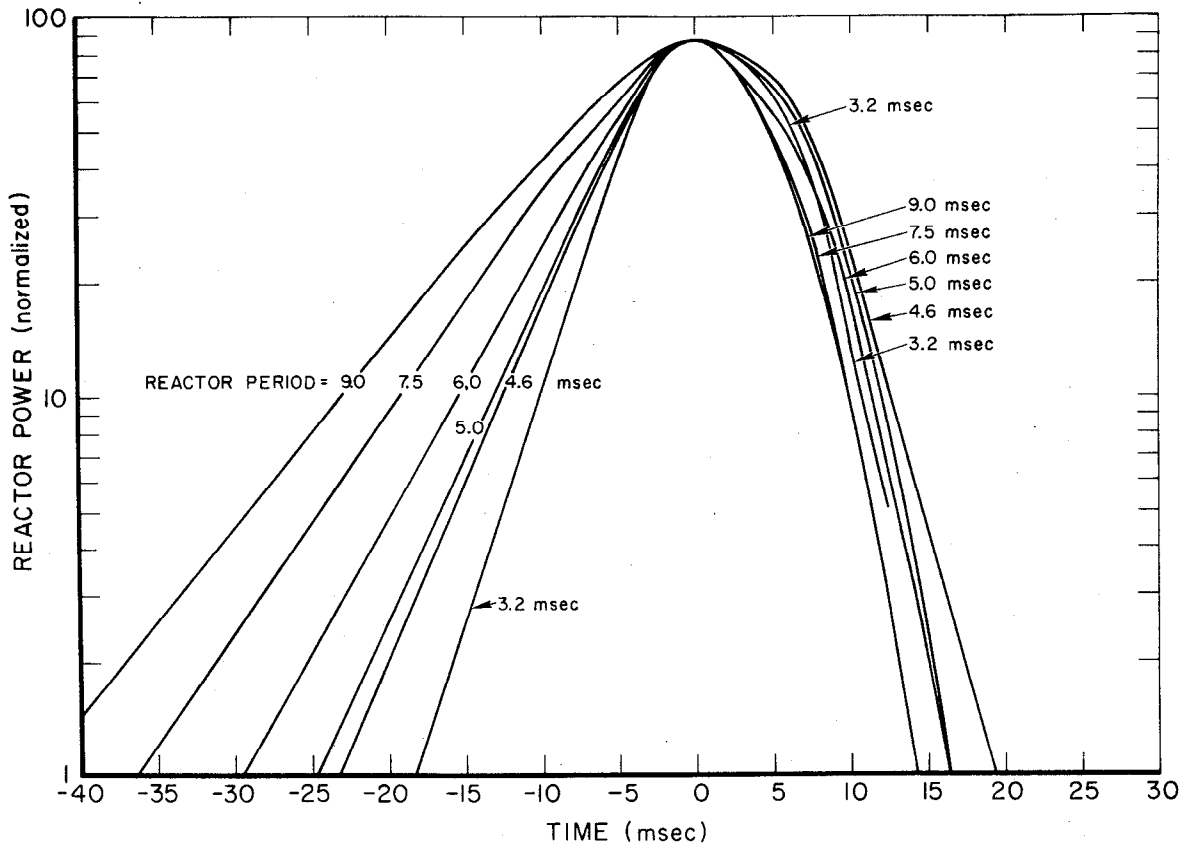
Fig. 14 Various power profiles for several different periods normalized at peak power.

15

boiling arise, resulting in the production of a larger amount of steam and, therefore, increasing the rate of production of shutdown reactivity. The eventual sharp power decline after peak power, which becomes sharper with shorter periods, might thus be associated with a break in film boiling.

To study the specific compensated reactivity, $\triangle k_c$, responsible for the change in burst shape, the time dependent reactivity was computed, for several excursions in the short period region, by solving the space independent kinetics equation (Figure 15). The results of this study showed that the rate of reactivity compensation during tests in the intermediate period range, say between 20 msec and about 8 msec, is characterized by a curve such as that in Figure 15 corresponding to $\tau_0 = 9.5$ msec, which demonstrates a fairly rapid but smooth compensation to several dollars. However, an inflection in the compensation reactivity curve was observed to occur at periods of about 7.5 msec (not shown) and this inflection became more abrupt at shorter periods. For $\tau_0 = 6.4$ msec, peak power is established as the value of $\triangle k_c$ passes through about 1.30$. Fully another dollar is compensated before the inflection occurs, so that for this case, at least, considerable power decline occurred before the shutdown rate was significantly reduced by the inflection.

TIME (5 msec/division)

Fig. 15 The time dependent compensation of reactivity for several short-period power excursions of decreasing period. The occurrence of peak power is indicated on each curve and is coincident with the compensation of the prompt reactivity.

For tests with shorter periods, around 5 msec, peak power was established at about the beginning of the inflection, and shutdown of the power was consequently delayed. Finally, for $\tau_0 = 3.2$ msec, peak power occurred during (rather than before) the inflection resulting in the observed broadening of the burst both before and after peak power.

Two conclusions are drawn concerning this behavior of the reactivity compensation. First, it might be expected that at still shorter periods ($\tau_0 < 3$ msec) the inflection in the compensation curves would occur prior to peak power, giving somewhat the effect of a transient with two periods (ie, the initial asymptotic period will be followed by a transition region as initial compensation takes place and, then, during the inflection another and longer "period" may be established).

Second, since the compensated reactivity is primarily a consequence of the steam content within the core, the inflection indicates an inhibition in the rate of void growth, which might have resulted from a nonuniform process in the rate of steam void production under transient conditions such as exponentially heating of fuel plates.

Behavior somewhat of this nature was anticipated from the results of previous in-pile studies of transient boiling [6] conducted at Spert. These studies revealed that during short-period power excursions, the initial growth of steam bubbles was often suppressed momentarily and that complete vapor blanketing of the fuel plate finally arose from a second generation of bubbles.

16

The calculations of reactivity compensation are obtained from the space-independent kinetics equations and would not reflect the above described void behavior unless nearly all regions of the core gave rise to the same process of boiling simultaneously. However, during very short-period power excursions, the time-lag between high and low flux regions of the core is correspondingly decreased, and the specific behavior of boiling void production (and condensation) should become increasingly apparent in the reactivity calculations. It is possible that this effect is responsible for the enhancement of the reactivity inflection noted in Figure 15 as shorter periods are achieved.

2.6 Maximum Reactivity Compensation

The maximum reactivity compensation attained during a power excursion, $\Delta k_c(\max)$, has also been computed for several of the shortest period tests and values ranging between 6\$ and 7\$ have been found. It is not apparent from these data just what functional relationship exists between $\Delta k_c(\max)$ and the reciprocal period in this region, but it does appear that in the region investigated (ie, between $\alpha_0 = 150$ and $\alpha_0 = 312$ sec^{-1}), $\Delta k_c(\max)$ is not rapidly changing. The excess reactivity, Δk_0, however, increases rapidly over this region (Figure 12) and it can be expected that at some period complete shutdown will become difficult. As the calculations indicate, such a condition may arise for initial reactivity insertions above 6\$ which would yield periods less than about 1.6-msec.

2.7 Fuel Plate Damage

After each test in which measured temperatures exceeded a few hundred degrees, fuel plates were inspected in order to ascertain the amount of damage sustained from thermal distortion. The first indications of permanent warping were obtained in a test with a period of 7 msec, for which the maximum recorded temperatures were about 400°C.

During shorter period tests, damage to the plates gradually increased from slight, lengthwise bowing to more localized bowing around the hot spot of the plate, succeeded by a type of sinusoidal rippling along the length of the fuel plates. The amplitude of these ripples was greatest a few inches below the center of the plate at a position corresponding to the peak flux, and attenuated toward either end of the plate in low flux regions.

Rippling of the plates was apparently caused by the constraint against expansion existing within the fuel plates both by the cladding and the edge of the fuel plates since these nonfuel-bearing materials remained comparatively cold during the power excursions while the central meat was heated.

It was observed that following excursions in which high plate temperatures were reached (ie, 550 to 650°C) the ripples became flat-topped or "square-wave" in profile, creating, as a consequence, regions on the plate of very high curvature. Failure of the clad by cracking was common in these regions.

Warping of the fuel plates was sufficient in several cases to cause complete channel blockage. The amplitudes of the ripples were often greater than the plate spacing (0.179 inch), and occasionally adjacent plates having rippled in opposite directions would come together and close off the water channel.

In the test with a period of 5 msec, eruptions of molten fuel occurred over about a 6-inch-high region on each of the six fuel plates in the central fuel

assembly, and over a small region of one additional fuel plate in an adjacent fuel assembly. About 0.5 percent of the total fuel plate area of the core showed signs of melting. Figures 16 through 22 show several damaged fuel plates of the central assembly from this test. Rippling and particularly the "square-wave" character of thermal deformation is apparent in most of the photographs.

Failure of the cladding by hot short cracking was widespread but most severe at the corners of the ripples. The actual surface of the cladding does not appear to have melted during the 5.0-msec period test. The molten material seen in the photographs from this test was mostly the uranium-aluminum alloy which had escaped through clad fractures. Eruptions of molten fuel (Figures 17 and 22) were preferentially located in high curvature regions.

Hot short cracking of the cladding is characteristic of the aluminum alloy used for these plates (6061 alloy) and probably promoted early failure of the clad. As seen in several of the photographs, the melted metal occurring in the 5.0-msec period test appears to have originated in the meat portion of the fuel plate and escaped through fractures in the yet unmelted clad. It is possible that another alloy of aluminum (such as 2S) less susceptible to hot, short cracking might have contained the molten fuel in this test. The results of a metallographic examination of the fuel plates are discussed in Appendix H, and a more complete discussion of fuel plate damage may be found in Reference 10.

For the test with a period of 4.6 msec, fuel plate thermal distortion and melting were more severe as seen in Figures 23 through 28. In this test, nearly 80 percent of the plates were warped and rippled to the extent that they could not be reused for subsequent tests. The region of melting was again centered about the hot spot of the core with a diameter (on a horizontal plane) of about six inches and a height of about nine inches. About two percent of the total plate area of the core was affected by melting and most of the melted plates were fused to adjacent plates as shown in Figures 26 through 28. Figure 23 illustrates the extent of melting as it occurred during the 4.6-msec test on a single plate located in the center (transient rod) assembly. It may be seen that, in contrast to the damage observed in the 5.0-msec test, melting of the clad surface did occur during the 4.6-msec test. Several plates from the same assembly, Figure 25, show severe constriction as a consequence of fuel melting and subsequent runout.

Maps of the melting regions for both the 5.0-msec and 4.6-msec tests are shown in Appendix D.
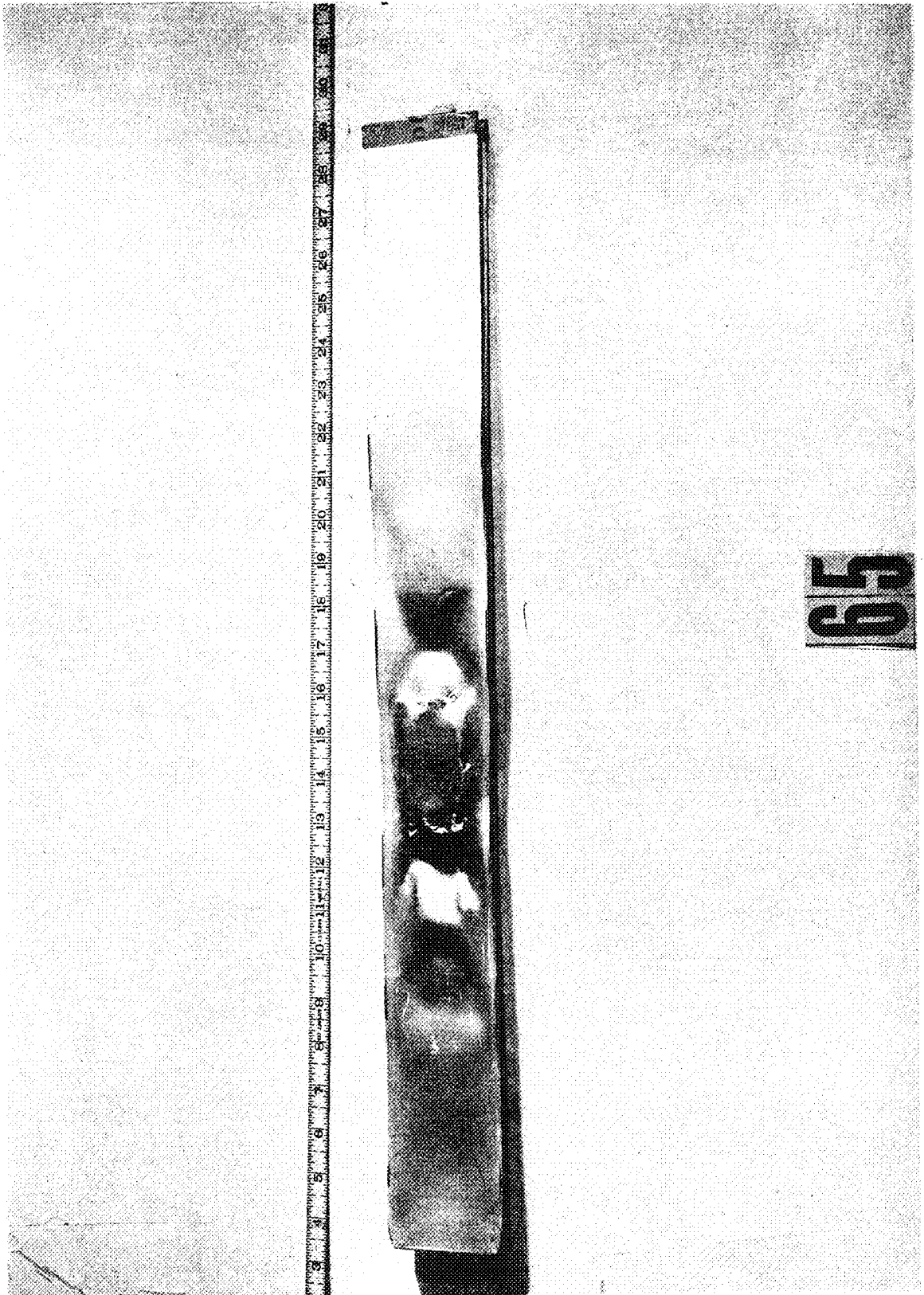
Fig. 16 Two fuel plates warped and fused together as a result of a 5-msec test.
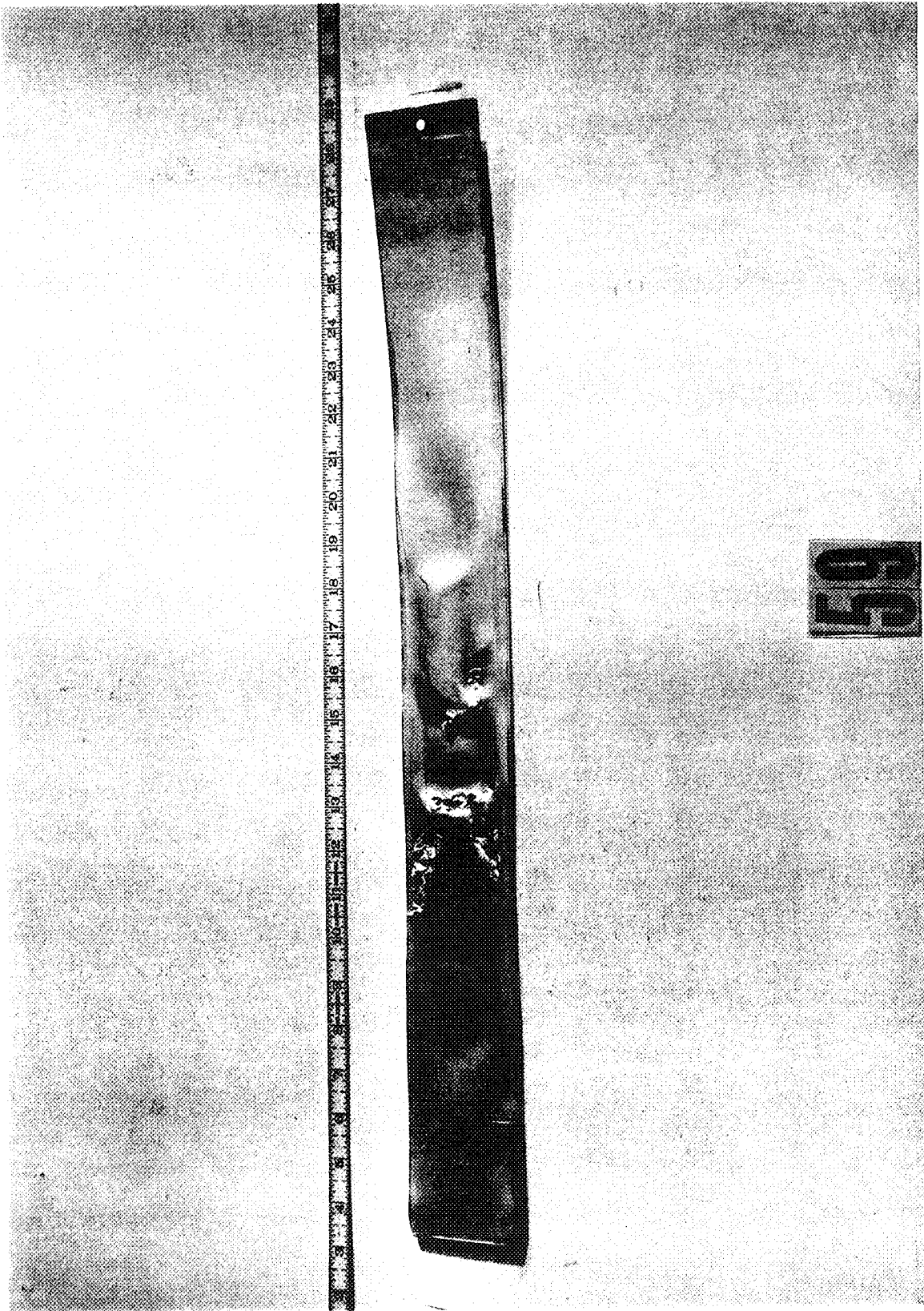
Fig. 17 Fuel plate from 5-msec test showing melting and warping.
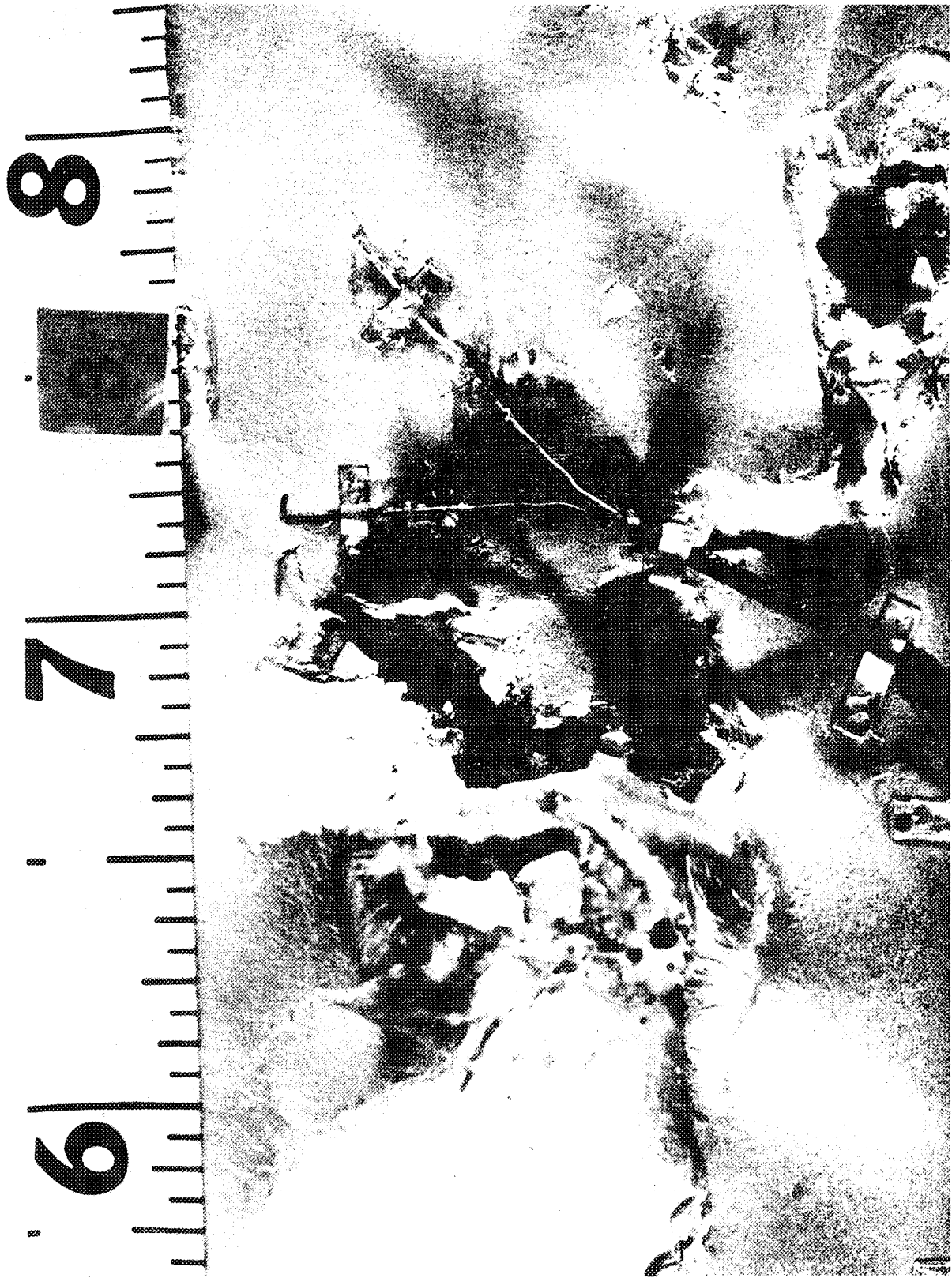
Fig. 18 Close view of fuel plate showing melt region, cracking of clad, and a thermocouple -- 5-msec test.

21
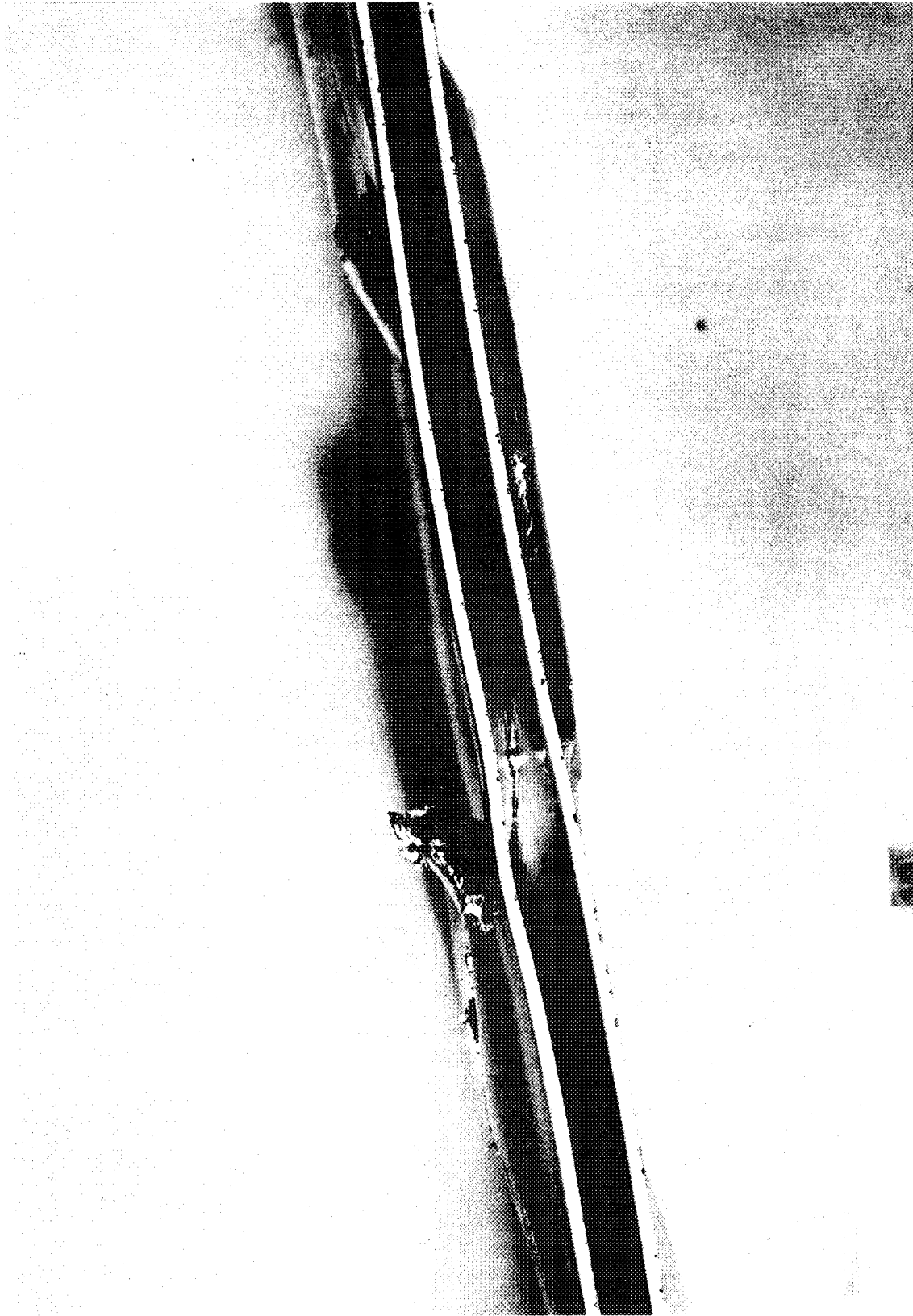
Fig. 19 Two fuel plates fused together -- 5-msec test.
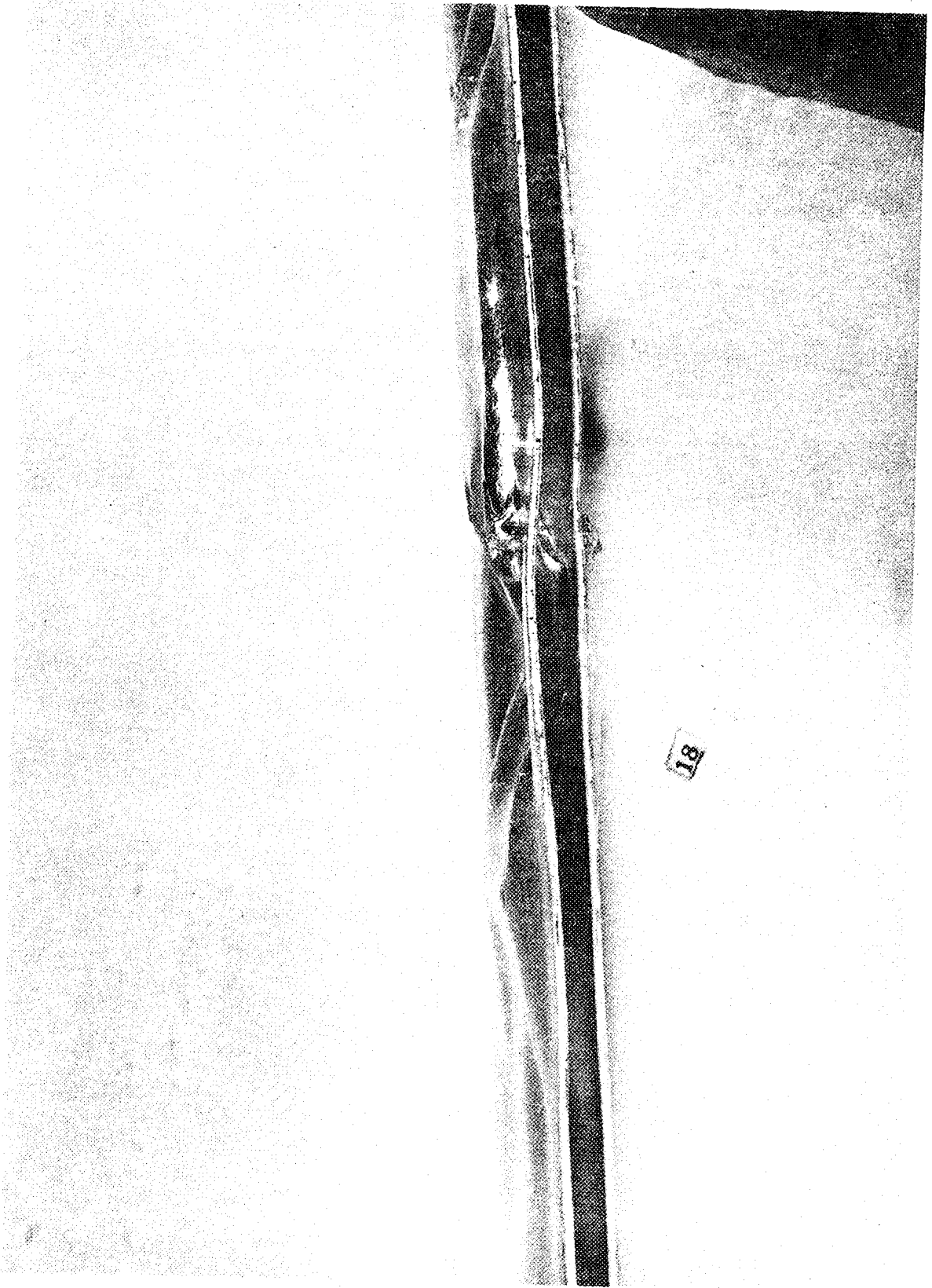
Fig. 20 Two fuel plates fused together -- 5-msec test.
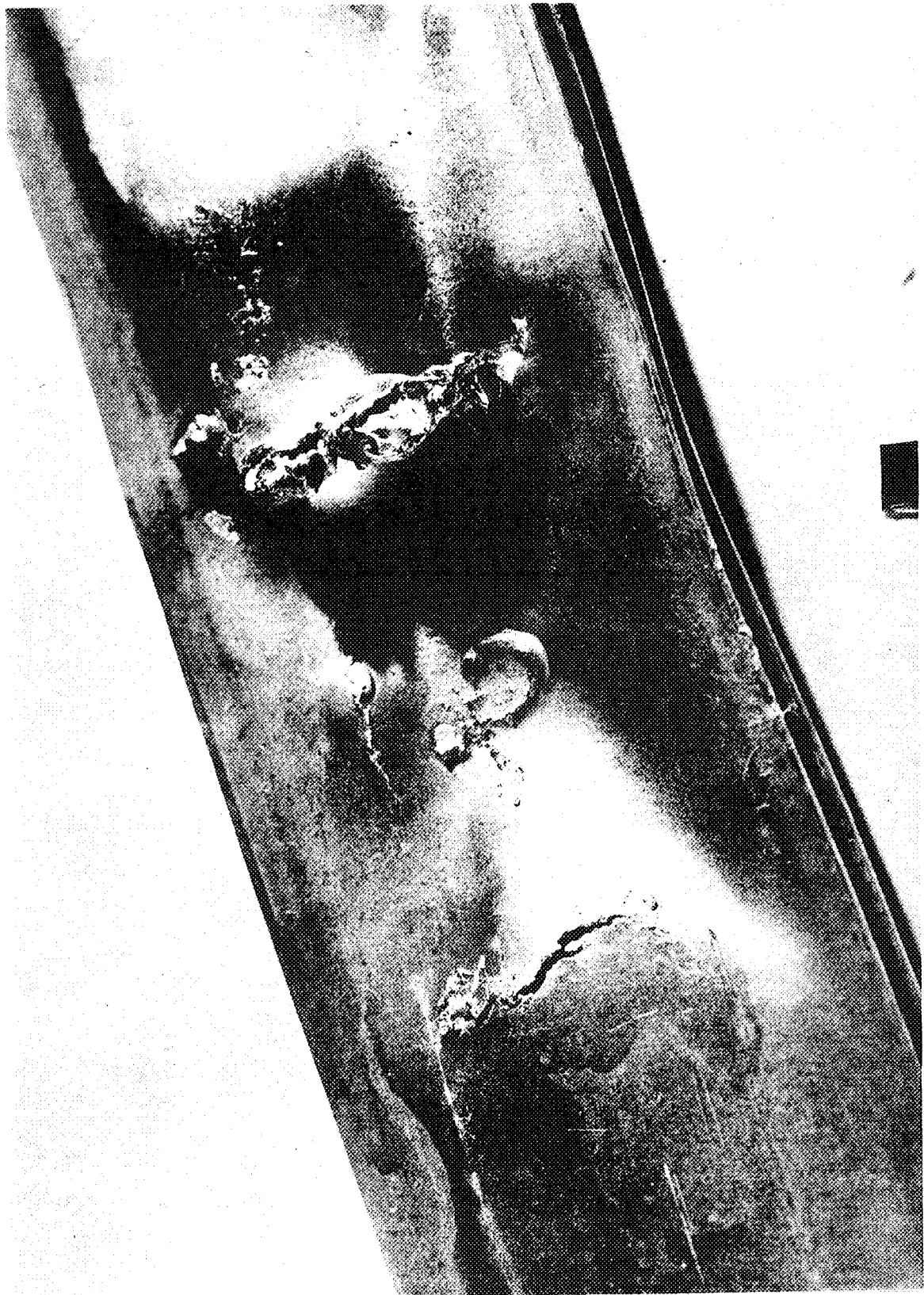
Fig. 21 Typical melt eruptions and clad fracture of fuel plate -- 5-msec test.

24
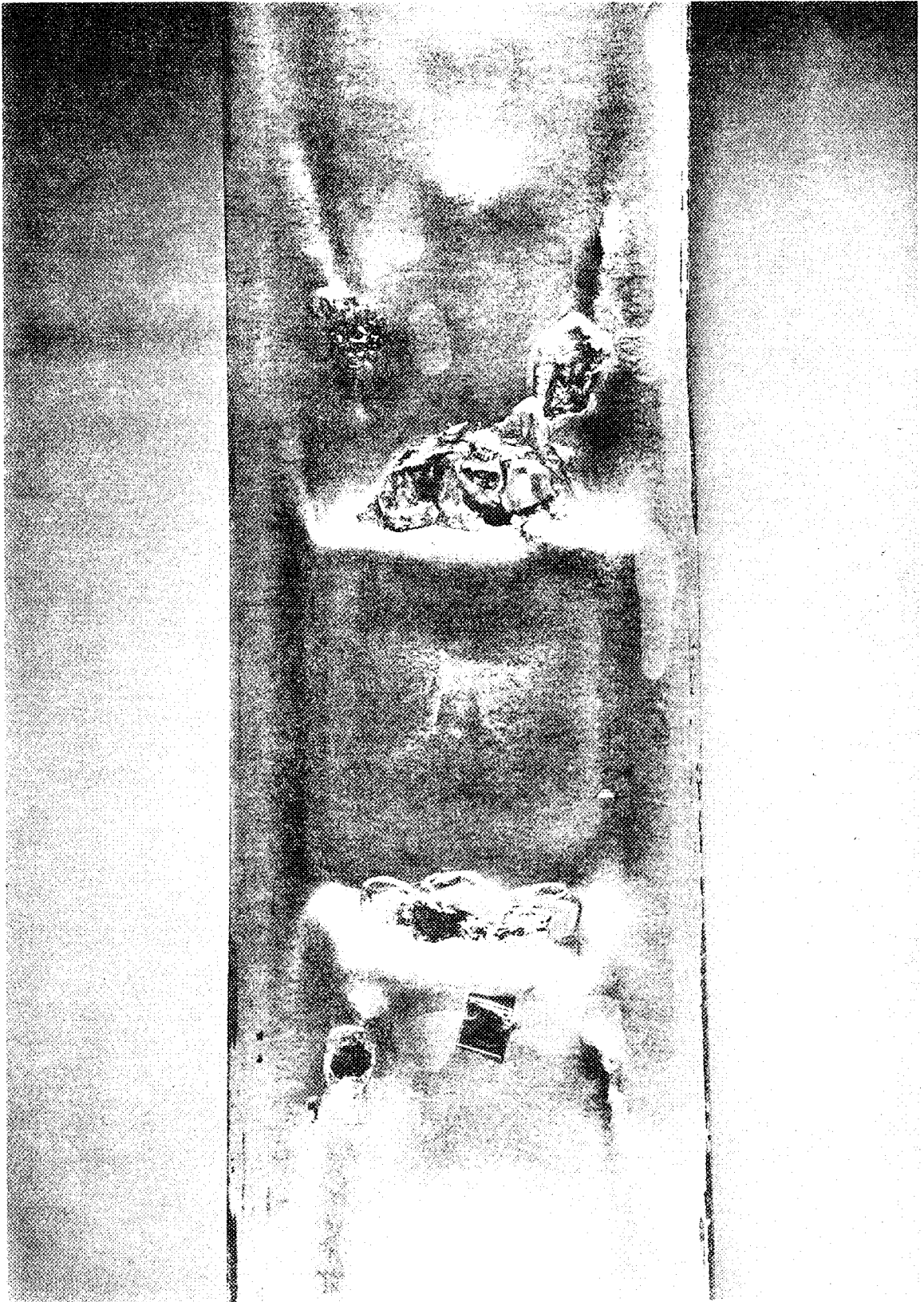
Fig. 22 Typical square-topped ripples and melt of fuel plate -- 5-msec test.

UNMELTED CLADDING

MELTED CLADDING
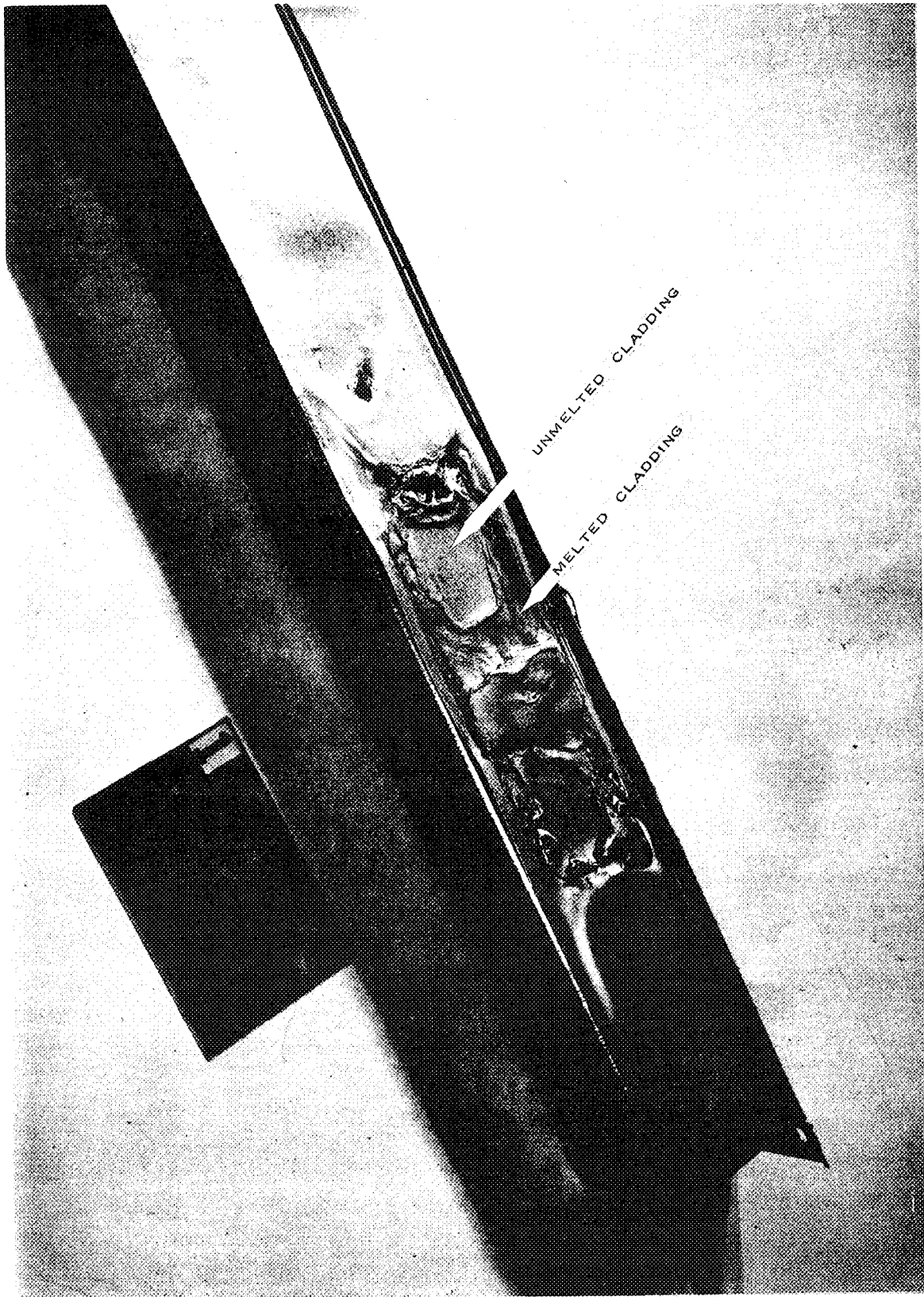
Fig. 23 Top fuel plate of central assembly showing warpage and melting -- 4.6-msec test. Regions of complete clad melting are visible.
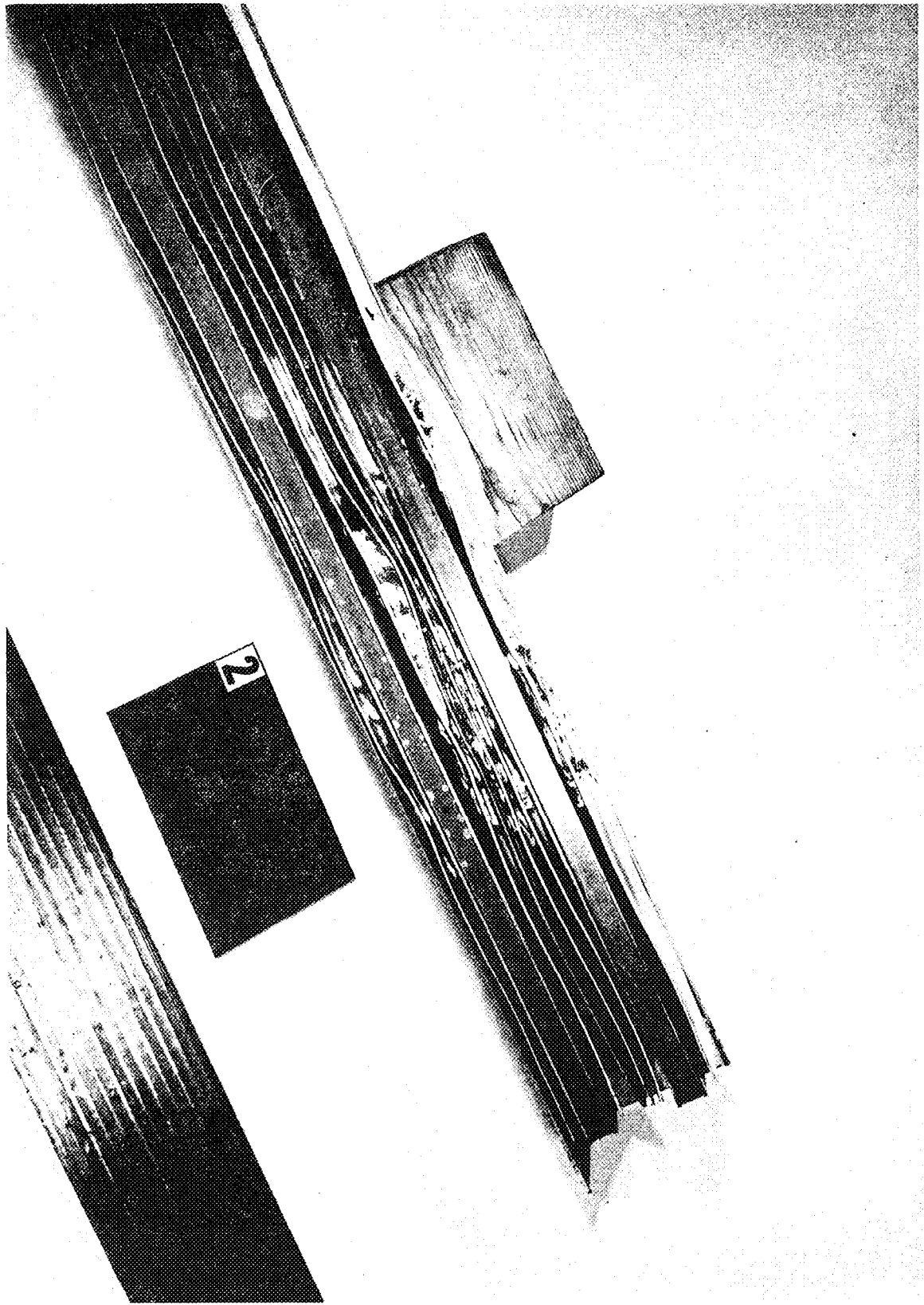
Fig. 24 Side view of central assembly showing extent of plate fusion -- 4.6-msec test.
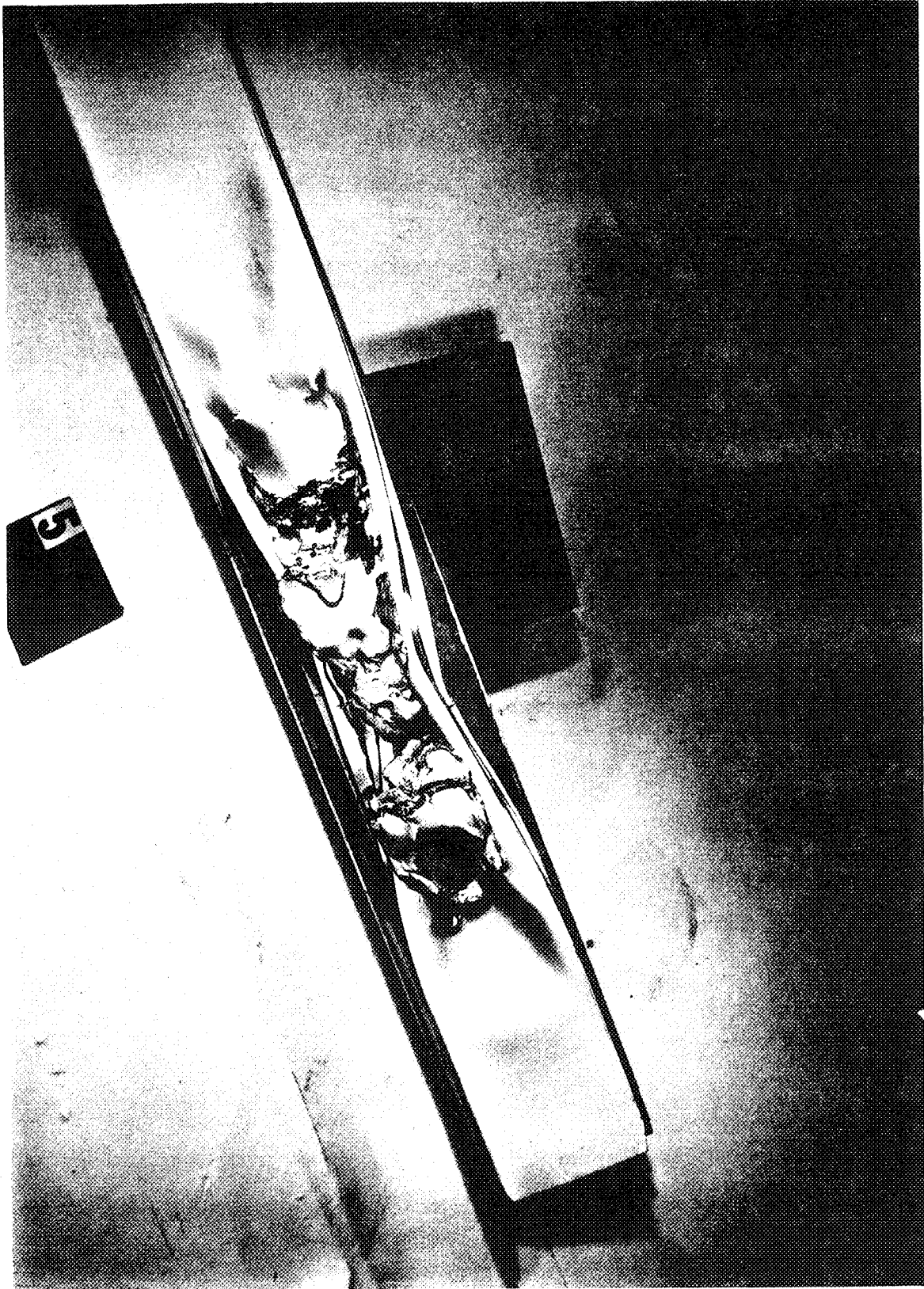
Fig. 25 Melting and plate constriction in center assembly -- 4.6-msec test.
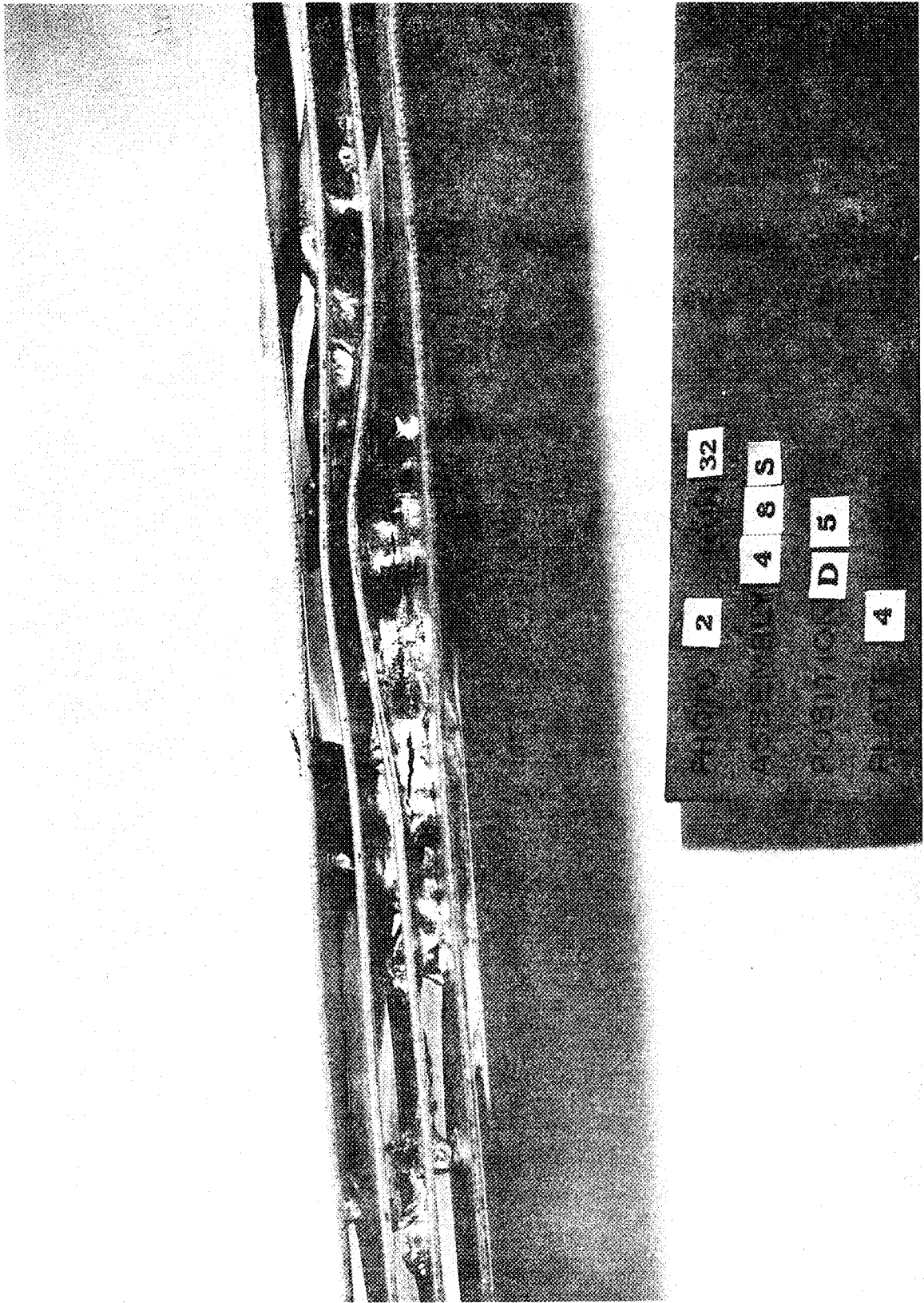
Fig. 26 Edge view of fused plates, position D5 -- 4.6-msec test.
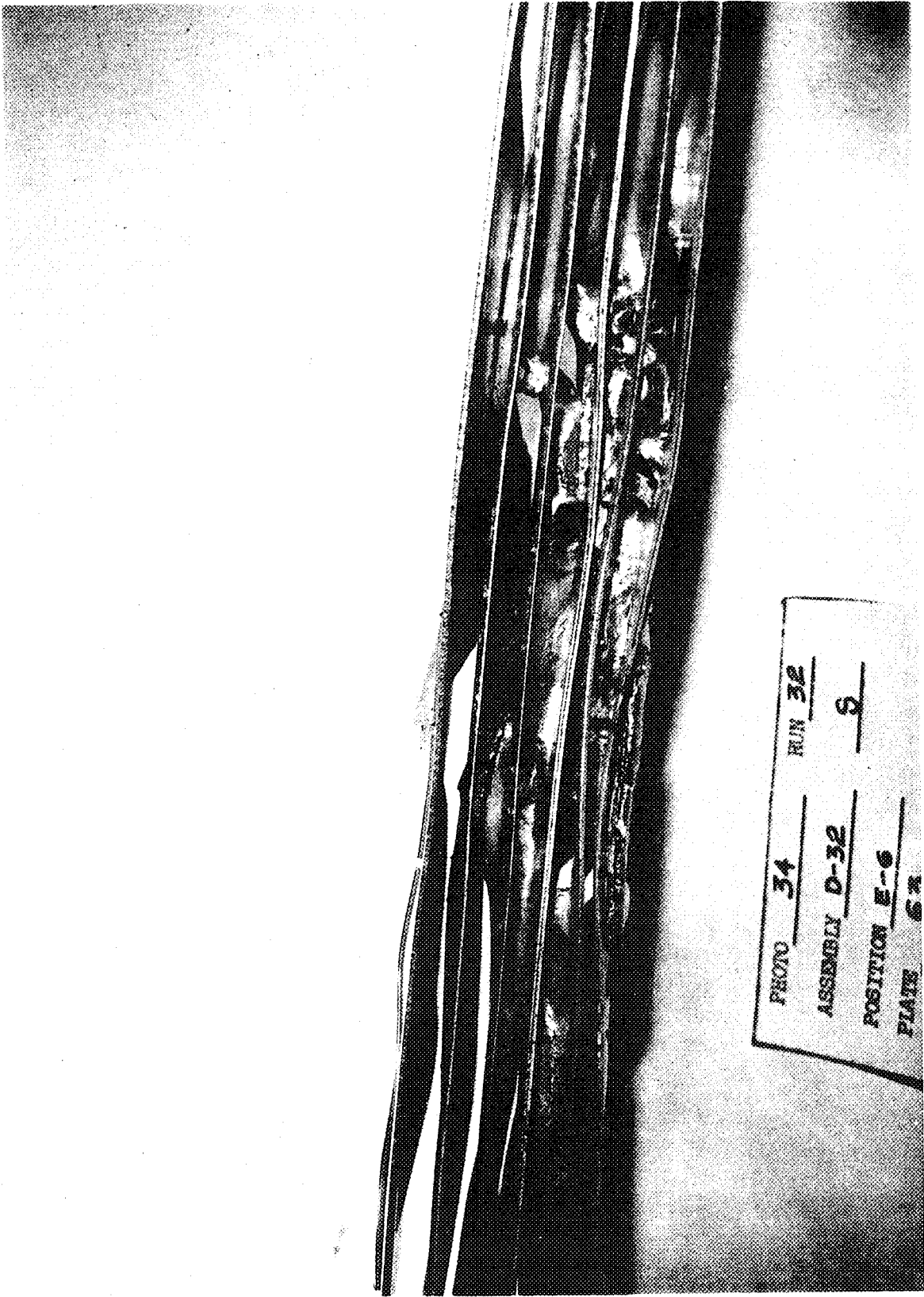
Fig. 27 Edge view of fused plates, position E6 -- 4.6-msec test.

PHOTO _12_

ASSEMBLY _D-42_ RUN _32_

POSITION _F-5_ _N_

PLATE _1949_
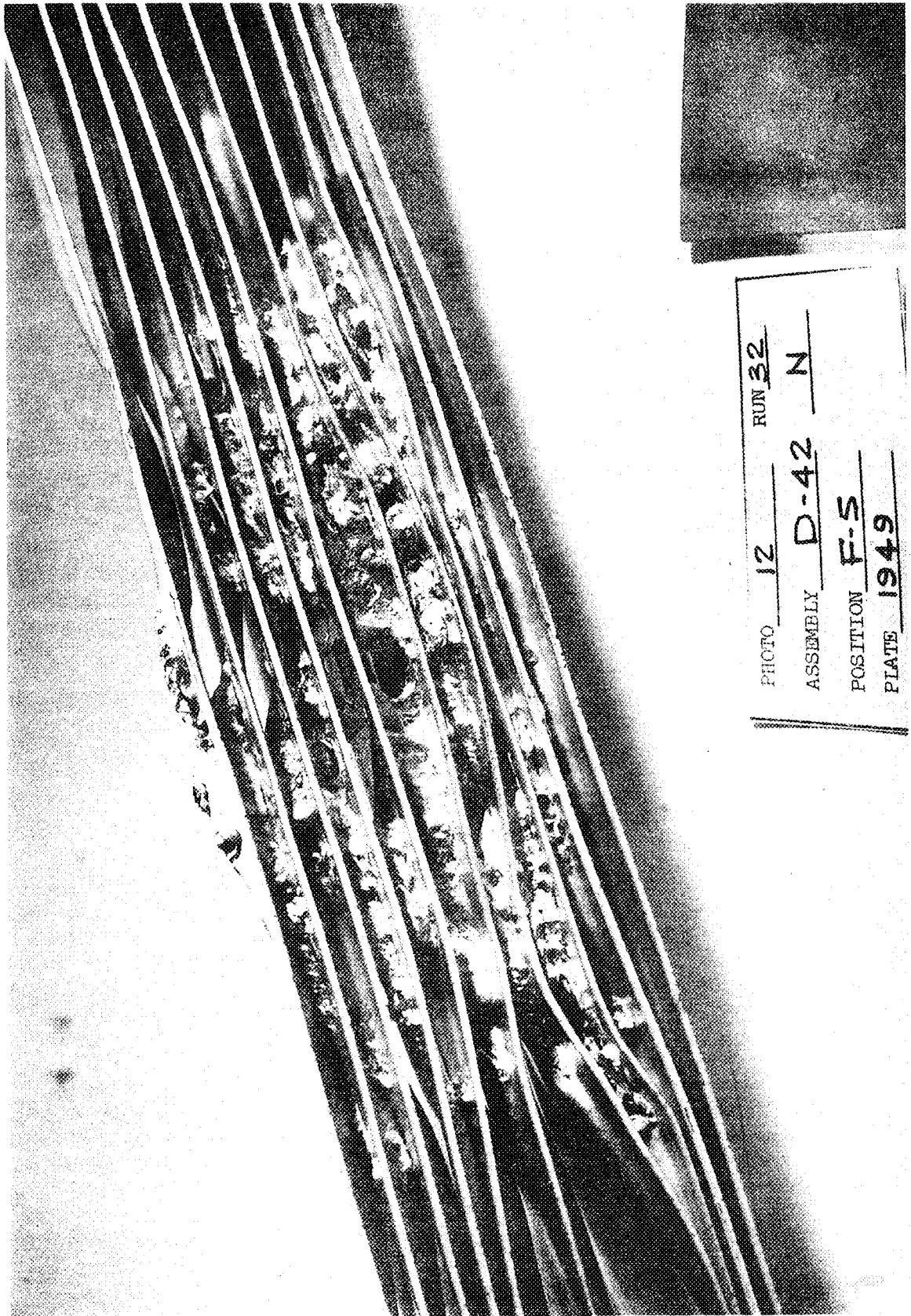
Fig. 28 Edge view of fused plates, position F5 -- 4.6-msec test.

IV. THE DESTRUCTIVE TEST

1. PREDICTABILITY OF TEST RESULTS

In accordance with the objectives of this program, power excursions were to be initiated with successively larger reactivities to obtain data on the nature and extent of damage encountered in the short period region and to probe for factors which might be responsible for the type of destructive pressure pulses which apparently occurred in the Borax test in 1954 [2] and more recently in the case of the SL-1 accident [11, 12].

The results of experiments leading up to the destructive test have been discussed in the preceding section but will be briefly reviewed with regard to extrapolability of the data to shorter periods. As discussed in the previous section, the measured power, energy, temperature, pressure, and the compensated reactivity had all shown regularity and predictability as the period was shortened. No evidence was observed in any of the data which would indicate the occurrence of unusual or unpredicted behavior in the period region just below 4.6 msec.

Although damage from thermal deformation had been produced in nearly 80 percent of the core and melting in about 3 percent, neither of these phenomena had produced a tendency toward the generation of large pressures despite the fact that fuel plate temperatures in many cases exceeded the critical temperature of water. In the 5.0-msec period test and the 4.6-msec period test, both melting and warping occurred, yet their occurrence was accompanied neither by the generation of significant pressures nor the displacement of materials.

2. TEST CONDITIONS

In the absence of any known threshold at periods proximal to 4.6 msec, the last test was approached with the specific objective of reducing the period by a substantial amount and establishing melting over a large fraction (about 40 percent) of the core. As with all preceding tests with periods below about 6.0 msec, the last test was conducted with the anticipation that an explosion such as occurred in the Borax-I test might occur although such could not be extrapolated or predicted. The period for the test was selected to be that which would produce fuel plate temperatures in the range 1000 - 1700°C. The 1000°C lower range limit was selected to ensure widespread core melting and the upper range limit of 1700°C was selected to avoid enhancement of the potential chemical reaction since studies at other laboratories [19] had indicated that near this temperature the chemical reaction between aluminum and water becomes more rapid.

A period of 3.3 msec was selected which required the insertion of about 3.5$ excess reactivity. A peak power of 2.3 GW and a total nuclear energy of 33 MW-sec were predicted for this test.

In preparation for the test, a pneumatically operated transient rod ejection system was installed which was capable of ejecting the entire transient rod in about 85 msec.

The test was conducted under special procedures and with specified weather conditions. Safeguards which were adopted included evacuation from the area of all personnel not essential for the test and an alert status with various safety support services at the National Reactor Testing Station. Weather requirements for the test consisted of lapse conditions with no rainfall, wind from the southwest (190 to 250°) between 10 and 20 mph and a three hour predicted persistence of these conditions after the test. The wind direction was chosen to prevent a possible release of radioactive fissides from being airborne to other NRTS installations.

An extensive radiological effort (Appendix B and G) was planned, including ground-level dose measurements on a grid system extending downwind of the reactor building, and cloud tracking by airplane.

The area surrounding the reactor was inspected by airplane just prior to the test in order to assure that personnel were not inadvertently close to or downwind from the reactor.

Special instrumentation and reentry procedures were adopted to ensure the safety of personnel engaged in the reentry operation following the test since it could not be assured that normal control of the reactor would be possible nor that the usual operational information on the reactivity status of the reactor would be available.

Following completion of all pretest preparations, a period of about two weeks was spent in a state of readiness before meteorological conditions favorable for the test developed. The test, Run 54, was initiated at 12:25 p.m. on November 5, 1962.

3. TEST EVENTS

Immediately following ejection of the transient rod, a loud noise in the reactor area was heard over the intercom systems and a plume of water was observed to rise about 80 feet above floor level of the reactor building (Figure 29). Pictures on both television monitors in the control room were immediately lost apparently as a result of water hitting the cameras which were aimed directly at the core. It was found that the reactor control-rod-drive system could not be operated normally and that positive indication of the control rod positions could not be obtained. However, neutron-levels (as indicated by neutron sensitive chambers) were declining normally.
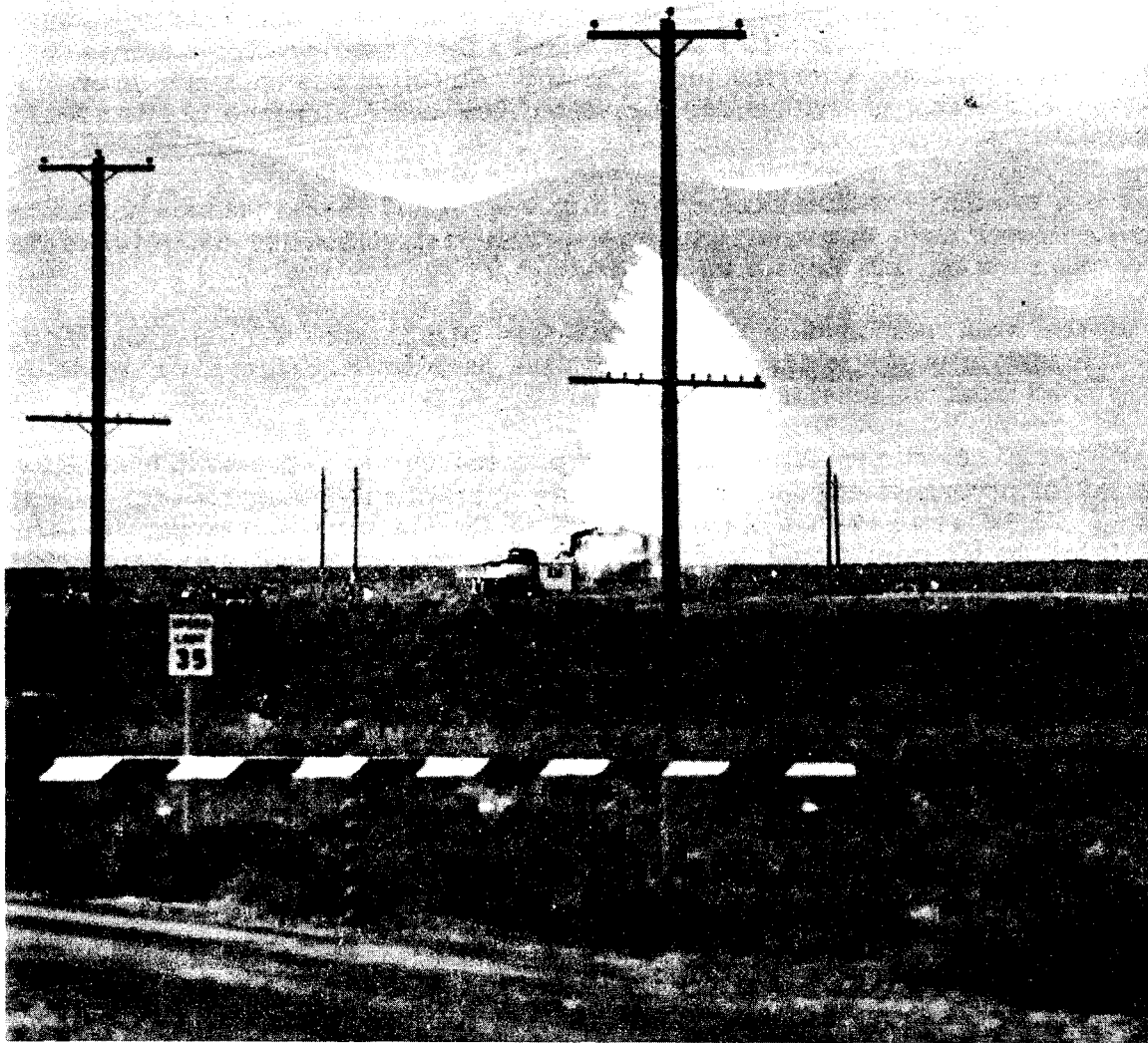
Fig. 29 Plume of water rising about Spert I during 3.2-msec test.

4. REENTRY

In accordance with procedures for reentry which had previously been established in the event that a positive indication of the shutdown condition of the reactor could not be determined (by means of the control system and the nuclear instrumentation), all water in the reactor vessel was drained by remote activation of a sump pump. As the water level reached 6-inch and 3-inch levels

above the vessel floor, a float-actuated, blast-protected, water level instrument [a] provided this information to the Control Center. Verification of the proper operation of this device was accomplished by partially refilling and redraining the vessel to test repeatability. Draining was completed and personnel reentry began about four hours after the test.

The first reentry team, equipped with several layers of protective clothing, self-contained breathing apparatus, and radiation monitoring equipment, approached the reactor while in radio contact with personnel in the Control Center and established that radiation levels in the reactor area were sufficiently low to permit recovery operations to begin around the reactor building. Short-time visual examination of the destroyed core in the vessel also was possible even though the normal shielding of water was absent. Although air activity in the reactor area was negligible following the test, all personnel in the first several reentry teams were required to use filter breathing apparatus for protection against contaminated particulate matter which might be airborne by the strong wind blowing at the time.

The radiation level at floor level over the open vessel (about 10 feet from the normal core center) was about 25 r/hr at the time of first reentry (3 hours and 55 minutes after the test). Other radiation measurements taken at this time indicated dose rate levels of 1.1 r/hr at roof level directly above the vessel (about 18 feet from the core), 85 mr/hr at "head" level about 5 feet from the edge of the vessel, and approximately 2 mr/hr at floor level about 50 feet in front of the reactor building.

After checking radiation levels, the reentry teams removed all motion picture cameras from the reactor area. The films were removed and processed immediately.

---

[a] See Appendix B for a description of this instrument.

V. DESTRUCTIVE TEST RESULTS

1. DAMAGE TO THE CORE AND FACILITY

Immediately following the test it was possible to see that some of the control-rod-drive extensions were bent. Figure 30, a photograph showing a view of the front of the reactor building shortly after the test, shows the bent rod-drive extensions extending from the upper bridge (supporting the drive motors) to the magnet plates and dash-pots mounted on the lower bridge just below the lip of the tank. The lower bridge (visible at about floor level in Figure 30, and again in a rear view, Figure 31) had been raised and tilted. The lower bridge is normally about three feet below floor level and supported at each end by I-beams welded to metal plates in the concrete floor of the building. These end supports can be seen at each side of the reactor vessel. One end of the bridge had been thrust upward about three feet by the explosion and came to rest about two feet above normal level. Some debris and an overhead light from the reactor building can be seen on the floor in front of the vessel.

As shown in Figures 32 and 33, one of several roof support beams of the reactor building was bent upward, presumably by the water ejection.

Figure 34 shows the appearance of the reactor core prior to the test and Figure 35 is a similar view after the test showing the extent of destruction achieved by this test. The lower bridge, seen at the top of both figures, supports several items including instrument leads, control and transient-rod blades, and a periscope (the large black tube in the center of Figure 34). Figure 36 is a close-up view of the debris in the vessel. The periscope can still be seen at top, center. Immediately to the left of the periscope can be seen the transient rod extending down to the two aluminum blades, which have been spread into an inverted Y-shape. The transient rod blades are normally parallel and reside in a fuel assembly in the center of the reactor.

The condition of these blades suggests that a destructive pressure pulse probably originated between them in the central assembly of the core. Just to the front and to the right of the transient blades can be seen two of the four control-rods. The control rod blades, by contrast, are pressed together into a crescent shape.

On the right of the picture, Figure 36, the reactor vessel can be seen to be bulged outward between reinforcing rings which were attached to the exterior of the vessel. Since the vessel was back-filled, the bulging would have caused displacement and compaction of the surrounding earth. Other items identified in Figure 36 and in Figure 37 include ion chambers, core support structure, several damaged fuel assemblies, many fragments of fuel plates, underwater lamps, pressure transducers, etc.

Figures 38 and 39 show the general types of damage obtained in fuel assemblies and plates. In general, the central portions of fuel plates have been melted and subsequently disintegrated, leaving only the tops, bottoms, and the unfueled edge strips still intact. Further photographs of the test damage are presented in Appendix E.

36

CONTROL ROD
DRIVE MOTORS

UPPER
BRIDGE

CONTROL
ROD
EXTENSIONS

LOWER
BRIDGE
SUPPORT
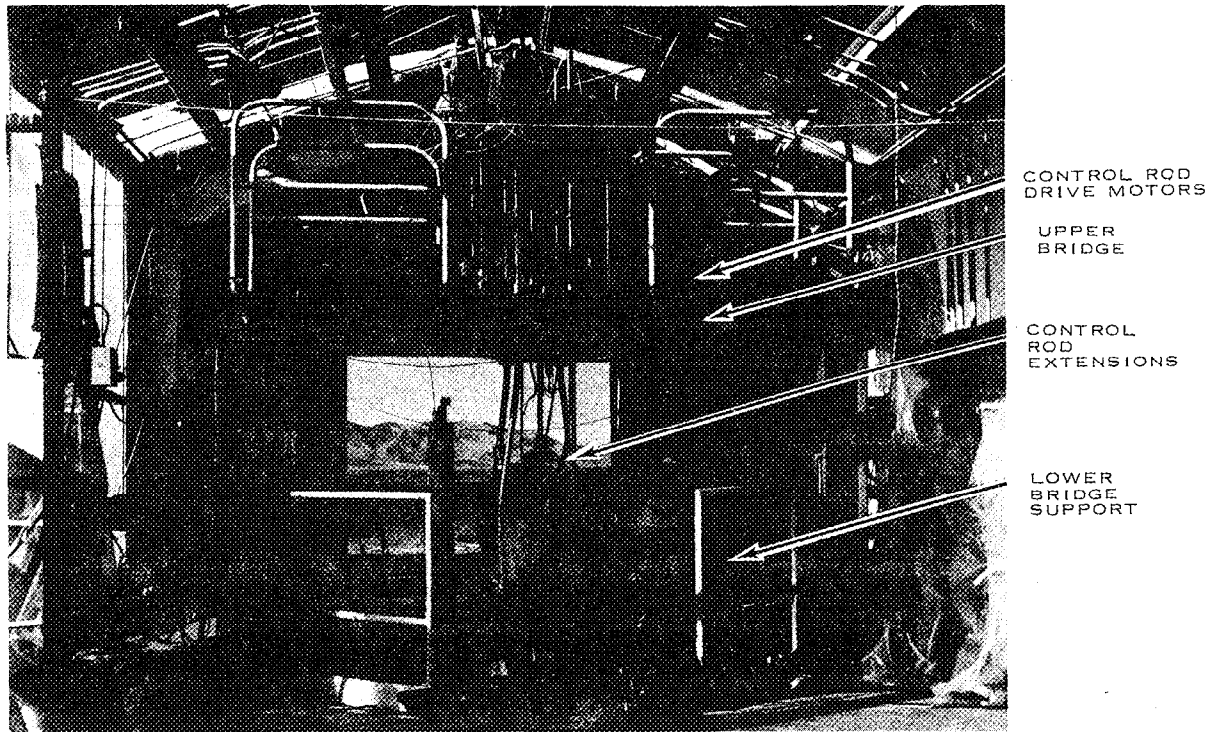
Fig. 30 Front view of reactor building showing damage incurred to control rods.

PERISCOPE

LOWER
BRIDGE
SUPPORT
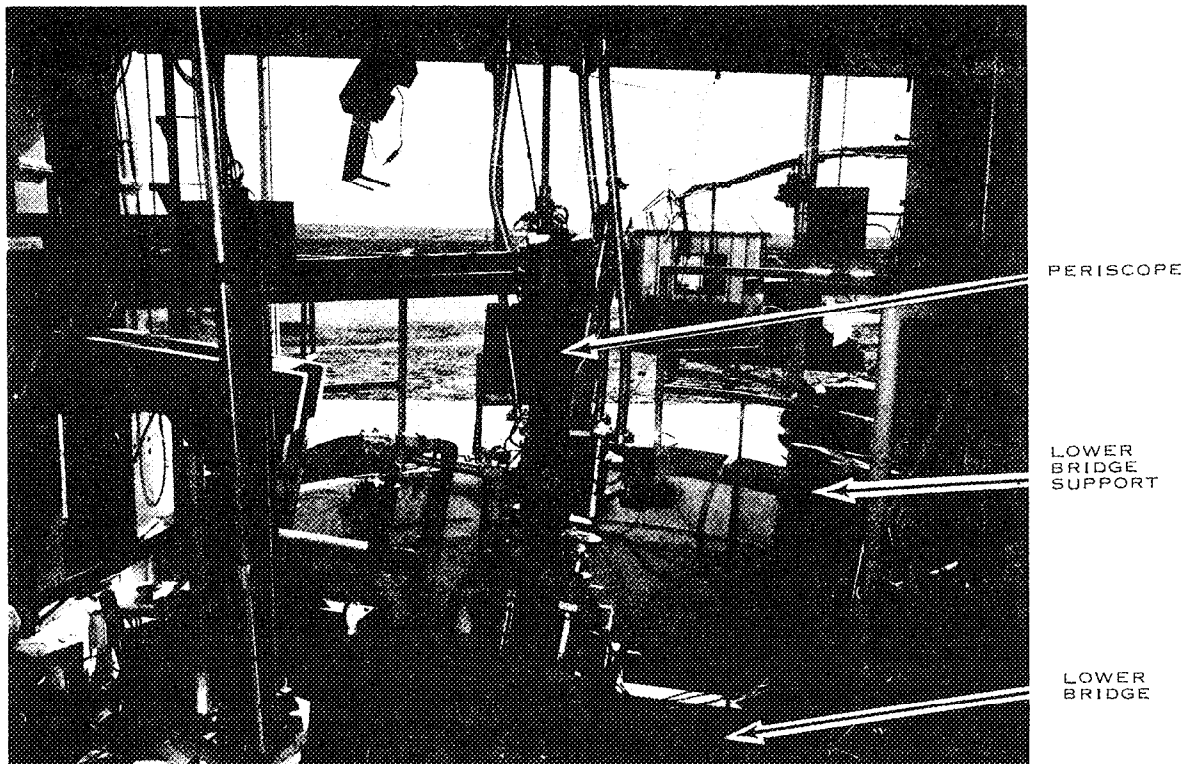
LOWER
BRIDGE

Fig. 31 Rear view of control rods and lower bridge.
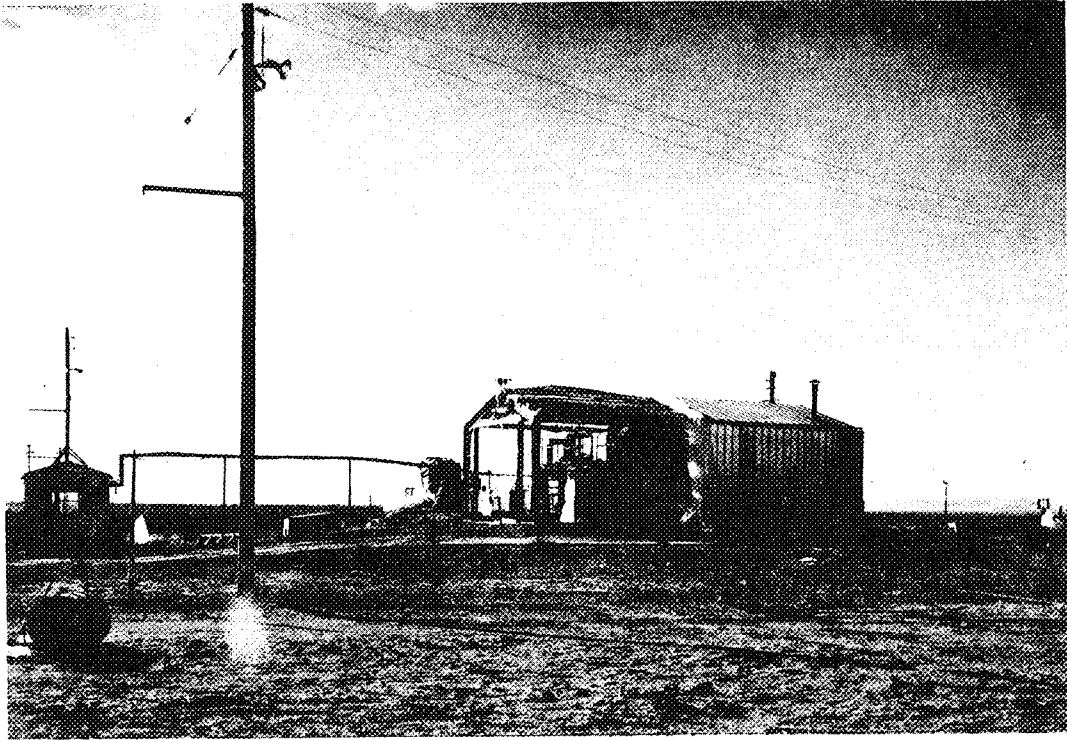
Fig. 32 Side view of reactor building showing bent roof purlin.
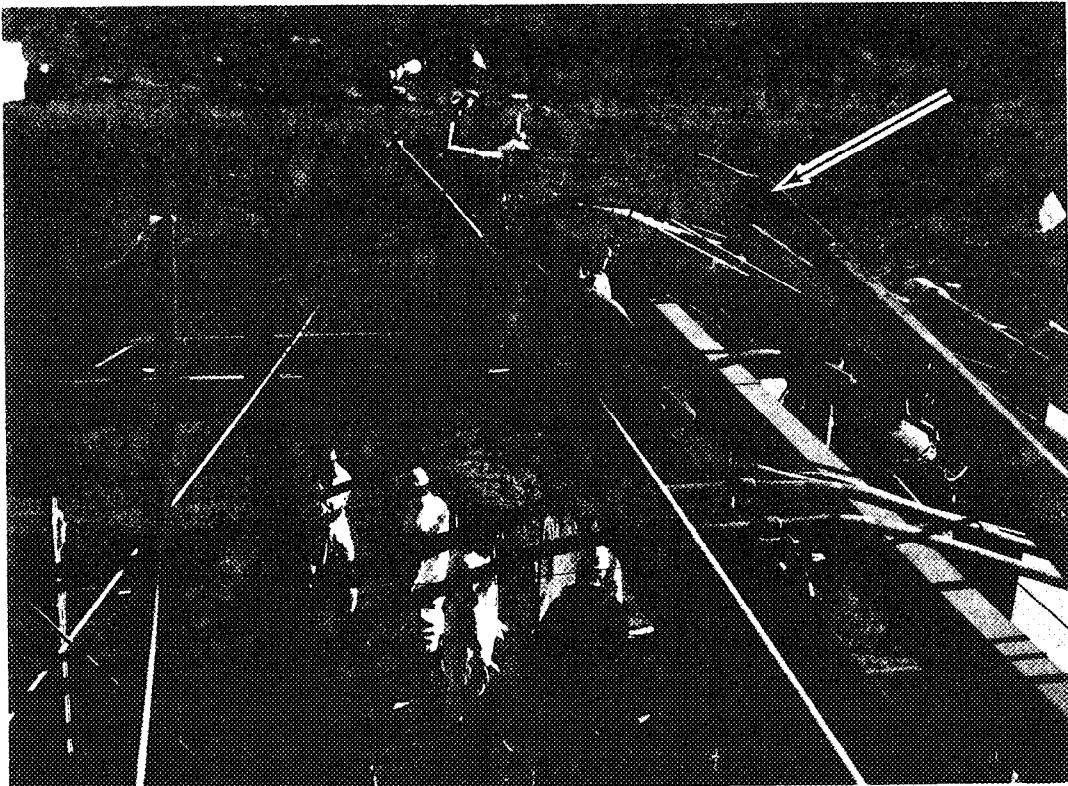
Fig. 33 Close view of bent roof purlin.

PERISCOPE

LOWER
BRIDGE

PRESSURE
TRANSDUCER
HARNESS

CONTROL
RODS

CORE
SUPPORT

FLOOD
LIGHTS
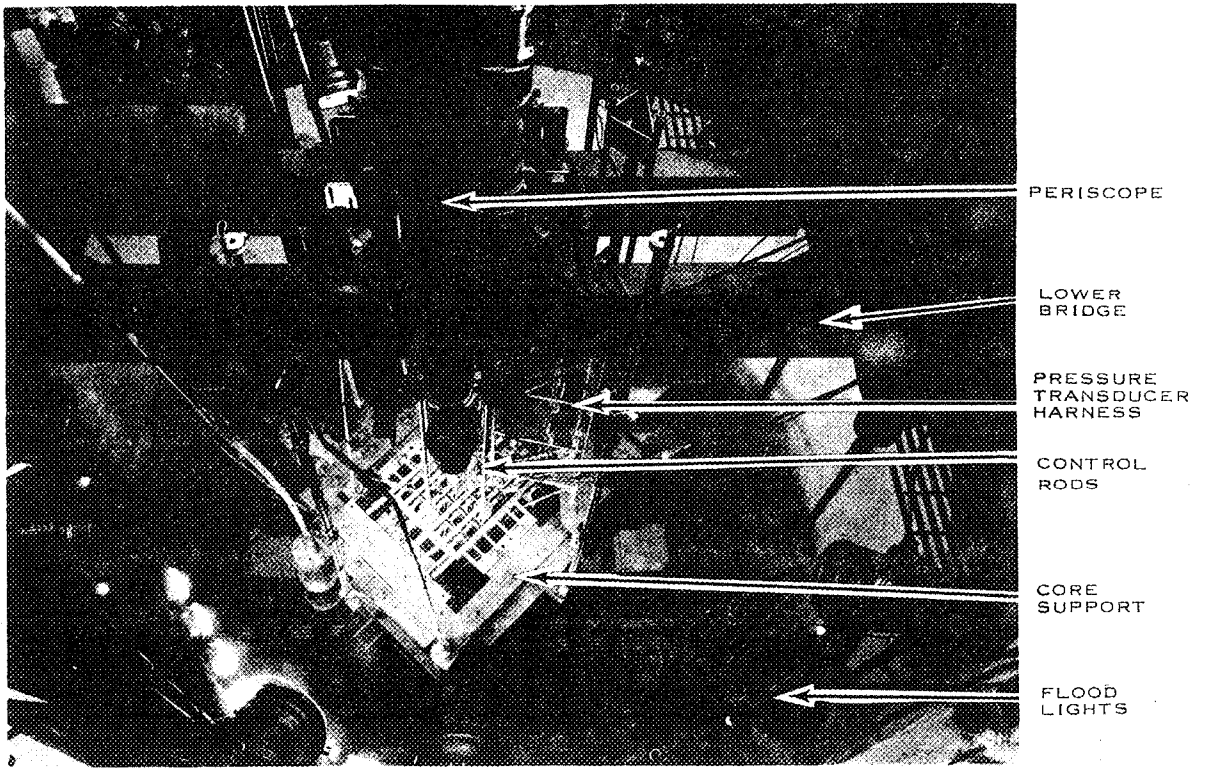
Fig. 34 View of reactor before destructive test.

TRANSIENT
ROD
BLADES

CONTROL
ROD
BLADES

CORE
SUPPORT
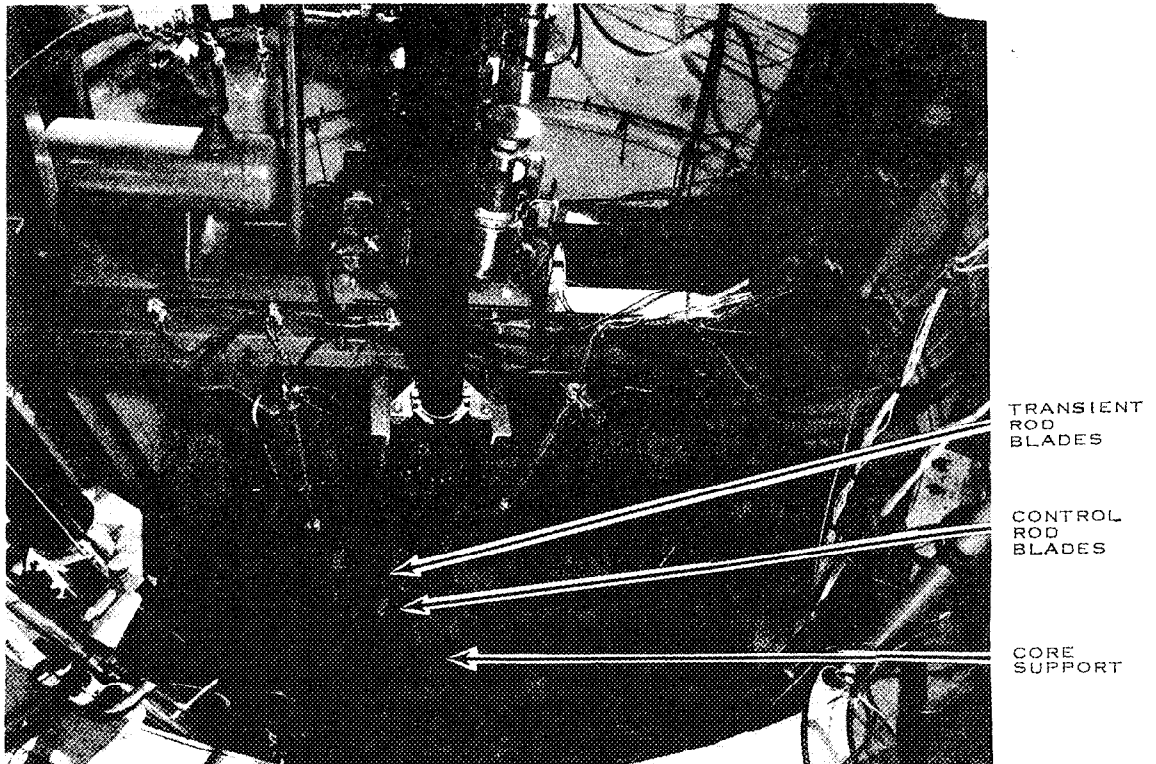
Fig. 35 View of reactor after destructive test.

TRANSIENT
ROD

CONTROL
ROD
BLADES

Fig. 36 Close view in vessel after destructive test.

TRANSIENT
ROD
BLADES

ION
CHAMBER
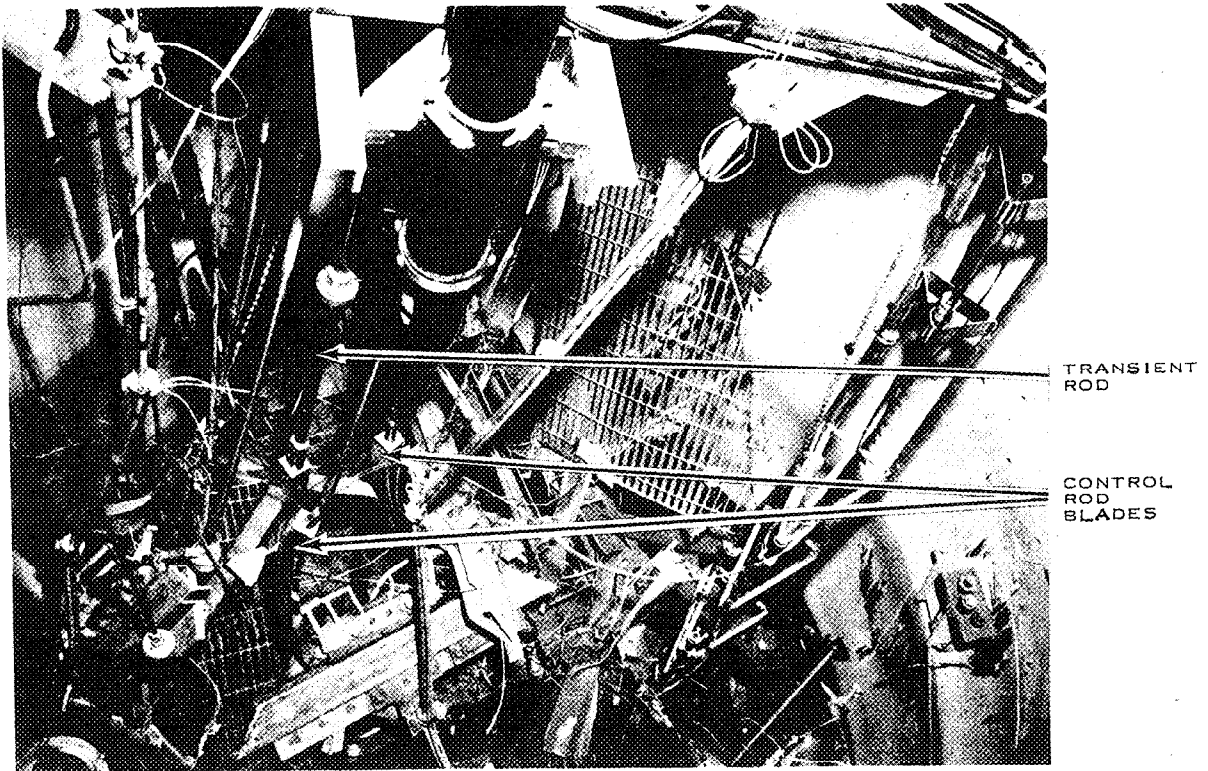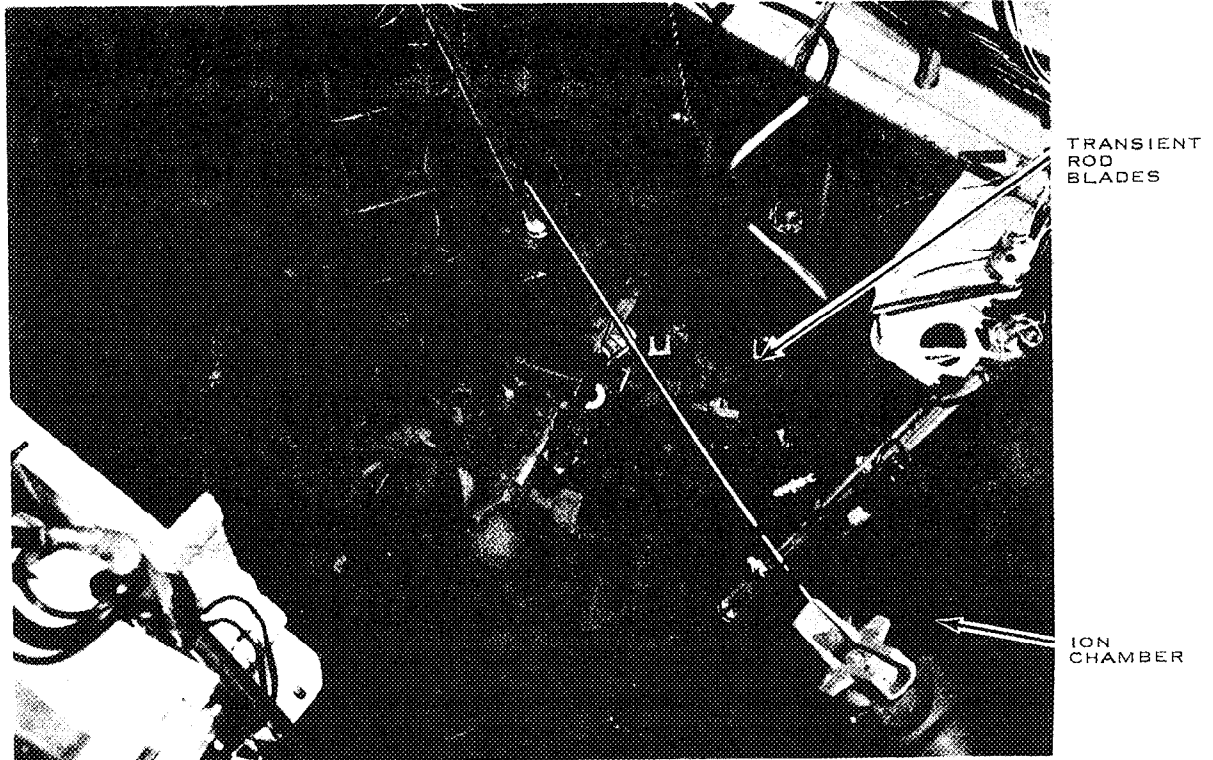
Fig. 37 Close view in vessel after destructive test.
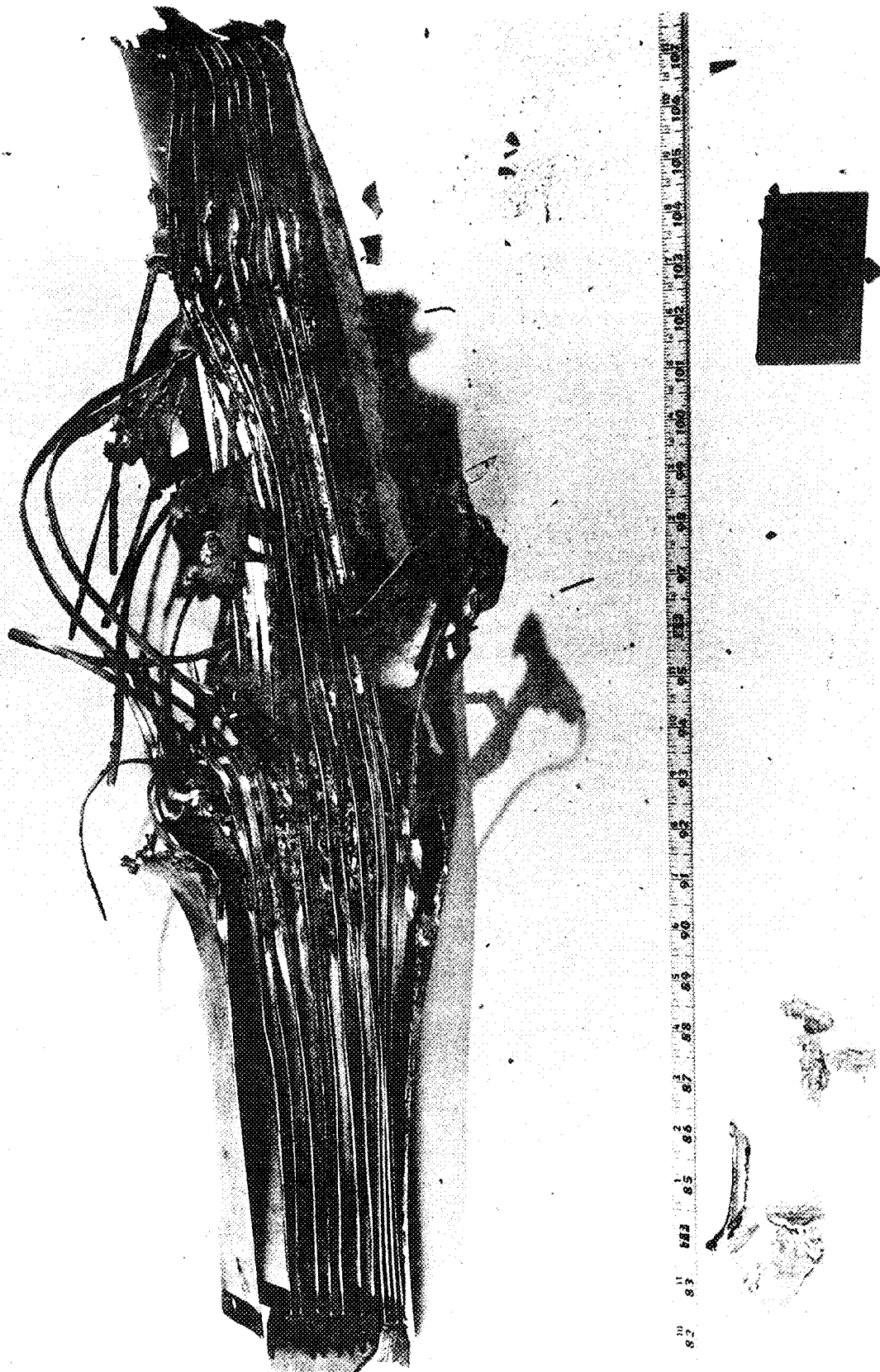
Fig. 38 Typical plates from peripheral assembly-edge view, position G6.

41
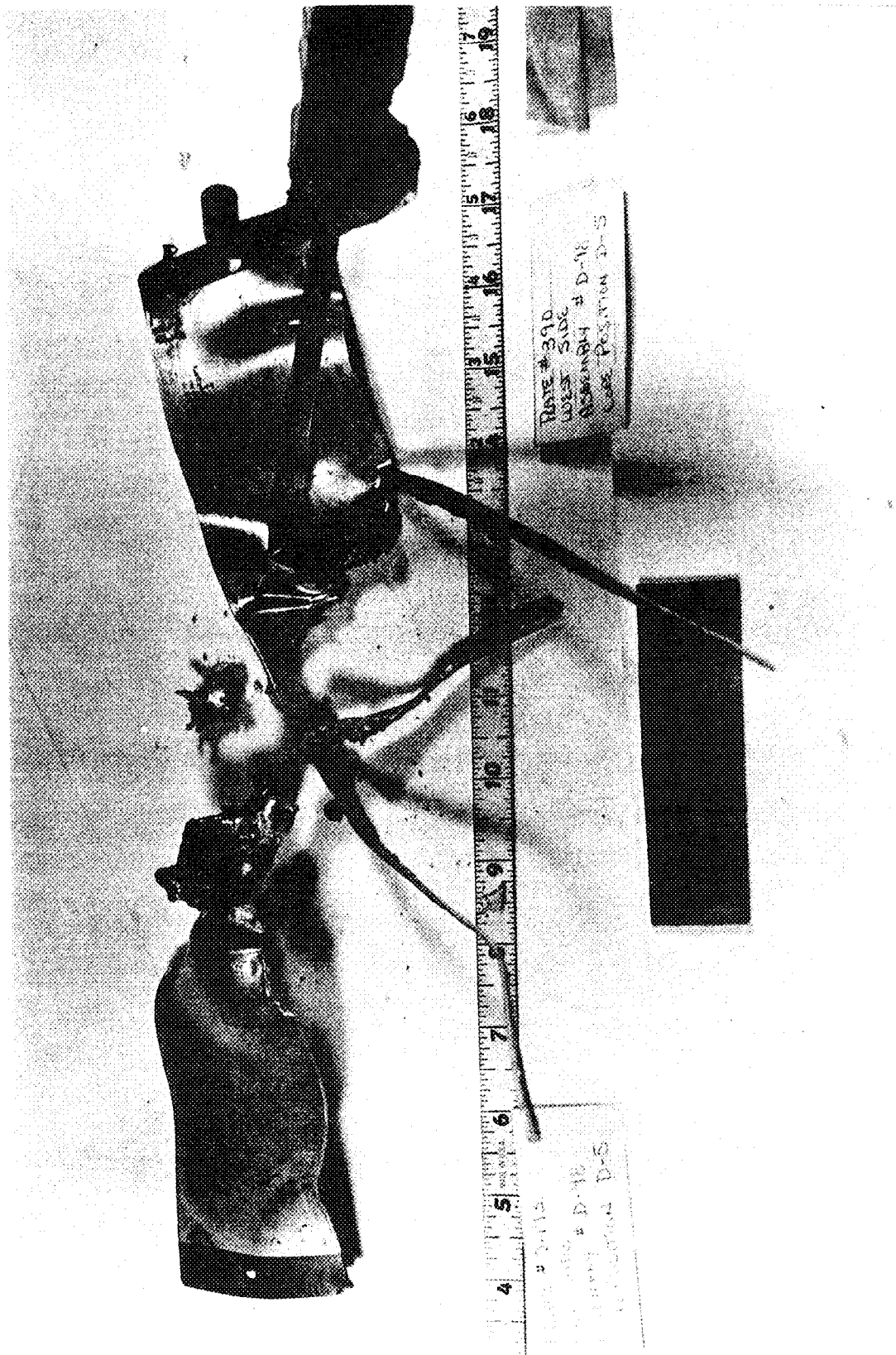
Fig. 39 Fuel plate end fragments from assembly D5.

2. TEST DATA

2.1 General Behavior

Data from the destructive test indicate clearly that the power excursion was essentially complete and the reactor in a typical post-burst shutdown condition at the time the explosion began. The power, shown in Figure 40, had completed a normal excursion, with a period of 3.2 msec and a peak of 2.3 GW. The total nuclear energy release was 31 MW-sec. The reactivity compensation as inferred from the burst shape reached about 6.5$ total compensation prior to the explosion. At the time of the first indication of the explosion, the power had declined to a level less than five percent of peak, and it is estimated that less than 0.6 MW-sec of nuclear energy was released in the remainder of this power excursion after the explosion began. In other words, the power excursion had released essentially all of the expected nuclear energy before the explosion.
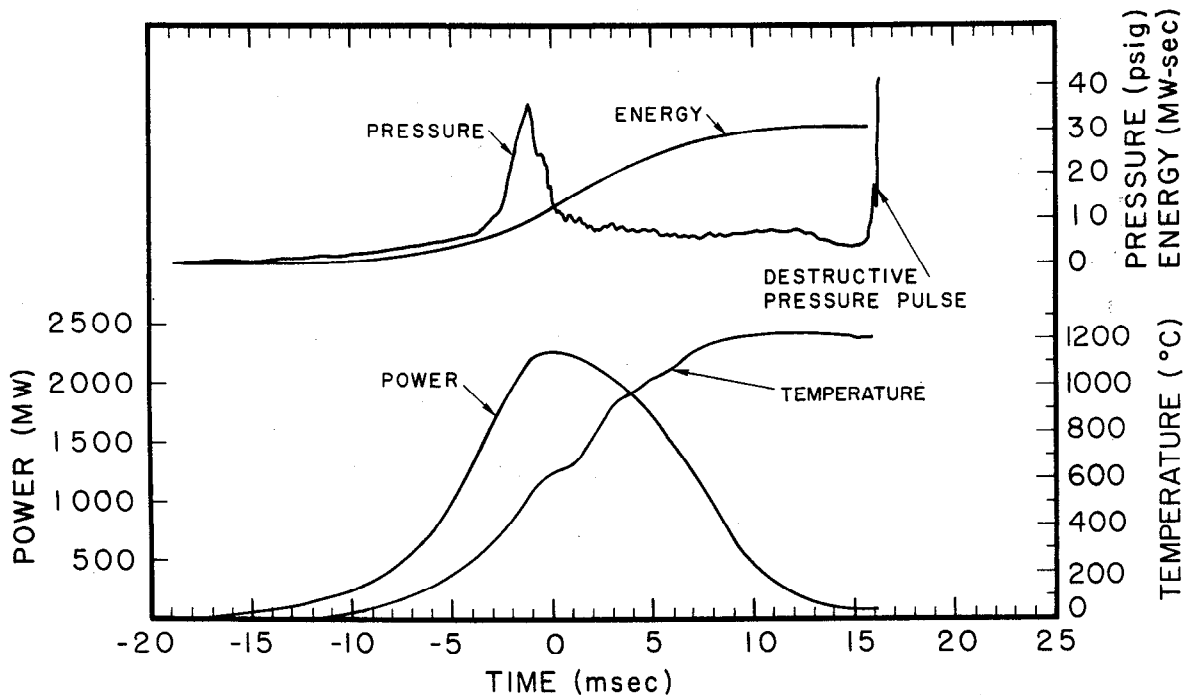
Fig. 40 Plot of data from Run 54, the destructive test.

This sequence of events, that is, a complete power excursion (including shutdown) taking place before the explosion, is in apparent contrast to the Borax-I destructive test. In the Borax test, the data do not permit a definite separation of the two events (in time) and seem to indicate the occurrence of some explosive effects even before peak power.

Since the nuclear energy release was nearly complete before the first indication of an explosion, the temperatures of the fuel plates very likely had reached their maxima and were beginning to decline. Measurements of fuel temperatures obtained from fuel capsules (Appendix B) which approximate actual fuel plate meat temperatures indicate that maximum temperatures were probably reached several milliseconds before the explosion (Figure 40). Con-

ventional thermocouples attached directly to the fuel plates near the core hot-spot, however, had either failed or were considered to be inaccurate at the above-melting temperatures attained.

Calculations of fuel plate temperature at the core hot-spot (see Reference 13 and Appendix F) indicate that maximum meat temperatures did not exceed 1400°C and that at the moment of the initial explosive pressure, fuel plate surface temperatures were probably near the melting point of aluminum (660°C).

The pressure trace shown in Figure 40 is typical of several traces obtained during the destructive test from low-range pressure transducers up to the time of the explosion. As with all previous pressure data, the pressure pulses appearing at about the time of peak power are associated with the onset of boiling in the core. Maximum shutdown (or boiling) pressure for this test (shown in Figure 11) was about 35 psig which constitutes a significant increase above the 9 psi pressure obtained from the 4.6-msec period test and which is slightly higher than predicted.

Additional plots of destructive test data are shown in Appendix C including temperature, pressure, strain, and power. Details of measurements of the total energy release, and maximum temperatures are given in Appendices B and F, respectively.

As a consequence of breakage and electrical shorting of many of the transducer cables during the explosion, the data recorded on oscillograph records (Figure 41) are extremely difficult to read. Most of the instrumentation which was located in and adjacent to the core was immediately destroyed by the explosion and produced erratic signals on the oscillograph record which tended to mask much of the remaining data.
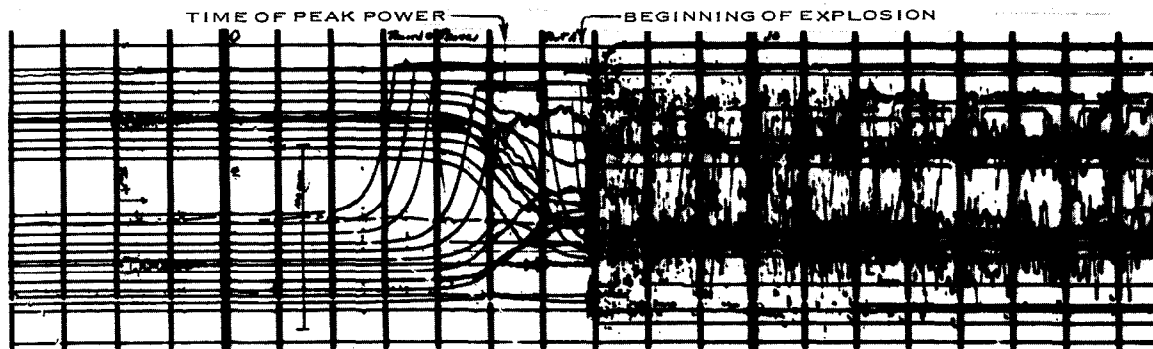
Fig. 41 One of four oscillograph records obtained during Run 54, the destructive test. The time elapse between vertical lines is 10 msec.

2.2 Discussion of the Destructive Pressure History

Detailed analysis of the oscillographic records has resulted in the conclusion that the initial rise of destructive pressure in the water near the core was extremely fast and probably was not recorded accurately due to the inadequate bandwidth of the recording galvanometers (nominally, 5 kc). The indicated rate of the pressure rise varies considerably from one transducer signal to another but the oscillograph trace which could be followed and measured with the greatest confidence (Figure 42) indicates that the pressure increased from zero to a first

44

peak of about 2800 psig in less than 300 μsec, with a rise time (ie, 10 to 90 percent) of about 150 μsec. Many other traces which could not be followed all the way to a first maximum also indicated rise times of 150 μsec and less: One pressure signal recorded on magnetic tape was observed to rise from 0 to 30 psig in about 20 μsec (close to the rise time limit of that system).

The 2800 psig maximum pressure recorded at the beginning of the explosion (Figure 42) is open to some question because of the difficulty in following the trace and because the pressure pulse itself apparently contained a broader

Fig. 42 Pressure recording obtained during Run 54, the destructive test. Dashed line indicates region in which original recording was too faint to follow with confidence.

frequency spectrum than the galvanometer was capable of recording. Data from several other transducers were not usable because of interference from other traces and also, more commonly, because of failure of the transducer. A single 100,000-psig range transducer, which did not fail, yielded a small amplitude signal which was difficult to measure accurately. Oscillations of this trace, both negative and positive, could be contained within an envelope of ± 3000 psig during the first two milliseconds of the pressure burst and within about ± 8000 psig for several more milliseconds before becoming quiescent.

At the onset of destructive pressures, nearly all of the low-range pressure transducers failed (as expected) usually within the first millisecond. The failure of some high-range transducers (ie, 0 to 10,000 psig), such as the one which provided the data shown in Figure 42, was unexpected since the pressures apparently did not exceed the rated range values of these transducers. Such failures, it has since been learned, are attributable to a characteristic of the strain-gauge type transducers which leads to fracture of the strain-gauge wires whenever the environmental pressure contains frequencies approaching (or above) the resonant frequency of the transducer, which in most cases was between 10 and 20 kc.

Although it was possible to establish that destructive pressures commenced to develop only after the nuclear excursion was essentially complete, ie, about 15 msec after peak power, it is not possible to deduce with certainty from any of the recorded data the exact nature of the pressure history after the pressure rise was initiated. For instance, there is no recorded evidence that the explosion consisted of just a single pressure pulse. In fact, preliminary studies based upon photographic measurements of the time and velocity of water ejected from the reactor vessel strongly suggest that a considerable fraction of the total pressure impulse occurred at a much later time, viz, more than 40 msec after peak power, such as might occur as a result of a series of pressure pulses covering a time span (from the first pulse to the last) of at least 25 msec or more.

It was possible to obtain additional data on the maximum pressure from an examination of damaged pressure transducers. Several of the pressure transducers used for the destructive test were of the diaphragm type rated for relatively low pressures (0 to 300 psig), and permanent deformation of the diaphragm occurred during the explosion. Laboratory studies of these transducers indicated
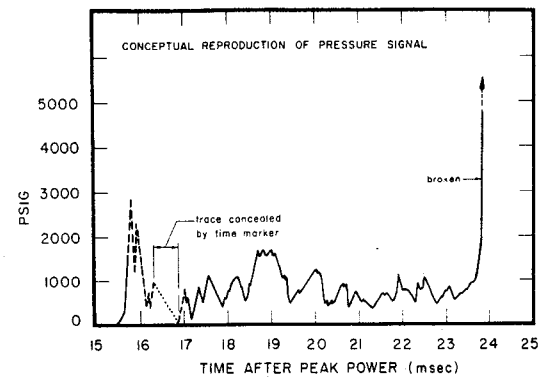
45

that such diaphragm deformations could be calibrated for both static and dynamic (or pulsed) pressure. Pulses with rise times as short as $100\,\mu\,sec$ were generated to establish the calibrations, and in Figure 43 the results are shown for a typical transducer rated at 0 to 300 psig.

From the calibration of Figure 43, and the deformations observed on six different transducers used during the destructive test, peak pressures were established for several points external to the core. These pressures together with the single recorded pressure of Figure 42 (at position No. 12) are shown on a schematic of the core in Figure 44.

Pressures of about 4000 psig are indicated at symmetrical positions 8 and 13, each about 10 inches from the sides of the core. Positions 3 and 4, respectively, 11 inches and 8 inches from the top and bottom of the core (on the Z-axis) also show similar pressures around 2500 psig. A higher, and seem-
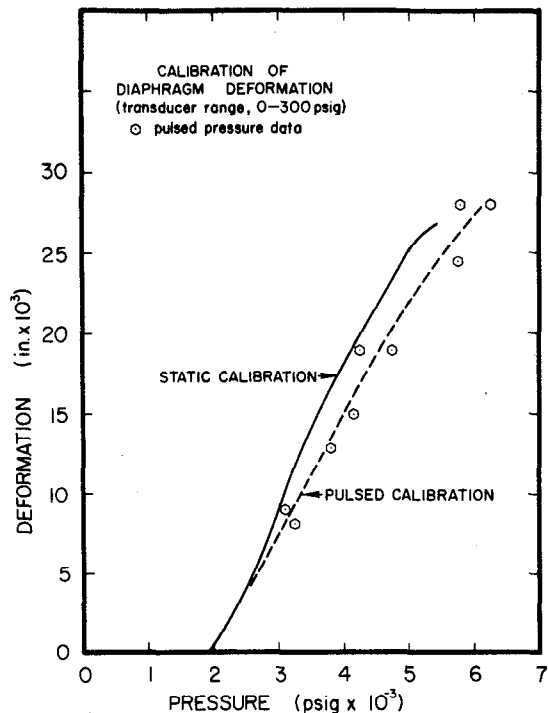
Fig. 43 Static and pulse calibration of permanent deformation of diaphragms of 0 - 300 psig range pressure transducers.

ingly anomalous, pressure at position 6 is attributed to reinforcement as a result of pressure reflection from the concrete floor of the vessel.

Studies of deformation also were made of the deformation of other selected items near the reactor, but these were generally inconclusive due to the complexities of geometry, materials, and pressure distribution. For the bulged vessel itself, yield pressure is about 140 psi but the actual pressure required to cause the vessel damage could not be computed due to the presence of the earth backing. Inside of the core, a crushed, air-filled tube indicates that pressures probably exceeded 3600 psig (Figure E-11).

2.3 Fisside Release

An array of air monitors had been placed on a grid system extending downwind of the reactor to measure the release of radioactive material from the reactor. Data obtained from these

Fig. 44 Map of peak pressures around core during destructive test. All pressures were obtained from measurement of deformed diaphragms except at position 12 which was obtained by recording. See Table B-II for actual locations.

46

samples are presented in Appendix G together with a description of the method used in computing the total release of fissides to the atmosphere. Based upon these calculations, (which use the $t^{-1.2}$ rule-of-thumb decay rate) it is estimated that about 2.4 x 10^5 curies were released to the atmosphere as a result of the destructive test. The fisside inventory of the core at the time of the release was almost totally due to the fissioning which took place during the power excursion with only a small contribution from the long-lived radioisotopes from previous tests. Using a value of the nuclear energy release of 31 MW-sec, it is estimated that the total fisside content of the core was 6 x 10^7 curies and that, therefore, this calculation indicates the fraction of this inventory which was released to the atmosphere to be of the order of 0.4 percent.

The fisside release calculation is severely limited in precision since only a few isotopes could be collected and corrected by decay back to the time of release. It appears that those isotopes which were collected were released as gases. No solid products were collected.

Improvements in the calculation of fisside release have been continued by the USAEC-ID Health and Safety Division. These calculations, which are still preliminary[a], take into account the specific decay schemes of the collected isotopes, Sr^{91}, Sr^{92}, and Ba^{139} as well as an improved computer calculation of the noble gas inventory of the core at the time of the release. It has been calculated on this basis that about 7 percent of the noble gases were released to the atmosphere. Since neither solid products nor radioiodines were found, it is, therefore, estimated that the fisside release consisted mainly of the noble gases and amounted to about 0.7 percent of the total fisside inventory.

Although radioiodines were not detected following the destructive test, it has been possible to calculate the maximum release of radioiodines which could have taken place undetected. By this approach, it has been established that less than 0.01 percent of the radioiodines were released to the atmosphere[a].

Most of the fisside release was swept out of the reactor building by the strong winds ($\approx$20 mph) which were blowing at the time so that contamination both in the building and on the ground downwind of the reactor was slight (ie, about 40/disintegrations/min/cm^2 on smears taken from the reactor floor about 20 hours after the test).

---

[a] These results were obtained by the USAEC-ID Health and Safety Division and communicated personally by W. P. Gammill of that Division. This information along with the data and calculations is expected to be published as an IDO report in the near future.

VI. ANALYSIS

1. METAL-WATER CHEMICAL REACTION

1.1 Chemical Analysis

Studies which have been carried out on the oxidation of molten aluminum in the presence of water indicate that this reaction can proceed at high rates with the release of a considerable amount of thermal energy. A review of some of these studies (References 14 through 21) was, therefore, made to help determine the feasibility of explaining the Spert I explosion on the basis of a rapidly reacting metal-water reaction.

For melted aluminum at about 660°C, this reaction takes the form:

$$2Al + 3H_2O \longrightarrow Al_2O_3 + 3H_2 + 4199 \text{ cal/g Al} \quad ,$$
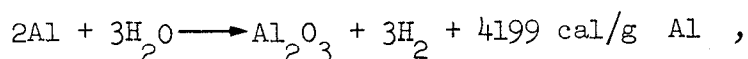
where the product oxide is usually in the form, α-Al$_2$O$_3$ (alpha alumina). Other reactions are possible which lead to forms of alumina other than the α-phase and to various hydrates of alumina; but the above reaction appears to be the principal reaction at elevated temperatures such as were obtained during the destructive test [22].

Normally, in laboratory tests a quantitative measure of the extent of the oxidation reaction is obtained from the hydrogen reaction product which is collected. Since this was not possible during the Spert destructive test, a chemical analysis of the destructive test core debris was made. This method is based on the assumption that the α-Al$_2$O$_3$ product is quantitative, and that the accuracy of measuring the amount of this product in the radioactive debris recovered from the reactor vessel is adequate.

The debris collected from the reactor vessel originally contained all sorts of "foreign" material including nuts, bolts, paint, glass, sand, etc, in addition to fragments of fuel plates and selective removal of these items was necessary before the samples could be chemically analyzed. All foreign materials large enough to be conveniently seen and grasped with handling tools were removed from the debris as were all intact portions of the fuel plates (Figure 39) since unmelted aluminum would not have contributed significantly to the reaction.

A total of about 22 kg of debris was collected, and, of this, six samples totaling about 1420 grams were chemically analyzed at the Idaho Chemical Processing Plant. In order to remove as much metal from the samples as possible and to increase the relative concentration of α-Al$_2$O$_3$, the samples were initially dissolved in HCL. Figure 45 outlines a complete typical analysis procedure. X-ray diffraction methods were used to detect and measure the alumina but, due to the presence of large quantities of ordinary sand in the x-ray samples, results were not precise.

Alpha-alumina was found separately in the form of small globules or spheres (the order of 0.004-inch diameter) and as incrustations upon aluminum metal

ORIGINAL SAMPLE 5629 grams

Screen	On Screen	Dissolve	Residue	X-Ray Diffraction	
#4 MESH SCREEN	96.3 grams ON SCREEN	DISSOLVE IN 6N HCL+H_2O_2	RESIDUE 2.99 grams	$<2\%$ α AL_2O_3 OR <0.06 grams	FUSED
#16 MESH SCREEN	179.4 grams ON SCREEN	DISSOLVE IN 6N HCL+H_2O_2	RESIDUE 26.59 grams	$<2\%$ α AL_2O_3 OR <0.53 grams	FUSED
#100 MESH SCREEN	206.6 grams ON SCREEN	DISSOLVE IN 6N HCL+H_2O_2	RESIDUE 38.88 grams	23% α AL_2O_3 OR 8.8 grams	FUSED
#200 MESH SCREEN	50.1 grams ON SCREEN	DISSOLVE IN 6N HCL+H_2O_2	RESIDUE 26.0 grams	7% α AL_2O_3 OR 1.82 grams	FUSED
PAN	30.5 grams ON PAN	DISSOLVE IN 6N HCL+H_2O_2	RESIDUE 19.5 grams	$<2\%$ α AL_2O_3 OR <0.4 grams	FUSED

SOLUTE → TOTAL SOLUTE ANALYZED FOR CONSTITUENTS

Fig. 45 Diagram of analysis and results of a typical sample of metallic debris collected from the Spert I vessel after Run 54.

fragments of all sizes. Many tiny globules and fragments were found in grab-samples of the debris. Analysis of individual globules in a Debye-Shirrer X-ray powder camera revealed that α-alumina was a principal constituent along with several other undetermined crystal components.

Prior to chemical analysis two large samples of debris collected from the floor of the vessel were screened in order to obtain an approximate size distribution of the particles. The results of this size fractioning are plotted in Figure 46. Mean particle diameters appear to be in the range of 600 to 800 microns. It should be noted that the data in Figure 46 were taken directly from the screenings and no interpretation is made as to effective spherical size or as to the amount of exposed surface area.

From this analysis, it was determined that α-alumina constituted between 1.6 and 2.0 percent by weight of the original cleaned samples of debris.
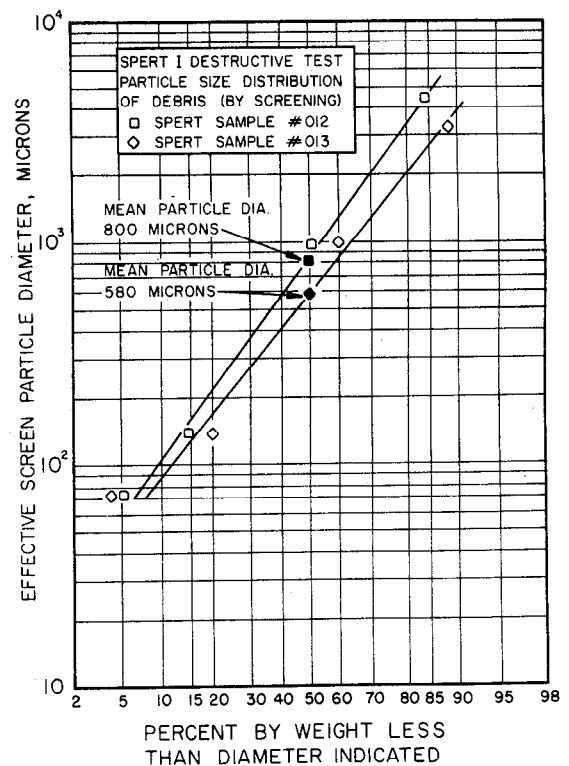
Fig. 46 Particle size distributions obtained from two samples of debris taken after the Spert Destructive Test.

Other constituents of the debris included aluminum 65 percent by weight, uranium 6.7 percent by weight, and the remainder consisting of sand, glass, etc.

Based upon an average content of 1.8 percent α-alumina in a total of 22 kg of debris, it appears that about 200 grams of aluminum metal (or 0.4 percent of the aluminum in the core) was consumed in the reaction releasing, as a consequence, about 4 MW-sec of energy.

1.2 Interpretation

From a review of the results of several studies of the chemical reaction kinetics, it is concluded that the chemical reaction between aluminum and water would not be explosive under the conditions which were attained in the Spert I reactor before the explosion. After initiation of the explosion, it appears that dispersion of the molten fraction of the core could have produced conditions conducive to a rapid metal-water reaction, although, even under these conditions there is little experimental evidence to indicate explosive reactions.

Higgins and Schultz [17] report that the chemical "reactivity" of aluminum is nil at temperatures up to 1170°C, but that aluminum becomes more reactive at temperatures above 1170°C. The completion fraction depends importantly upon the particle size, becoming greater with small particles. It was found by Higgins and Schultz that as a result of dispersing molten metal into water to produce fine particles, pressure pulses were generated which were due primarily to the libration of hot hydrogen gas, and that the rise time of the pressure pulses were sufficiently long that the metal-water reaction could be separated from the domain of "high order explosions". In two samples given [17] with metal temperatures of 1399 and 2021°C, the pressure pulses required 15 msec and 10 msec, respectively, to attain peak magnitude (73 psia and 191 psia, respectively). These results are in contrast with the Spert destructive test results which, although starting from a condition of somewhat intact, fuel plates apparently attained several thousand psig pressures in a fraction of a millisecond.

Extensive research done more recently both in-pile and out-of-pile at ANL also has failed to produce pressure pulses with the rise times required to explain the initiation of the Spert I explosion. Nor did an additional and specific test, in which sections of a Spert D-core fuel plate were subjected to ANL fast heating tests in the TREAT reactor, give any indication of an explosive reaction [15, 16].

The ANL tests have shown that aluminum reacts slowly up to temperatures around 1750°C and that above these temperatures the reaction rate increases but still is not "explosive". The reaction rate is apparently controlled by incrustations of oxide on the metal surfaces, and it appears that explosive rates of reaction are possible only if the metal is first finely divided.

It has been concluded, therefore, that the initial short rise-time pressure pulse of the Spert I explosion probably was not the result of a metal-water reaction. However, the chemical reaction very likely did proceed rapidly after initial deflagration of the core, and contribute energy to the explosion. For a metal-water chemical reaction to have initiated the Spert explosion would have apparently required first that the core be finely and violently fragmented, a condition which is tantamount to requiring another explosion of a different source to occur first.

50

2. CONDITION OF THE CORE AT THE TIME OF THE EXPLOSION

From the data of previous transient tests in which core damage was confined to thermal distortion and limited melting, it is possible to construct a model of the core conditions which probably existed to some degree in the few milliseconds just prior to the explosion. This is shown as the following sequence of events:

(1) During the early part of the power excursion, fuel plate temperatures increased exponentially to the boiling point of water and above;

(2) Nucleate boiling began and produced a pressure pulse which was measured outside of the core at about 35 psi;

(3) Nucleate boiling next subsided to film boiling as fuel plate surface temperatures exceeded about 200°C;

(4) After vapor blanketing was established, the fuel plate temperature increased rapidly but was probably arrested or even reversed occasionally by momentary collapse of the steam layer. Collapse of the void is postulated to be the result of a water hammer effect as water returned to the core after being accelerated out of the core by initial void growth;

(5) While still below melting temperature, the fuel plates deformed into typical configurations (Figures 24 through 28) and met opposing fuel plates in the water channel. Such behavior is expected to create multiple channel blockages, entrapments of steam and water, and additional momentary collapse of voids;

(6) Subsequent to thermal distortion, molten fuel escaped through cracks in the unmelted clad.

This sequence of events, although not directly observed during the destructive test, is consistent with many other observations of kinetic boiling behavior and fits the progressive nature of fuel plate damage observed in longer period tests. It also establishes the core in the condition which most probably existed at the time that the specific phenomena -- causitive to the explosion began to occur.

The intimacy of melted and nearly melted aluminum with water trapped in warped water channels and with water which has effected void collapse appears to approximate conditions described by Long [23] which are conducive to "steam explosions". After producing and studying many steam explosions, Long states that ". . . violent explosions occur when a thin layer of water is trapped under a sudden rush of molten metal . . .". In his study, designed to duplicate industrial metal spills, the "sudden rush" of metal is a description of the experimental method used.

As a consequence, then, of the rapidity of melting, warping, and void collapse in the destructive test and the resulting potential for generation of superheated water in contact with hot fuel, the "steam explosion" hypothesis is readily admissable as an explanation of the origin and perhaps also the development of the Spert I explosion.

VII. CONCLUSIONS

Having described in some detail the objectives, observations, and studies of this destructive testing program with a plate-type core, an attempt is made here to summarize the various results, conclusions, and implications. In general, many of the results have been essentially equated to types of damage observed and are presented here in order of increasing severity of the test from which they were derived.

In the period region around 10 msec and less, thermal distortion of fuel plates was the principal type of damage. This damage, arising from large thermal gradients generated within the fuel plates, was characterized by bowing, rippling, and clad failure and eventually led to channel blockage when adjacent plates touched and fused together in the water channels. Such distortions are concluded to be the result of an expanding meat section of the fuel plates which is constrained by the colder cladding, by the unfueled edge strips which remain relatively cold, and by binding of the fuel plate edges in the assembly side plates. In conventional assembly construction this situation is further aggravated since the fuel plates are welded in place, to a nonfuel bearing assembly side plate.

The occurrence of melting in the D-core was first seen as a result of a 5.0-msec period test, in which melting affected about 160 inch^2 of the fuel plate surfaces. For the 4.6-msec period test, melting affected over 600 inch^2 of fuel plate surface. The nature of the melting in both tests indicates that the flow of molten fuel does not occur very rapidly; ie, there is no evidence that the fuel is expelled from the plate under any pressure, such as might be anticipated to arise from high internal stresses. Melted portions of the fuel remained with the plates themselves. There were no fragments of fuel found separated from fuel plates. The transient pressures measured during these tests give no indication of any increase with the occurrence of melting and thus substantiate the conclusion that the simple fact of fuel plate melting does not of itself constitute a sufficient condition for the generation of destructive pressures.

Both of the aforementioned damage responses, ie, thermal distortion and melting, were superimposed for periods of 5 msec and less and led to the touching and fusing-together of adjacent plates. The mechanism whereby fuel plates fuse together appears to be one in which warping first causes the fuel plate to rapidly extend far out into a water channel where it touches another plate. Melting, which occurs subsequent to the warping, then fuses the plates together. Since warping is expected to take place only during the short interval of time in which the temperature is increasing above about 100°C but still below the melting point at 640°C, it is reasonable to expect that the warping process was very rapid during the 3.2-msec period test, and that the entrapment of water and steam between plates is a likely consequence of this process.

During the 3.2-msec period test, a violent explosion occurred immediately after the power excursion. In this test complete fuel plate melting is estimated to have occurred in approximately 8 percent of the core and partial (ie, internal fuel) melting in about 35 percent of the core (ie, approximately 12×10^3 inch^2 of fuel plate area). Little recorded information is available about the nature of the explosion which destroyed the core after this melting; however, a number of postulates have been advanced and there is a significant amount of indirect

information to support the hypothesis of a steam explosion resulting from a momentary superheating of water.

Of major significance from this 3.2 msec test is the observation that, prior to the initiation of the destructive pressure burst, which occurred 15 msec after the power-peak, the reactor underwent a complete self-limiting power excursion with burst parameters systematically predictable from longer period tests. It should be further noted that the reactor evidenced no difficulty in effecting self-shutdown for such short periods (reactivity insertions as large as 3.5$).

The maximum reactivity compensation data obtained during several of the shortest period excursions indicate that, for this core, rapid compensations in excess of 6$ are possible from thermal and boiling shutdown mechanisms. However, a tendency toward the production of high superheats and consequent pressures at the onset of boiling during such excursions and an apparent depression of the void growth rate during the initial steam formation may lead to an unpredictable increase in energy release and to core damage at periods shorter than those tested, ie, periods less than 3.2 msec.

It should be further noted that since the explosion occurred at a time after nuclear shutdown was complete and when the power, the reactivity, and fuel plate temperatures were all decreasing, conditions leading to the explosion do not appear to be directly a consequence of the excess reactivity, the period, or the shutdown process, except insofar as these factors determine the energy release. In other words, the major differences of initial core conditions between the 3.2-msec period destructive test and, say, the 4.6-msec period test lie in the domain of energy release effects such as maximum temperature and degree of melting.

The time at which the Spert I explosion took place (about 15 msec after peak power) may be a consequence both of the internal fuel plate temperatures and the rate of heat transfer from the meat to fuel plate surfaces. Calculations of fuel plate temperature distributions [13] indicate that fuel plate surfaces at the core hot spot may have been passing through the melting temperature at the time of the explosion. Centerline meat temperatures at the core hot spot possibly reached 1400°C maxima but are calculated to have decreased to about 1000°C at the time of the explosion. Thus, it is expected that during a shorter period power excursion with a consequent increase in the amount of energy released, complete fuel plate melting would occur earlier, and possibly, even before nuclear shutdown was complete.

An analysis was conducted to determine the extent of a possible metal-water chemical reaction, and it was determined that approximately 4 MW-sec of energy may have been released in this process. However an evaluation of the results, in the light of the pressure and temperature conditions obtained in the reactor during the 3.2-msec period test and those used in out-of-pile studies of this chemical reaction, indicates that the chemical reaction was not responsible for initiating the observed explosion. The reaction rates required to support such a postulate and the temperatures obtained in the test are not consistent with current experimental information on the kinetics of the chemical reaction. In fact, it is necessary to postulate a separate explosion or trigger mechanism to even establish the necessary condition for the high rates of the metal-water reaction itself. It is, therefore, concluded that the observed metal-water reaction (amounting to the consumption of roughly 200 grams of

aluminum) was a "side reaction" which proceeded as a consequence of the explosion, and added energy to it.

Another significant result of the destructive test concerns the release of fissides to the atmosphere resulting from melting and violent dispersal of the core. It has been calculated that about 0.7 percent of the total core inventory was released to the atmosphere in the form of noble gases. Solids were not detected in the atmosphere. Radioiodines also were not detected and, as a consequence, less than 0.01 percent of the iodines are calculated to have been released.

The conclusions which have been drawn here regarding the explosion in the Spert I reactor and regarding the conditions which existed in the core prior to the explosion may bear significance in the analysis of the two other cases of reactor explosions, the Borax test explosion in 1954, and the accidental SL-1 explosion in 1961. In all three reactors, the materials and geometries of of the cores were similar (ie, low-melting point (aluminum) metal in plate-type water moderated systems), and the energy release in each case was sufficient to induce melting, and, a prior, severe warping of the plates.

Thermal warpage in both Borax and SL-1 cores probably was sufficient to cause adjacent fuel plates to touch each other. In the Spert core, ripple amplitudes greater than 0.22 inch have been observed (following a nonexplosive, 4.6-msec period test) whereas the water channel thickness was only 0.18 inch. There is a distinct possibility then that warping in the Borax core could have been sufficient to span the 0.117-inch plate spacing and cause adjacent fuel plates to touch, even though a stiffener plate was used in that core which reduced the effective fuel plate width to about half of the nominal 2.8-inch-wide plate in Spert I.

Plate and channel dimensions in the SL-1 core were considerably different from either Spert I and Borax but, there again, it seems that touching of plates is highly probable in any excursion attaining temperatures at or near melting. SL-1 plates had a free width of 3.5 inches, and the coolant channel thickness was 0.310 inch. If the Spert I ripple amplitude mentioned above is scaled-up by the ratio of plate widths, then amplitudes of deformation in SL-1 of about 0.275 inch can be expected which are considerably in excess of the half-channel thickness.

As was noted above, the increased energy expected at shorter reactor periods would be expected to result in melting of fuel earlier in the excursion possibly before nuclear shutdown was complete or even during the power rise, a situation which may have been evidenced in the Borax test.

Also with regard to the Borax test, it should be noted that the pressures derived from the momentary superheating of water prior to the onset of boiling may have played an important role in initiating that explosion. If the Borax explosion occurred around the time of peak power, then shutdown pressures associated with initial boiling of the moderator in colder fractions of the core could still have been occurring at the beginning of the explosion. Thus, the need for a separate triggering mechanism is not nearly as evident in the Borax test as it appears to be in the Spert I test. Shutdown pressures in a 2.6-msec period power excursion may be sufficient to initiate dispersion of melted fuel plates.

One implication of the Spert I test results arises from the fact that in the Spert I core, as with Borax and SL-1, each assembly (consisting of 12 fuel plates) was separated from adjacent assemblies by the unheated assembly walls which remain cold and, therefore, strong and rigid during each test. Thus, it is reasonable that only one assembly need be considered in formulating a model for a triggering mechanism (recognizing that pressure disturbances may "couple" more than one assembly). Also it was noted that the center assembly which had the highest fuel plate temperatures also produced the highest pressures, and also may have been the source of the initiation of the explosion. Because of the placement of the transient rod blades, the largest group of fuel plates in this assembly is four plates. Thus, the very distinct possibility of being able to conduct meaningful investigations of the nature of the initiation of the explosion in small scale mechanism experiments is evident.

The possibility that only a small number of fuel plates may have been responsible for initiating the Spert I explosion combined with the fact that the explosion does not appear to be involved in any aspect of integral core kinetics (ie, shutdown behavior, etc) points out the possibility of performing other tests in small sub-assemblies, possibly even with nonnuclear heat.

Another conclusion resulting from the Spert I destructive test is again based upon the yet unproved assumption that melted fuel plates are essential to produce the explosion. That is, it appears that the use of higher melting point metals for fuel plate cladding (ie, zirconium- stainless-steel, etc) would be effective in reducing the probability of either a steam explosion or a metal-water chemical reaction simply because of the higher melting temperatures (provided of course, that other effects of these materials such as lower heat conductivity and thinner cladding thicknesses do not abrogate the advantage of a higher melting point).

Some advantage also may be obtained with aluminum by using an alloy which is less susceptible to hot-short cracking than is the 6061 alloy used here. In most of the very short period tests, clad cracking was extensive and contributed to the early release of molten fuel even though the clad surface was not itself melted.

With regard to creating conditions within the core which deter or prevent an explosion, the relative merits of fuel plates which are constructed either "thick" or "thin", or with either thick cladding or thin cladding are not certain. A core consisting of plates with thick cladding, for instance, will have a higher heat capacity and will be able to sustain excursions with greater energy release; however, it appears that the thicker clad also may delay the onset of boiling and the completion of nuclear shutdown with the result that a higher energy release necessarily takes place. It also is possible that the reduced flexibility of thick plates would lead to cracking and rupture earlier in a transient than their thin counterparts.

Finally, it is felt that a significant volume of information has been added to the study of plate core reactor kinetics as a result of this program and that the justification of pursuing the investigation of the many facets of the destructive test in subassembly test programs has been more firmly established.

VIII. REFERENCES

1. T. F. Wimett et al, Time Behavior of Godiva Through Prompt Critical, LA-2029 (April 1956).

2. J. R. Dietrich, Experimental Investigation of the Self-Limitation of Power During Reactivity Transients in a Subcooled, Water-Moderated Reactor. Borax-I Experiments, ANL-5323 (March 1957).

3. A. H. Spano and R. W. Miller, Spert I Destructive Test Program Safety Analysis Report, IDO-16790 (June 1962).

4. R. W. Garner, An Analysis of Nonboiling Reactivity Feedback Mechanisms in Pressurized Power Excursions in the Spert III Reactor, IDO-16819 (January 1963).

5. G. O. Bright (ed.), Quarterly Progress Report - October, November, December, 1957, IDO-16437 (March 1958) p 58.

6. R. W. Miller, "An Experimental Study of Transient Boiling During Spert I Power Excursions", Trans. Am. Nucl. Soc., 4, 69-70, June 1960.

7. R. W. Miller, Calculations of Reactivity Behavior During Spert I Transients, IDO-16317 (June 1957).

8. F. L. Bentzen (ed.), Quarterly Progress Report - October, November, December, 1959, Reactor Projects Branch, IDO-16537 (September 1958) pp 52-61.

9. G. F. Brockett and E. Feinauer, Summary Data Report for Spert Transient Pressure Measurements in the Interval 1955-1961, IDO-16930 (April 1964).

10. J. Dugone and L. L. Wieland, Fuel Plate Experience During Spert I Destructive Test Series with an Aluminum-Clad Plate-Type Core, IDO-16885 (July 1963).

11. Final Report of SL-1 Recovery Operation, May 1961 through July 1962, IDO-19311 (July 1962).

12. J. F. Kunz (ed.), Additional Analysis of the SL-1 Excursion, IDO-19313 (November 1962).

13. J. E. Houghtaling, Alain Sola, and A. H. Spano, Transient Temperature Distributions in the Spert I D-12/25 Fuel Plates During Short-Period Power Excursions, IDO-16884 (June 1964).

14. R. C. Liimatainen et al, Studies of Metal-Water Reactions at High Temperatures II. Treat Experiments: Status Report on Results with Aluminum, Stainless Steel-304, Uranium, and Zircaloy-2, ANL-6250 (January 1962).

15. Reactor Development Program Progress Report, ANL-6658 (November 1962) p 68.

16. R. O. Ivins, "A Study of the Reaction of Aluminum/Uranium Alloy Fuel Plates with Water Initiated by a Destructive Reactor Transient", Trans. Am. Nucl. Soc., 6, 101-102, June 1963.

17. H. M. Higgins and R. D. Schultz, The Reaction of Metals with Water and Oxidizing Gases at High Temperatures, IDO-28000 (April 1957).

18. W. F. Zelezny, Metal-Water Reactions: Rates of Reaction of Aluminum and Aluminum-Uranium Alloys with Water Vapor at Elevated Temperatures, IDO-16629 (November 1960).

19. L. F. Epstein, "Correlation and Prediction of Explosive Metal-Water Reaction Temperatures", Nucl. Sci. Eng., 10, 247-253, July 1961.

20. H. M. Saltsburg, Metal-Water Reactions, KAPL-1495, April 1956.

21. S. C. Furman, Metal-Water Reactions: V. The Kinetics of Metal-Water Reactions-Low Pressure Studies, GEAP-3208, July 1959.

22. R. O. Ivins and L. Baker, Argonne National Laboratory, Personal Communications.

23. G. Long, "Explosions of Molten-Aluminum in Water -- Cause and Prevention", Metal Progress, 71, 107-112, May 1957.

24. F. de Hoffman, Intensity Fluctuations of a Neutron Chain Reactor, MDDC-382, October 1946.

25. F. Schroeder (ed.), Quarterly Technical Report, Spert Project, January - March, 1962, IDO-16788 (August 1962) pp 5-9.

26. R. L. Johnson, A Statistical Determination of the Reduced Prompt Neutron Generation Time, Λ/β, in the Spert IV Reactor, IDO-16903 (July 1963).

27. M. R. Zeissler, Non-Destructive and Destructive Transient Tests of the Spert I D, Fully Enriched, Aluminum-Plate-Type Core: Data Summary Report, IDO-16886 (November 1963).

28. U. S. Weather Bureau, Meteorology and Atomic Energy, AECU-3066, July 1955.

29. C. A. Hawley, Jr., et al, "Radiological Data from the Destructive Test", Trans. Am. Nucl. Soc., 6, 139-140, June 1963.

APPENDIX A

START-UP AND STATIC EXPERIMENTS

APPENDIX A

START-UP AND STATIC EXPERIMENTS

1. INITIAL CORE LOADING

Initial loading of the D core began on March 3, 1962, and an initial critical loading was achieved with 20 fuel assemblies and the control rods withdrawn 17.95 inches on March 5, 1962. The associated critical mass was approximately 2.8 kg of U-235. Loading then proceeded until an operational core consisting of 25 assemblies containing 3.8 kg of U-235 was achieved on March 6, 1962. The reactor was critical at ambient temperature with the control rods withdrawn 9.20 inches. The available excess reactivity of the core was determined to be ≈8.2$ and the shutdown reactivity margin to be ≈ 4.4$; these were considered adequate for the proposed test program.

2. ROD CALIBRATIONS

2.1 Control Rod

The differential reactivity worth of the control rods over the range of rod travel from the critical position to the fully-withdrawn position was measured by the reactor period method. Both boric acid solution and transient rod poison insertion were used as reactivity shims to permit measurements of reactor period over the range of control rod travel.

Differential and integral reactivity worths of the control rods are shown in Figure A-1. Scatter in the differential reactivity worth data is attributed to uncertainties of + 0.02 inch in the rod position increment and to possible inhomogeneity in the concentration of the boric acid solution used to shim the reactivity. The integral curve indicates an available excess reactivity of 8.2$, which, if inserted as a step, would result in about a 1-msec period power excursion.

A shutdown reactivity of 4.4$ was inferred from integration of a linear extrapolation of the differential rod worth curve from 9.20 inches to zero inches withdrawn.

2.2 Transient Rod

Reactivity worth of the transient rod was determined by intercalibration with the control rods, and the integral transient rod reactivity worth is shown in Figure A-2. The total worth of the transient rod was 7.1$, which indicated that the minimum period possible for test purposes was about 1.3 msec, based upon a measured reduced prompt neutron lifetime of 8.2 msec.
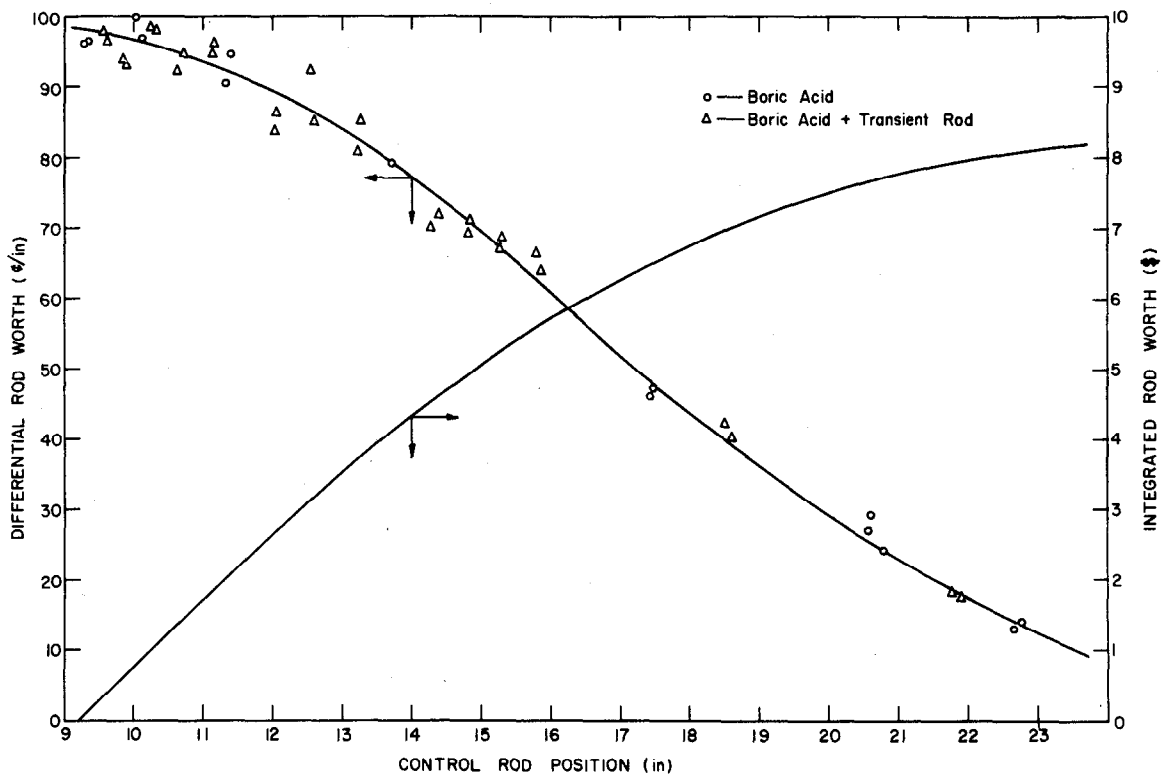
Fig. A-1 Differential and integral control rod calibration curves.
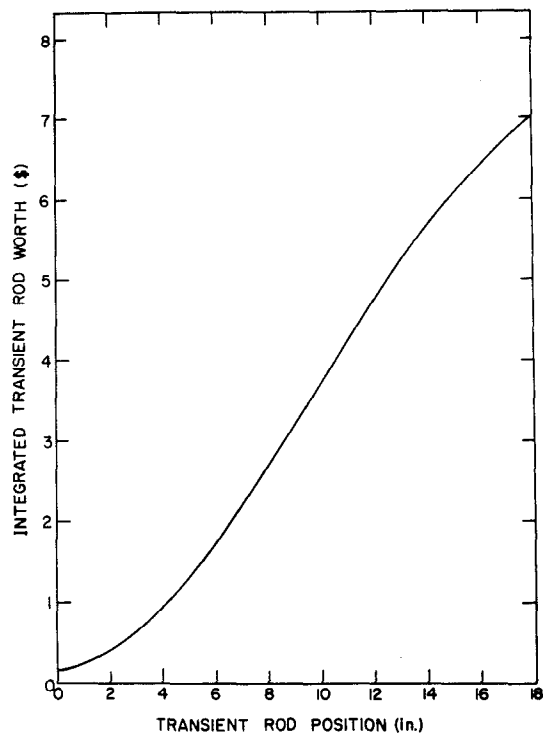
Fig. A-2 Integral transient rod calibration curve.

3. VOID COEFFICIENT

Void coefficient measurements were made for uniformly distributed voids in the core and for voids distributed at various axial positions in the central region of the core. The influence of a change in the volume of the void in the peripheral regions of the core on the value of the central void coefficient also was studied.

3.1 Uniform Void Coefficient

The measurement of the uniform void coefficient was performed by inserting 30-inch long by 0.610-inch wide by 0.159-inch thick magnesium strips in alternate channels of each non-rodded fuel assembly to simulate a uniform distribution of voids throughout the core. The lateral positions of the magnesium strips in the channels were staggered to reduce interaction. Following the determination of the critical position of the control rods with all the strips in place,

selected strips were removed, a new critical position established, etc, until all the strips were removed from the core. Reactivity loss for each set of strips removed was obtained from the change in the calibrated control rod positions. The void coefficient was calculated by correcting the reactivity effect for neutron absorption by the magnesium and by considering only the magnesium within the active length of the fuel assembles as a void. No correction was made for neutron scattering. Results of these measurements, shown in Figure A-3, indicate a value for the coefficient of 36¢/% decrease in moderator density (or -0.067¢/cm^3 of water removed).

3.2 Central Void Coefficient

Central void coefficient measurements were performed by use of 4-inch long by 0.610-inch wide by 0.157-inch thick magnesium strips located in the central region of the core. Each strip was attached to the transient rod drive mechanism to enable remote vertical positioning of the voids. The vertical profile of the void coefficient was obtained from the control rod worth by determining the critical rod position as a function of void position. The results of this measurement are shown in Figure A-4. The peak of the local void worth curve occurs at a void position of about 8.5 inches above the bottom of the fuel. The maximum central void coefficient was about -84¢/% decrease in moderator density (or -0.16¢/cm^3 of water removed). This coefficient was determined to be independent of void volume for void volumes as large as 370 cm^3.
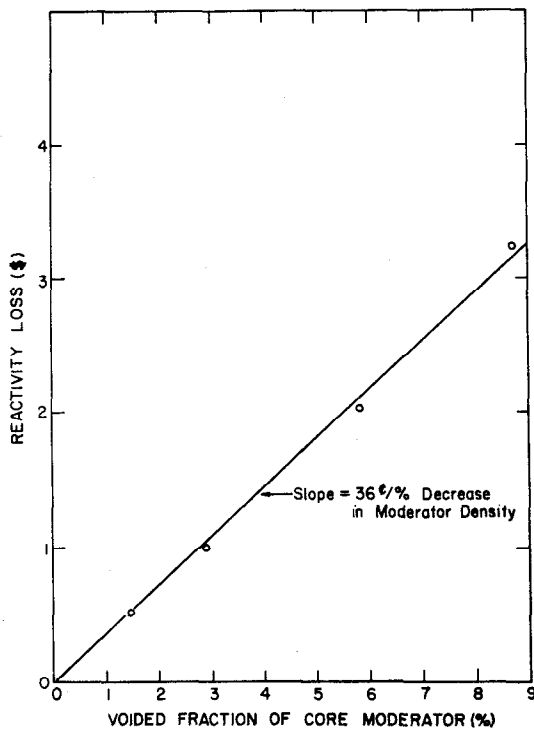
Fig. A-3 Reactivity loss as a function of void fraction for a uniform distribution of voids.
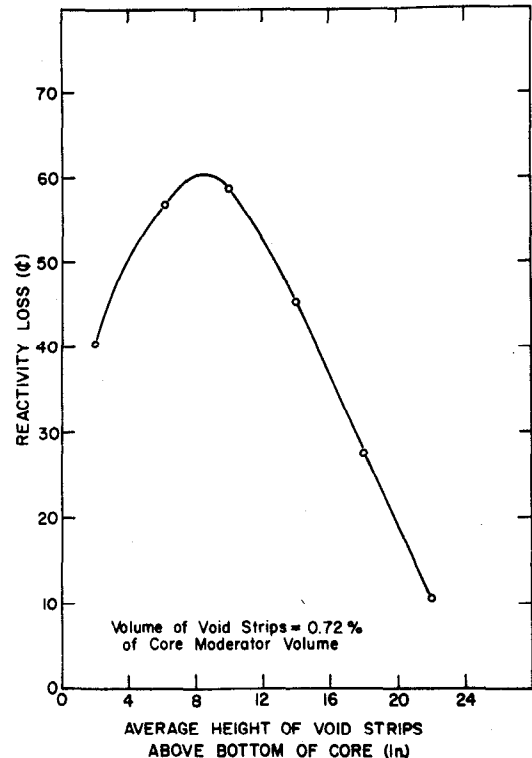
Fig. A-4 Reactivity worth of centrally-located, 4-inch long void strips as a function of height above the bottom of the core.

63

3.3 Void Interaction of Central and Peripheral Regions

The void distribution during a transient probably does not correspond to a uniform void only, or to a central void only, but is rather some more complicated distribution which changes rapidly with time as the boiling point is exceeded. For example, it is likely that during a short-period self-limiting excursion, water channels in the centermost regions of the core are almost completely voided while water channels in the peripheral region of the core, which receive less heating, are only slightly voided. A strongly voided core, by virtue of the consequent redistribution of neutron flux, might be expected to have a markedly different void importance distribution from that obtained in the previous measurements. Additional void worth measurements were, therefore, conducted to determine if the central void coefficient was significantly affected by the presence of voids in peripheral regions of the core.

Four experiments were performed using aluminum strips (26 inches long x 3/4 inch wide x 1/8 inch thick) to simulate voids. For these experiments a 6- x 6-inch region centered about the transient rod was defined to be the "central region", with the remainder of the core defined as the "peripheral region". The four experiments included one in which the central and peripheral regions were voided uniformly, and three experiments in which the central region was more heavily voided than the peripheral region. The reactivity effect due to each of the various void distributions was measured from the change in the critical position of the calibrated control rods. Specific values for the four void configurations along with the results of the experiments are listed in Table A-I.

TABLE A-1

VALUES FOR THE FOUR VOID CONFIGURATIONS AND EXPERIMENT RESULTS

Experiment No.	Region	Number of Strips in Region	Void Volume (cm^3)	Region Voided (%)	Reactivity Change From Unvoided Critical Core (ϕ)	Central Region Void Cofficient[a] (ϕ/cm^3)
1	Central and Peripheral	95	3503	6.68	-315	---
2	Central	40	1475	17.81	-455	-0.096
	Peripheral	80	2950	6.68		
3	Central	40	1475	17.81	-345	-0.090
	Peripheral	44	1622	3.67		
4	Central	40	1475	17.81	-214	-0.090
	Peripheral	0	0	0		

[a] Void coefficients are corrected for absorption cross section of aluminum only.

The results show that the central void coefficient as measured with voids only in the central region is not significantly affected by void fractions as large as seven percent in the peripheral regions. Higher void fractions in both regions would probably have accentuated any interaction between voids. However, the experiments described here were sufficient for present purposes since they produced reactivity decrements in excess of the reactivity compensations necessary for the destructive test program.

An additional result of these experiments has been a comparison of the relative void coefficients obtained by using two different materials, magnesium and aluminum, to simulate voids. The independent calculations of these two determinations yield $-0.067\cancel{c}/cm^3$ for magnesium and $0.063\cancel{c}/cm^3$ for aluminum which agree within 10 percent when both values are corrected for the absorption cross sections of magnesium and aluminum, respectively.

4. NEUTRON FLUX DISTRIBUTION

The steady-state neutron flux distribution was determined from activation of 29 cobalt wires located in the core as shown in Figure A-5. The wires extended the full length of the fuel plates and were irradiated for 135 minutes at power level of about 90 kW.
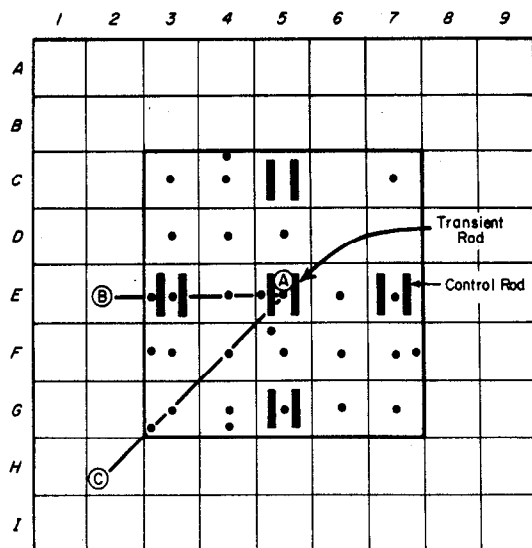

Fig. A-5 Flux wire activation positions.

Figures A-6 through A-10 illustrate representative vertical and horizontal flux profiles at selected core positions. The normalized flux distributions are plotted as functions of height above the bottom of the core or distance from the core centerline. The maximum flux was determined to be in position E5-5 at about 8 inches from the bottom of the core (E5-5 means the 5th water channel numbered from the west or left side of the fuel assembly in the E5 grid position). The peak-to-average flux ratio was determined to be 2.4. Individual values of the flux are estimated to be accurate within 20 percent: 15 percent due to uncertainty in the exact location of the wire detector and 6 percent due to the counting error.

5. POWER DISTRIBUTION IN A VOIDED CORE

The flux distributions discussed previously were obtained during an experiment in which the power level of the reactor was kept at low values insufficient to raise the temperature of the core above the boiling point of water. By contrast, however, many of the transients anticipated during the destructive test program would cause boiling to occur over large fractions of the core; and, the following experiment was designed to determine to what extent the power distribution in the core would be affected by the presence of a nonuniform void distribution such as might be produced during one of these tests.

The experiment consisted of measuring the power distribution both with and without simulated voids in the core. Thin foils of a 93 percent enriched uranium-aluminum alloy (5/32 inch diameter by 0.006 inch thick) were used to monitor
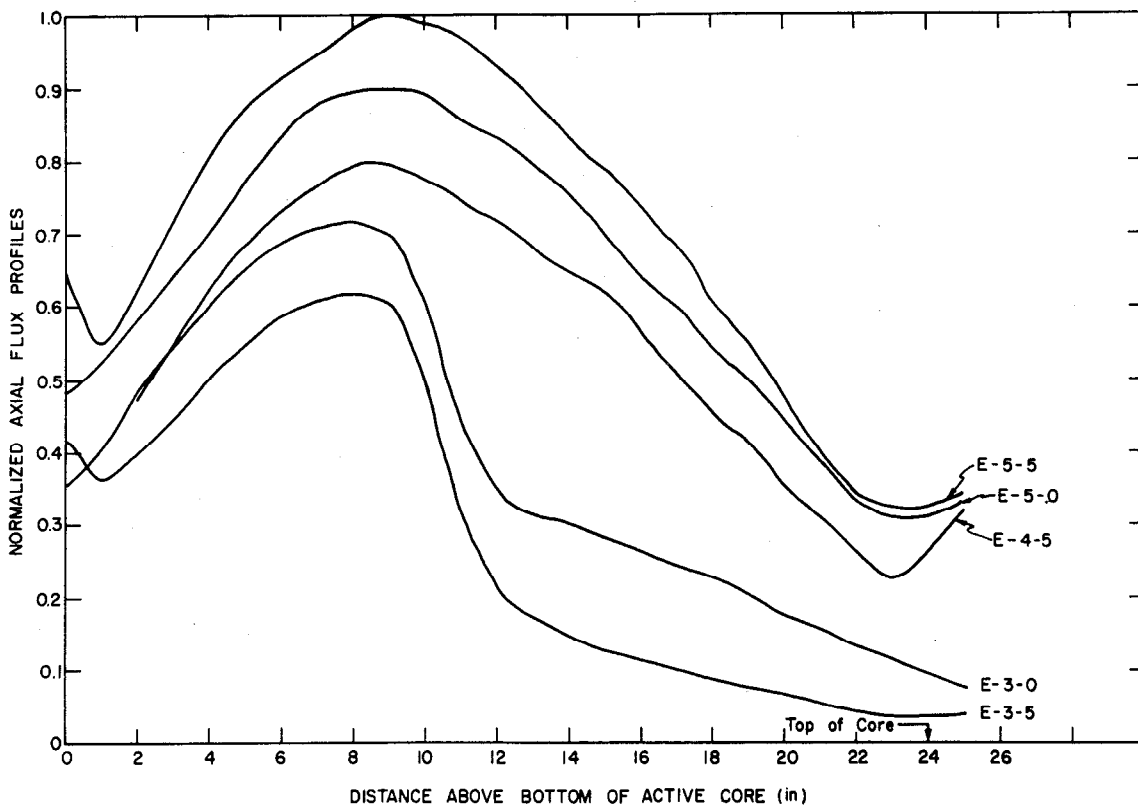
Fig. A-6 Vertical flux profiles in fuel assemblies E-3, E-4, and E-5.
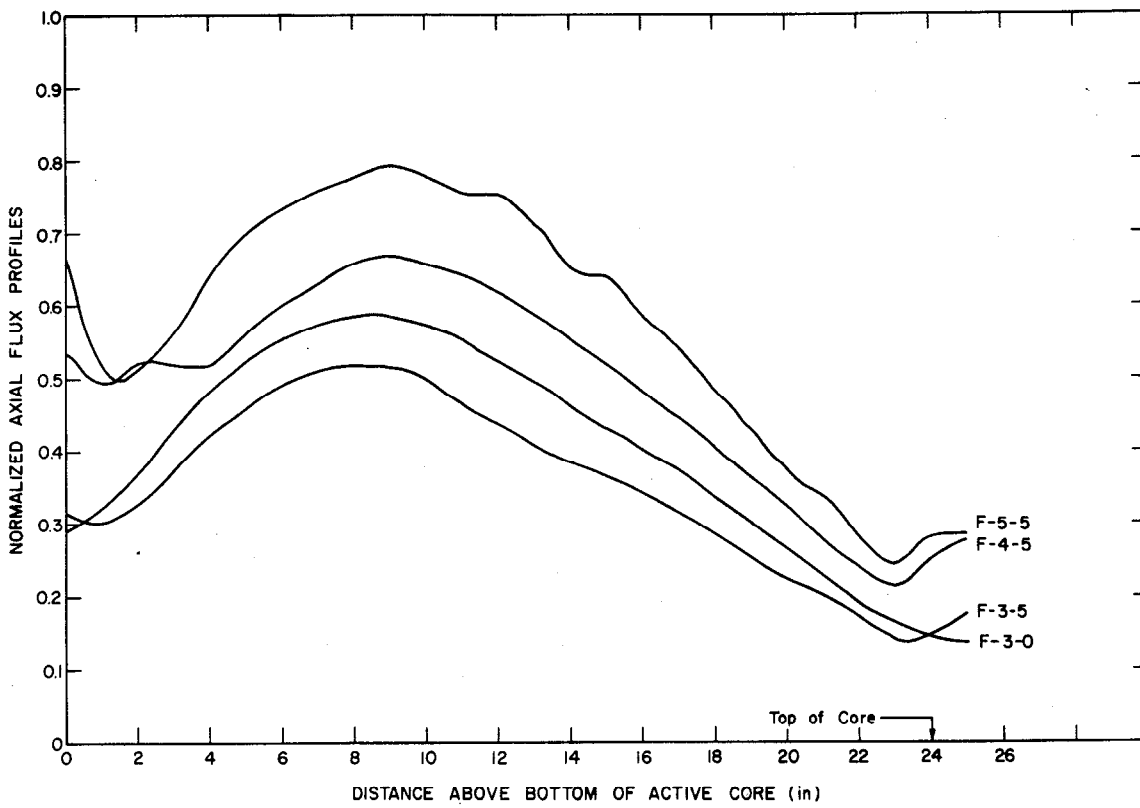
Fig. A-7 Vertical flux profiles in fuel assemblies F-3, F-4, and F-5.

66
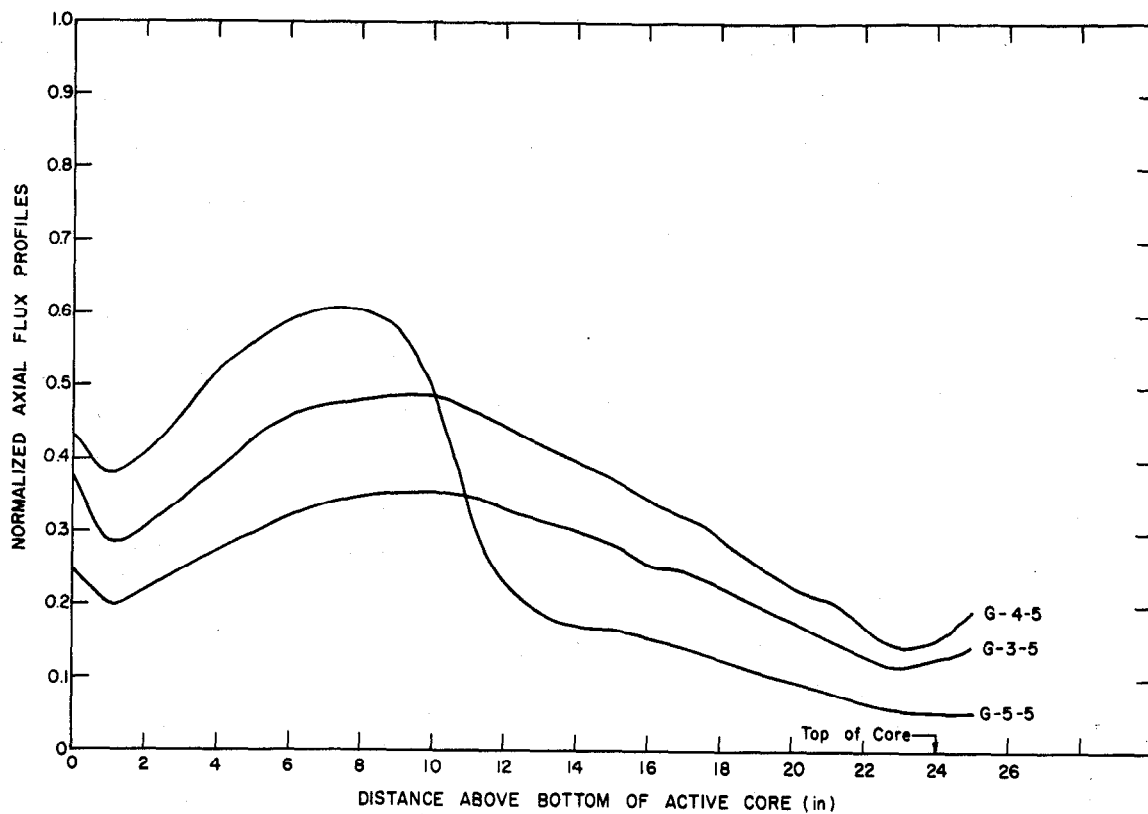
Fig. A-8 Vertical flux profiles in fuel assemblies G-3, G-4, and G-5.
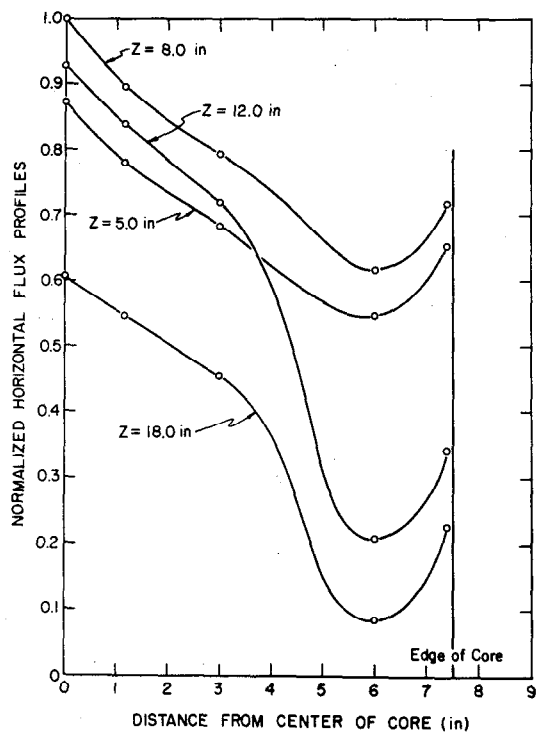

Fig. A-9 Horizontal flux profiles along direction A-B (Fig. A-5). Lines drawn in to connect data points.
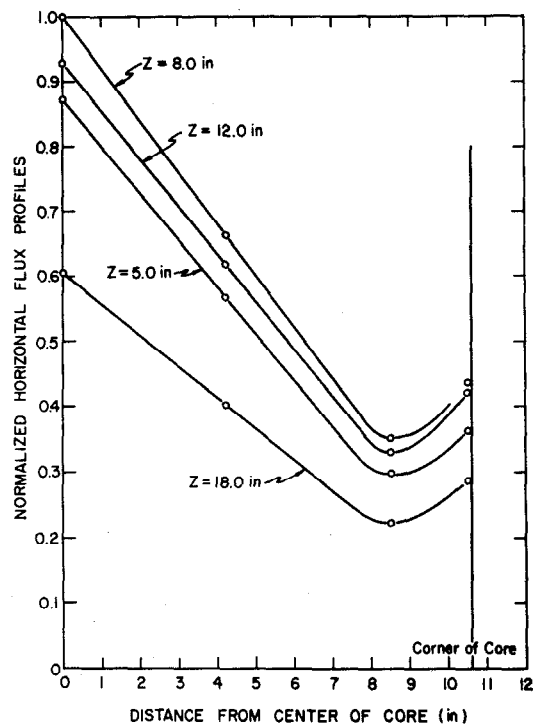

Fig. A-10 Horizontal flux profiles along direction A-C (Fig. A-5). Lines drawn in to connect data points.

the flux, and aluminum strips were used to simulate the voids. Only a central region (shown in Figure A-11) was voided to simulate the void distribution which might occur during the early part of an excursion. This region was voided to about 18 percent.

The foil locations used for both the voided and unvoided activations are shown in Figure A-11. The foils were mounted on plexiglass strips with mylar tape, and the strips were positioned in one quadrant of the core; since analysis of the cobalt wire activations obtained during the power calibration indicated quadrant symmetry, only one quadrant was investigated. The total weight of U-235 in all foils was only 1.5 g in each experiment. Figure A-12 shows the results of these flux measurements.

Fig. A-11 Location of uranium-aluminum alloy foils for comparison of the flux in voided and unvoided core.

O= Foils located at +3, 0, -4, -7, -10, -13, -16, -19, -22, -25, and -28 inches.

⊙= Same as 0 with addition of cadmium covered foils at +1-1/2, -1-1/2, -8-1/2, -14-1/2, -17-1/2, -20-1/2, and -26-1/2 inches [a].

●= Foils located at 0, -7, -13, -16, -19, and -25 inches[a].

⊗= Same as 0 with an additional foil at -17-1/2 inches; this was the master foil used in the counting analysis[a].

[a] All dimensions are from the top of the core; ie, +3 indicates a position three inches above the top of the core.

6. ISOTHERMAL TEMPERATURE COEFFICIENT

An isothermal temperature coefficient of approximately -2.1¢/°C was determined from the change in control rod critical position during a 9.6°C temperature rise obtained during the flux distribution measurement.

7. REDUCED PROMPT NEUTRON LIFETIME

A value of the reduced prompt lifetime, $\ell/\bar{\beta}$, for the D-12/25 core was determined from an analysis of subcritical statistical behavior of the neutron population [24, 25, 26]. The value of the reduced prompt neutron lifetime obtained in this experiment was $\ell/\bar{\beta}$ = 8.3 ± 0.4 msec as compared to a value of 8.16 ± 0.04 msec obtained from step-transient tests. The quoted uncertainty in the second value is the standard deviation based on the deviation of the data points from a least squares fit and is probably an underestimate.

PROFILE ALONG LINE A B

PROFILE ALONG LINE A C

Z=0.0 in

Z=0.0 in

Z=-7.0 in

Z=-7.0 in

Z=-13.0 in

Z=-13.0 in

Z=-16.0 in

Z=-16.0 in

Z=-19.0 in

Z=-19.0 in

Z=-25.0 in

Z=-25.0 in

END OF CENTRAL VOIDED REGION

EDGE OF CORE

RELATIVE POWER

DISTANCE FROM CORE CENTER (in)
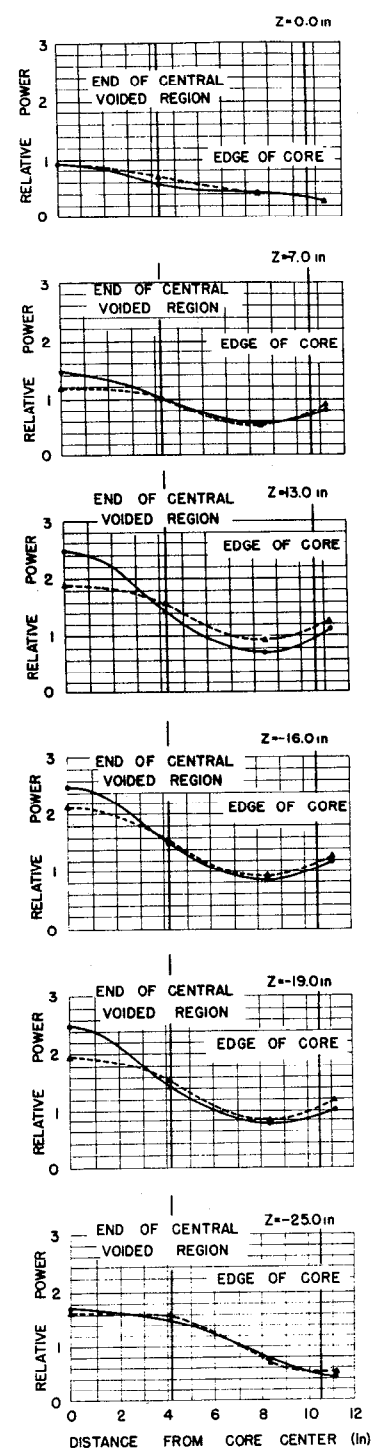
LEGEND

——■ POWER DISTRIBUTION IN UNVOIDED CORE

——■ POWER DISTRIBUTION IN CORE WITH CENTRAL REGION VOIDED 18%

Fig. A-12 Comparison of horizontal flux profile in voided and unvoided core. Z is the distance from the top of the fuel plates. For the voided case the control rod position was Z = -13 inches. For the unvoided case the control rod position was Z = -15.3 inches. The power normalization was obtained by taking the ratio of the local count rate to the average core count rate for each of the two conditions.

69

APPENDIX B

DETAILS OF TRANSIENT INSTRUMENTATION FOR RUN 54

APPENDIX B

DETAILS OF TRANSIENT INSTRUMENTATION FOR RUN 54

1. POWER

Measurement of the reactor power level during the excursion was accomplished by seven neutron-sensitive ionization chambers variously located in the reactor core, in the reflector water, and in underground tubes immediately adjacent to the reactor vessel. Those chambers located in the reflector water and subject to damage from large pressure excursions were contained within heavy-walled watertight canisters for protection. Three of the chambers were of miniature size (about 1/8 inch diameter x 1 inch long). The relatively insensitive miniature chambers were placed in and adjacent to the core. The location of these miniature chambers is indicated in Table B-I.

TABLE B-I

MINICHAMBER LOCATIONS [a]

Chamber	X (in.)	Y (in.)	Z (in.)
GE-176	- 9.7	9.62	9.5
GE-679	- 3.0	8.5	- 6.0
GE-686	- 1.3	- 1.6	- 3.0

[a] Dimensions are in inches from the geometric center of the core. The X, Y, and Z coordinates form a left-handed system with the Z dimension pointing vertically up from the core. The core itself is approximately 15 inches square x 24 inches high.

With provision for duplication and multiple-ranging of some of the power instruments in order to provide power coverage from a few watts to about 200 GW, a total of 28 power signals was recorded by optical recording galvanometers. Six of these power traces also were recorded on magnetic tape to provide better frequency response, and easier reduction and preparation of data for analysis.

2. ENERGY RELEASE

The energy release from the excursion was obtained by integration of the power data recorded as described above. During the destructive test, six cobalt wires also were placed in the core in order to provide additional information on the nuclear energy release by activation measurements.

3. TEMPERATURE

Fuel plate temperatures in the core were measured by 34 thermocouples installed on 16 different fuel plates. Of these, 12 were surface-type and 22 were buried-type thermocouples. The surface-type thermocouples (Figures B-1 and B-2) consisted of 10-mil diameter chromel-alumel wires, flattened and trimmed
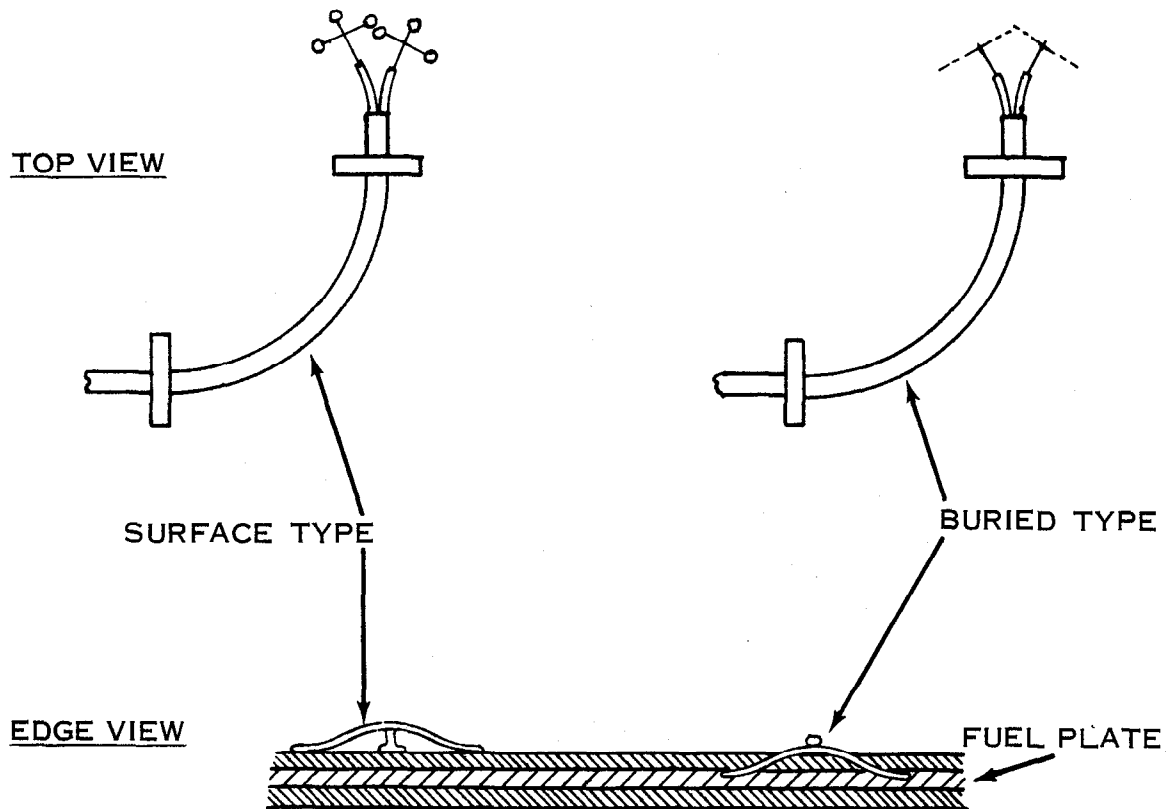

Fig. B-1 Mounting technique for thermocouples.

to tabs approximately 0.5 mil thick, which were resistance-welded to the surface of the fuel plates to establish a low-mass junction. The buried-type thermocouples consisted of two chromel-alumel wires imbedded into the meat of the fuel plate with the cladding peened over the top of the wires to hold them in place (Figure B-1). These buried thermocouples provided thermal and electrical contact with the plate for a longer time after plate melting than would have been the case for the wires attached to the surface and were, therefore, used in regions of the core that were expected to exceed the melting point of aluminum. In the attempt to obtain a measure of the actual fuel temperature in the core during the destructive test, two special capsules were constructed and installed in the core prior to the test. These capsules consisted of a small quantity of the fuel alloy (from a conventional plate) contained in a high-melting-point container along with high-melting point thermocouples. Upon melting, the meat alloy was constrained to remain in contact with the thermocouples. The capsule consisted of a type-304 stainless steel cylinder, 3/16 inch in diameter, 3/4 inch long, with 20-mil walls, crimped into an elliptically shaped container. One end of the container was welded closed
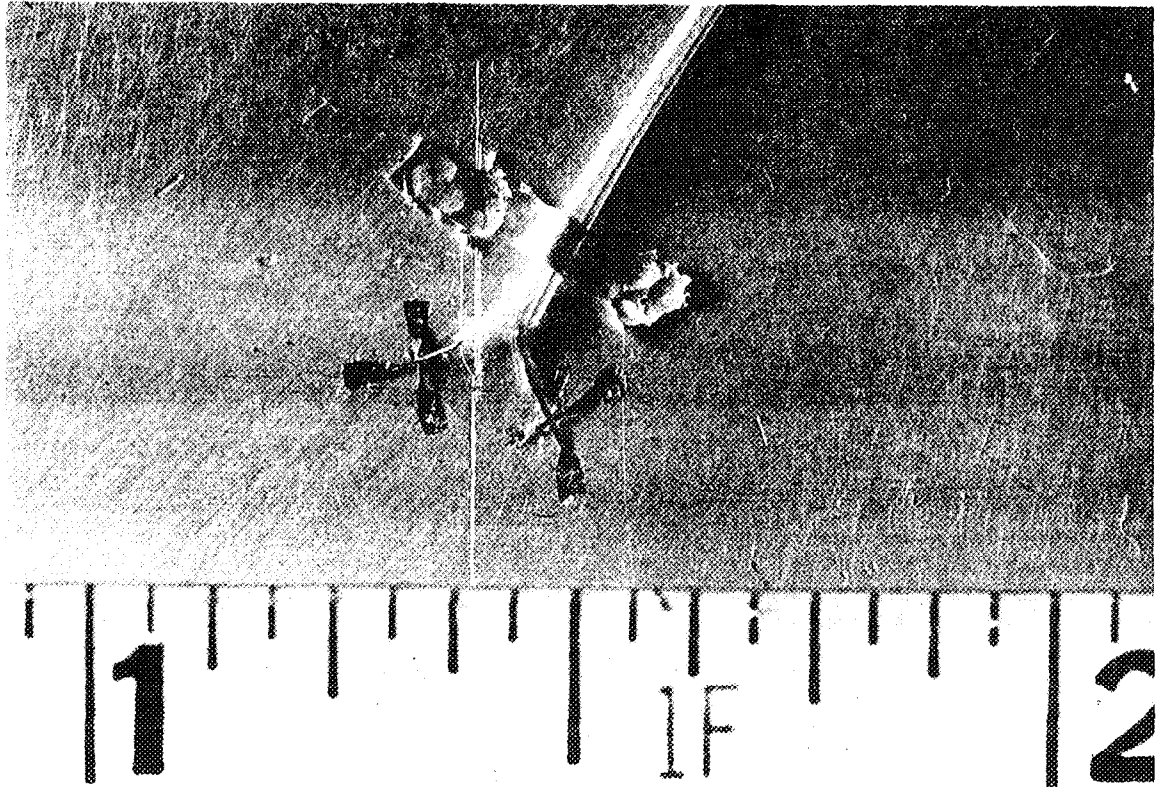
Fig. B-2 Photograph of typical surface-type thermocouple. (Welded tabs are ≈0.5 mil thick.)

with 0.125 inch of stainless steel. Two slabs of U-Al alloy from a regular fuel plate were placed in the container, forming a fuel slab about 0.04 inch thick. A tungsten, tungsten-rhenium thermocouple pair, contained in a stainless steel sheath, was placed in the fuel. The stainless steel sheath extended into the cylinder but not into the fuel. The top of the container was then welded closed with stainless steel, adding 0.250 inch of stainless steel on the top side of the fuel capsule. The capsule was again crimped and heated past the melting point of the uranium-aluminum alloy to ensure good contact between the thermocouple wires and the fuel. Figure B-3 is a photograph of the fuel capsule.

One of the fuel capsules was placed near the central hot spot of the reactor core and the other at a point just outside the expected melting region of the core.

4. PRESSURE

A total of 19 pressure transducers at 15 different locations surrounding the reactor core was used during the destructive test. The location and ranges of these transducers are shown in Figure B-4 and in Table B-II. The location of pressure transducers used during all other tests also appears in Table B-II. This arrangement was selected to provide information on the time behavior of transient pressures as a function of position surrounding the core. More than one transducer was located in some of the positions in order to cover the range from the modest pressures extrapolated from previous data to the destructive pressure pulses anticipated for the series. No pressure measurements were made

75

Fig. B-3 Photograph of fuel-bearing capsule.
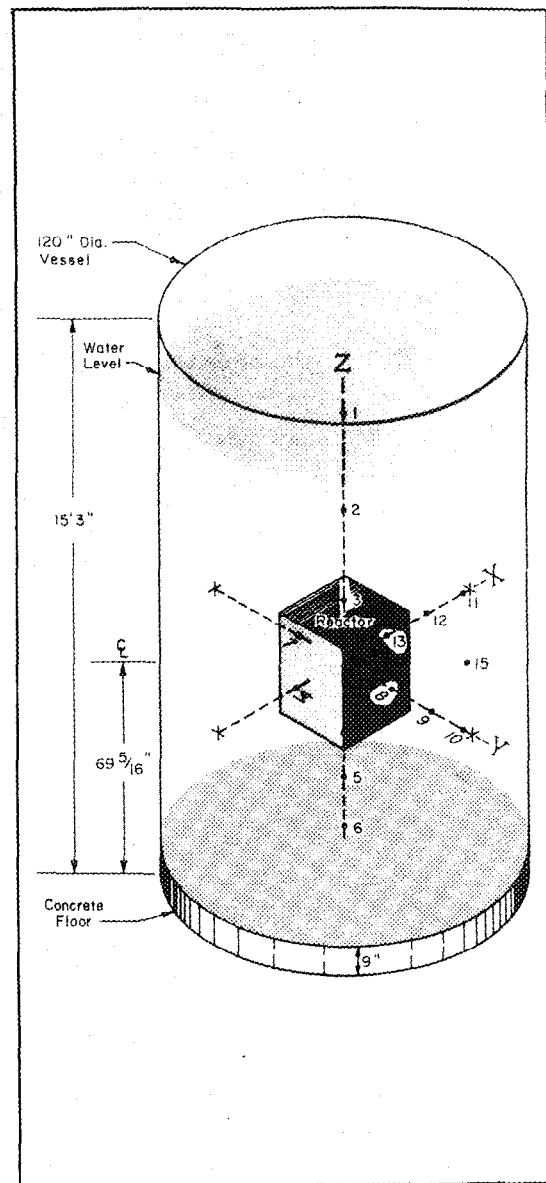
Fig. B-4 Location of pressure transducers for destructive test.

within the reactor core since no transducers were available which were sufficiently small to fit between the fuel plates and at the same time sufficiently insensitive to the radiation burst to permit useful measurements. The pressure transducers were carefully selected to minimize the radiation sensitivity of the transducer while at the same time preserving a maximum available frequency response. A total of 24 pressure signals was recorded by the optical recording galvanometers during the test.

5. STRAIN

Strain gauges were placed on several items in and around the reactor during the destructive test, utilizing strain measurement techniques which had been

76

PRESSURE TRANSDUCER INSTRUMENTATION

Transducer Serial No.	Location (See Fig. B-4)	Coordinates (in. From Core Center)			Pressure Range (psig)
		X	Y	Z	
1960	1	3	2	58.5	100
2444	1	6	3	58.5	1000
1976	1$_d$	3	3	62	-15 to 35
2444	2$_d$	3	3	39	-100 to 900
1975	3	3	3	19.5	100
2655	3$_d$	5	5	23	-10 to 20 and -50 to 250
2060	3$_d$	3	3	23	-100 to 700
16106	4	3	3	-27.5	100
2077	4$_d$	3	-4.5	-20	-300 to 2700
2628	4$_d$	3	-3.5	-20	-10 to 20 and -30 to 270
2074	5$_d$	3	2	-36	-350 to 3150
16237	6	-4	-3	-51	100
2281	6	-2.5	3	-52	3000
2638	6$_d$	3	2	-53.5	0 to 300
2208	7	0	-25	0	2500
2192	7$_d$	3.5	-16.5	0	0 to 10,000
3949	8	0	10.5	0	150
2062	8$_d$	1.5	16.5	0	0 to 3500
1977	8$_d$	-1	17	0	-8 to 17 and -25 to 225
2639	9$_d$	1	36.5	2.5	0 to 300
16275	10	-4.5	54	0	100
2232	10	5	53	0	1000
1990	10$_d$	1	53.5	2	-7 to 58 and -200 to 450
1976	11	54	4	0	100
2192	11	54	-6	0	10,000
2196	11	55	8	0	8000
2475	11$_d$	52.5	1	1.5	0 to 300
1977	12	25.5	0	0	250
2196	12$_d$	35	0	2	-800 to 7200
3948	13	10.5	0	0	150
2281	13$_d$	17	1	-1	0 to 3000
2646	13$_d$	17	-2	2	-15 to 85 and -30 to 270
2553	14$_d$	-17	1.5	0	0 to 1000
20123	15$_d$	17.5	-22.5	-48.5	-10,000 to 90,000

Note: Locations of pressure transducers used during the 3.2-msec destructive test are designated by the letter "d". The pressure ranges indicated for the transducers used during other tests are maximum pressure ranges and were adjusted before each test by varying the gain of the connected amplifiers.

developed during the nondestructive portion of the testing program. The following specific items were instrumented with strain gauges during the test: the hold-down bars which provided vertical restraint on the fuel assemblies in the core -- longitudinal tension; the core clamps which provided lateral support to the core -- longitudinal compression; the core-support legs which support the core structure from the bottom of the reactor vessel -- longitudinal compression; a peripheral fuel assembly -- instrumented for strains in bowing and bulging of the assembly; and the reactor vessel -- hoop stress or bulging. A total of eight signal channels was recorded for the measurement of strain during the destructive test.

6. FLOW

The flow of moderator from the reactor core during short-period excursions is of interest because of its applicability to the study of the transient shutdown processes. Both the thermal expansion of the fuel plates and boiling of the moderator in the core lead to the expulsion of moderator from the core. Since these mechanisms apparently constitute the major shutdown processes occurring during short-period excursions, information as to the time and rate at which shutdown occurs can be obtained from the measurement of moderator flow from the top and bottom of the core.

Two different devices were utilized for the measurements of flow from fuel assemblies in the core. The first consisted of a small circular disc suspended on the end of a cantilevered beam over the center of the flow. The force on this drag disc was monitored by a strain gauge mounted on the beam and the force then related to the velocity of flow. While this device provided a sensitive indication of the initial flow motion of the moderator, the relationship between the force on the disc and water velocity was such as to make quantitative flow information difficult to obtain from the device. A more quantitative measurement of flow was obtained from a displacement transducer which utilized positive motion of a piston in a cylinder, with the velocity of the piston being measured by a moving-magnet technique. This flowmeter consisted of two separate piston-cylinder units mounted on each end of a fuel assembly (Figure B-5). Flow from the assembly was constrained to move into the cylinders and cause the pistons to move outward. Attached to each piston was a magnet moving through a coil to produce a signal proportional to the velocity of motion. For the destructive test, two drag-disc-type and two displacement-type flowmeters were in use, mounted on two fuel assemblies adjacent to the central assembly of the core.
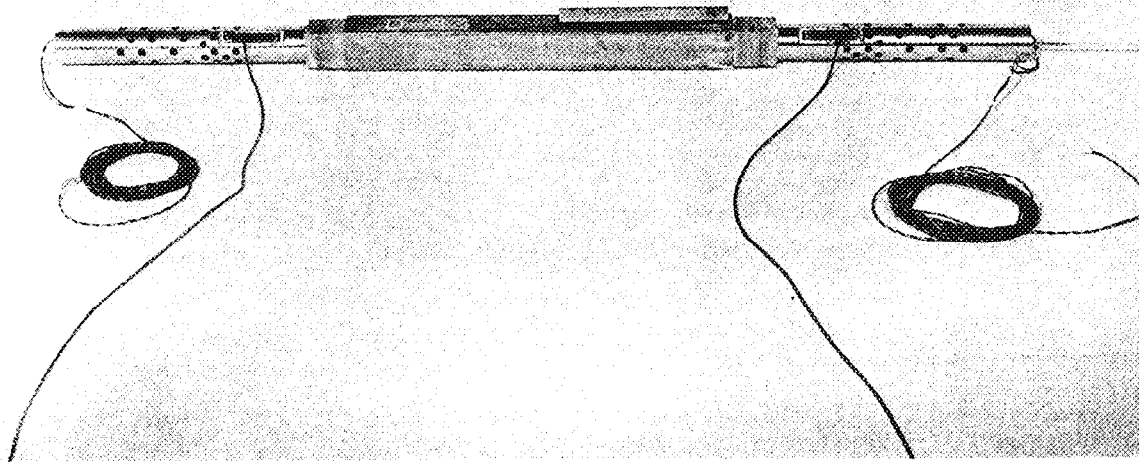

Fig. B-5 Photograph of displacement transducers mounted on fuel assembly.

7. PHOTOGRAPHY

For the destructive test, two high-speed (500 fps) cameras were used in conjunction with the periscopes to provide an underwater view of the reactor core.

A third, medium-speed (128 fps) camera viewed the core from above through a mirror. Six cameras ranging from high speed (600 fps) to conventional speed (24 fps) were variously positioned to record the expulsion of water from the vessel, disruption of the control structure, and ejection of missiles. Table B-III lists all the cameras which were used for the destructive test with their locations and speed.

TABLE B-III

LOCATION AND SPEED OF CAMERAS FOR DESTRUCTIVE TEST

Camera No.	Type	Speed (fps)	Location
1	Waddell	500	North edge of reactor tank using periscope to view across top of core
2	Waddell	500	North edge of reactor tank using periscope to view top of core
3	Waddell	600	Rear doorway of reactor building viewing directly over reactor vessel
4	Bell & Howell	128	Near reactor tank viewing top of core through mirror
5	Bell & Howell	64	Approximately 50 ft southeast of reactor viewing front of reactor building
6	Bell & Howell	24	Approximately 100 yd southeast of reactor viewing front of reactor building
7	Bell & Howell	128	Roof of Spert I terminal building viewing west side of reactor building
8	Arriflex	48	At the Control Center approximately 1/2 mi from the reactor
9	Bell & Howell	24	Approximately 125 ft west of Spert II reactor building, about 1/2 mi from the Spert I reactor

8. RADIOLOGICAL MEASUREMENTS

The radiological measurements obtained during the destructive test were conducted as a joint effort by personnel of Phillips Petroleum Co. and the Health and Safety Branch of AEC Idaho Operations Office. The measurements made included: (a) measurement of the integrated neutron and gamma dose as a function of position relative to the reactor vessel, including separate determination of the integrated dose during the power burst and the total integrated dose for about four hours after the test; (b) direct-radiation dose-rate measurements made with six remote-area monitors at several points for the purpose of estimating hazard to reentry personnel; (c) airborne radioactive contamination, using high-volume air samplers located in and around the reactor area; (d) the neutron spectra and the gamma-to-neutron ratios as a function of position relative to the

core, by use of nuclear accident dosimeters (NAD) suspended over the reactor; (e) the fission product inventory in the reactor water after the test, by water sampling; (f) air activity and fallout rate, at several grid positions downwind of the reactor; (g) the Na-24-induced activity in ordinary blood, as a function of proximity of the blood sample to the edge of the reactor vessel, in order to determine biological effects; (h) body absorption factors for a reactor excursion accident, by simultaneous exposure of film badges and bottles of tissue-equivalent solution; (i) comparison of several methods for accident analysis, by placement around the vessel of materials (small tools, various metals, etc) which might normally be found around a reactor which had undergone an accident; (j) determination of fallout by the use of grass plots, fallout plates, etc, positioned on the downwind grid; and (k) fisside cloud activity and progress by means of both airborne and surface mobile tracking equipment located downwind for a distance of 25 miles.

9. SPECIAL EQUIPMENT FOR DESTRUCTIVE TEST

In addition to the instrumentation described above and the normal control instrumentation for the reactor, a number of special items of equipment were provided specifically for the destructive test. Two television monitors were provided to view the reactor core and the top of the vessel. Monitors for these channels were placed in the reactor control room to provide information for post-test analysis of the condition of the core and facility prior to reentry.

In addition to the conventional water-level indicator for the reactor vessel, a separate, ruggedized, float-actuated device was mounted on the floor of the reactor vessel to provide indication when the water level reached six and three inches above the bottom of the reactor vessel. This was provided in anticipation that the normal full-range water-level indicator might be damaged by the violence of the test and to provide positive indication of successful draining of the vessel prior to personnel reentry of the area.

A remotely operated soluble-poison injection system also was provided to inject gadolinium nitrate solution into the reactor vessel in the event that, because of damage to components and hardware, it might not be possible to drain the water from the reactor vessel.

Figures B-6 through B-11 illustrate typical transient instrumentation for Run 54.
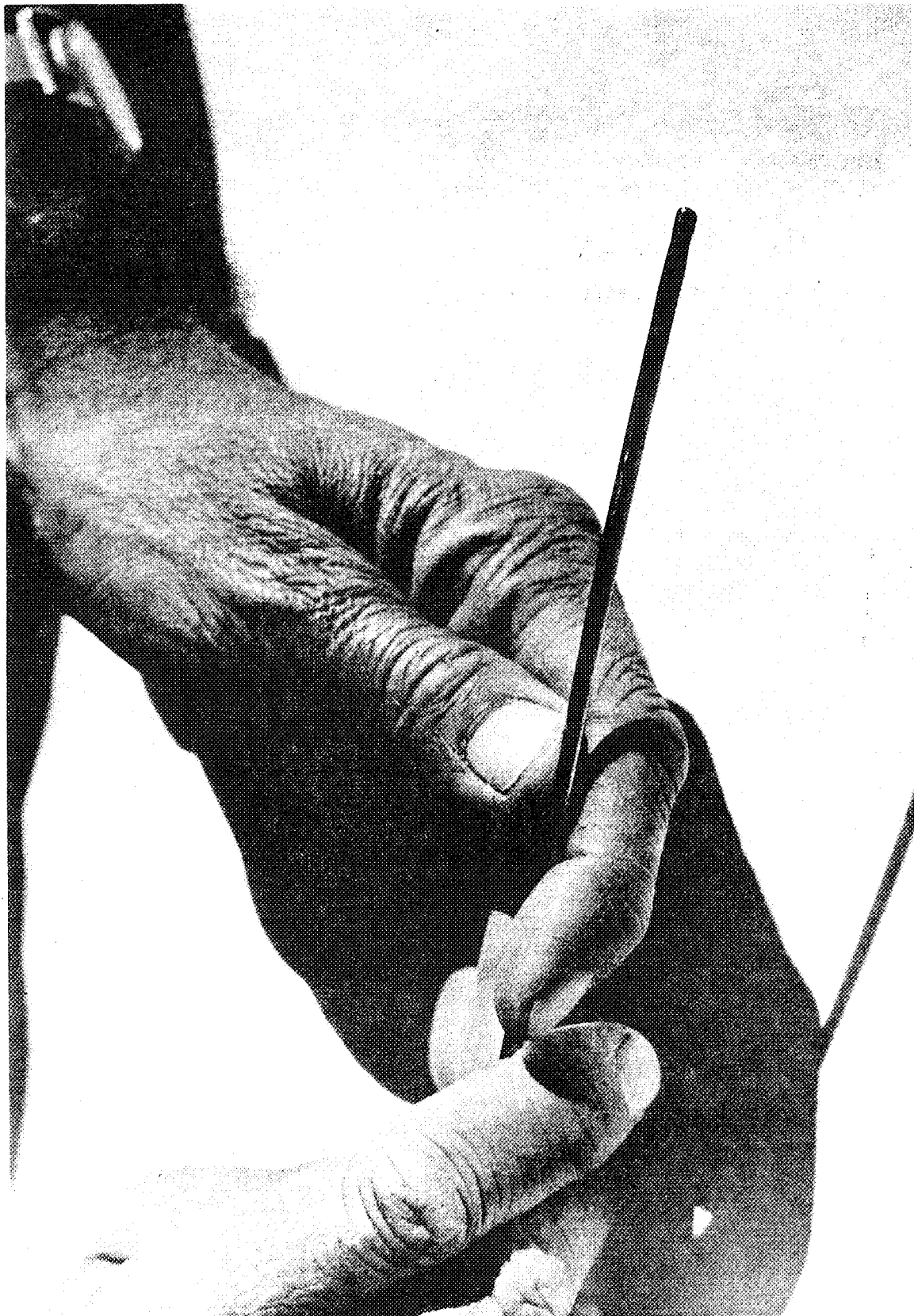
Fig. B-6 Miniature ionization chamber used for in-core power level monitoring.

Fig. B-7 Typical installation of pressure transducers. Three transducers are shown attached to wall-mounted bracket. Lead wires exit through steel tubing.
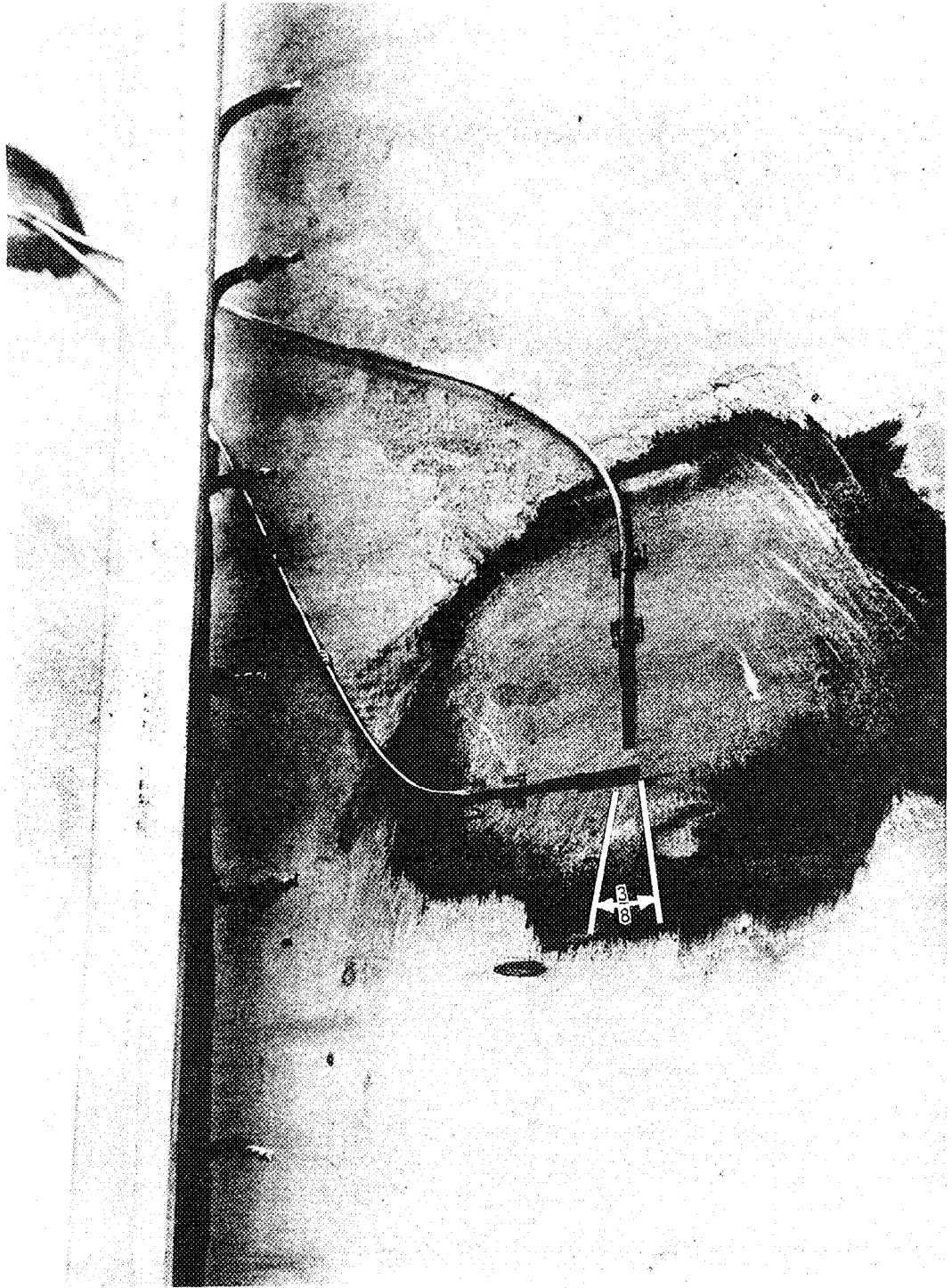
Fig. B-8 Typical installation of strain gauges. Two strain gauges are shown attached to the wall of the reactor vessel, one vertical and one horizontal.
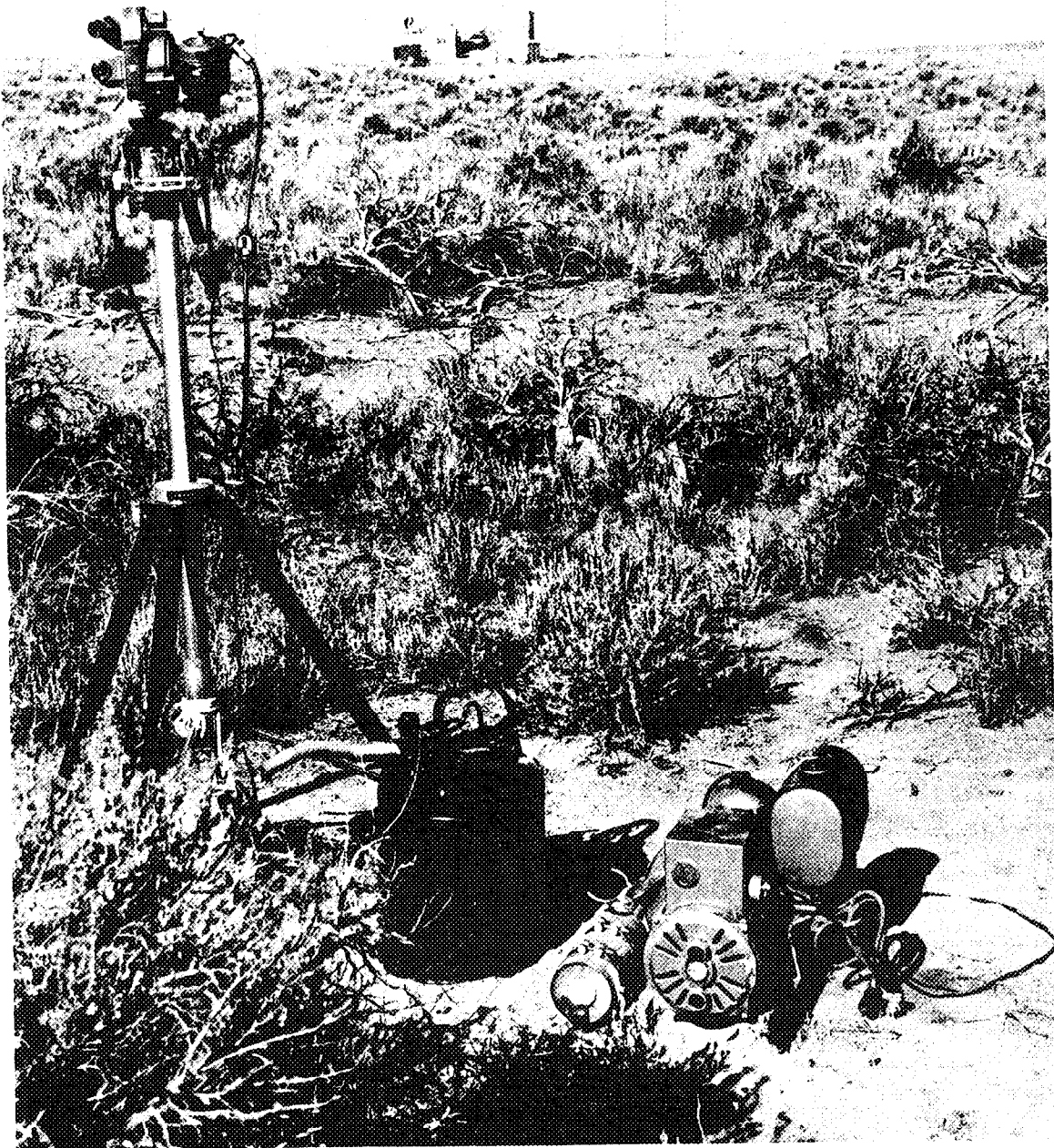
Fig. B-9 Installation of camera #6 for long distance photography. Camera has independent power supply and is started remotely by a sequence timer at the control center.
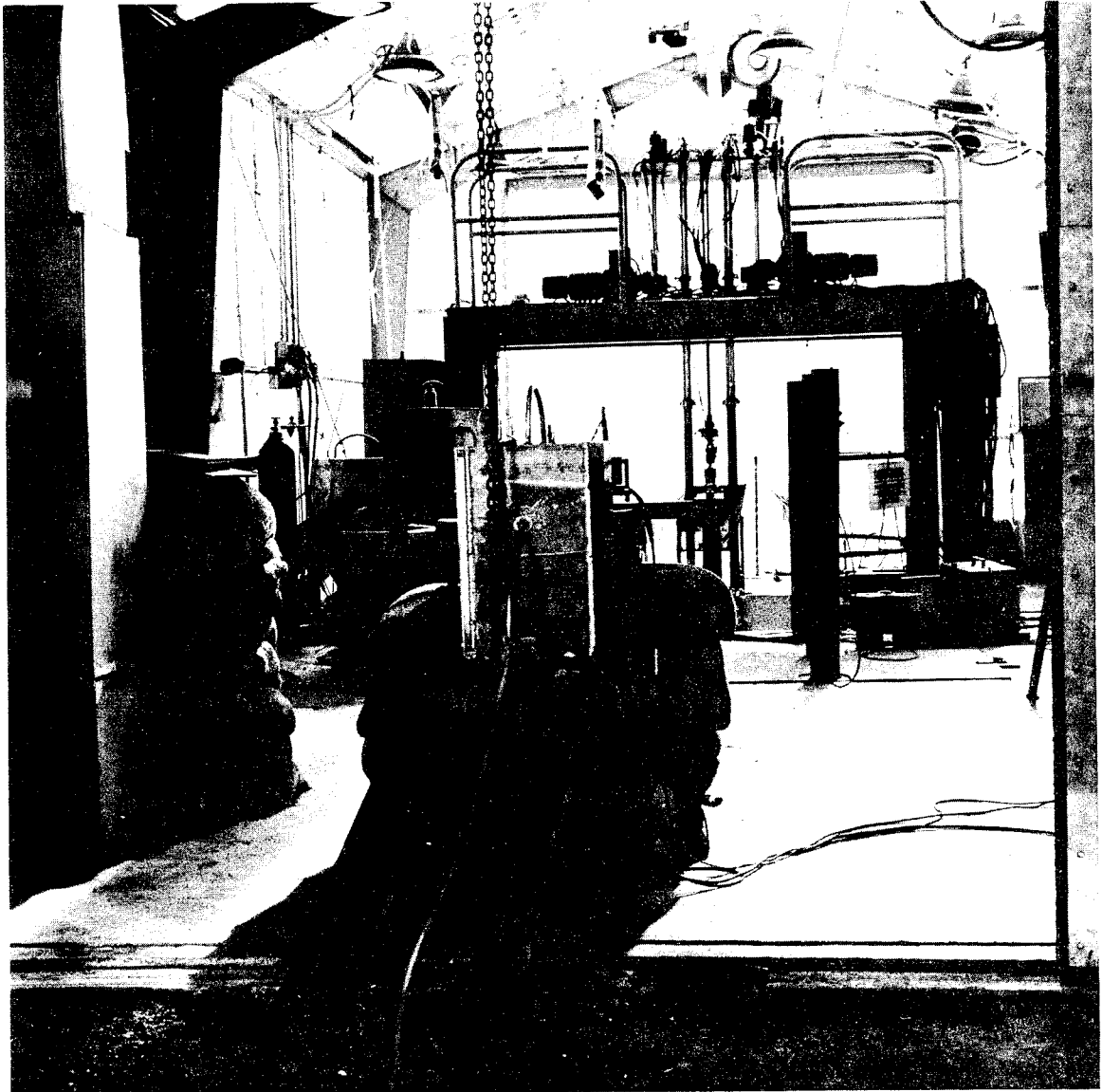
Fig. B-10 High speed (600 fps) camera #3 installation at the rear of the reactor building. Rope (attached at rear of housing) and inclined track are for remote removal of camera.
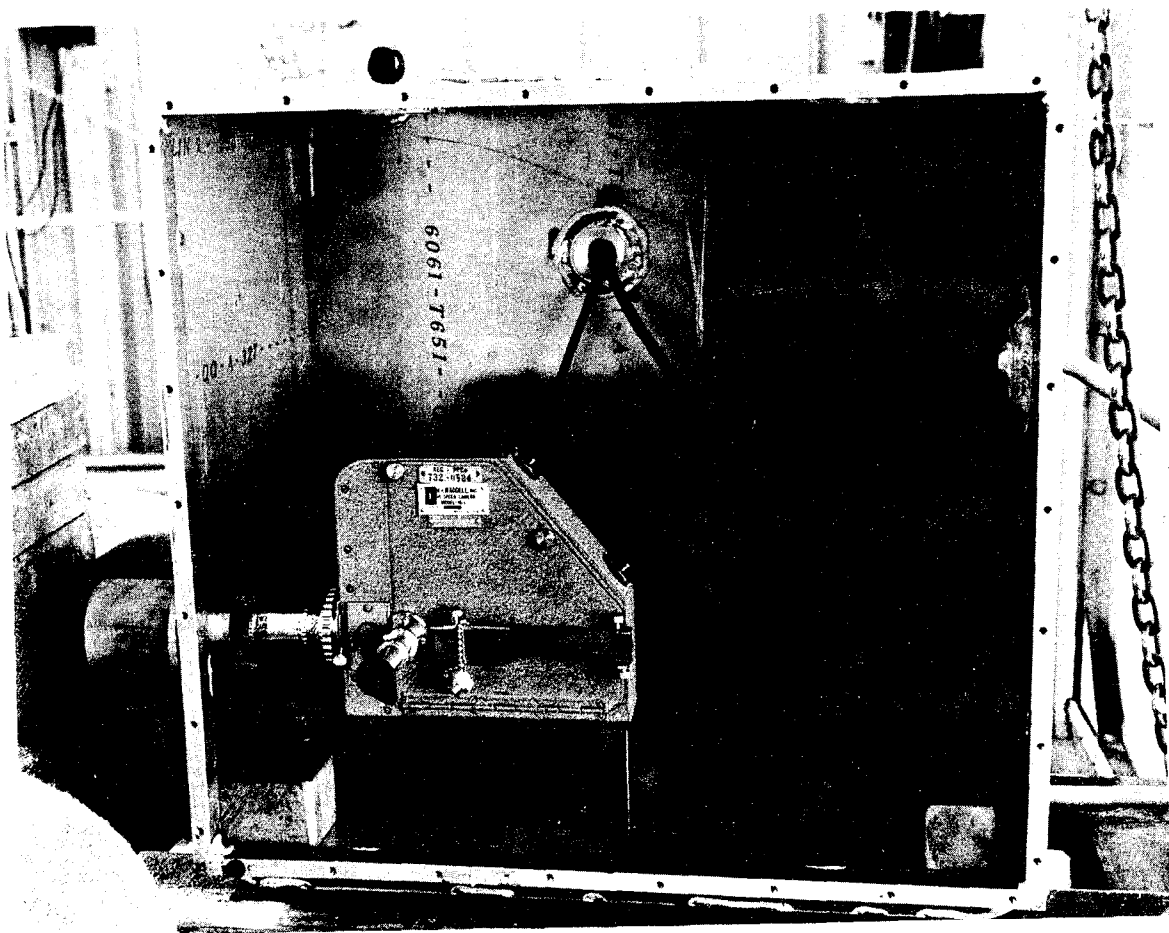
Fig. B-11 View of high speed camera inside of protective housing. Cables supply power for motors and light-timing device.

APPENDIX C

DATA SUMMARY

APPENDIX C

DATA SUMMARY

This appendix contains representative data taken from selected tests during the Destructive Test Series. For a more complete data summary see Reference 27. In the figures to follow, nomenclature designating the location of the measuring instrument is assigned to each temperature and pressure response curve. The location of pressure transducers is specified by a left-handed, Cartesian coordinate system having its origin at the center of the core (Figure B-4). A number which corresponds to specific coordinates (Table B-II) is assigned to each pressure transducer. The location of thermocouples is specified by a symbol having five characters: the first two specify the fuel assembly (Figure D-1); the third specifies the fuel plate (fuel plates are numbered 1 through 12, number 1 is the first fuel plate on the west side of the fuel assembly); the fourth specifies the side of the fuel plate to which the thermocouple is attached; and, the last is the z coordinate of the thermocouple location (z = 0 is at the vertical center of the core).

Figures C-1 through C-7 are general behavior plots of power, temperature, and pressure (pressure traces are shown only when a significant deflection was recorded) for the period region from 880 msec to 6 msec. Figures C-8 through C-10 are general behavior plots showing power, temperature, and pressure for a 5-msec period test. Figures C-11 through C-13 are general behavior plots of power, temperature, and pressure for a 4.6-msec period test. Figures C-14 through C-20 are behavior plots from the destructive test. Figure C-21 shows the maximum recorded temperatures for the Destructive Test Series.

Figure C-22 is a plot of burst parameter versus reciprocal period for all of the data recorded during the Destructive Test Series. The burst parameter is defined as $\phi(t_m)/E(t_m)\alpha_0$. If the power increase to peak follows a pure exponential, then $\phi(t_m)/\alpha_0$ is the energy release up to the time of peak power, $E(t_m)$. As α_0 increases the power rise becomes sharper thus approaching a pure exponential and the burst parameter approaches unity. The change in slope and eventual decline of the burst parameter (shown in Figure C-22) for α_0 greater than about 100 sec^{-1} is due to burst broadening before peak power which is discussed in Section III-2.5.

Table C-1 contains a list of the initial step injection of reactivity, Δk_0; the period, τ_0; reciprocal of the period, α_0; peak power, $\phi(t_m)$; energy release at the time of peak power, $E(t_m)$; total energy release, E_T; maximum temperature at the time of peak power, $\theta(t_m)$; and maximum temperature, θ_{max}, for each of the 54 tests performed during the Destructive Test Series.

The best values of τ_0, $\phi(t_m)$, and E_T for the destructive test are 3.21 $\pm$ 0.04 msec, 2260 $\pm$ 60 MW, and 30.7 $\pm$ 0.6 MW-sec, respectively. The quoted errors are the standard deviation of the experimental values. For $\phi(t_m)$ and $E(t_m)$ there also may be a possible 10 percent systematic error.
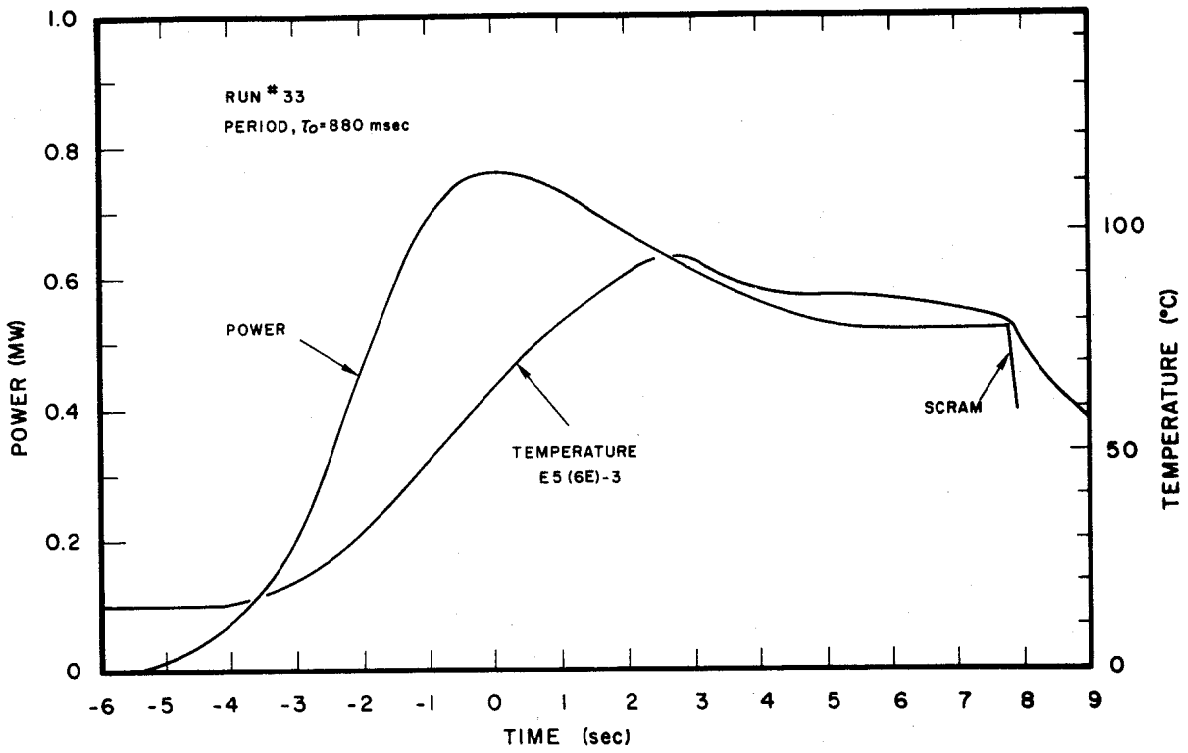
Fig. C-1 General behavior plot showing power and temperature for a 880-msec period transient test.
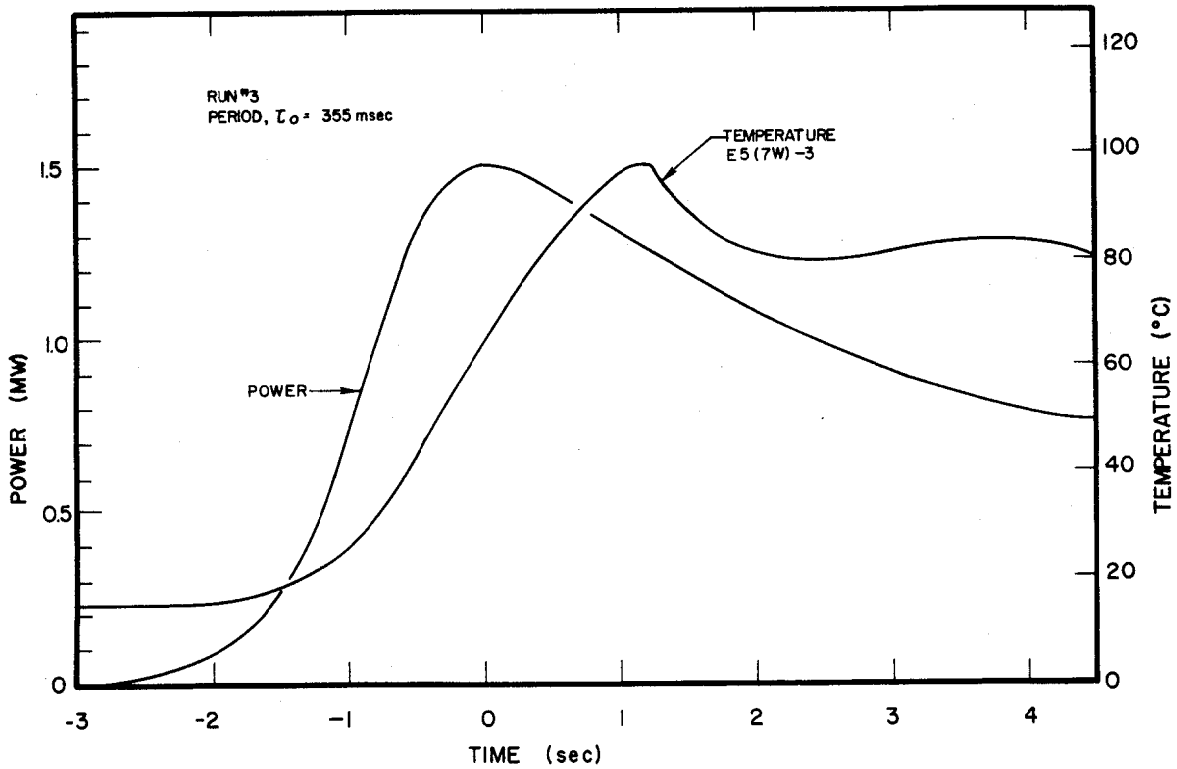
Fig. C-2 General behavior plot showing power and temperature for a 355-msec period transient test.

90
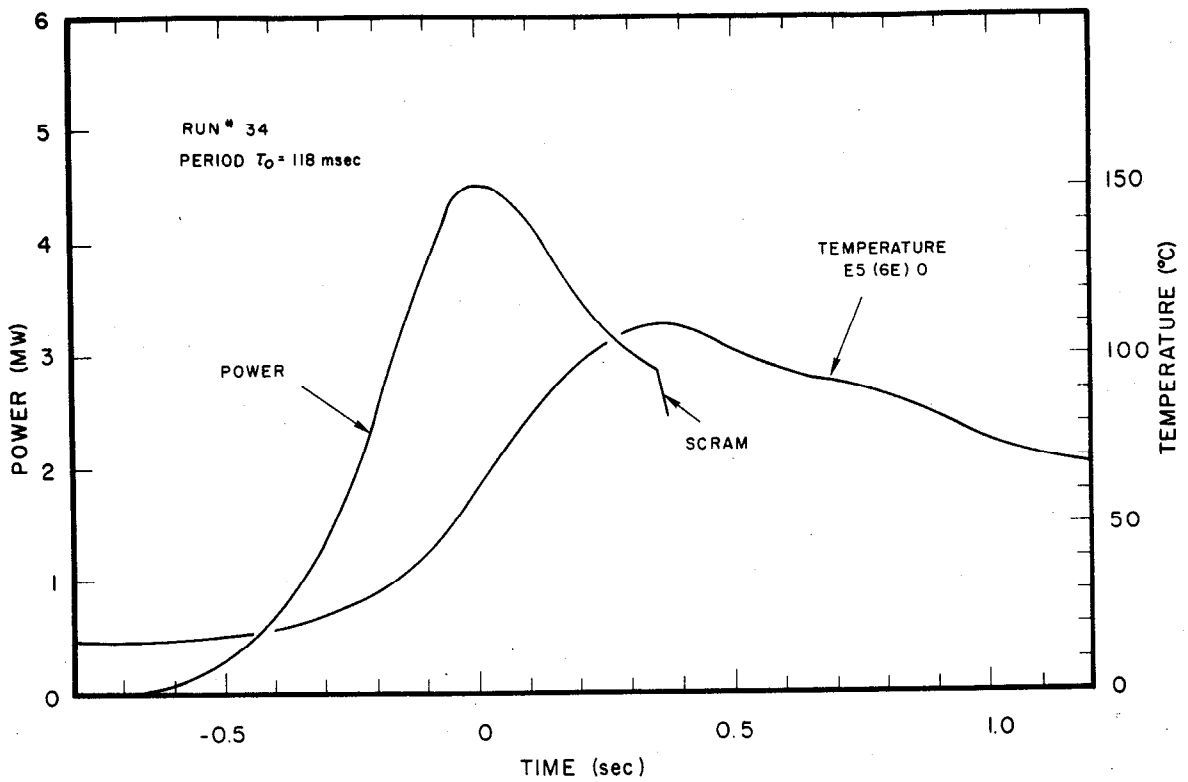
Fig. C-3. General behavior plot showing power and temperature for a 118-msec period transient test.
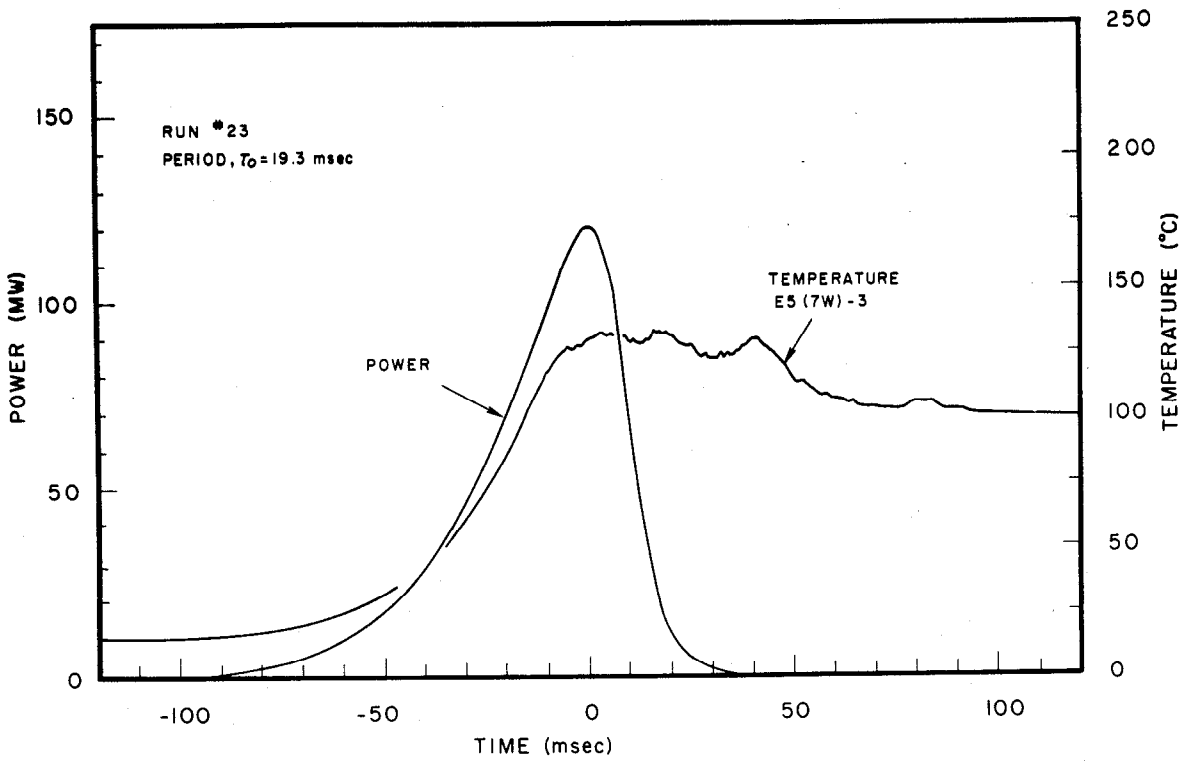

Fig. C-4 General behavior plot showing power and temperature for a 19.3-msec period transient test.

91
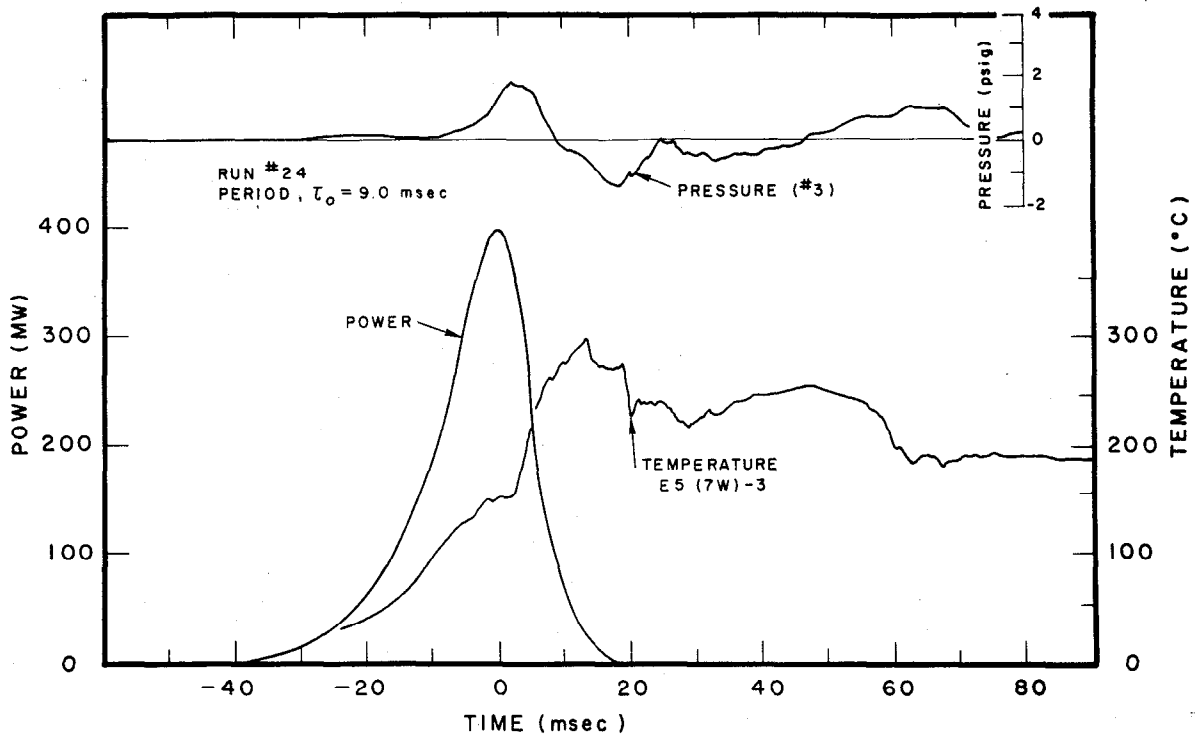
Fig. C-5 General behavior plot showing power, pressure, and temperature for a 9-msec period transient test.
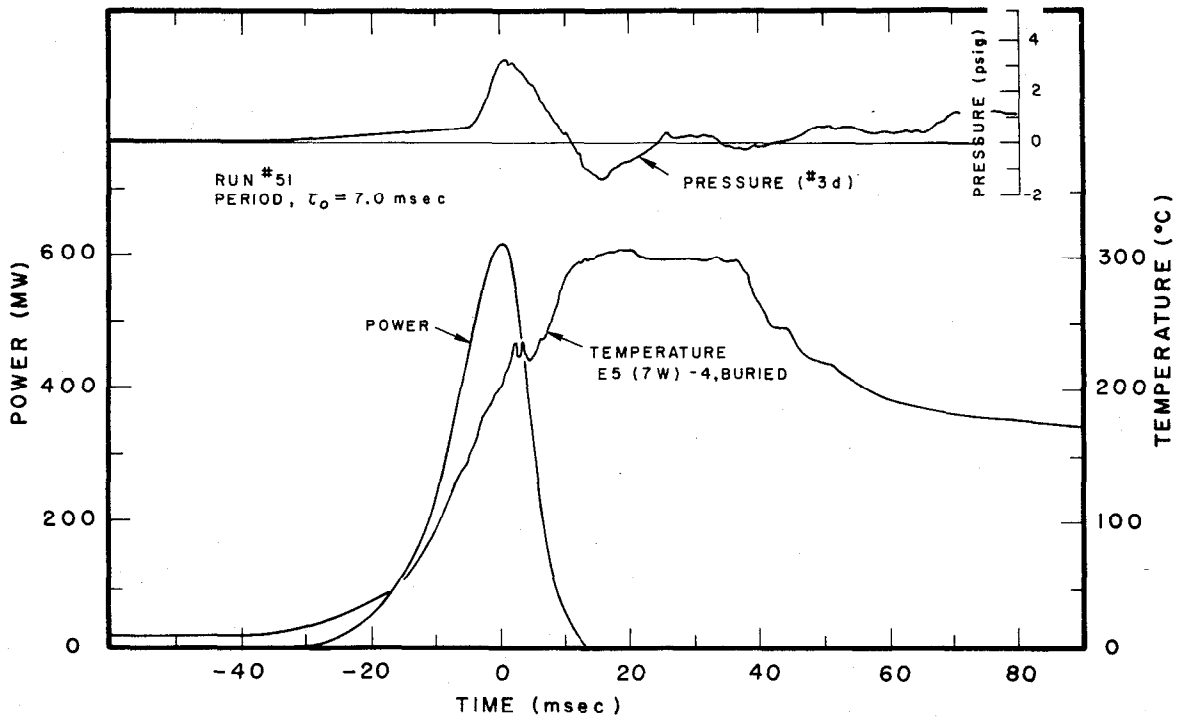
Fig. C-6 General behavior plot showing power, pressure, and temperature for a 7-msec period transient test.

92
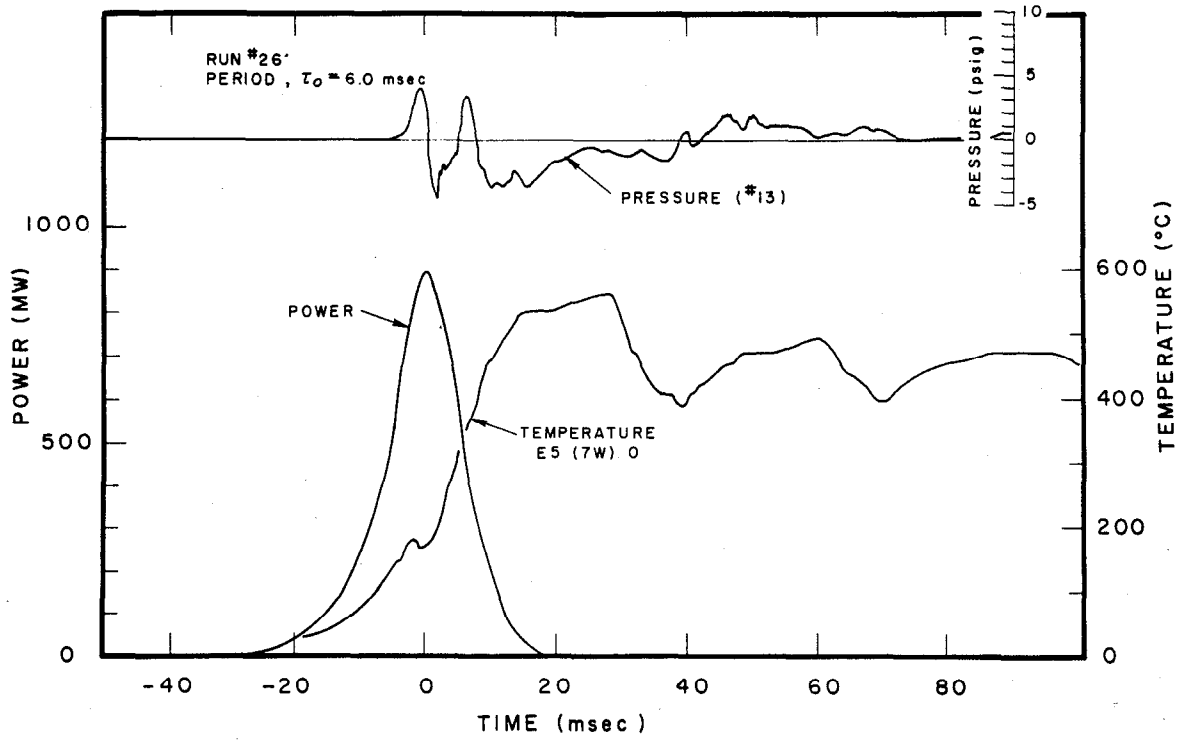
Fig. C-7 General behavior plot showing power, pressure, and temperature for a 6-msec period transient test.
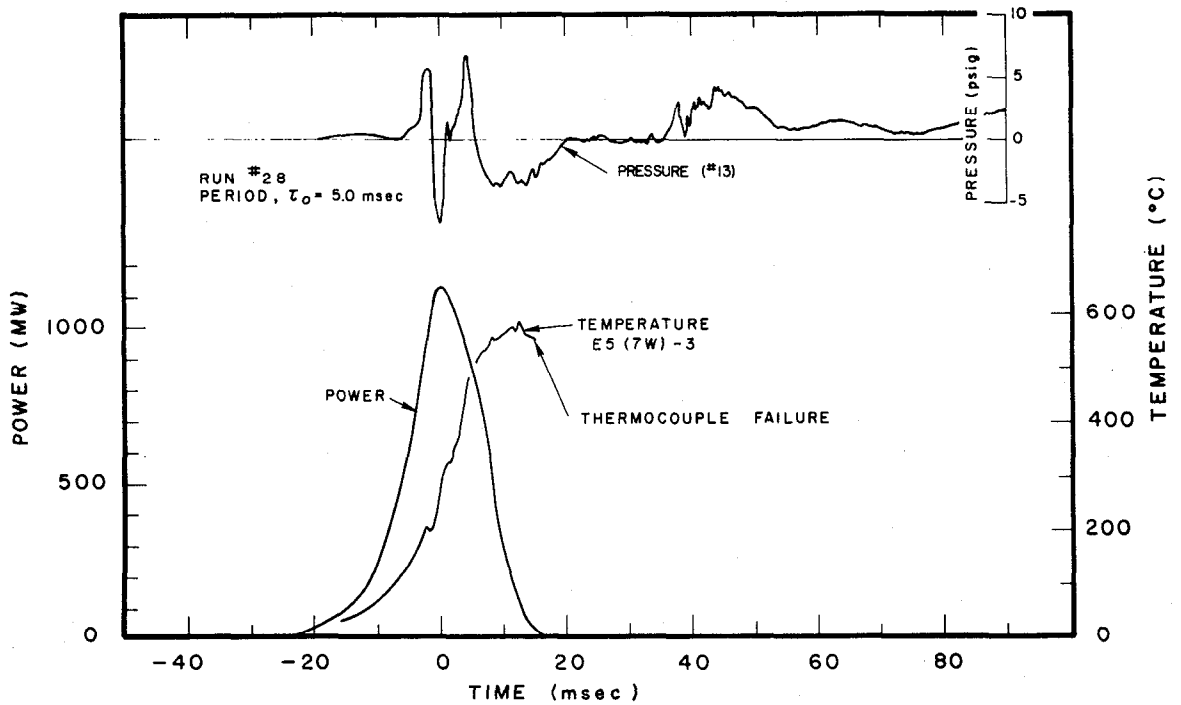
Fig. C-8 General behavior plot showing power, pressure, and temperature for a 5-msec period transient test.
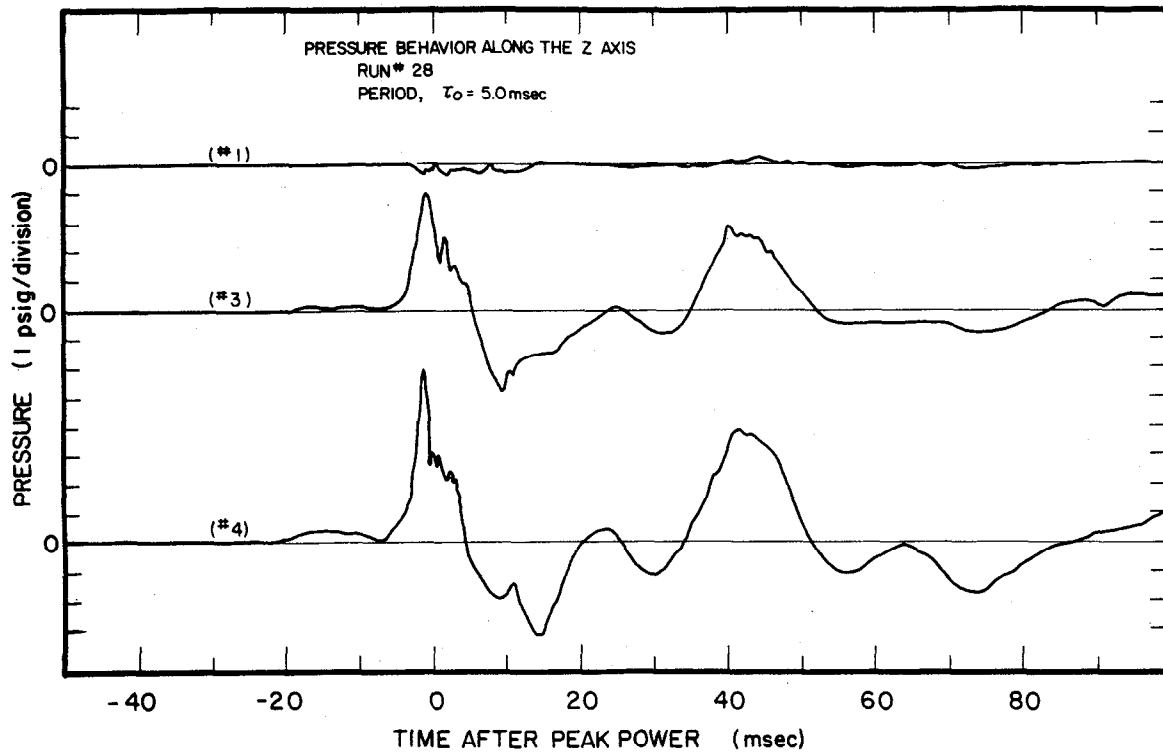
Fig. C-9 Vertical pressure profile showing pressure measured about five feet above the center of the core (#1), about two feet above the center of the core (#3), and 20 inches below the center of the core.
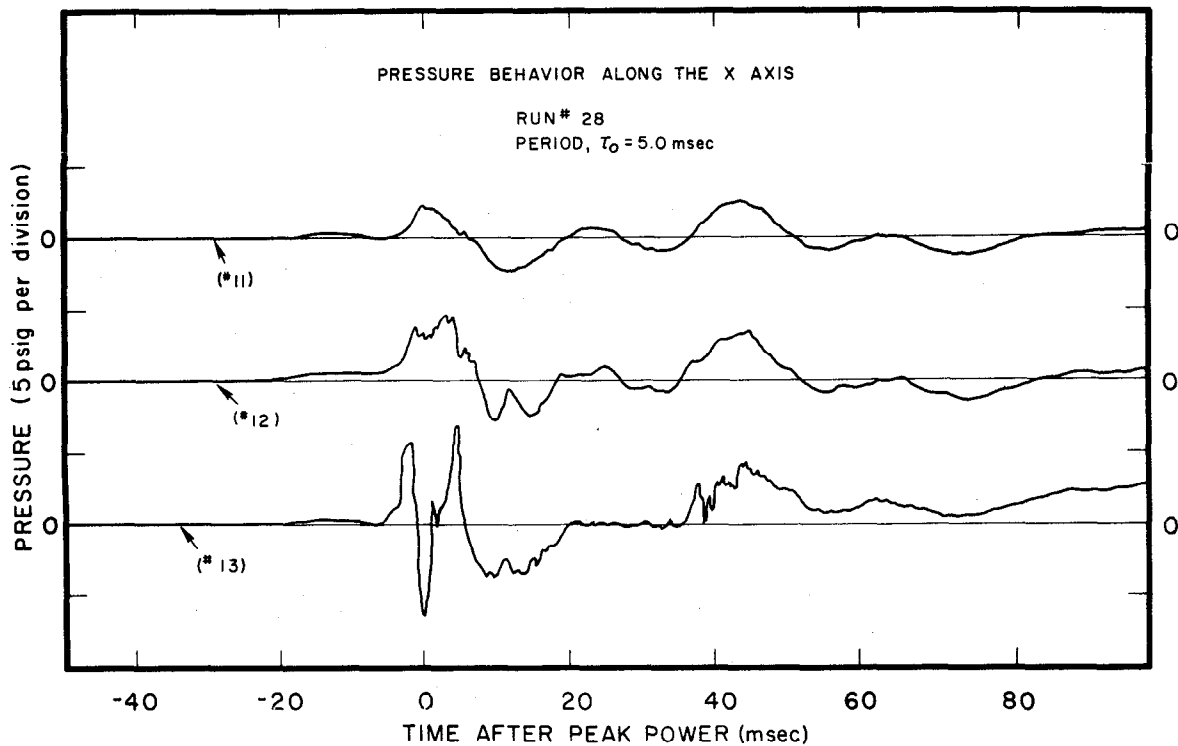
Fig. C-10 Horizontal pressure profile showing pressures measured respectively, 52 inches (#11), 35 inches (#12), and 17 inches (#13) horizontally from the core center.
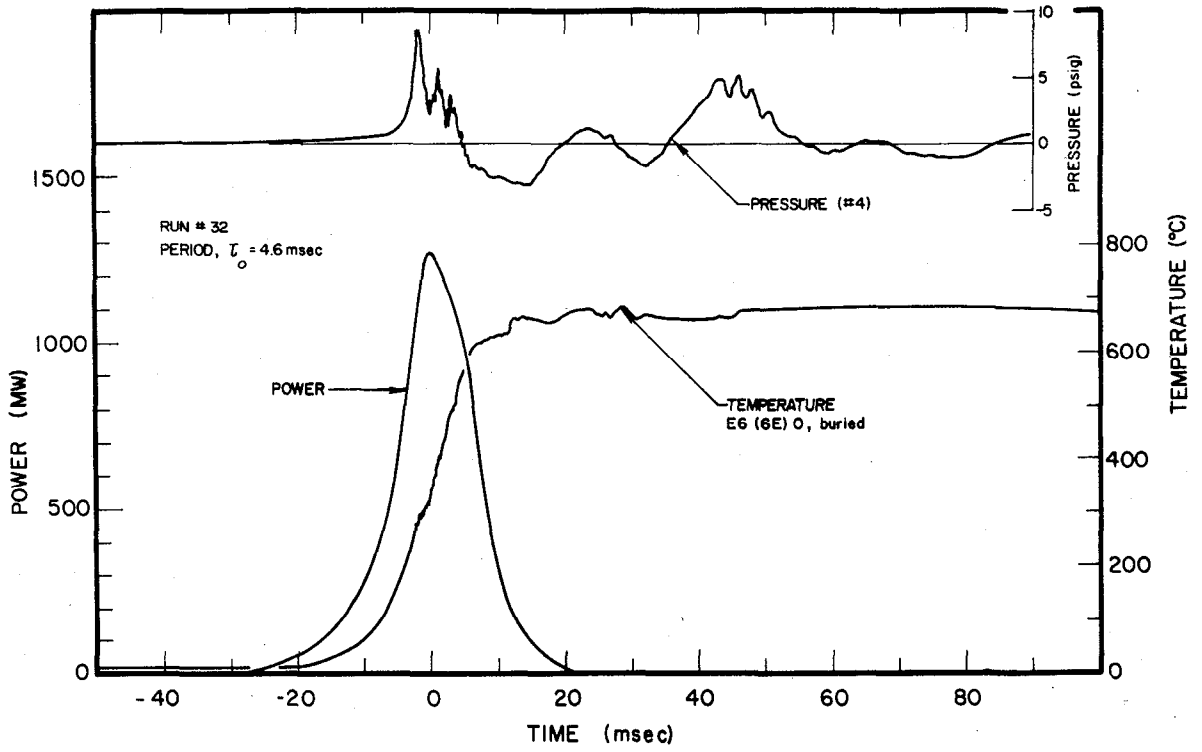
Fig. C-11 General behavior plot showing power, pressure, and temperature for a 4.6-msec period transient test.
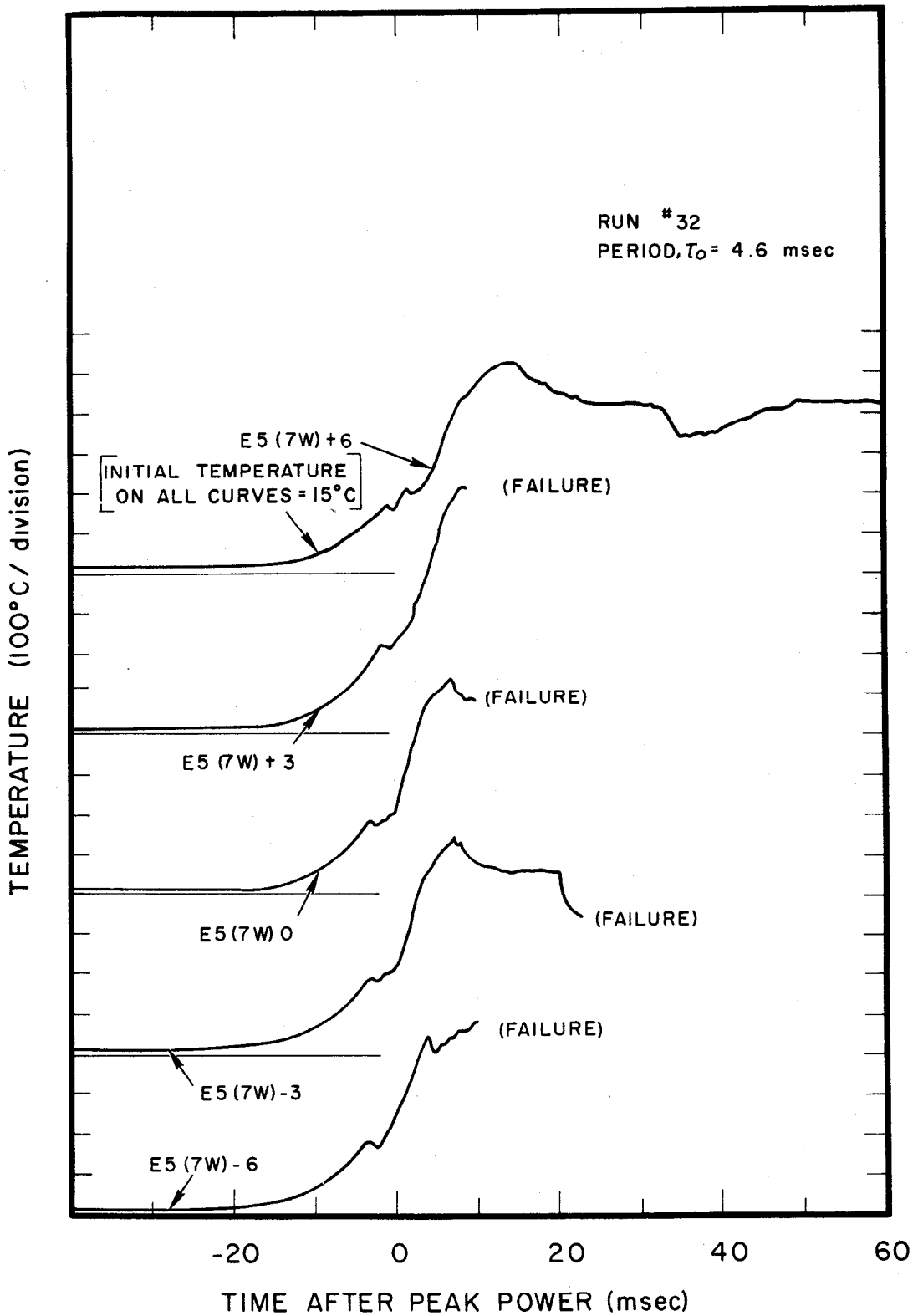
Fig. C-12 Vertical temperature profile measured on the west side of plate #7 in assembly E-5. The measurements were taken at the vertical center (z = 0) of the core and six inches and three inches above and below the vertical center by surface mounted thermocouples.

96

RUN #32
PERIOD, τ_o = 4.6 msec

[INITIAL TEMPERATURE
ON ALL CURVES = 15° C]

E5 (6E) 0, BURIED

THERMOCOUPLE FAILURE

E6 (7W) 0

D6(E6)0, BURIED

THERMOCOUPLE FAILURE

C7 (7W) 0
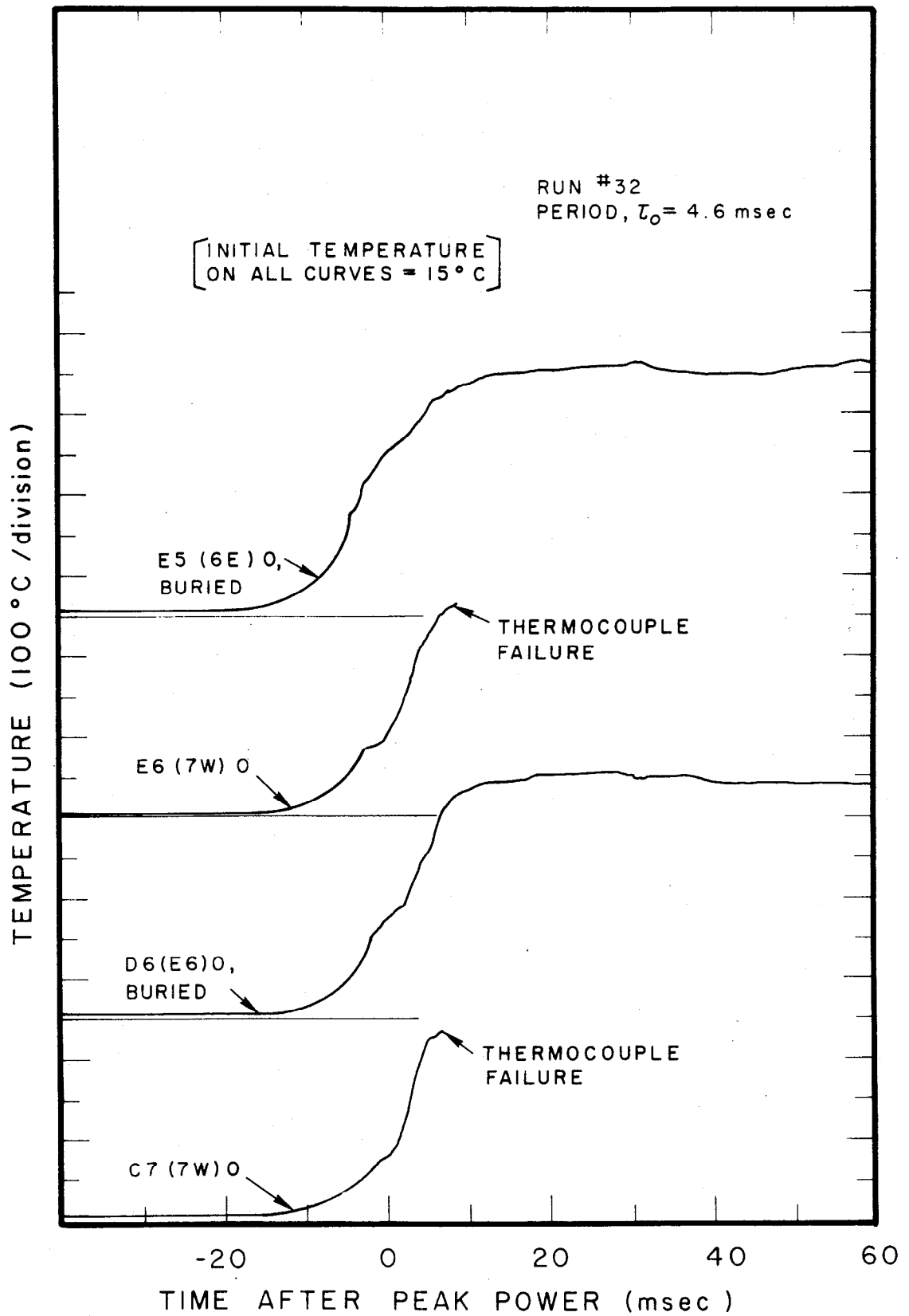
Fig. C-13 Horizontal temperature profile measured in the z = 0 plane.
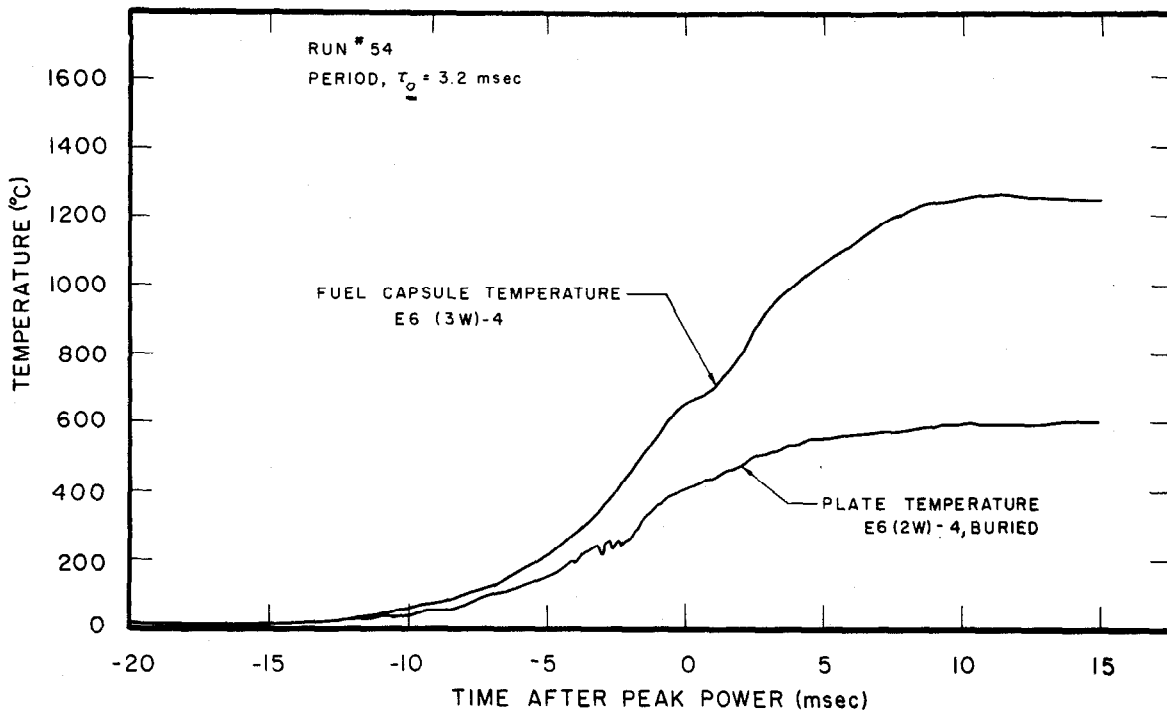
Fig. C-14 A comparison of fuel capsule and fuel plate temperatures during the destructive test.
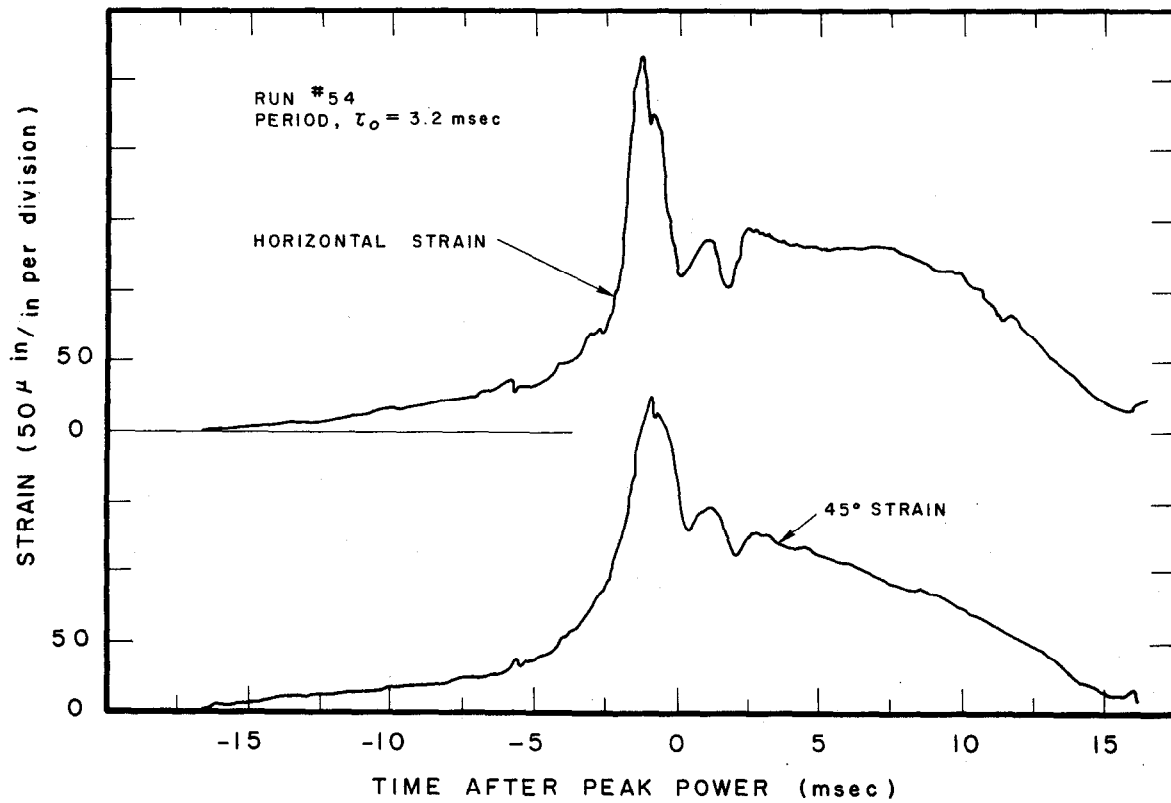
Fig. C-15 The strain response of the horizontal and 45° gauges of a rosette attached to the outside of a peripheral fuel assembly.

98

RUN #54, PERIOD, τ_o = 3.2 msec

E5 (7W)+ 8, buried

INITIAL TEMPERATURE
ON ALL CURVES =
15° C

E5 (7W) + 8

THERMOCOUPLE
FAILURE

E5 (7W) O

E5 (7W)-4, buried

TIME OF INITIAL
CORE DESTRUCTION

TEMPERATURE (100°C/division)

-15   -10   -5   0   5   10   15

TIME AFTER PEAK POWER (msec)
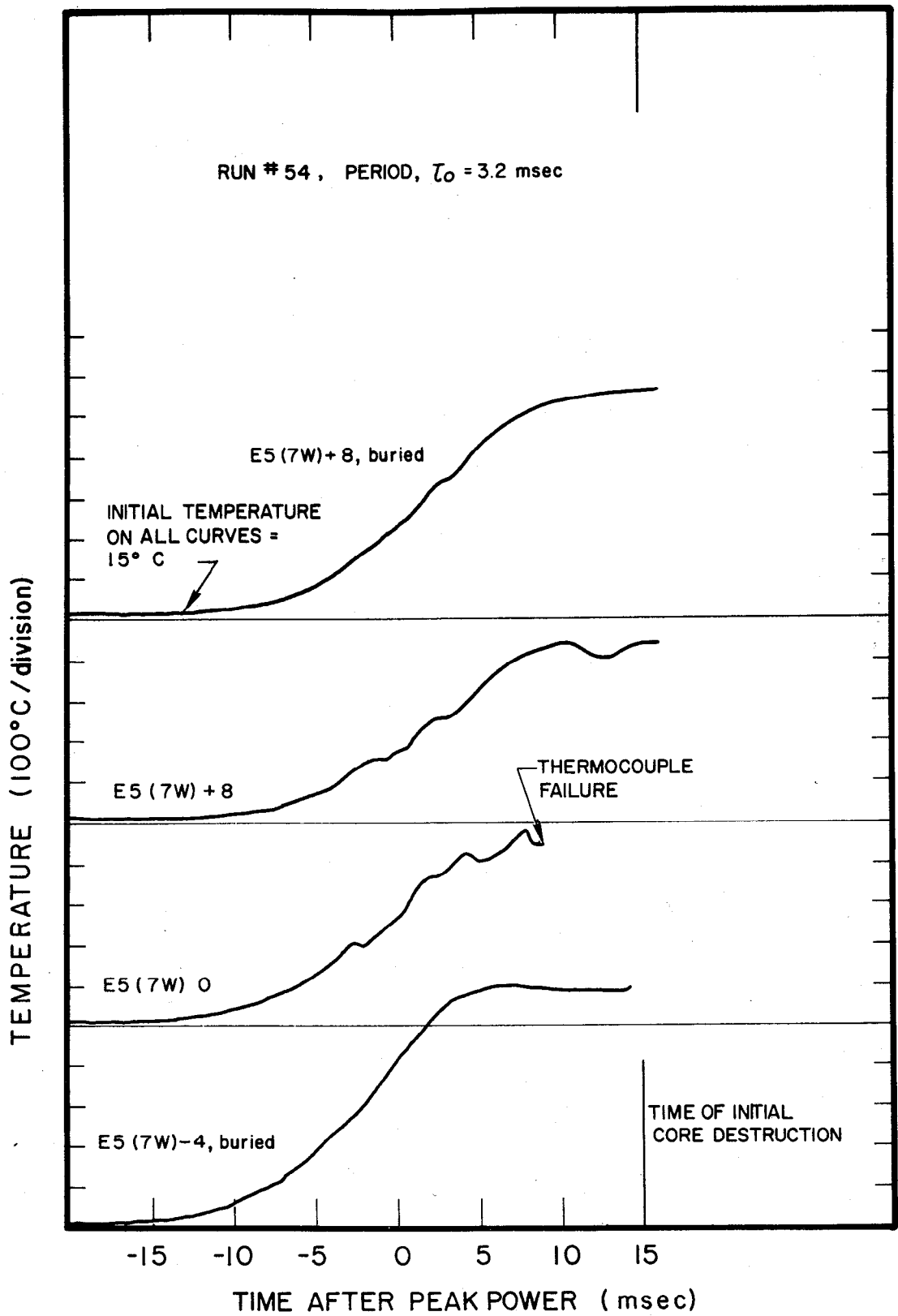
Fig. C-16 Temperatures measured on the west side of the plate #7, assembly E-5, during the destructive test.
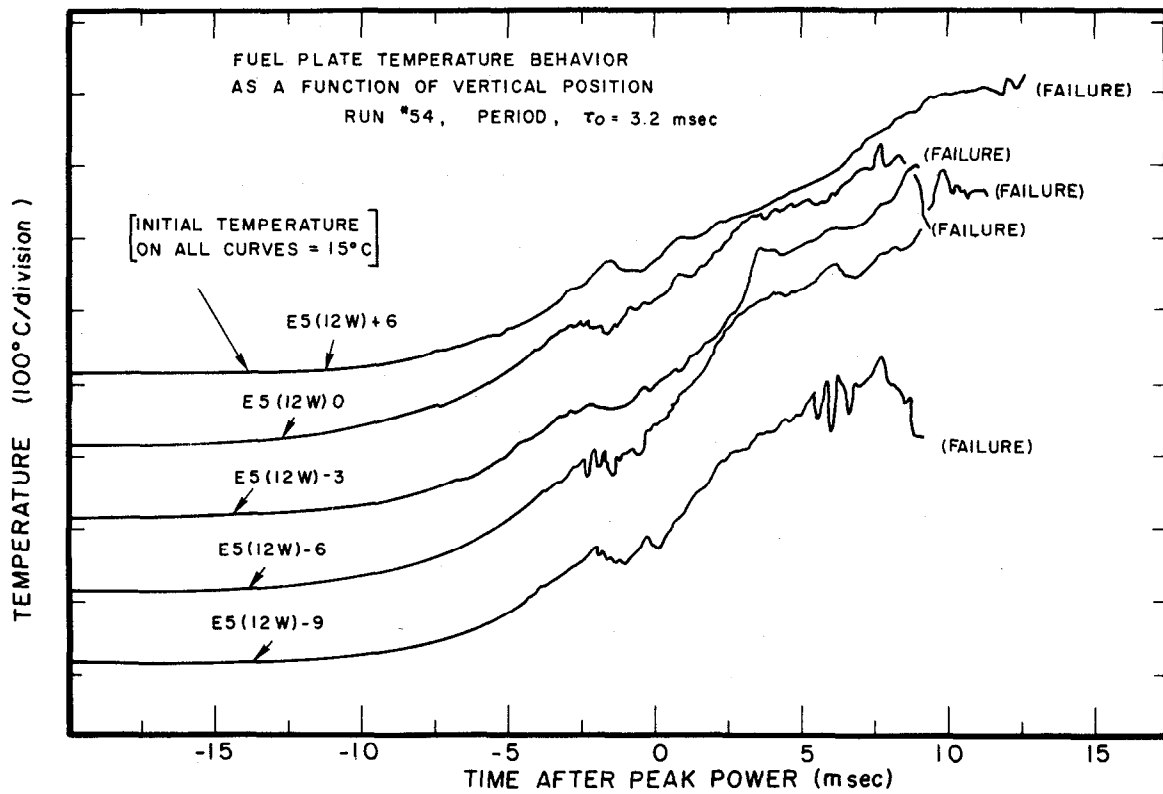
Fig. C-17 Vertical temperature profile as measured by surface-mounted thermocouples attached to the west side of plate #12, assembly E-5, during the destructive test.
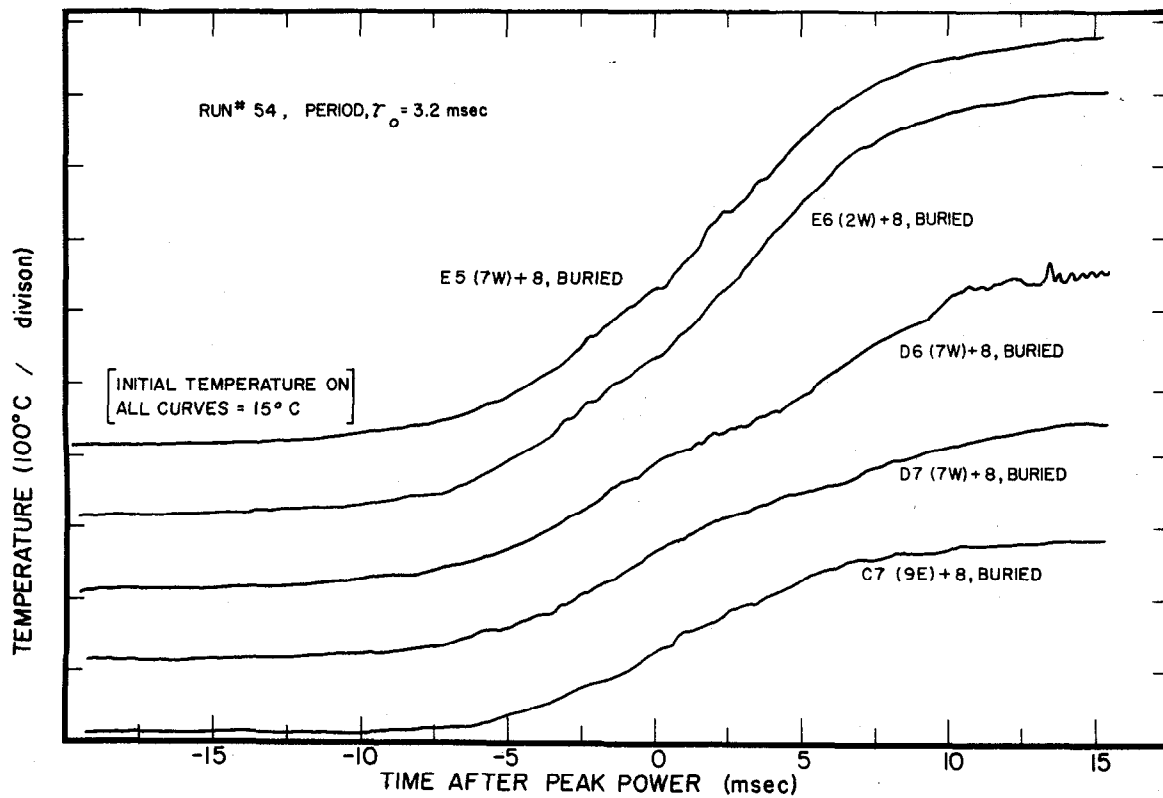
Fig. C-18 Horizontal temperature profile measured in the z = + 8 plane by buried thermocouples during the destructive test.
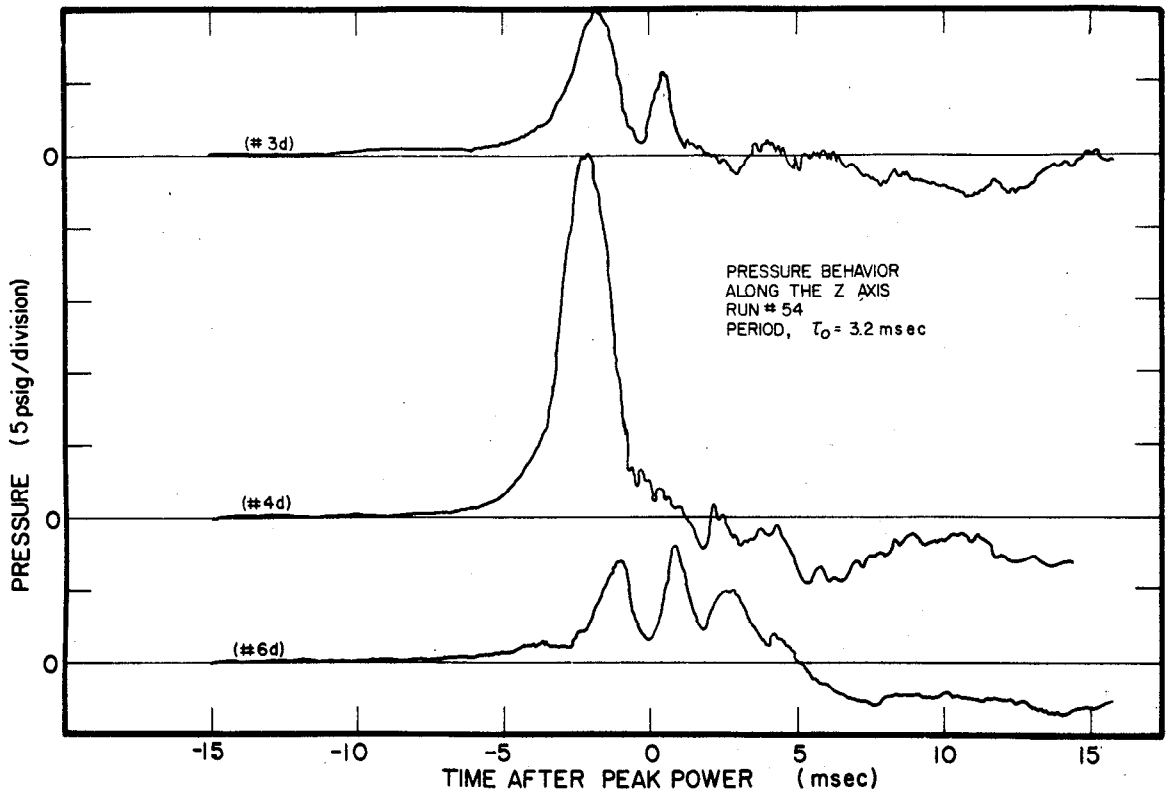
Fig. C-19 Pressure associated with moderator boiling as measured about 2 feet above the core center (#3 d), 20 inches below the core center (#4 d), and 53 inches below the core center (#6 d), during the destructive test.
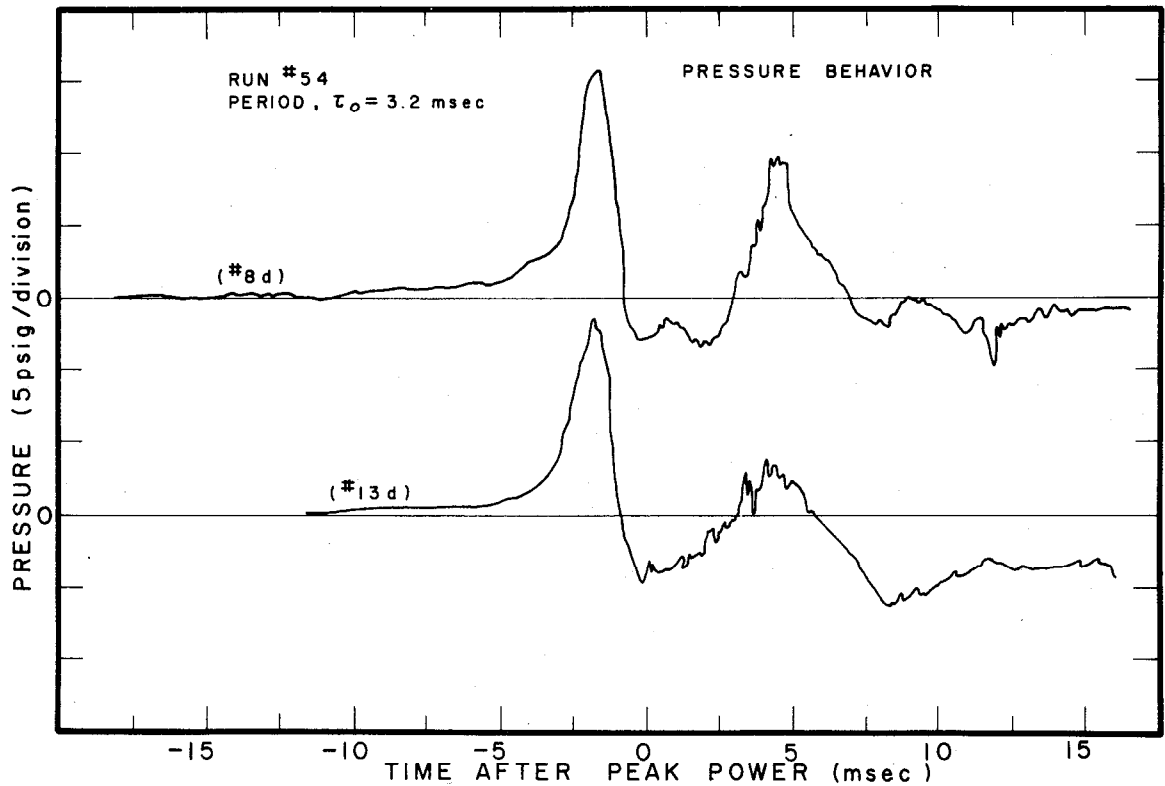
Fig. C-20 Pressure associated with moderator boiling as measured at the side of the core and 17 inches from the core center during the destructive test.
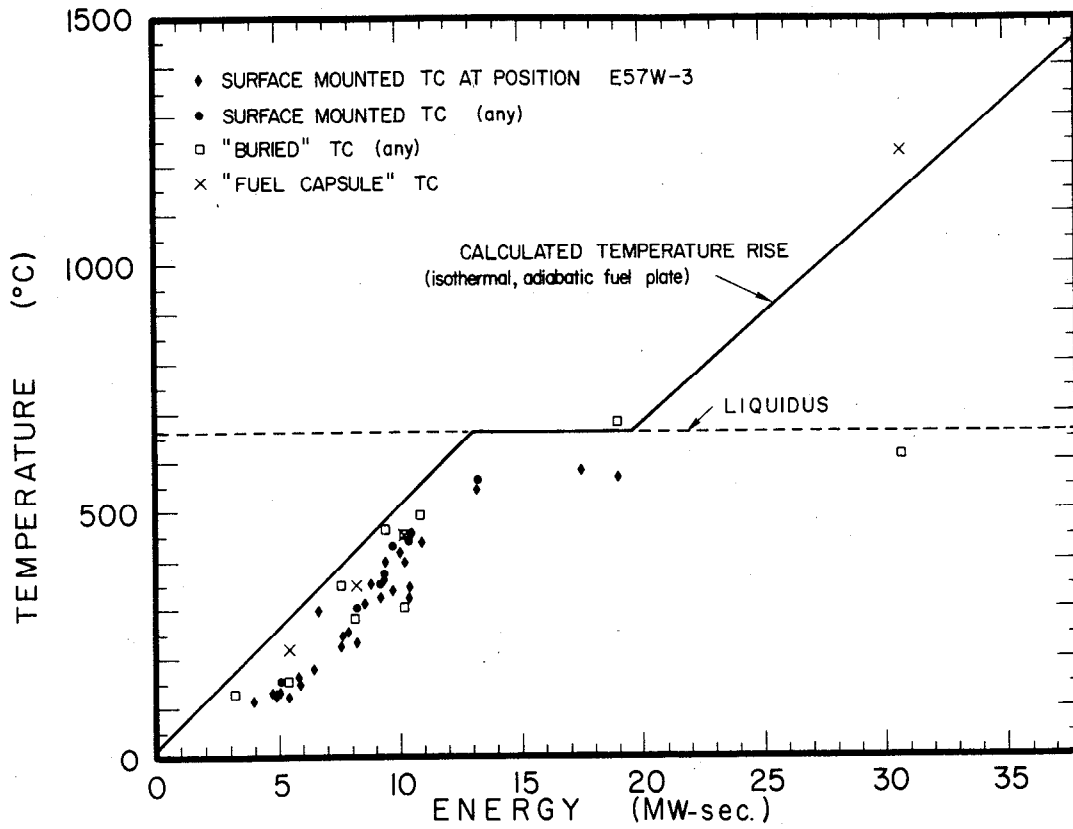
Fig. C-21 Maximum measured temperatures versus total energy release.
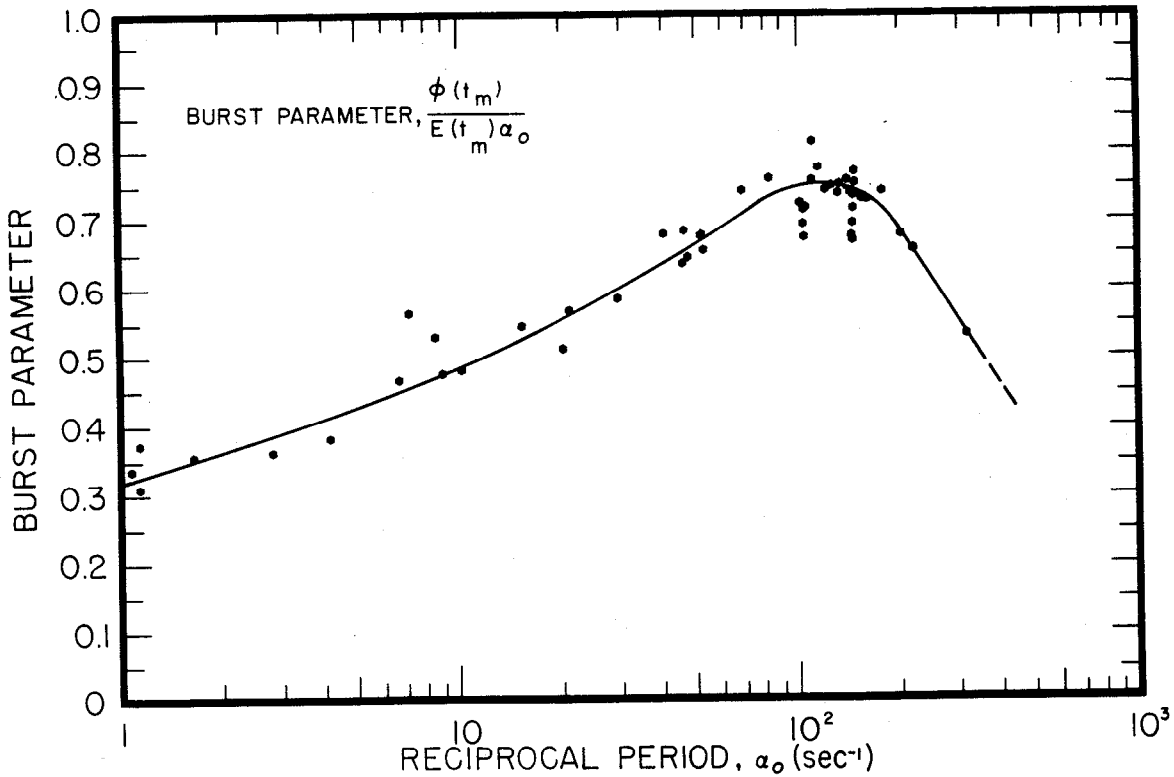
Fig. C-22 Burst parameter versus reciprocal period.

102

TABLE C-I

DATA SUMMARY - DESTRUCTIVE TEST SERIES

Run No.	τ_0 (msec)	α_0 (sec^{-1})	Δk_0 ($)	$\phi(t_m)$ (Mw)	$E(t_m)$ (Mw-sec)	E_T (Mw-sec)	$\theta(t_m)^*$ (°C)	θ_{max}^* (°C)	Date (1962)
									April
1	930	1.08	0.80	0.67	1.84	(d)	65(a)	89(a)	5
2	640	1.56	0.85	0.98	1.76	(d)	66	95	10
3	355	2.82	0.92	1.50	1.47	(d)	61	98	10
4	163	6.14	0.99	3.25	1.13	(d)	60	104 105(a)	10
5	98	10.2	1.05	6.60	1.34	(d)	73	110	11
6	65	15.4	1.10	14.2	1.68	(d)	92 93(a)	115	11
7	47	21.3	1.16	27.5	2.25	3.95	110	117	11
8	34	29.4	1.23	50.0	2.90	4.90	122	124	11
9	25	40.0	1.32	87.0	3.20	4.90	130	132	12
10	19	53	1.42	141	4.05	5.85	145	150	12
11	14.5	69	1.56	210	4.10	5.80	156 164(a)	165	12
12	12.1	83	1.67	290	4.60	6.45	166	180	12
13	9.8	102	1.80	380	5.15	7.55	180	227	12
14	9.5	105	1.85	430	5.70	7.85	188	255	13
15	8.2	122	1.99	530	5.85	8.55	181	315	16
16	7.2	139	2.13	630	6.00	9.32	181	360 375(a)	17
17	6.9	145	2.18	690	6.45	10.2	174 203(a)	400	17
18	6.8	147	2.20	685	6.05	10.00	188 198(a)	420	19
19	6.4	156	2.27	745	6.60	10.5	176 198(a)	455	19
									May
22	880	1.14	0.81	0.98	(d)	(d)	54(a)	94(a)	10
23	19.3	52	1.42	120	3.40	4.70	125	132	10
24	9.0	111	1.90	395	4.70	7.10	157	300	10
25	7.5	133	2.08	555	5.55	8.80	158	355	11
26	6.0	167	2.36	890	7.20	13.2	185 210(a)	545 560(a)	11
27	8.1	124	2.00	505	5.45	9.20	177	325	16
28	5.0	200	2.63	1130	8.35	17.5	320	585	18
									June
29	49.5	20.2	1.13	19.1	1.84	3.20	125(b)	129(b)	6
30	7.6	132	2.03	510	5.20	9.40	172 250(b)	400 465(b)	6
31	6.9	145	2.14	620	6.40	10.9	190 290(b)	440 490(b)	8
32	4.6	218	2.72	1270	8.90	19.0	240 420(b)	570 680(b)	11
									July
33	330	1.14	0.81	0.76	1.79	(d)	64(b)	94(b)	23
34	118	8.48	1.03	4.50	1.00	(d)	59 67(b)	102 109(b)	24
35	21.7	46.1	1.37	107	3.40	5.05	125 149(b)	128 155(b)	24
36	8.9	112	1.91	460	5.05	7.65	151 230(b)	242 350(b)	26
37	880	1.14	0.81	0.78	2.21	(d)	69(b)	87(b)	26
38	112	8.93	1.03	5.05	1.18	(d)	63 68(b)	99 117(b)	26
39	22.4	45.8	1.35	105	3.60	5.40	120 146(b)	124 154(b)	27
40	8.7	115	1.93	470	5.25	8.20	167 216(b)	234 305(b)	27
41	6.8	147	2.20	635	5.75	9.20	232(b)	355(b)	30
42	6.9	145	2.18	640	6.00	9.70	156 246(b)	340 430(b)	31
									August
43	6.9	145	2.18	660	6.35	10.4	160 243(b)	340 440(b)	1
44	6.9	145	2.18	665	6.60	10.4	161 250(b)	325 440(b)	2
									October
46	1310	0.76	0.75	0.39	1.49	(d)	65(b)	80(b)	18
47	243	4.12	0.95	1.43	0.91	(d)	61(a)	93(a)	19
48	140	7.14	1.02	3.80	0.94	(d)	62(a)	112(a)	22
49	21.1	47.4	1.38	110	3.60	5.40	148(b)	153(b) 220(c)	22
50	9.6	104	1.85	350	5.00	7.15	195(b)	232(b) 350(c)	22
51	7.0	143	2.16	620	6.45	10.2	223(b)	305(b) 455(c)	22
52	9.6	104	1.85	380	5.10	7.25	208(b)	229(b) 360(c)	24
53	9.7	103	1.84	360	5.05	7.45	204(b)	234(b) 350(c)	24
									November
54	3.2	313	3.55	2250	13.8	30.7	430(b)	615(b) 1230(c)	5

* Surface temperature measured at E5 (7W)-3.
(a) Highest surface temperature measured at a position other than E5 (7W)-3.
(b) Temperature measured using "buried" thermocouple (see Appendix B).
(c) Maximum temperature measured using special "fuel cell" thermocouple.
(d) Total energy undefined due to absence at long periods of a distinct power cutoff.

APPENDIX D

MELTDOWN DATA

# APPENDIX D

MELTDOWN DATA

Melting of fuel plates occurred for three of the power excursion tests conducted in the exploratory and destructive test series, with periods respectively of 5.0, 4.6, and 3.2 msec.

In the 5-msec period excursion test, melting occurred in seven fuel plates over a region about six inches high in the center of the core and involved about 0.5 percent of the total fuel plate area of the core. Photographs of several of the damaged fuel plates from this test have been shown previously in Figures 16 through 22. Figure D-1 is a cross section drawing of the Spert I core showing the radial distribution of the melted regions for this test. Figure D-2 shows the vertical distribution of the melted regions of the plates.

In the 4.6-msec period test, melting was obtained in 52 of the 270 fuel plates of the core, involving about two percent of the total fuel plate surface area of the core. Photographs of melted fuel plates from this test were shown previously in Figures 23 through 28. Figure D-3 is a cross section drawing of the Spert I core showing the radial distribution of the melted regions for this test. Figure D-4 shows the vertical melt pattern for each of the assemblies in which melting occurred.

In the 3.2-msec period destructive test, all of the 270 fuel plates in the core experienced melting to some degree. Figure 39 shows the top portions of typical fuel plates recovered from the reactor vessel. The unfueled edges of the plates can be seen still attached to the upper portions of the plates. The vertical pattern of fuel plate meltdown for the destructive test is shown in Figure D-5 for those recovered portions of the fuel plate which could be identified. The remaining pieces of fuel plates which were recovered, but which could not be identified as to position in the core, represent about 19 weight percent of the recovered plates. In Figure D-5 the vertical melt pattern is shown for each fuel plate of each assembly with the assemblies arranged in the appropriate positions of a horizontal cross section drawing of the core. The melt pattern was symmetrical about the central fuel assembly, which showed the largest amount of melting (approximately 78 weight percent). The damaged fuel assembly from core position G6 is shown in Figure 38. This assembly was recovered relatively intact and was cut open for disassembly before the photograph was taken. It can be seen that much of the melted region of the plates is missing but that most of the unmelted upper and lower ends of the plates are still connected by the unfueled edges.

The fuel plates of two of the corner assemblies (C3 and G7) remained in place even though the central portion of the plates was sometimes melted. The fuel plates from one of these two corner assemblies is shown in Figure E-1. The central portions of the plates were observed to crumble and flake easily.

Fig. D-1 Cross section drawing of the core showing distribution of melted regions on fuel plates after 5.0-msec test.

Fig. D-2 Vertical drawing of assemblies showing melted regions on fuel plates after 5.0-msec test.

Fig. D-3 Cross section drawing of the core showing distribution of melted regions on fuel plates after 4.6-msec test.
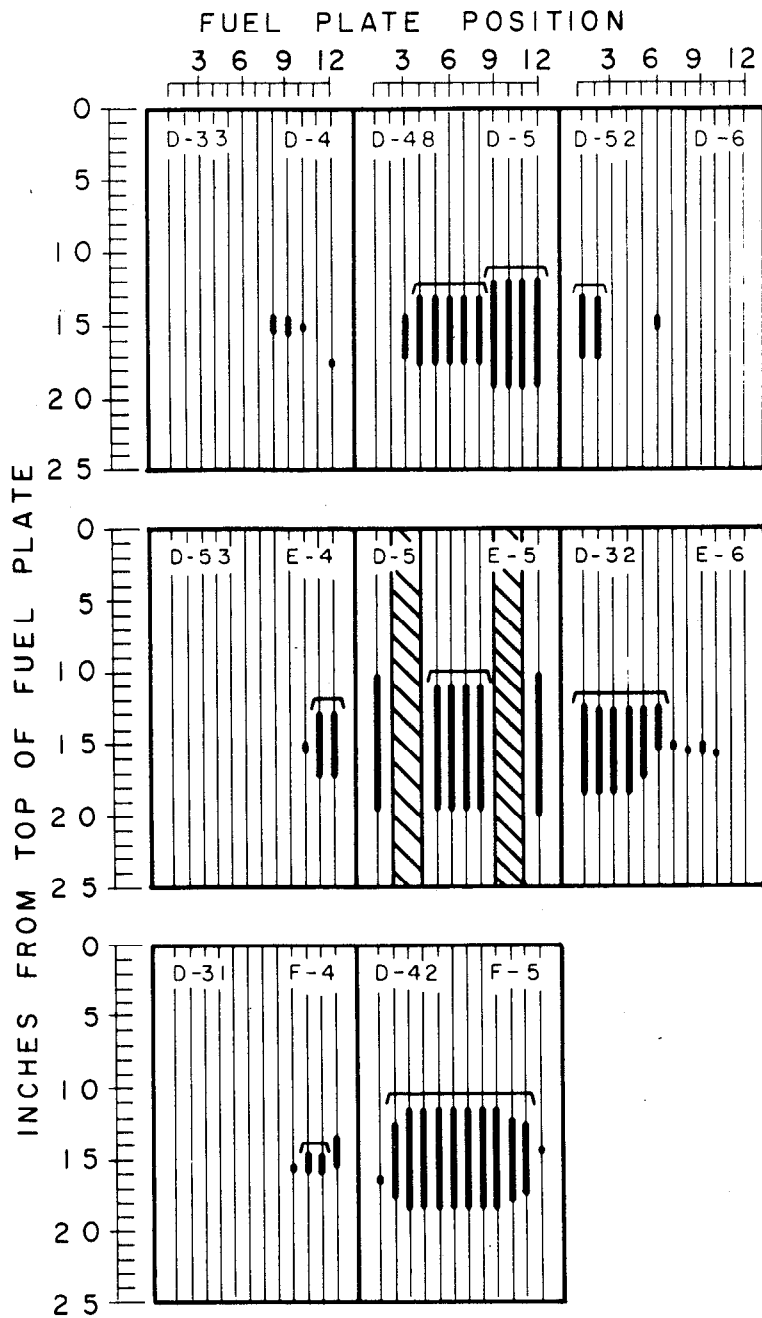
Fig. D-4 Vertical drawing of assemblies showing melted regions on fuel plates after 4.6-msec test.

111
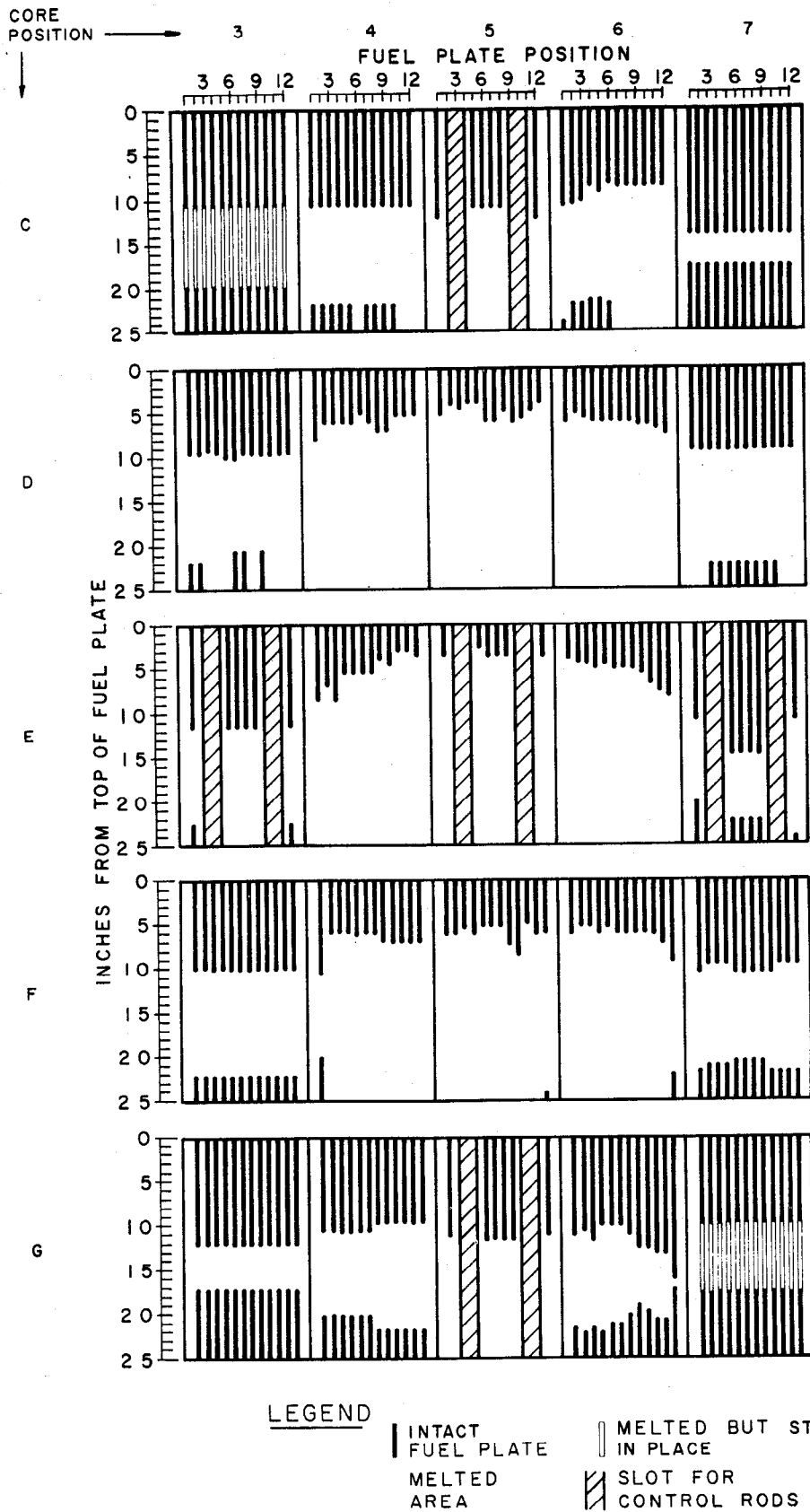
Fig. D-5 Vertical drawing of assemblies showing melted and disassembled regions of fuel plates after destructive test.

APPENDIX E

SUPPLEMENTARY PHOTOGRAPHS OF DESTRUCTIVE TEST RESULTS

APPENDIX E

SUPPLEMENTARY PHOTOGRAPHS OF DESTRUCTIVE TEST RESULTS

To further illustrate items which may be of interest, Figures E-1 through E-12 are included here as a supplement to Figures 30 through 44.

Figures E-13 through E-28 are selected frames from a motion picture taken of the destructive test by camera No. 6 (Table B-III). The camera was operating at about 24 frames per second and was located approximately 100 yards from the reactor building. The approximate time in milliseconds after peak power is indicated for each picture. The pictures shown are not necessarily successive frames.

Figures E-29 through E-44 are selected frames from a motion picture taken from the rear of the reactor building. The pictures shown are not necessarily successive frames. The camera was operating at approximately 600 frames per second, and the time after peak power is indicated for each picture.

The first motion observed in the motion picture is that of the floor as it is depressed around the lip of the vessel. (This motion is quite easily observed in motion projection but is difficult to see in individual pictures and, therefore, has not been included here.) Immediately following this, both periscopes (the large black tubes extending out of the vessel at the left and at the center) are observed to suddenly rise out of the vessel between t = 57 and t = 70 msec. Water finally emerges above floor level at about t = 70 msec.

Figures E-45 through E-60 are selected frames from a motion picture taken of the destructive test by camera No. 5 which was located approximately 50 feet southeast of the reactor building.
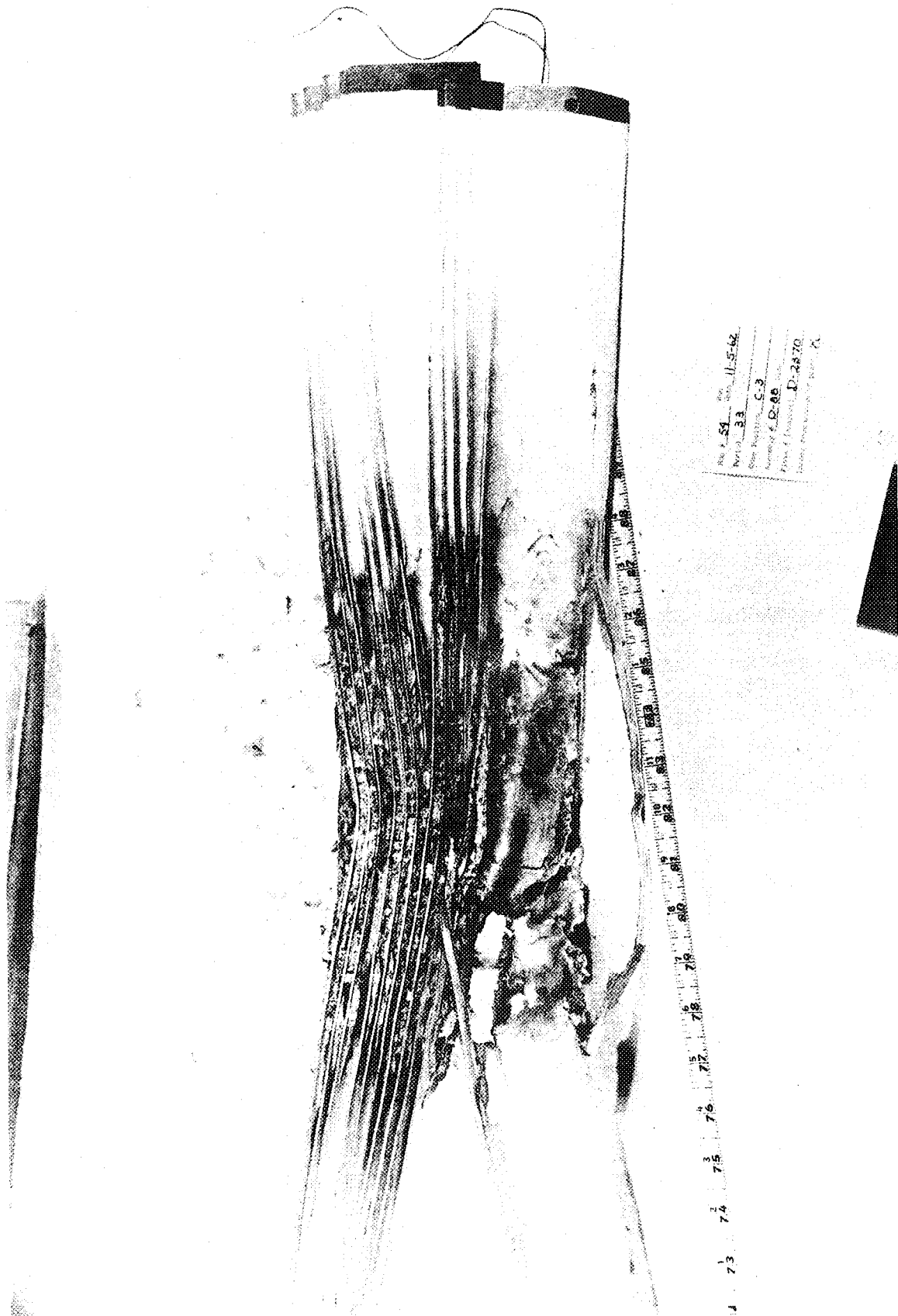
Fig. E-1 Fuel plates recovered from position C3 -- one of the two corners of the core in which the melted portions of the plates were relatively undisturbed. A cobalt wire used for integrated flux measurements is seen at the top.
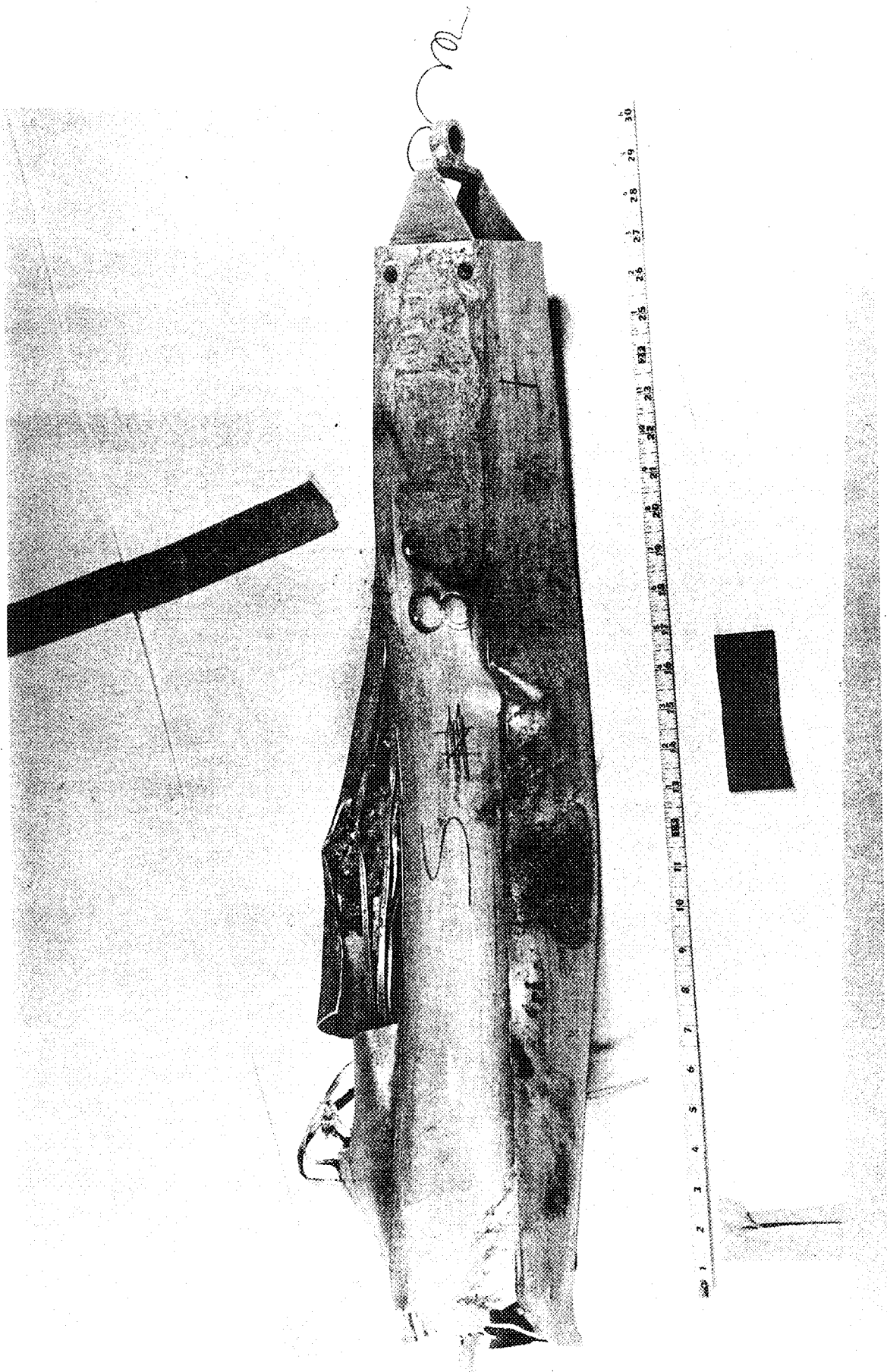
Fig. E-2 Assembly from position C4.

117
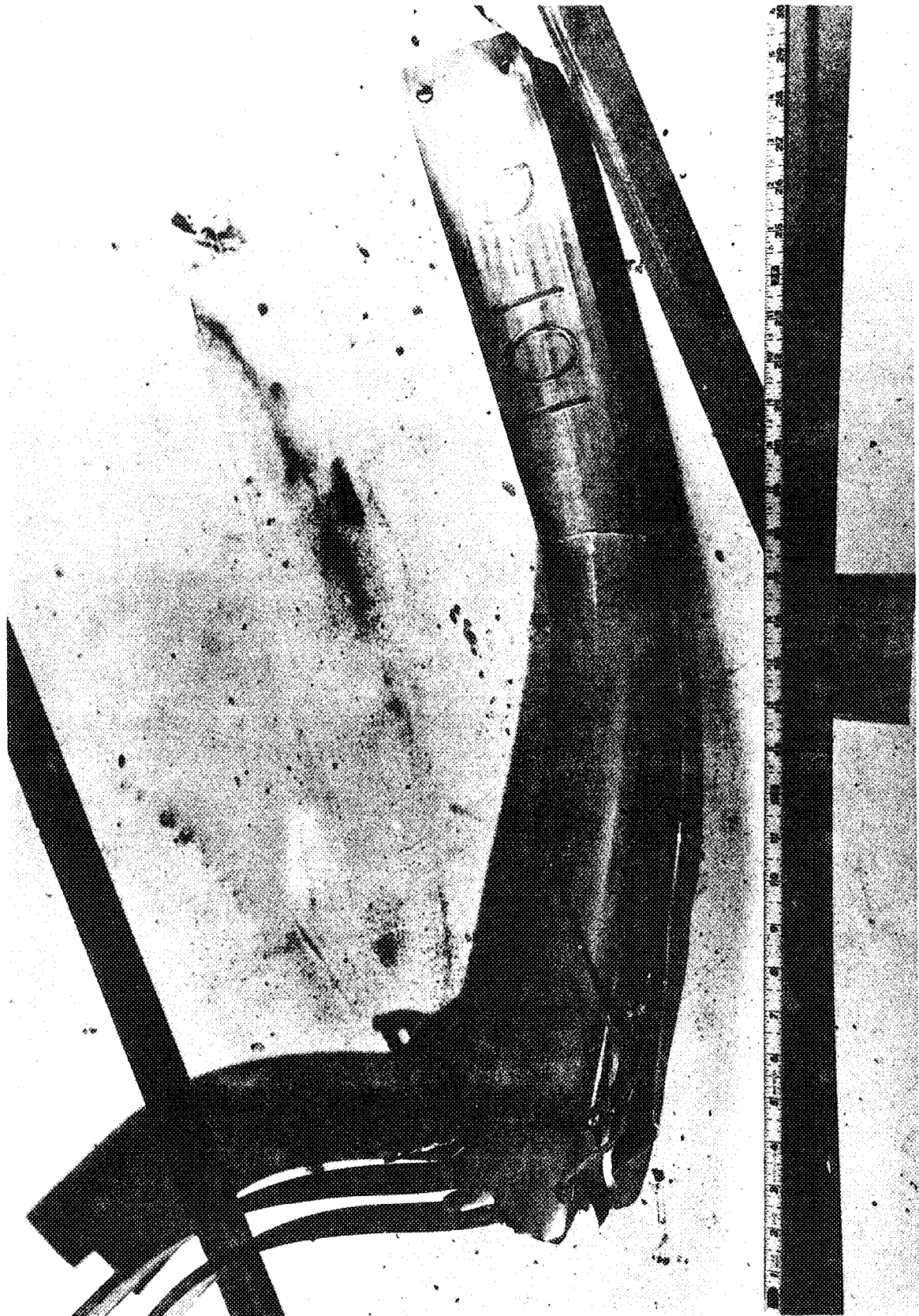
Fig. E-3 Control rod bearing assembly from position E7. Upper part of control blades has been broken away. Lower blade extensions can be seen emerging from the bottom of the assembly.
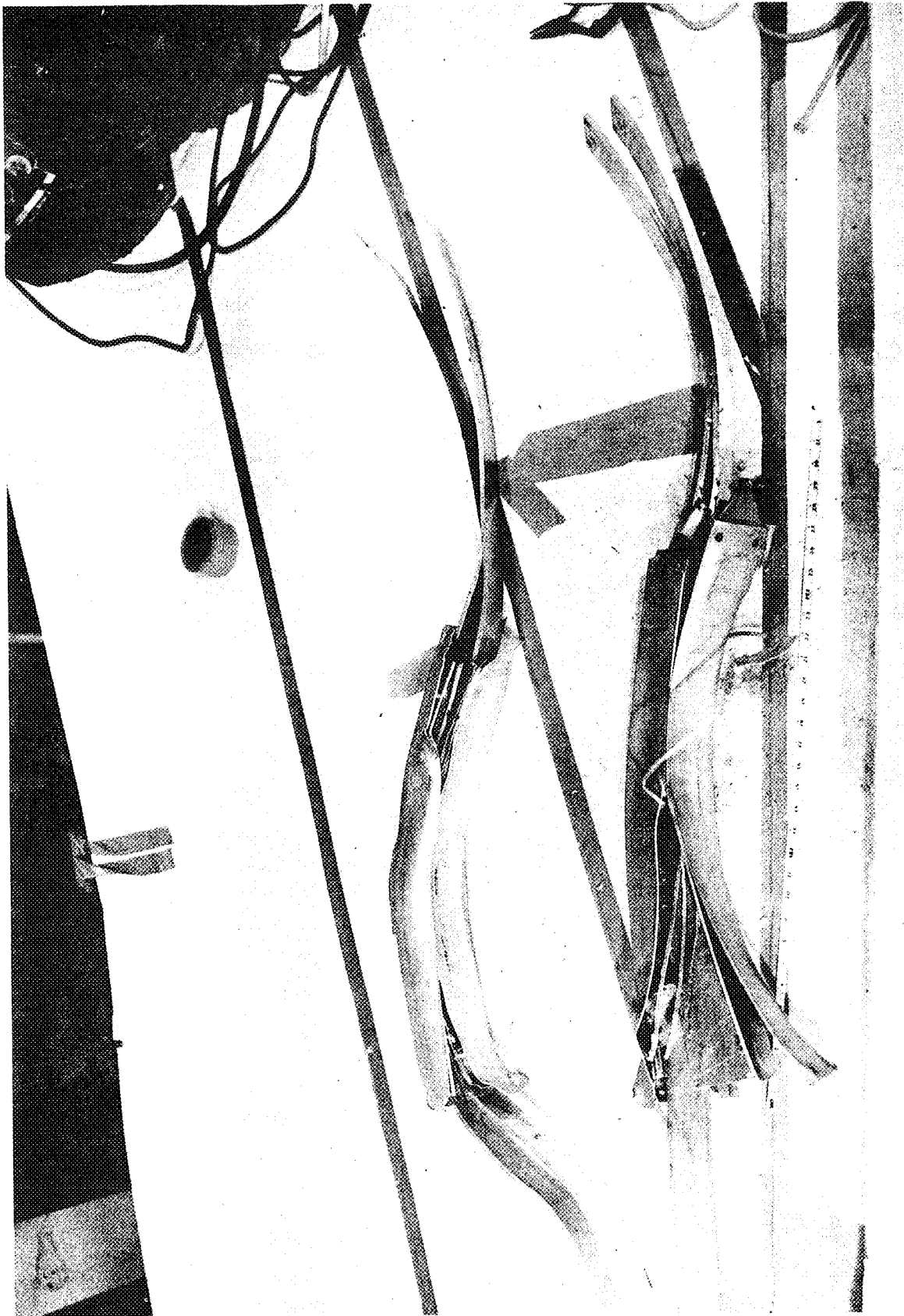
Fig. E-4 Control rod bearing assemblies from core positions G5 (left) and E3 (right).
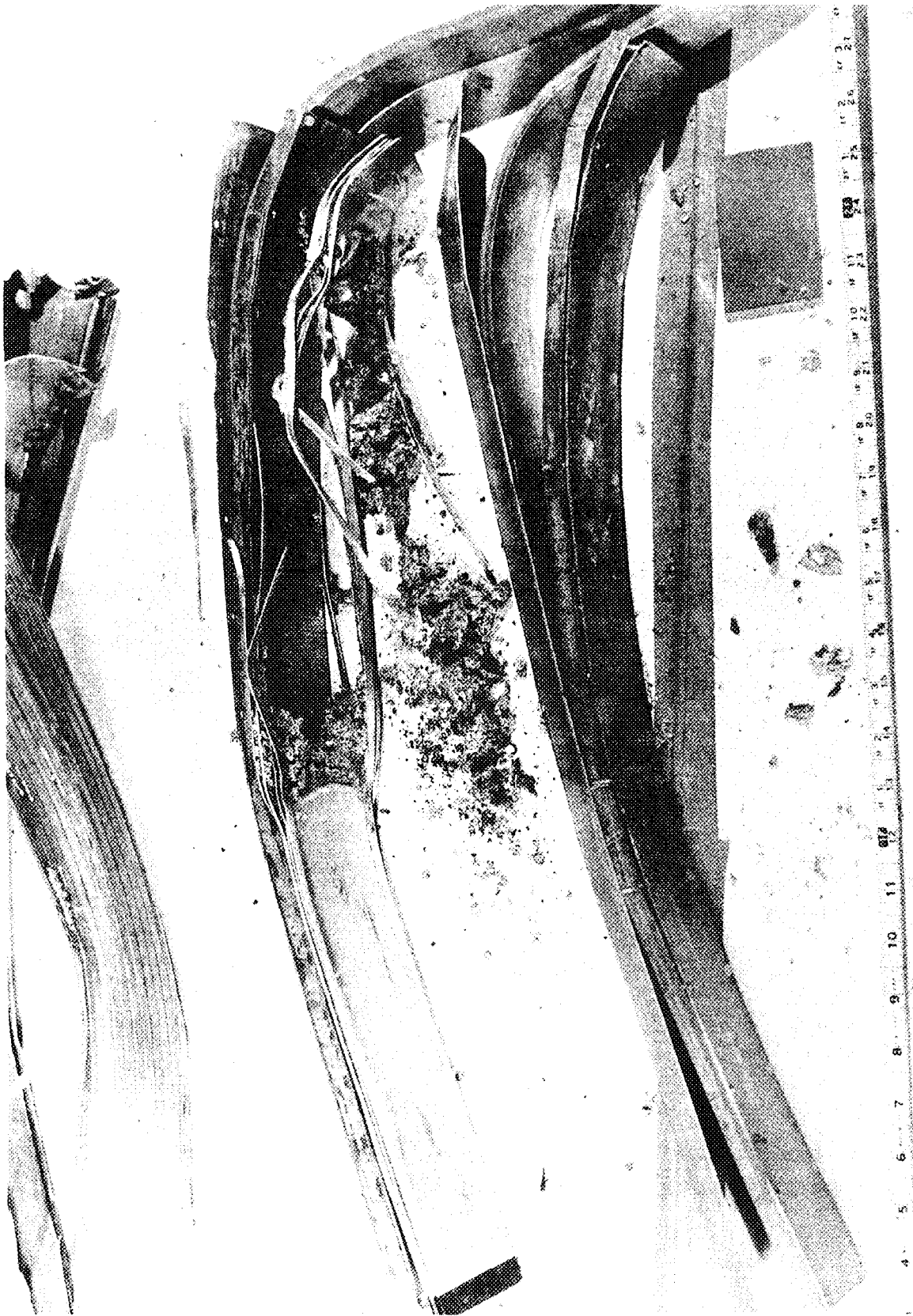
Fig. E-5 Control rod bearing assembly from position E7 after being opened for inspection. About half of the four fuel plates contained between the blades was melted and fragmented. The debris is typical of the material (in excess of 20 kilograms) collected.

120
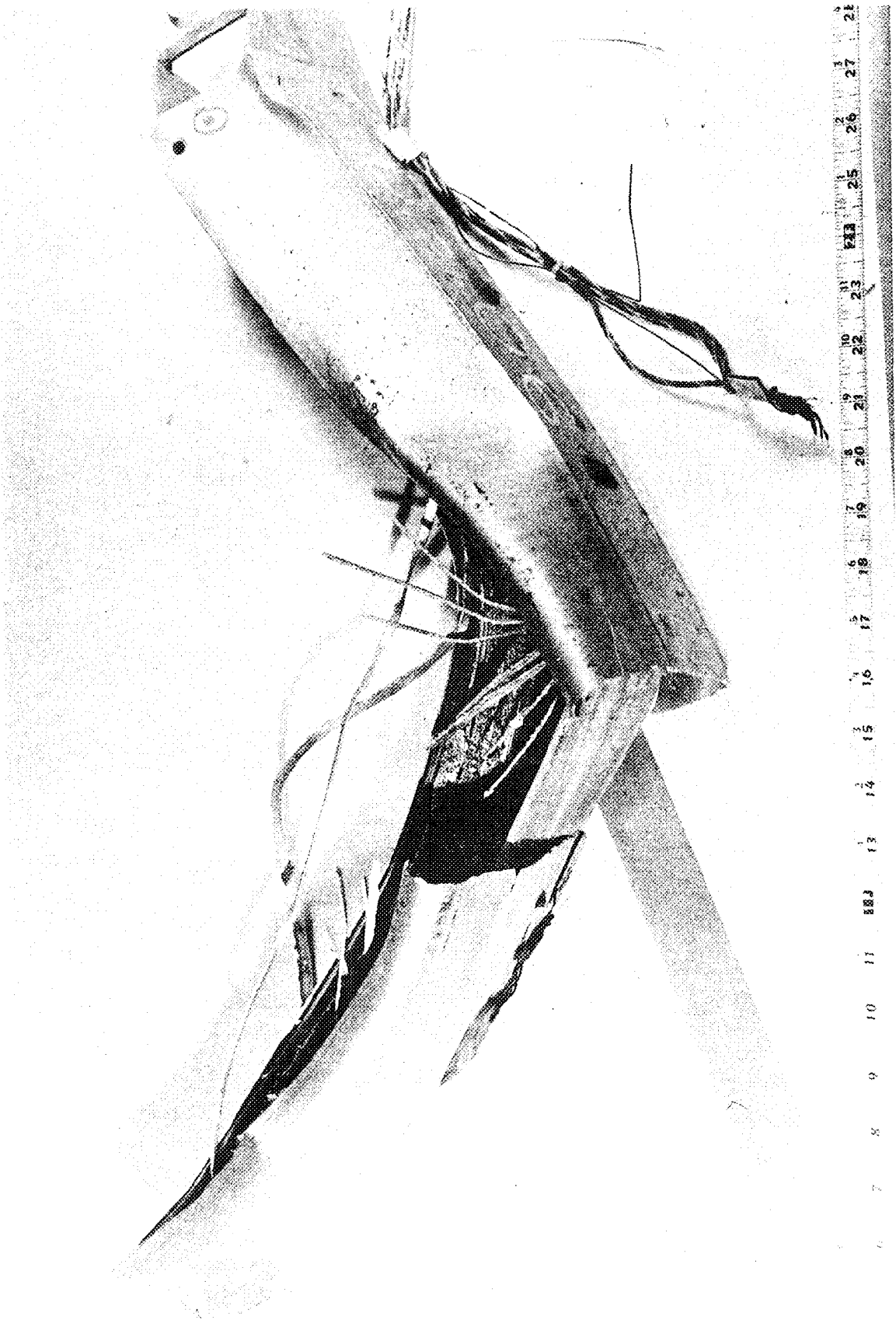
Fig. E-6 Assembly from position G4 showing damage typical for internal assemblies.

121
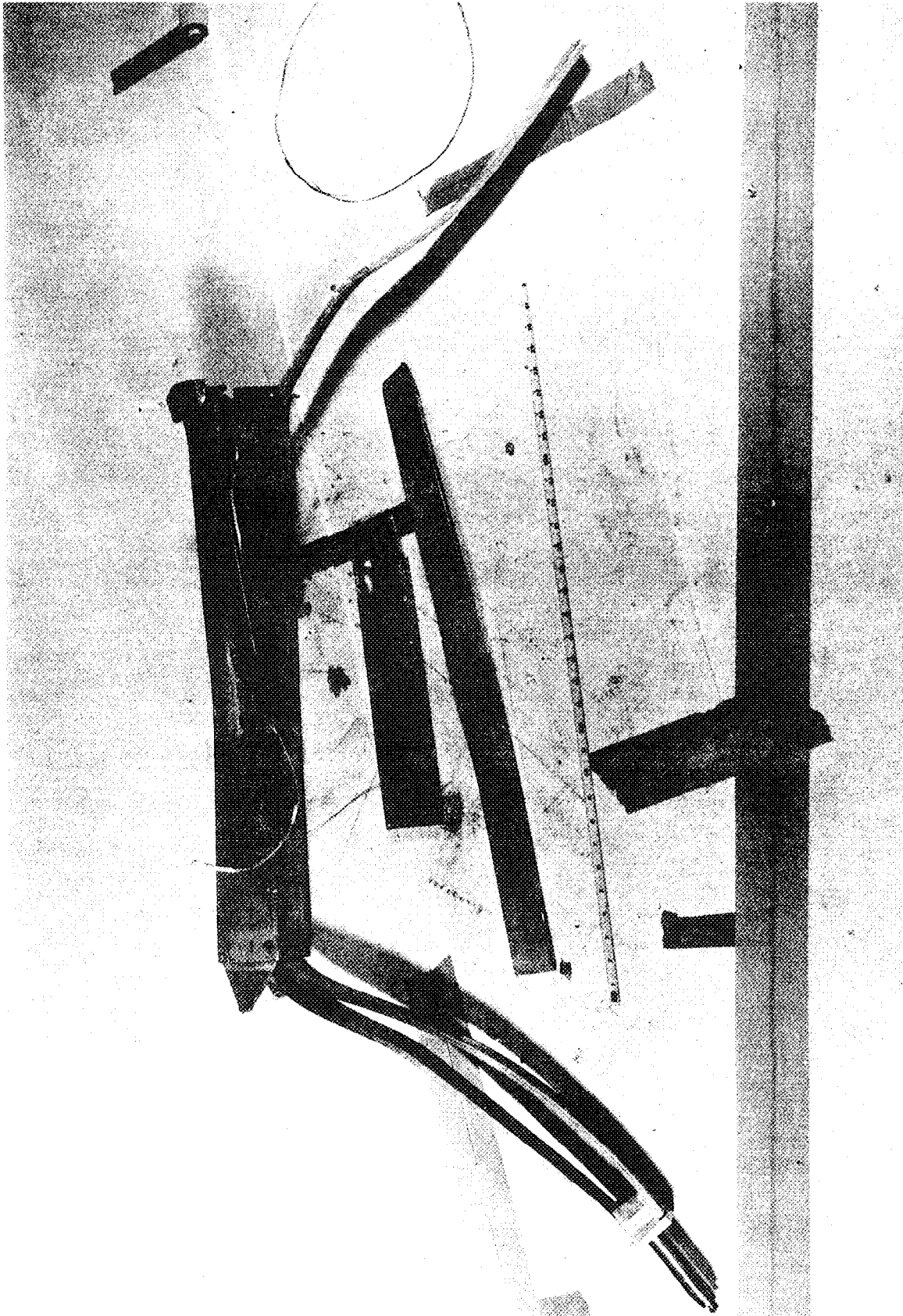
Fig. E-7 Control rod bearing assembly from position C5.
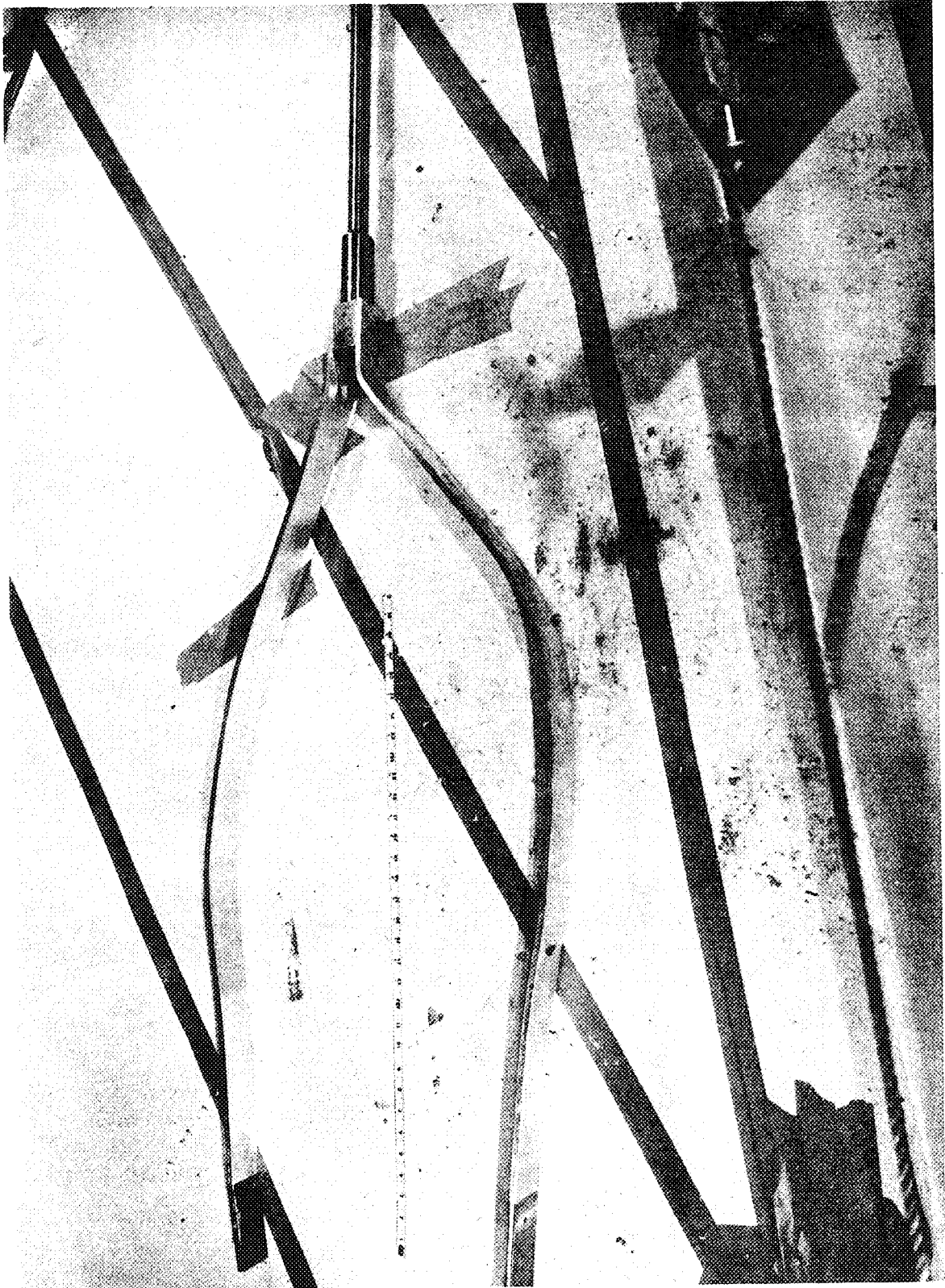
Fig. E-8 Upper (nonpoison) section of transient rod blades as recovered from the reactor vessel. The fuel assembly bearing this rod (position E5) was completely torn apart. The bottom (poison) section of one blade was broken away. The condition of this rod indicates that large magnitude pressures were created within the four fuel plates which are normally located between the two blades.
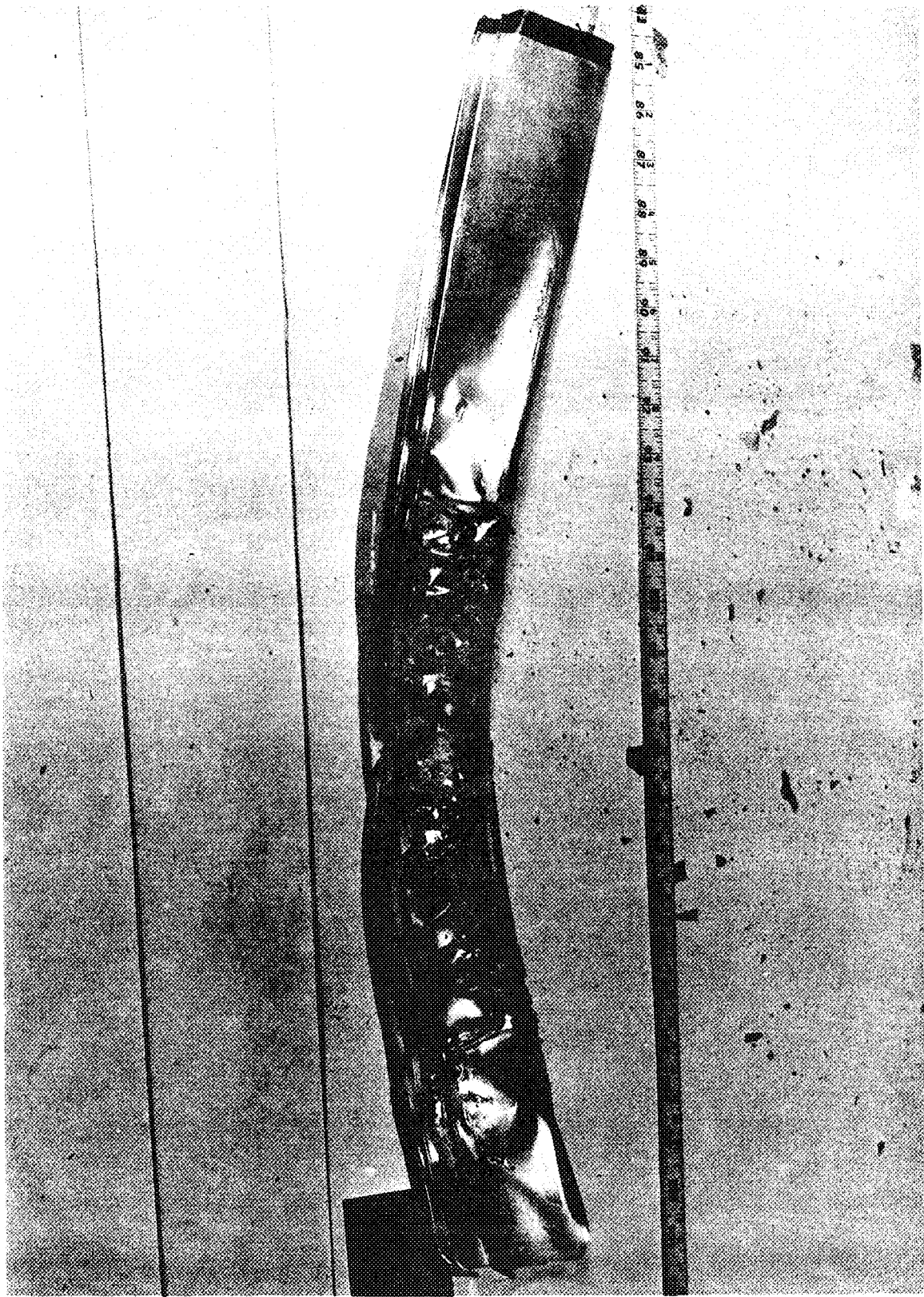
Fig. E-9 Several fuel plates from position G6 showing a stage in the progression from warping to melting and fusion of the plates. Wrinkles of soft but unmelted fuel plates at the extremities of the melted region probably blocked the channels and prevented pressure relief in the vertical direction of the core.
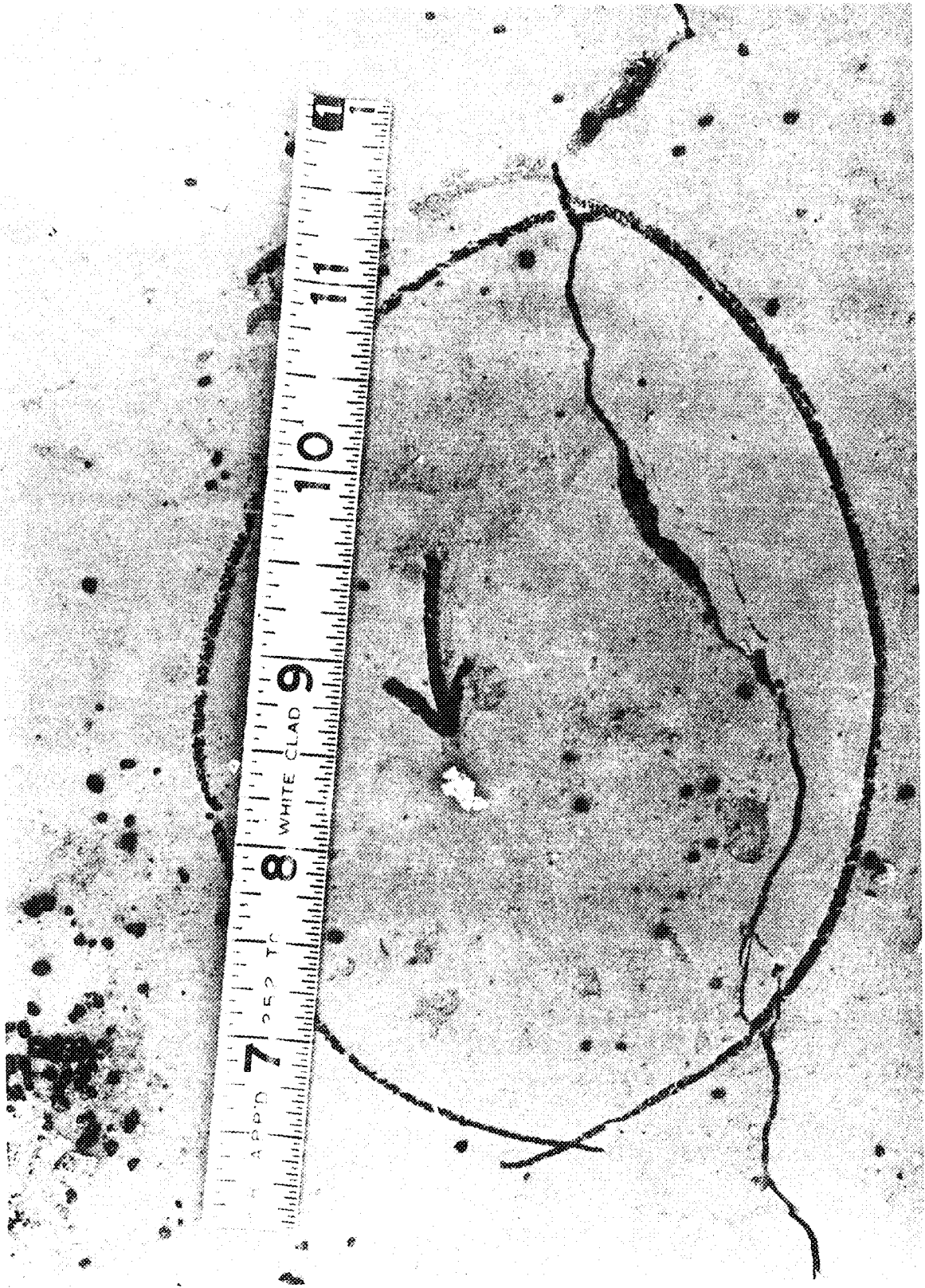
Fig. E-10 A fracture in the concrete floor which circumscribed the reactor vessel. In motion pictures, the lip of the vessel was observed to depress downward one or two inches and then to spring back up giving rise to this circumferential fracture. Arrow points to one of a few core fragments ejected from the vessel.

125
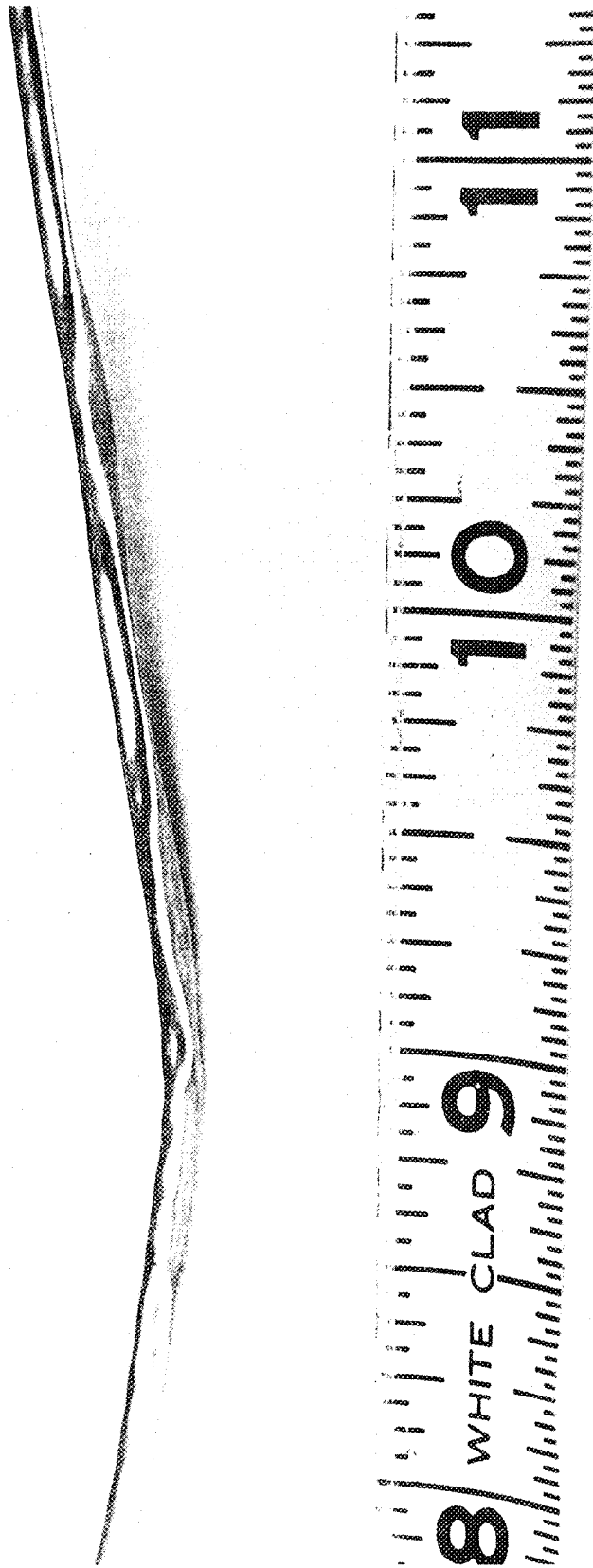
Fig. E-11 Section of an air filled tube located in the core during the destructive test. Pressure caused the tube to collapse as shown. It was estimated that over 3600 psi was required to cause this collapse.
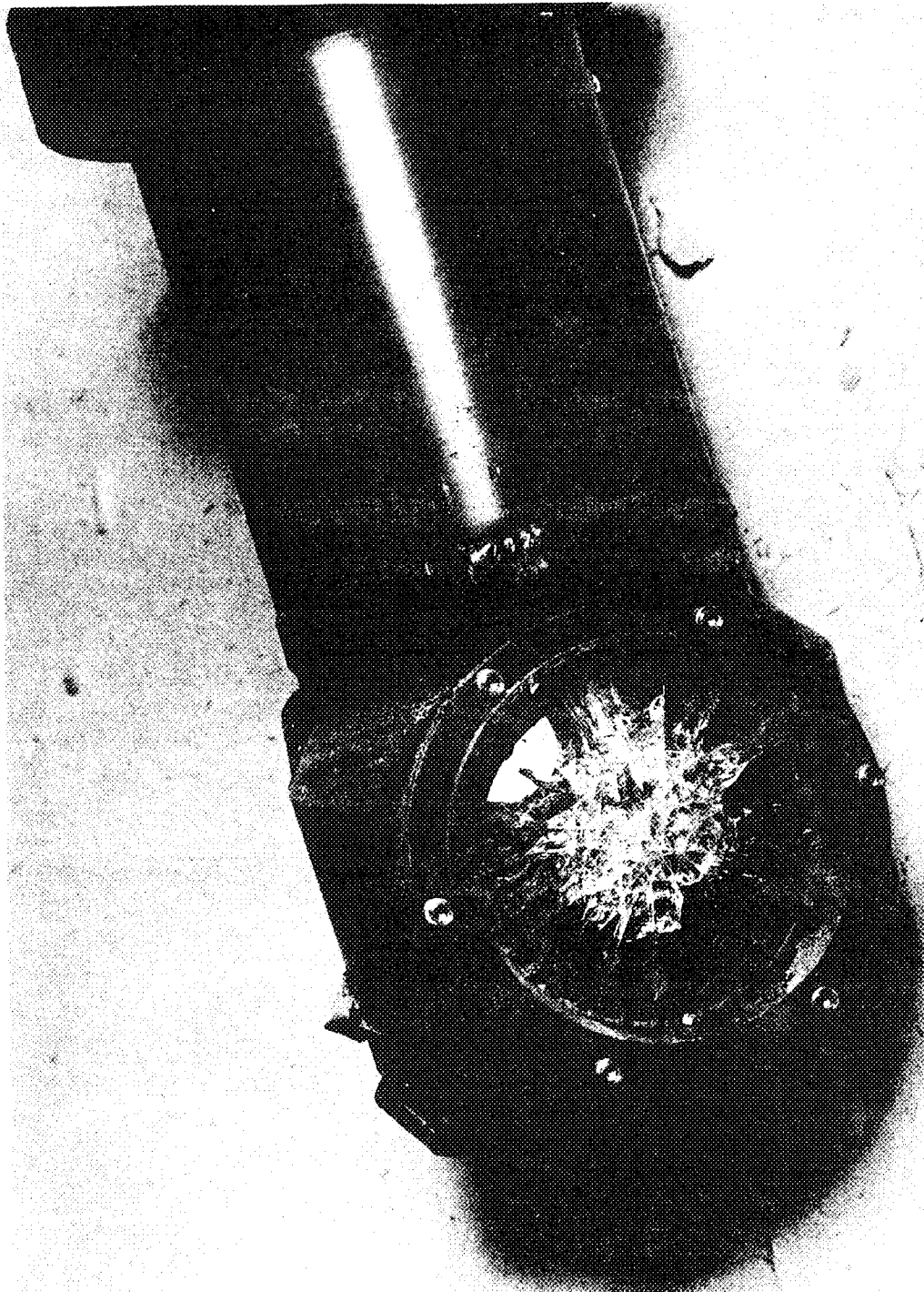
Fig. E-12 Objective lens of periscope. This lens was located at the vessel wall directly opposite the core (about 3-1/2 feet horizontally from core). Motion pictures taken at about 600 fps through this periscope revealed no apparent motion of the core prior to lens failure.

127
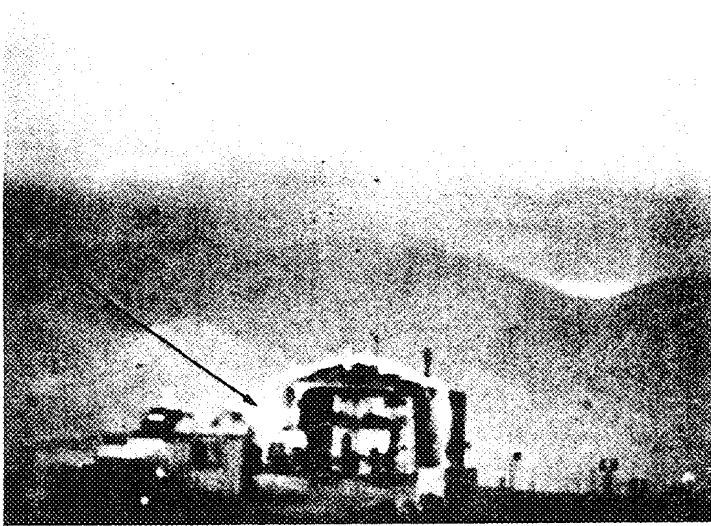
FLASH
BULB

Fig. E-13 t = -143 msec. Flash bulb indicates transient rod release.
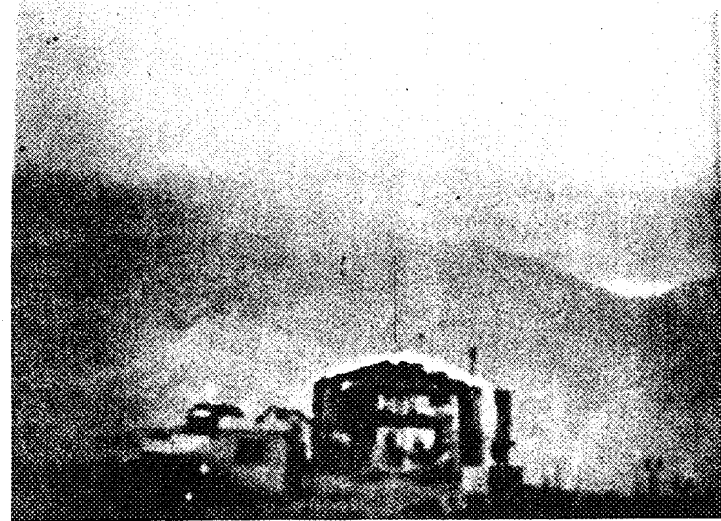
Fig. E-14 t = 87 msec.
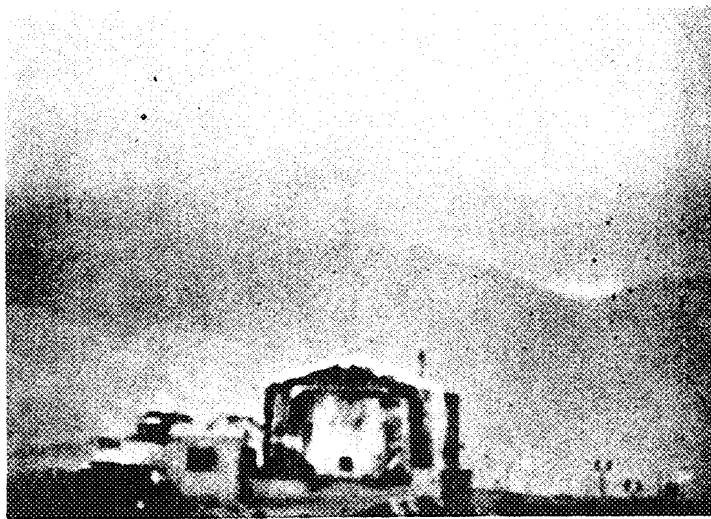
Fig. E-15 t = 130 msec.

Fig. E-16 t = 220 msec.

128
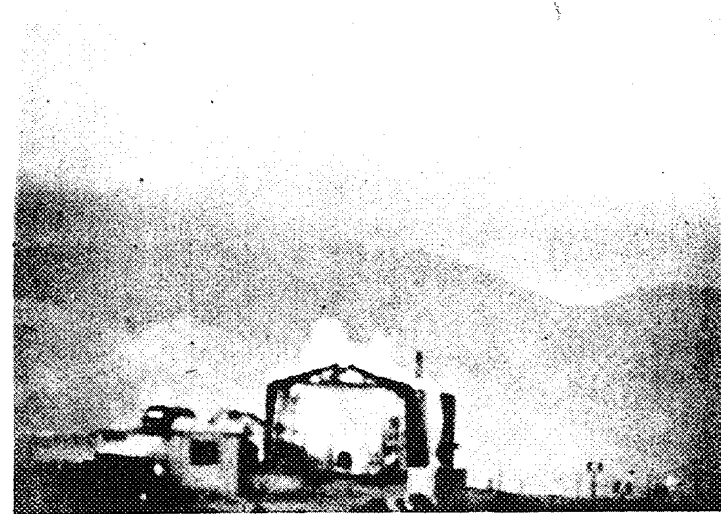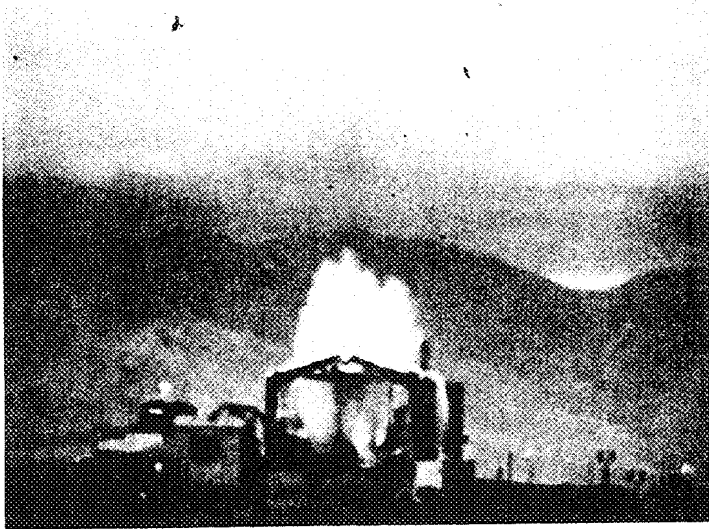
Fig. E-17   t = 360 msec.
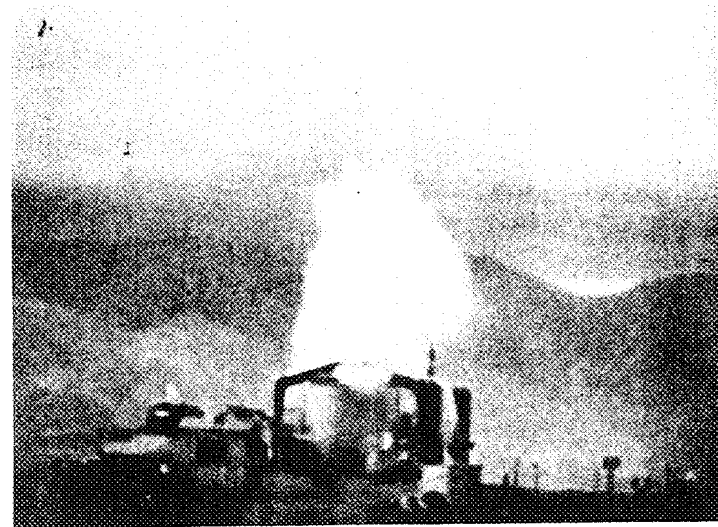
Fig. E-18   t = 620 msec.
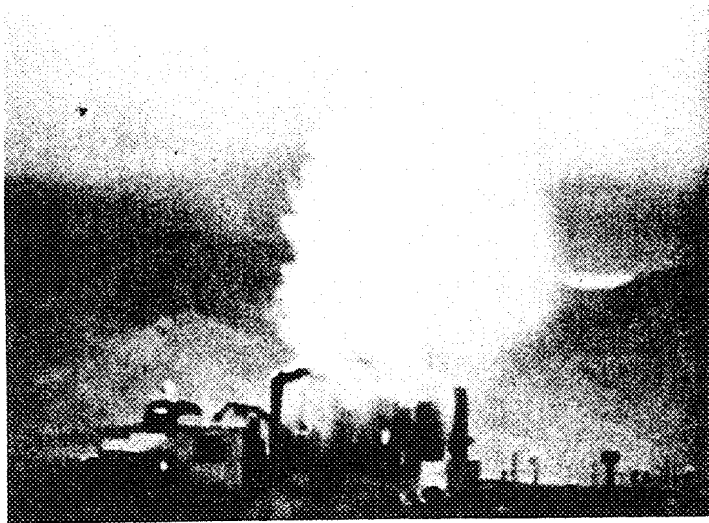
Fig. E-19   t = 900 msec.

Fig. E-20   t = 1030 msec.

129
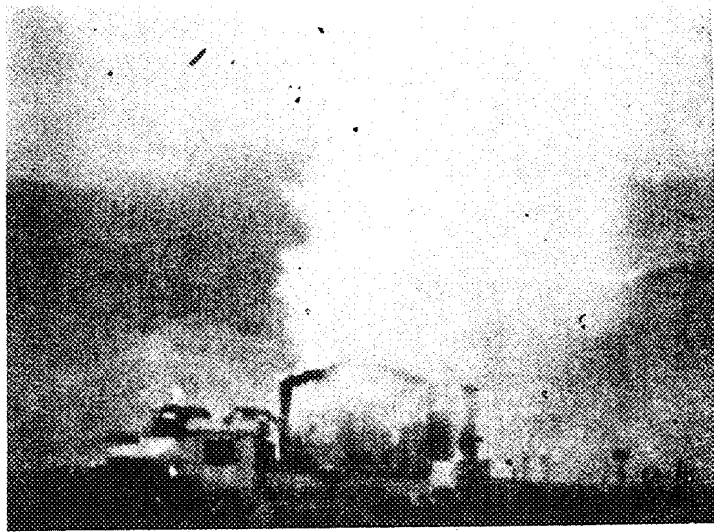
Fig. E-21 t = 1300 msec.
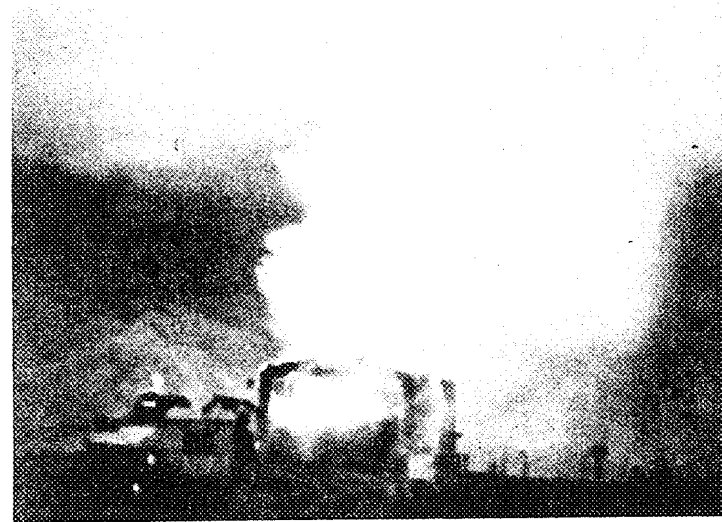

Fig. E-22 t = 1620 msec.

Fig. E-23 t = 2160 msec.


Fig. E-24 t = 2830 msec.

Fig. E-25 t = 3280 msec.

Fig. E-26 t = 3820 msec.
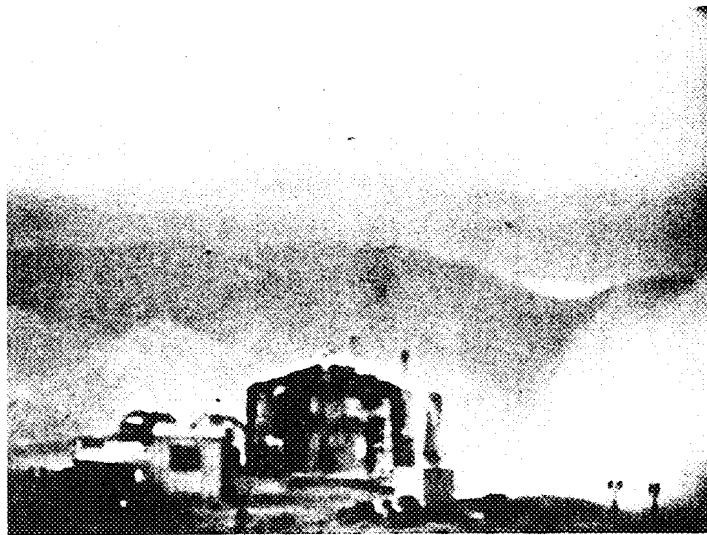
Fig. E-27 t = 4400 msec.

Fig. E-28 t = 5300 msec.

131

PERISCOPES

TRANSIENT ROD

LIP OF REACTOR VESSEL
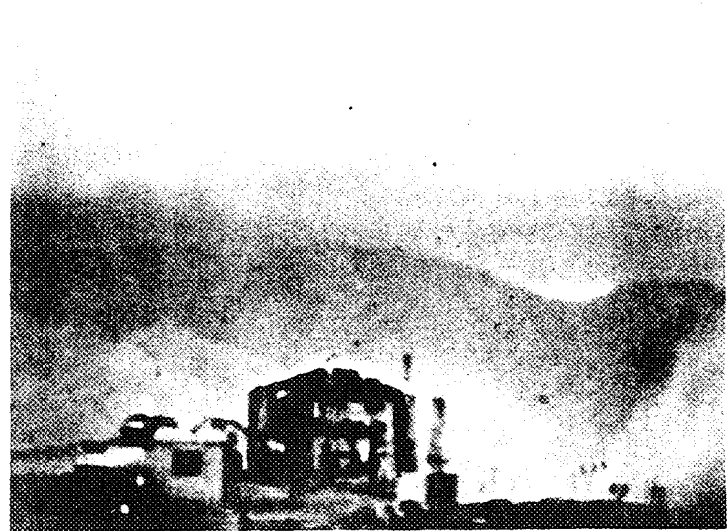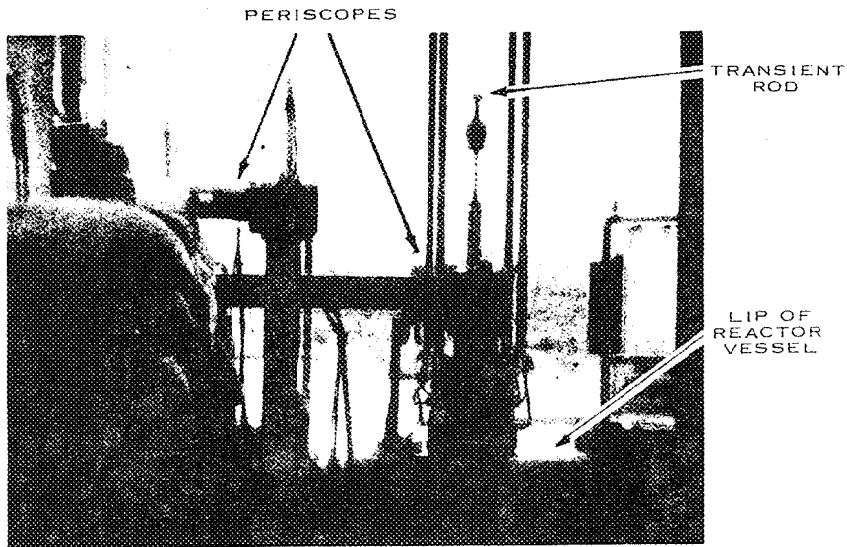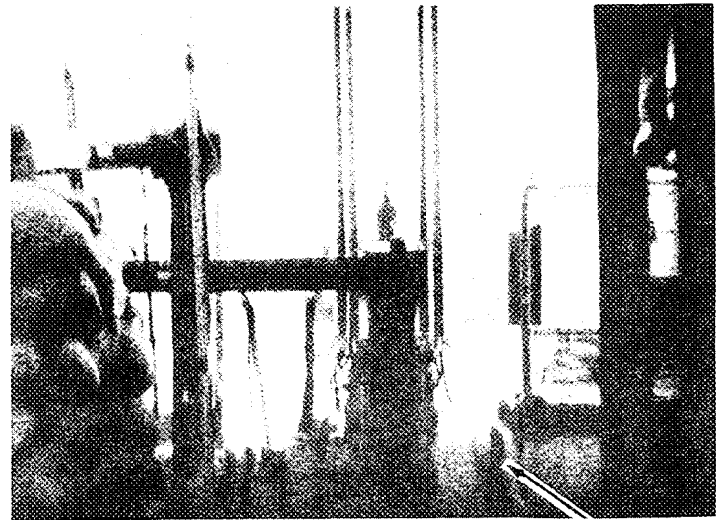
Fig. E-29 t = -73 msec.


PRESSURE TRANSDUCER MOUNTING BRACKET

Fig. E-30 t = 57 msec.
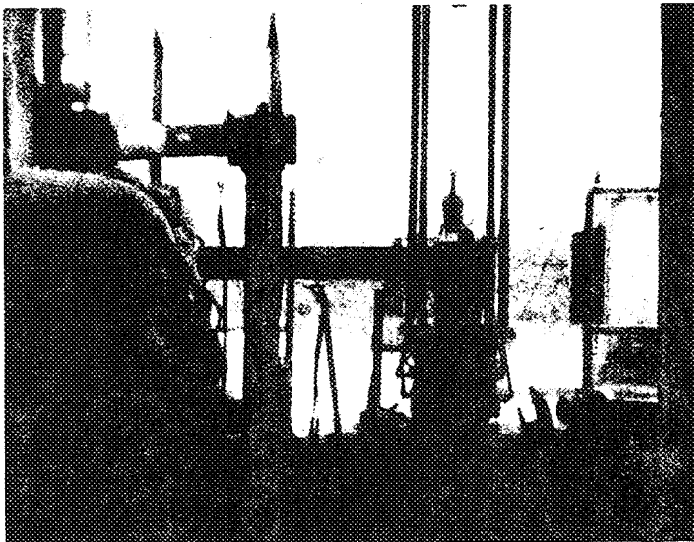
Fig. E-31 t = 65 msec.
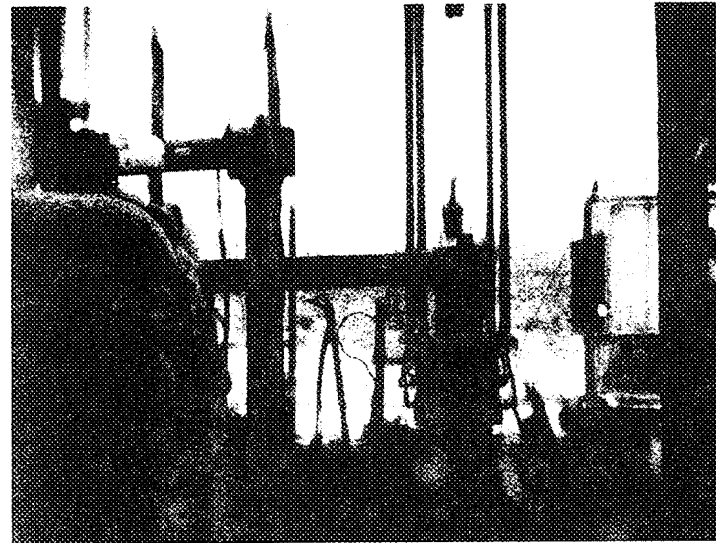

Fig. E-32 t = 70 msec.

Fig. E-33 t = 72 msec.
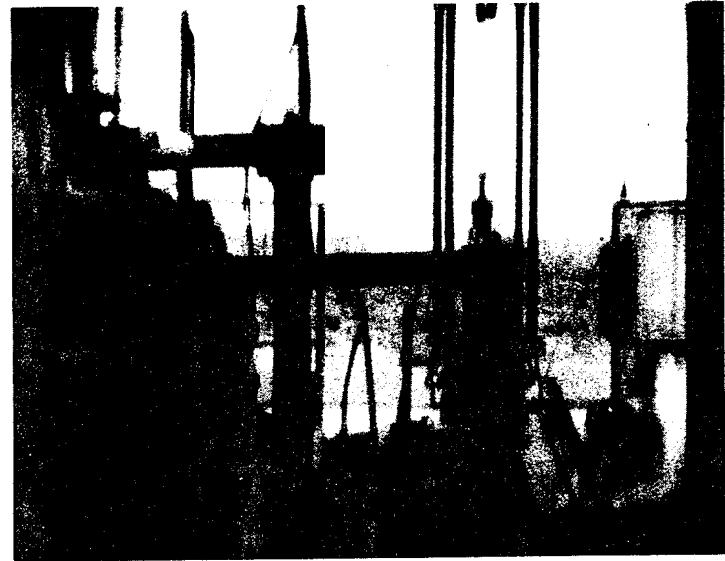
Fig. E-34 t = 74 msec.
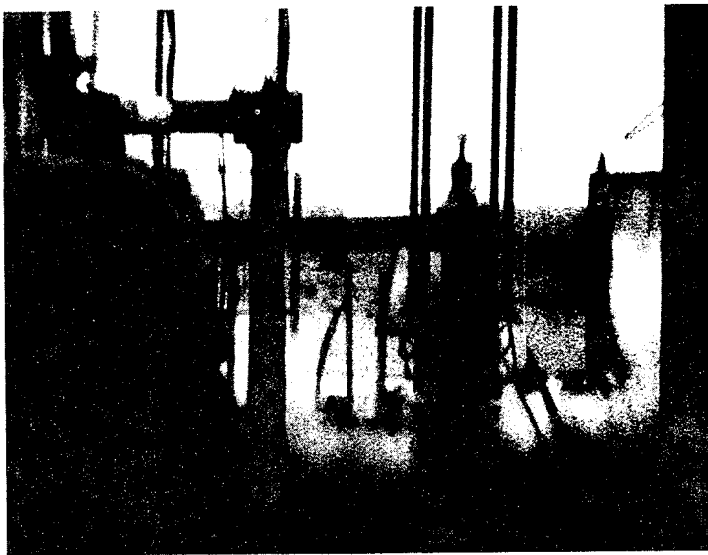
Fig. E-35 t = 79 msec.

Fig. E-36 t = 85 msec.

133
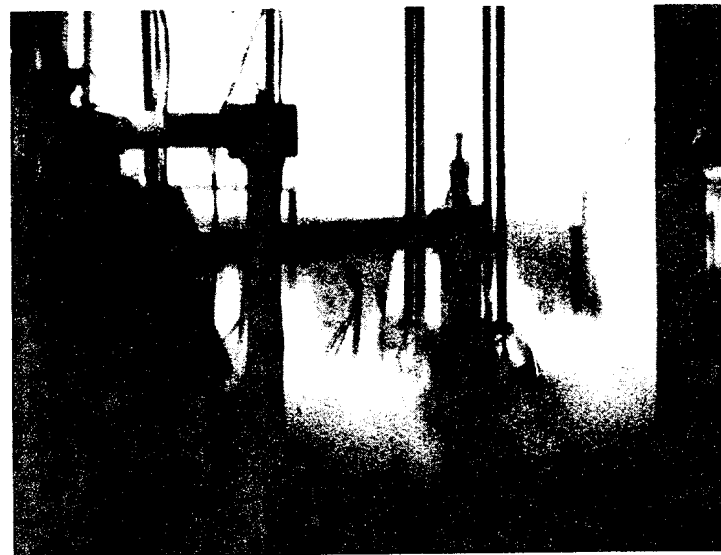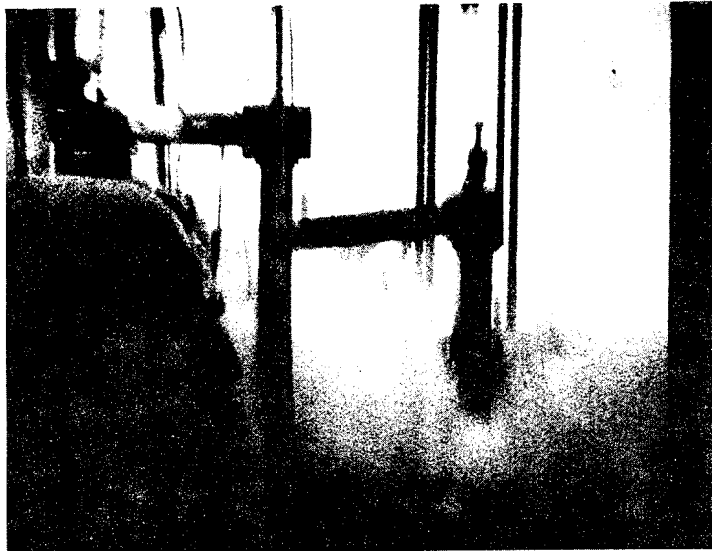
Fig. E-37 t = 94 msec.
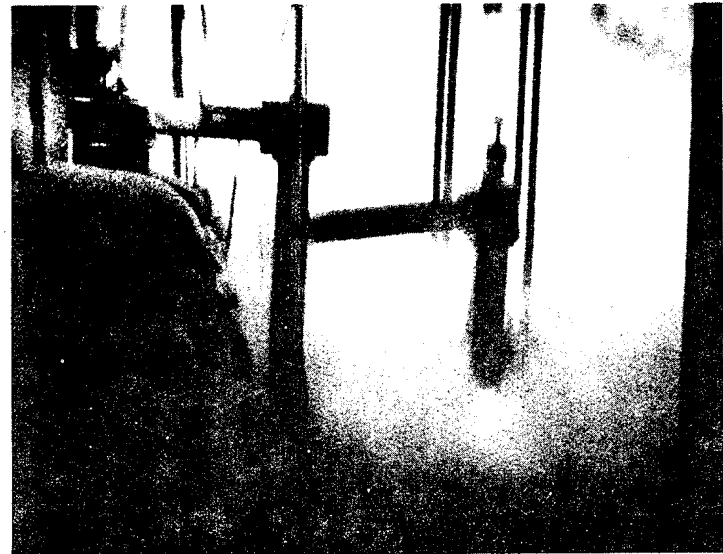
Fig. E-38 t = 97 msec.

Fig. E-39 t = 105 msec.

Fig. E-40 t = 114 msec.
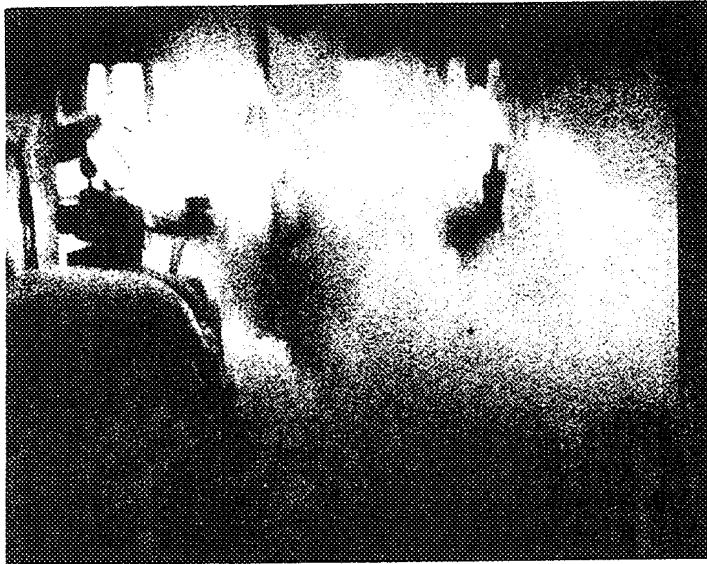
Fig. E-41 t = 124 msec.
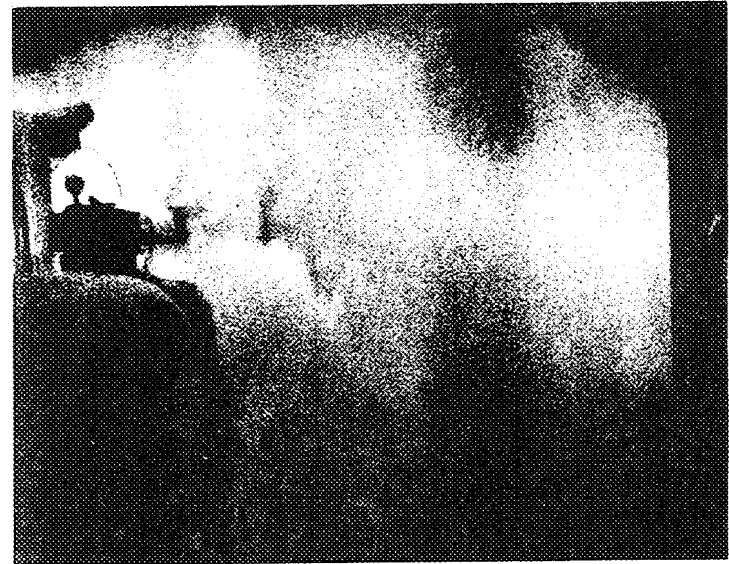
Fig. E-42 t = 135 msec.

Fig. E-43 t = 155 msec.
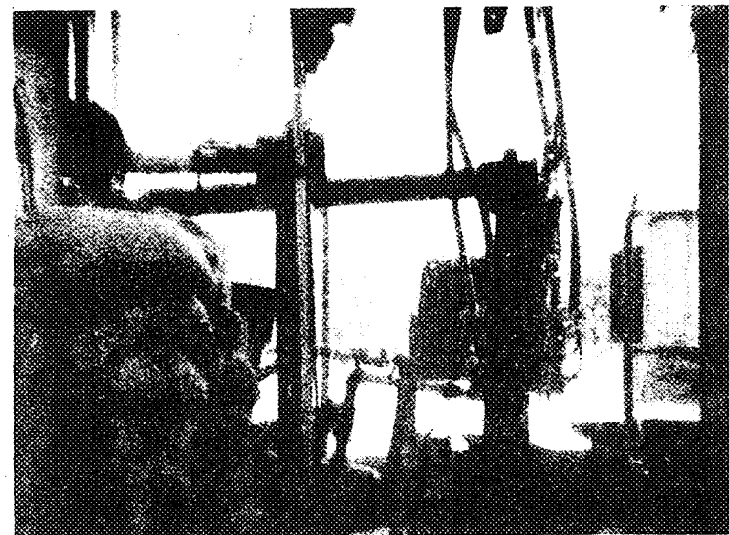
Fig. E-44 t ≈ 4 sec.

FLASH BULB
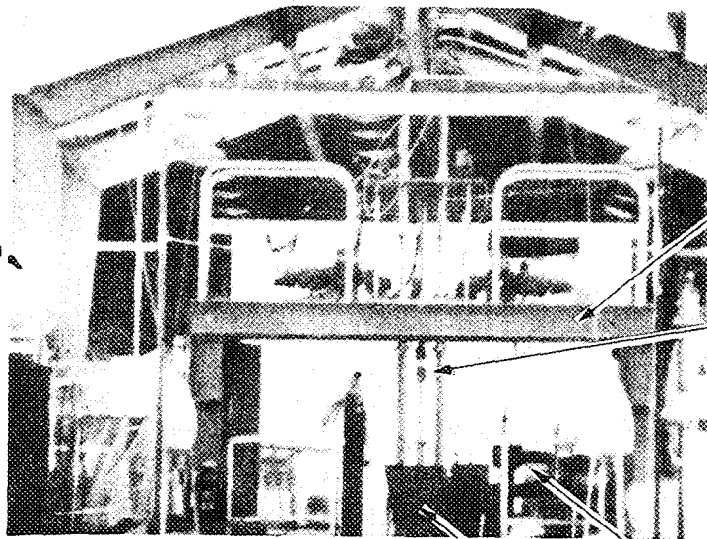
UPPER BRIDGE

TRAN-SIENT ROD

MIRROR   PERISCOPES

Fig. E-45 t = -153 msec.
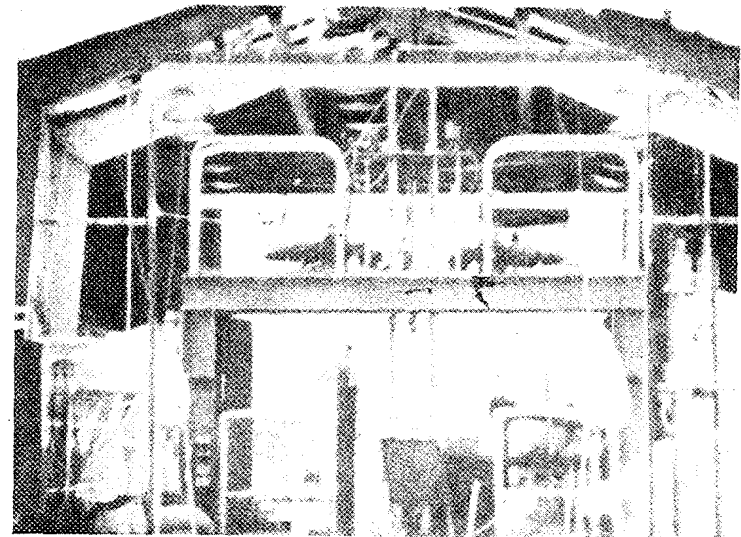
Fig. E-46 t = 70 msec.
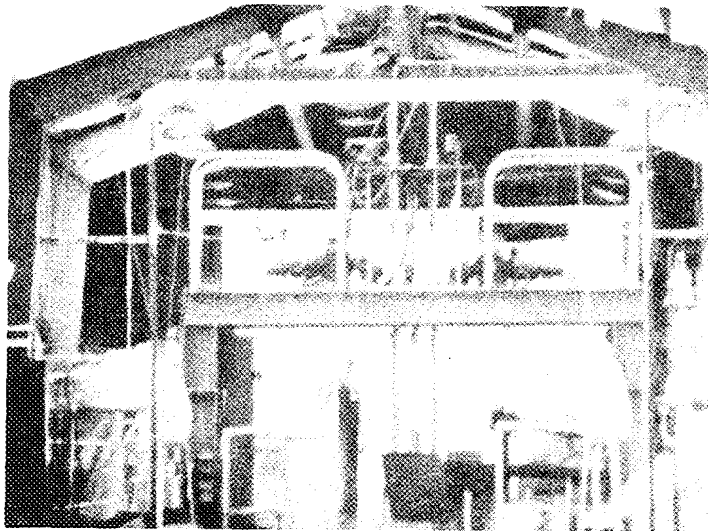
Fig. E-47 t = 85 msec.
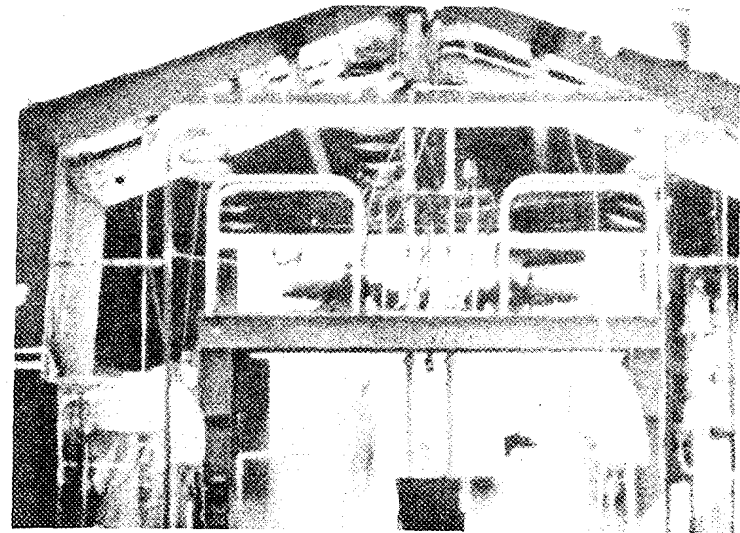
Fig. E-48 t = 100 msec.
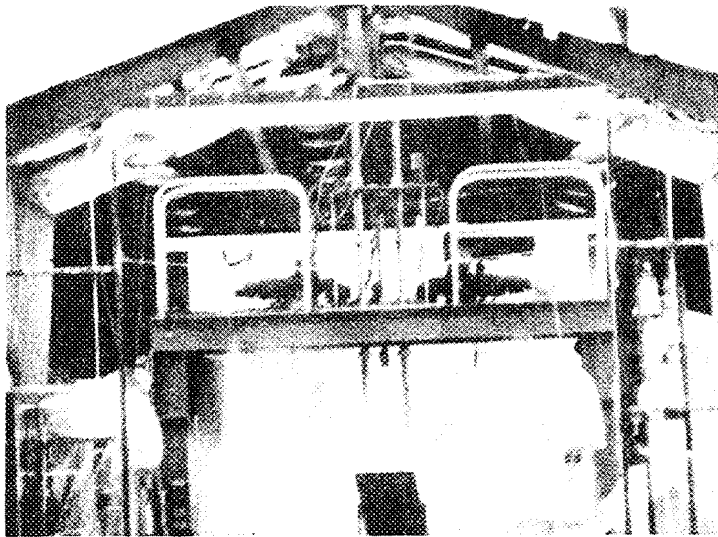
Fig. E-49 t = 115 msec.
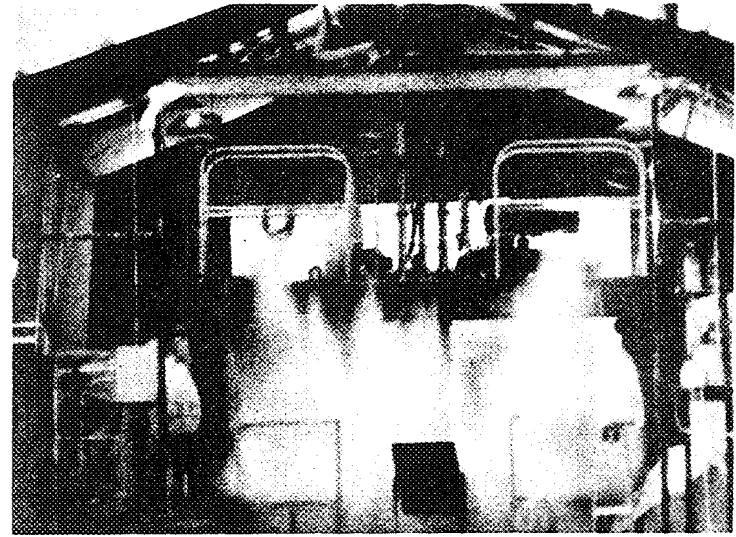
Fig. E-50 t = 130 msec.
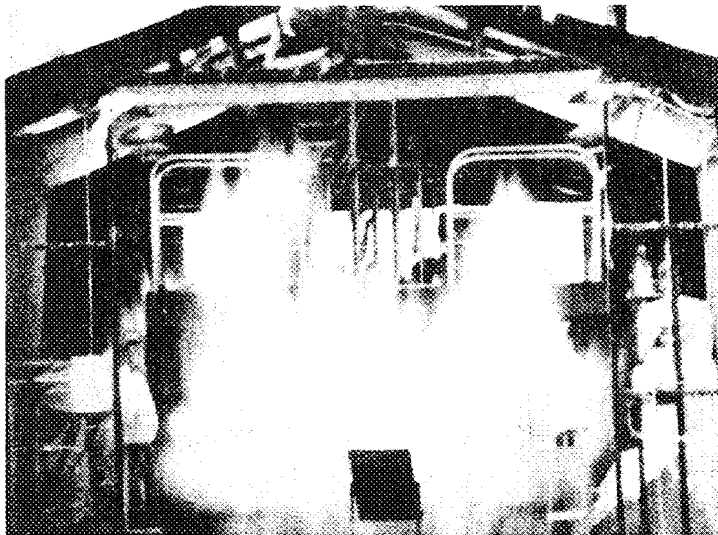
Fig. E-51 t = 145 msec.
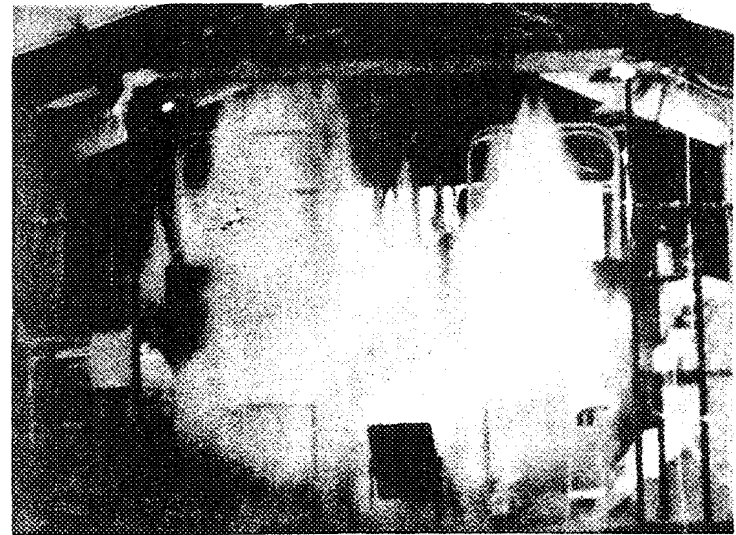
Fig. E-52 t = 160 msec.
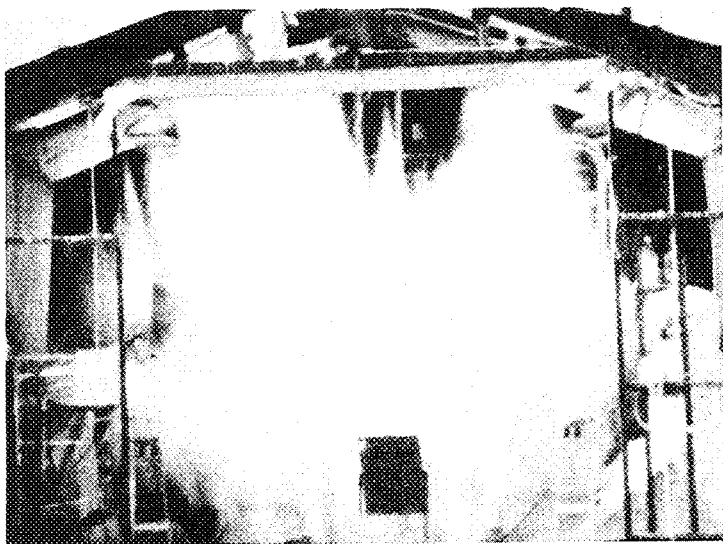
Fig. E-53 t = 175 msec.
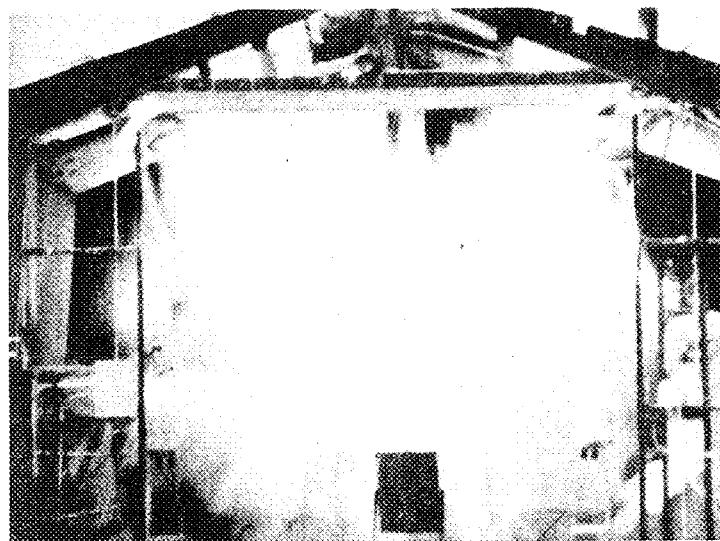

Fig. E-54 t = 190 msec.
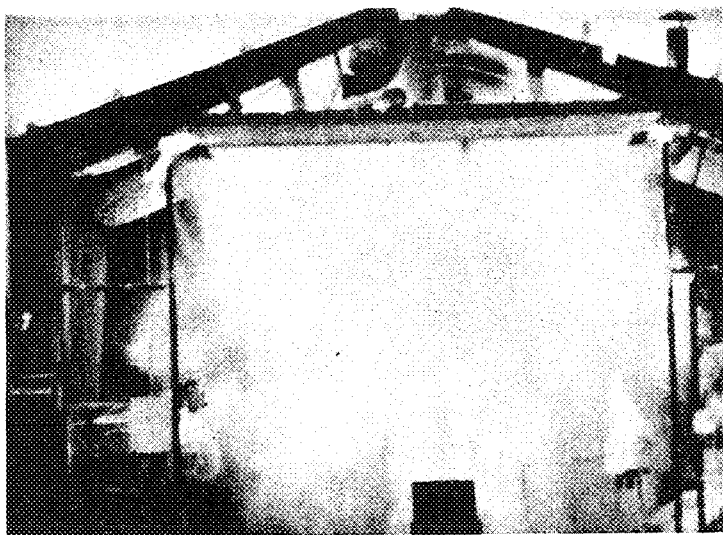
Fig. E-55 t = 205 msec.
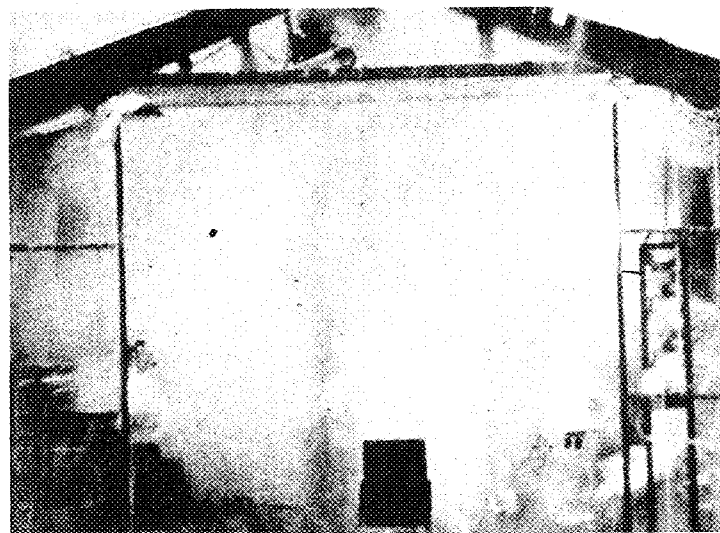

Fig. E-56 t = 295 msec.
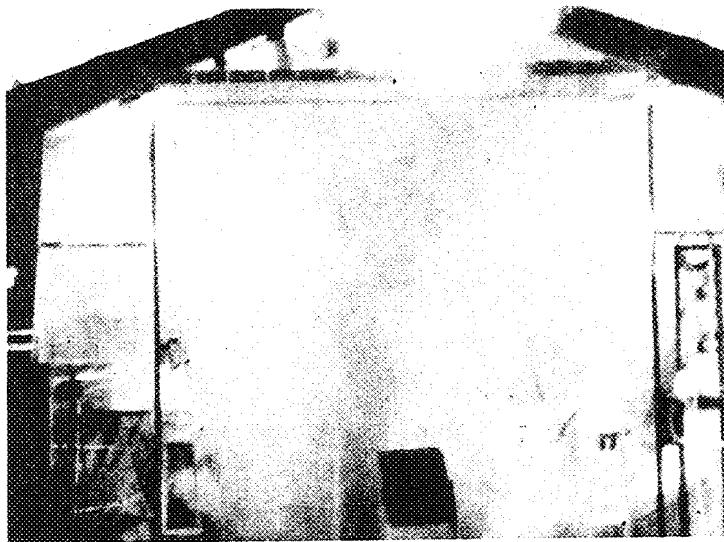
Fig. E-57 t = 445 msec.
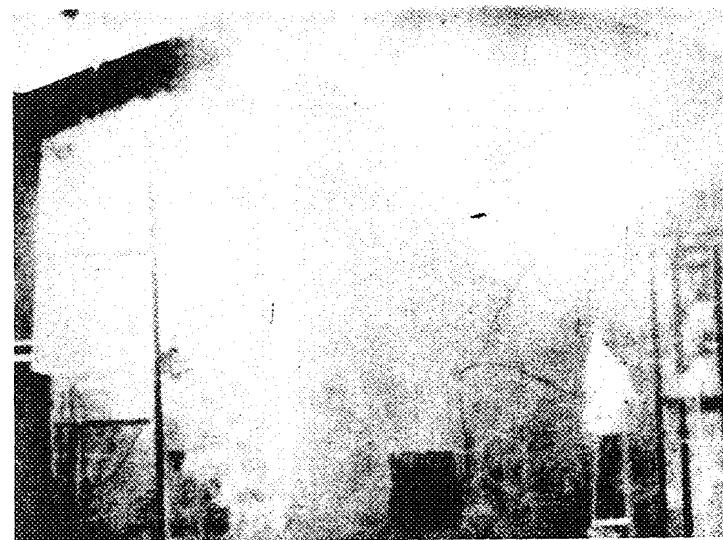
Fig. E-58 t = 1040 msec.
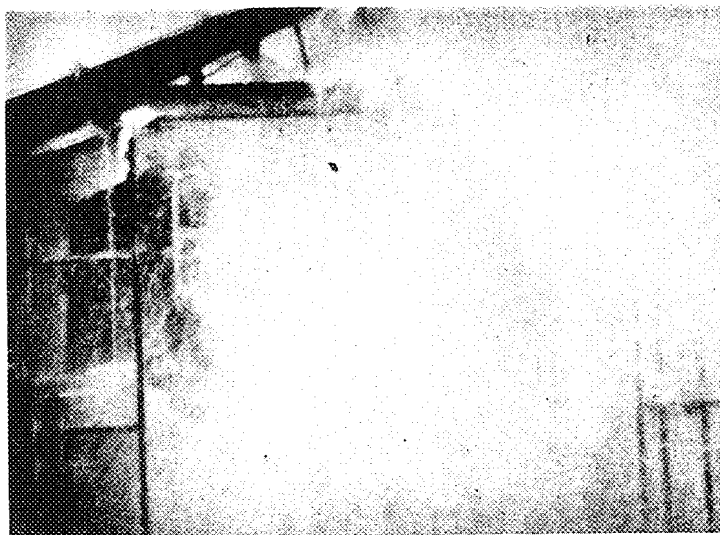
Fig. E-59 t = 1940 msec.
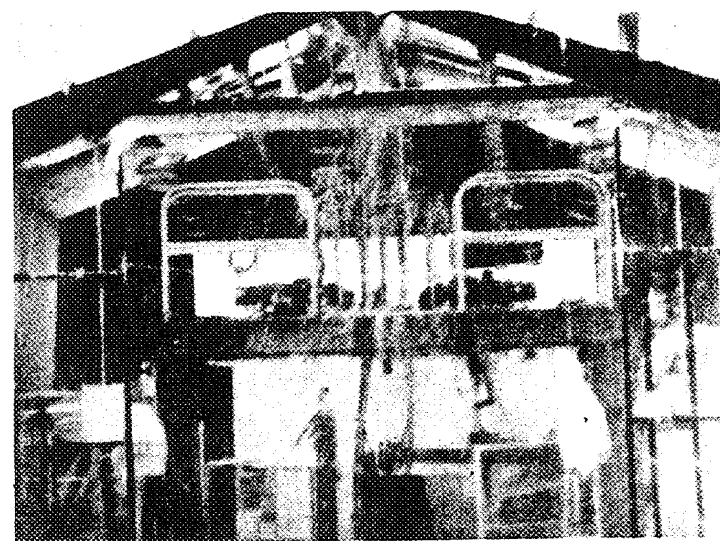
Fig. E-60 t = 4340 msec.

APPENDIX F

MEASUREMENT AND CALCULATION OF
MAXIMUM TEMPERATURE IN THE DESTRUCTIVE TEST

APPENDIX F

MEASUREMENT AND CALCULATION
OF MAXIMUM TEMPERATURE IN THE DESTRUCTIVE TEST

1. EXPERIMENTAL RESULTS

1.1 Surface Thermocouple Temperature Measurements

Only four of twelve surface thermocouples remained intact during the power excursion up to the time of the destructive pressure pulse. Listed in Table F-1 are the location of the four surface thermocouples, the temperature indicated at the time of the explosion, the maximum temperature indicated by the thermocouples, and the time at which the temperature was recorded.

TABLE F-I

SURFACE THERMOCOUPLE INDICATIONS

Location	Temperature at t = + 15 msec [a] (°C)	Maximum Temperature (°C)	Time at Maximum Temperature [a] (msec)
E5 (7W) + 8	452	452	+ 10.5 and + 15
E6 (7W) + 8	443	470	+ 10
D6 (7W) + 8	359	359	+ 15
C7 (9E) 0	396	396	+ 15

[a] Time is taken to be zero at peak power.

The other surface thermocouples failed at various times between 4.5 and 11.5 msec after peak power. At the time of failure, surface thermocouples were indicating between 385 and 580°C. These temperatures are lower than the melting temperature of 649°C for 6061 alloy aluminum. Failure of the thermocouples is attributed both to the differential thermal expansion between the meat and the clad and to internal cracking in the plate.

1.2 Buried Thermocouple Temperature Measurements

All buried thermocouples were intact at the time of the explosion. Table F-II shows for each thermocouple the indicated temperature at the time of the explosion, and for the five cases where a higher temperature was recorded before the time of the explosion, the indicated maximum temperature and the time at which this temperature occurred. Figure F-1 shows the temperatures indicated by buried thermocouples which were located in a plane eight inches above the center of the core at the time of the destructive pressure pulse.

143

TABLE F-II

BURIED THERMOCOUPLE AND INDICATIONS

Location	Temperature at t = + 15 msec (°C)	Maximum [a] Temperature (°C)	Time at [a] Maximum Temperature (msec)
E5 (7W) - 4	620	---	---
D6 (7W) - 4	601	---	---
D5 (7W) - 4	578	---	---
E6 (2W) - 4	608	---	---
C7 (9E) - 4	597	---	---
E5 (7W) + 8	576	---	---
D6 (7W) + 8	454	---	---
D6 (3W) + 8 South	461	---	---
E5 (12W) + 8	586	---	---
D5 (7W) + 8 South	561	---	---
D5 (7W) + 8 North	403	---	---
E6 (2W) + 8	598	---	---
E6 (11E) + 8	354	---	---
D4 (6E) + 8	493	---	---
D7 (7W) + 8	344	---	---
C6 (7W) + 8	349	---	---
C7 (9E) + 8	285	---	---
F4 (6W) + 8	467	482	+ 11.5
E7 (7W) + 8	135	158	+ 9
E7 (12W) + 8	177	230	+ 9
C5 (8E) + 8	144	166	+ 8
C5 (12W) + 8	160	186	+ 8

[a] Except when indicated the maximum temperature is the temperature at t = + 15 msec.

144

The temperatures indicated by buried thermocouples were always 10 to 25 percent higher than temperatures at equivalent positions indicated by surface thermocouples. (Compare, for instance, the values for E5 (7W) + 8 and D6 (7W) + 8 in Tables F-I and F-II.) Since the thermocouple junctions of the buried type lie in temperature gradients extending from the center of a fuel plate to the surface, the measured temperatures are, at best, a lower limit of the temperature existing at the center of the meat.

The fact that no temperatures above the melting point of aluminum were measured at any position does not indicate that melting did not actually occur. As seen below, a large part of the core meat (U-235 alloy in the center of each plate) did actually melt as well as some cladding material before the time of the explosion. The low (below melting) temperatures recorded with the buried thermocouples possibly may be due to the hot-short cracking of 6061 alloy aluminum

Fig. F-1 Temperatures at various points in the core in a horizontal plane eight inches above core center at about the time when destructive pressures arose (t = +15 msec).

which caused scales of unheated aluminum to separate from the molten interior of the plate. (See microphotographs in Appendix H which illustrate the separation of cladding.) Hot-short cracking was prevalent in hotter parts of the core and probably was instrumental in reducing heat transfer from meat to clad.

1.3 Fuel Capsule Temperature Measurement

In Appendix B is found a description of another device, called a fuel capsule, which was designed to provide a continuous indication of meat temperatures even above the melting point of aluminum. A fuel capsule was located at position E6 (3W) - 4 which is estimated to have a flux level about 15 percent lower than the maximum flux in the core. (The value of 15 percent was determined from a static flux measurement and may, therefore, differ slightly from the actual value during the transient test.) The fuel capsule yielded a peak temperature of 1245°C about 11 msec after peak power and a temperature of 1225°C at the time of the explosion, 4 msec later (see Figure C-14). Upon disassembly of the capsule it was found that the fuel alloy had melted but that the stainless steel surrounding the capsule fuel had not melted indicating that the temperature of the stainless steel wall of the fuel capsule had not exceeded 1400°C.

2. CALCULATIONS OF MAXIMUM TEMPERATURE

2.1 Maximum Average Temperature of a Fuel Plate Near the Core Hot Spot; Location E5 (7W) – 3

Using the measured energy release for the excursion of 30.7 MW-sec and values of the temperature dependent heat capacity of the plate, a calculation based upon the assumption that the plate was thermally insulated (adiabatic) indicates that the maximum average temperature across the thickness of a plate placed at the hot spot of the core would have been 1275°C. Due to the adiabatic conditions, this represents an upper limit of the average temperature across a plate during the test.

2.2 Maximum Average Temperature in the Capsule

Using a computational method identical to the one above the maximum average temperature in the fuel capsule was computed to have been 1400°C. This value is in reasonably good agreement with the measured value of 1245°C.

If the energy density in the capsule is increased by 15 percent to take into account the fact that the flux at the capsule location may have been 15 percent lower than the maximum flux in the core, it is concluded that the maximum average temperature in the capsule would have indicated no more than 1630°C. Since conditions for heat transfer from the meat of fuel plates are more favorable than from the meat of the capsule, it is reasoned that 1630°C represents an absolute upper bound of the adiabatic plate meat temperatures.

Applying the same 15 percent correction to the 1245°C measured peak temperature in the capsule indicates that had the capsule been located at the core hot spot it would have yielded a measured value of the peak temperature of about 1500°C. From considerations of the temperature distribution in the capsule at the time of the explosion, 1500°C probably represents an upper limit of actual fuel temperature at the core hot spot. Therefore, peak fuel plate temperatures are expected to be lower than 1500°C.

2.3 Temperature Distribution in Fuel Plate at E5 (7W) 0

Detailed machine calculations also were made [10] of the transient temperature profile inside several fuel plates located at various positions in the core and near the hot spot, by solving the one dimensional, second order heat transfer equations for the meat and the clad. Solutions were obtained for a two region slab model using regional, temperature-dependent values of the thermal conductivity and volumetric heat capacity, and a time dependent prompt heat source derived from the experimental transient reactor power. The model consisted of a primary heat source region of U-Al alloy and a clad region of aluminum 6061. Exterior boundary conditions used were the Neumann condition (temperature gradient goes to zero at the boundary) applied at the center of the plate with the experimental plate surface temperature used for the outer boundary temperature of the fuel plate.

Figures F-2 through F-7 show the results of several of these calculations. A more complete discussion of the calculations can be found in Reference 10 which discusses the computational method, meaningfulness of the measured temperature and calculated results, as well as assumptions that were made.
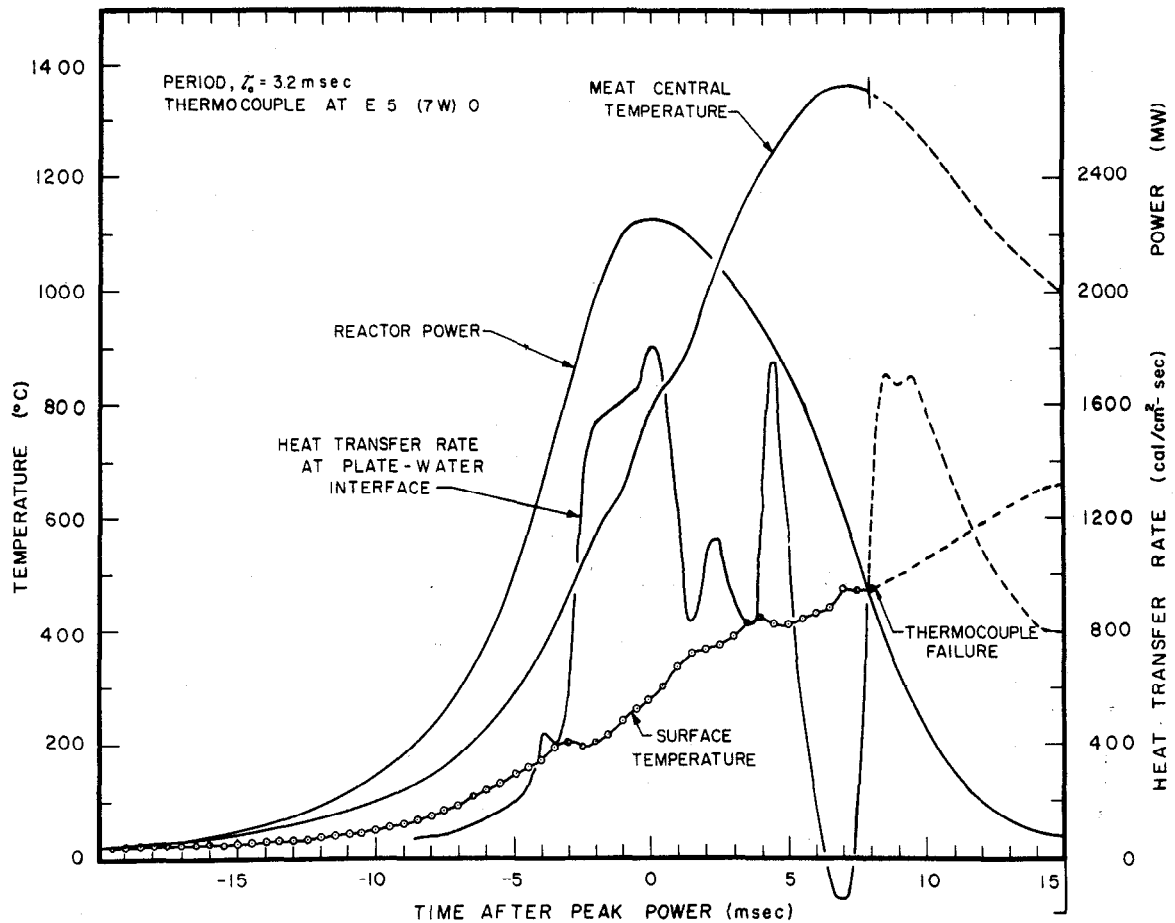
Fig. F-2 Calculated results of centerline meat temperature and of heat transfer rates from fuel plate surface to moderator. Experimental surface temperature (shown) was taken near core hot spot, E5 (7W) 0. Run 54.

Calculations of temperature distributions and heat transfer rates for a segment of fuel plate near the core hot spot, Figures F-2 and F-3, were complicated by failure of the thermocouple about 7 msec before the explosion. However, at this time the peak central temperature had apparently been reached and is calculated to be about 1360°C.

To continue the hot-spot calculation until the explosion, several "trial" or assumed surface temperatures were used, one of which is shown in Figure F-2 as the dashed portion of the surface temperature after thermocouple failure. Although a continuation of this surface temperature after thermocouple failure would reasonably go to lower temperatures (due to overall thermal relaxation and cooling of plate and rapidly decreasing power), the trial shown in Figure F-2 is based upon a nearly linear extrapolation of the temperature data and leads to a final surface temperature of about 650°C which is near the melting point of aluminum. Thus, this trial leads to a condition of incipient melting at the clad surface at the time of the explosion and a central temperature at this time of 1000°C (representing a 360°C drop from peak value)..

This "trial" is considered to be reasonable with regard to peak surface temperature. Nevertheless, another trial was taken which assumed that adiabatic conditions existed after the thermocouple failure in order to compute the highest central and surface temperatures possible at the time of the explosion. From this limiting type of calculation, values of 960 and 1080°C are found, respectively, for the surface temperature and centerline temperature.

From these calculations (with their inherent calculational models and assumptions) the conclusion is formed that at the onset of the explosion, the peak (unexposed) meat temperature at the core hot spot was about 1000°C and probably not exceeding 1100°C. Fuel plate surface temperatures at the same time probably did not exceed the melting point. However, if one assumes that the fuel plate was completely insulated during the last 7 msec prior to the explosion, then temperatures may have exceeded the melting point by as much as 300°C.

At other positions in the core, of course, temperatures were lower.
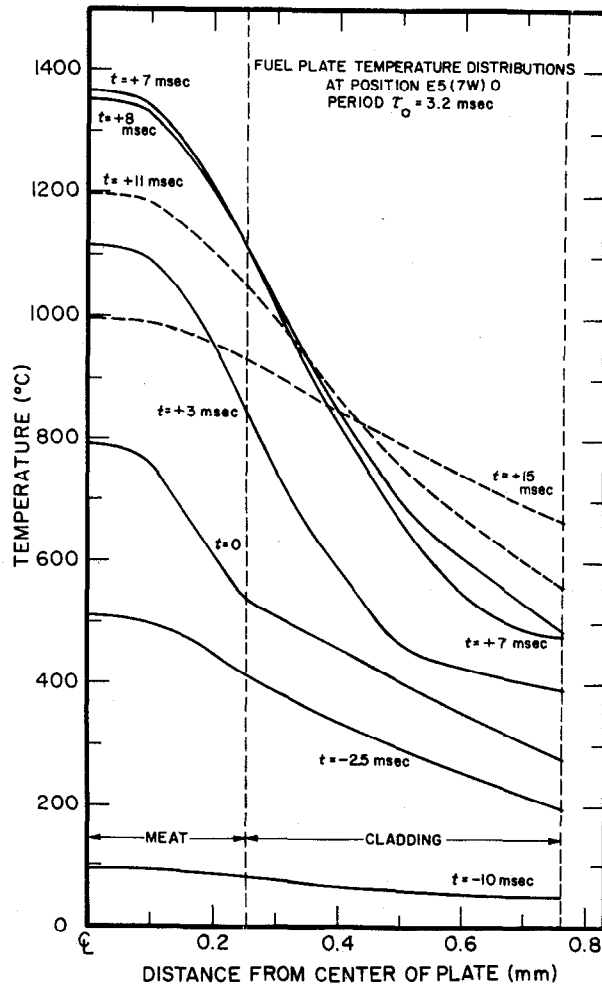
Fig. F-3 Calculated temperature distributions of a fuel plate section near the hot spot of the core. Times indicated are in milliseconds after peak power during the destructive test. Run 54.
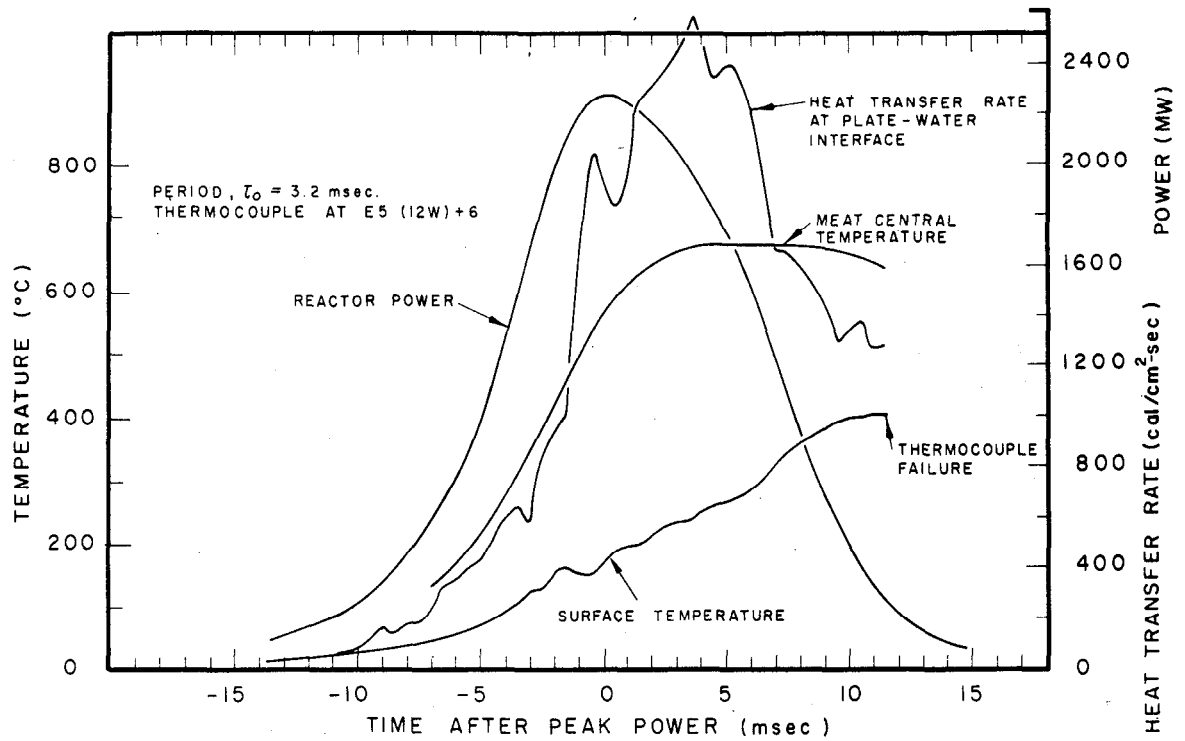
Fig. F-4 Calculated temperature and heat transfer rate shown with measured surface temperature at position E5 (12W) + 6. At this postiion, the thermal neutron flux was about 60% of the peak flux at the core hot spot. Run 54.
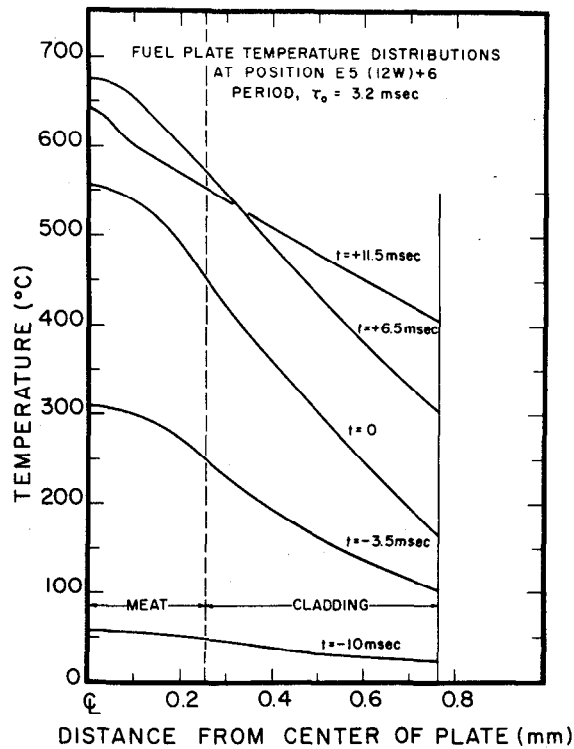
Fig. F-5 Calculated temperature distribution in a fuel plate segment at E5 (12W) + 6, (relative thermal neutron flux about 60% of peak at core hot spot). Times indicated are in milliseconds after peak power. Run 54.

149
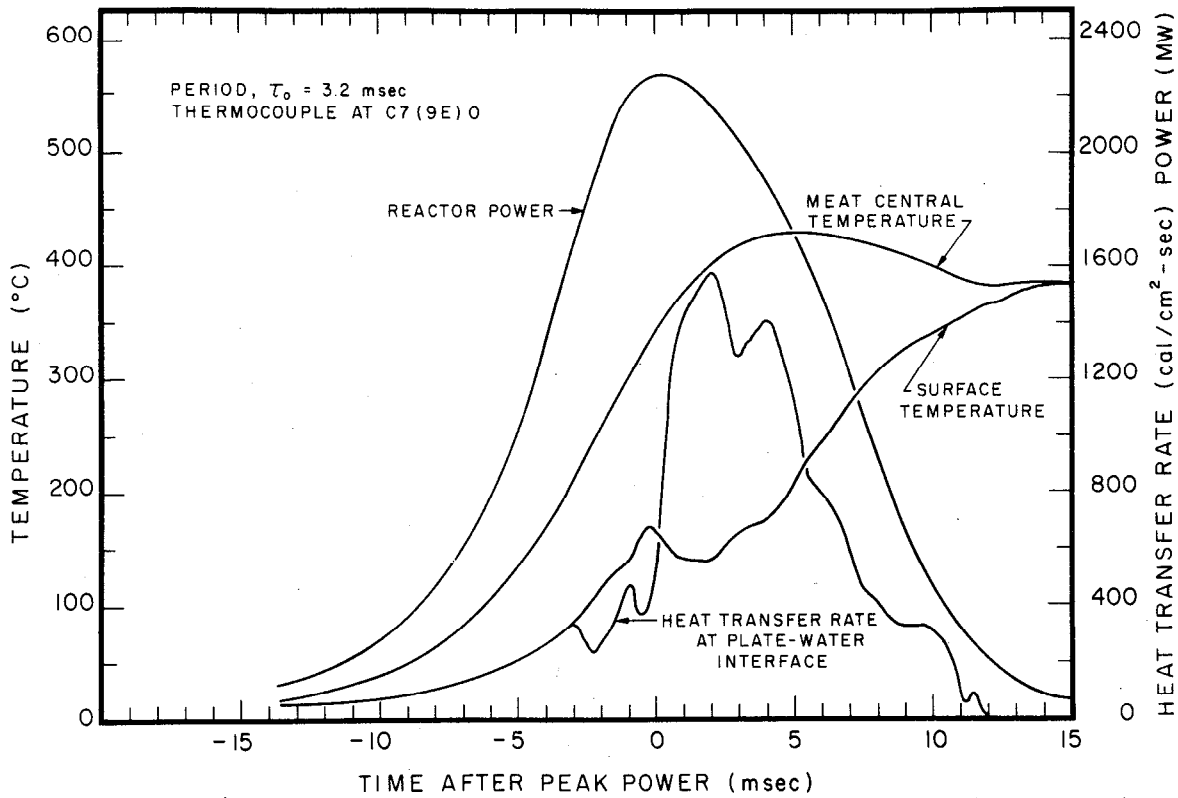
Fig. F-6 Calculated temperature and heat transfer rates shown with measured surface temperature at position C7 (9E) 0, during destructive test. Run 54. At this position the thermal neutron flux was about 45% of the peak at the core hot spot.
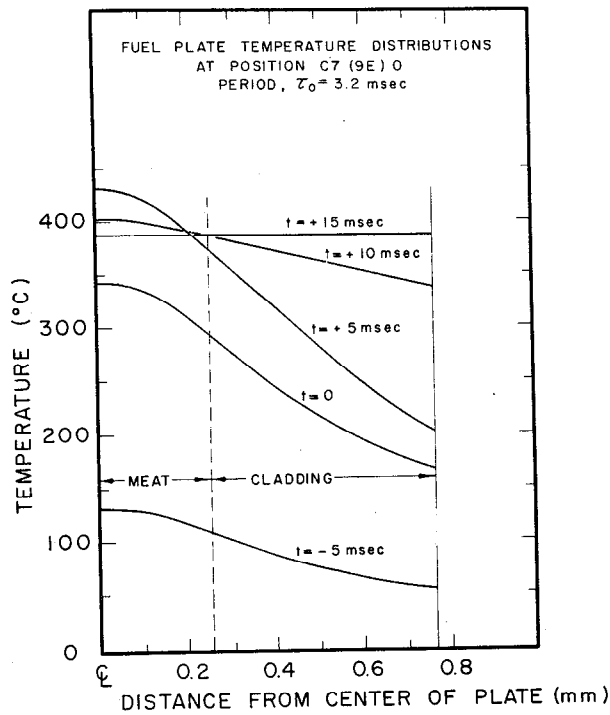
Fig. F-7 Calculated temperature distribution in a fuel plate segment at position C7 (9E) 0 (relative thermal neutron flux about 45% of peak at core hot spot). Times indicated are in milliseconds after peak power. Run 54.

150

APPENDIX G

CALCULATION OF FISSIDE RELEASE FROM THE DESTRUCTIVE TEST

APPENDIX G

CALCULATION OF FISSIDE RELEASE FROM THE DESTRUCTIVE TEST

The information presented in this section is based upon data provided by the USAEC-ID Health and Safety Division who cooperated with Phillips Petroleum Company in the performance of the destructive test and who had the responsibility for collection and analysis of fission product release data as well as coordination and collection of meteorological data for the destructive test. The data were taken from samples obtained with several prefilter, carbon trap, high volume air samplers placed on a grid system as indicated in Figure G-1.

The meteorological forecast conditions required for the destructive test were: wind direction $220° \pm 20°$, wind speed 10 to 20 mph, temperature lapse rate conditions and no precipitation for a three-hour period. Meteorological measurements recorded for the period between 1220 and 1420 Mountain Standard Time on November 5th are given in Table G-1. Values of the standard deviation of the wind direction variations are based upon instantaneous readings at one-minute intervals for the Spert I station and upon instantaneous readings at alternating two- and three-minute intervals for the three-mile arc station. The vertical temperature lapse rate was nearly neutral on the 250-foot meteorological tower at Central Facilities.
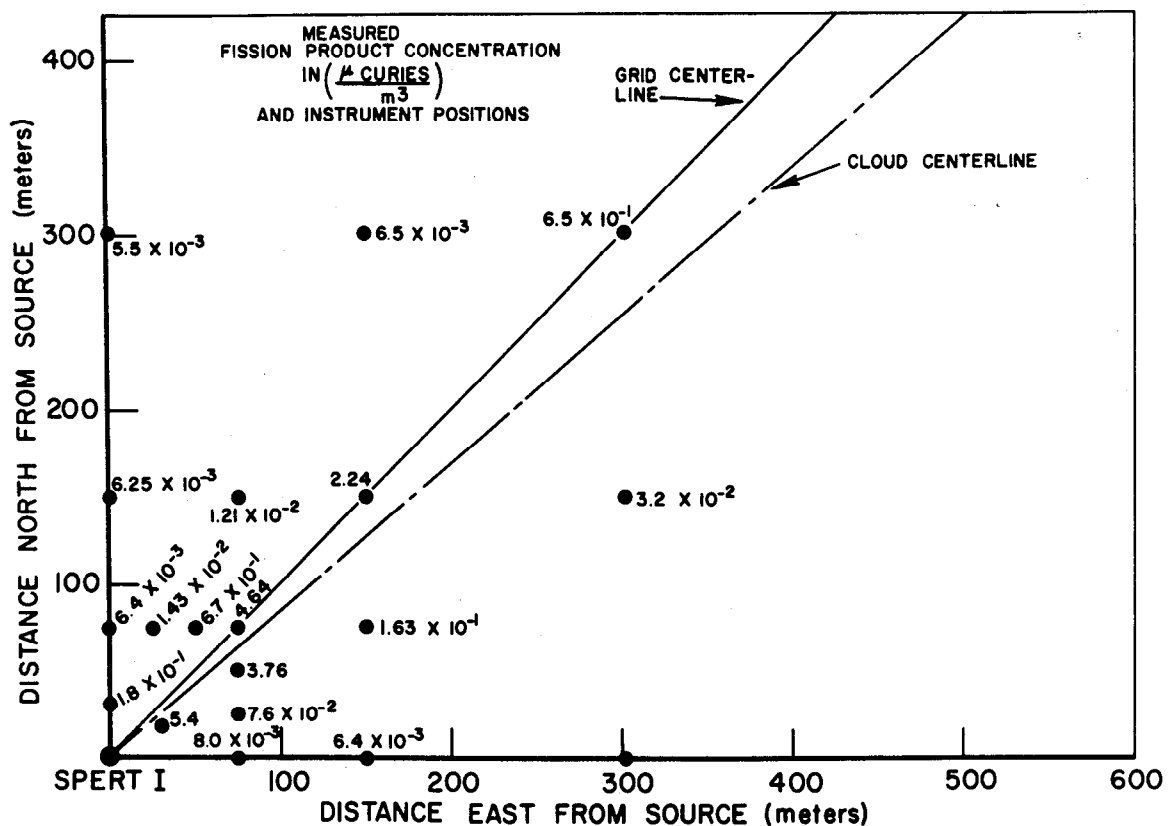

Fig. G-1 Air sampler locations and portion of the grid system showing values measured at each location (corrected to 1800 MST).

WIND MEASUREMENTS AFTER THE DESTRUCTIVE TEST

Station	Wind Speed $\bar{u}$ (mph)	Mean Wind Direction	Standard Deviation
Spert I	23	226°	10.9°
Three-Mile Arc	29	238°	11.9°

The destructive test was initiated at 1225, but counting data from the air samples were not available until 1800 due primarily to the time required for reentry after the test. Air sampler data corrected for decay back to 1800, along with instrument positions relative to the Spert I reactor building, are shown in Figure G-1. The values given in Figure G-1 are the concentrations in μ curies/m^3 rather than total integrated dose rates. Although cloud passage time was not actually measured, computed concentrations are based on the assumption that the cloud took two minutes to pass over the instruments. Concentrations in μ curies/m^3 were first plotted versus their respective distances from the grid centerline [a] on semi-log paper. Gaussian curves were fitted to the data for approximate downwind distances of 100, 200, 430, and 736 m (not shown in Figure G-1) and the maximum value of each Gaussian curve was then the interpolated cloud centerline which, when multiplied by the assumed two minutes of cloud passage time yields the total integrated dosage, TID, at the cloud centerline.

If it is assumed that the Spert I destructive test fisside release falls into the category of an "Instantaneous point source at ground level" [28], then, Q, the total curie release to the atmosphere of the test may be computed from Equation (1).

$$\text{TID} = \frac{2Q}{\pi C^2 \bar{u}(\bar{u}t)^{2-n}} \quad \frac{\text{curie-sec}}{\text{m}^3} \tag{1}$$

Sutton's parameters and other values used in this equation are:

$\bar{u}$ = mean wind speed = 26 mph

n = stability parameter = 0.25 (neutral)

C_2 = diffusion coefficient = 0.0210

$(\bar{u}t)$ = downwind distance on cloud centerline from point source to measuring instrument - 100, 200, 430, and 736 m.

---

[a] Grid centerline shown in Figure G-1.

The diffusion parameters used are typical for the NRTS during meteorological conditions such as those which prevailed during the destructive test. Computed values of Q were averaged to obtain an estimate of 1.51 curies for the instantaneous point source strength. Correction for 5 hours 35 minutes was estimated for the Way-Wigner equation, $A(o) = A(t) t^{1.21}$, which yielded 2.44 x 10^5 curies. This release is to be compared with a total fisside inventory in the core of about 5.7 x 10^7 curies immediately after the excursion (based upon 1.85 x 10^6 curies/MW-sec)[29] and amounts to about 0.4 percent. As noted earlier on page 47, however, recent calculations by the USAEC-ID Health and Safety Division (not published) indicate that the total release consisted only of about 7 percent of the noble gases or about 0.7 percent of the total fisside inventory. No solid products were collected after this test, and, although radioiodines were undetected, less than 0.01 percent of the iodines are calculated to have been released to the atmosphere.

APPENDIX H

METALLOGRAPHIC EXAMINATION OF
DAMAGED FUEL PLATES FROM THE DESTRUCTIVE TEST

APPENDIX H

METALLOGRAPHIC EXAMINATION OF
DAMAGED FUEL PLATES FROM THE DESTRUCTIVE TEST

A metallographic examination has been performed at the MTR hot cell on eight fuel plates which were melted as a result of the 3.2-msec period destructive test. The plates and their location in the core are shown in Table H-I.

TABLE H-I

METALLOGRAPHIC SAMPLE POSITIONS

Plate No.	Core Position [a]	Plate Position [b]	Approximate Length of Recovered Plate (in.)
D-2321	E-5	1	3-1/4
D-2433	E-5	12	3
D-1930	E-4	1	8-1/2
D-808	E-4	12	3-3/8
D-800	C-5	12	10-3/4 [c]
D-2392 [e]	C-3	4	25-1/8 [d]
D-1163	F-6	6	5
D-365	F-6	7	5

[a] See Figure D-5 for core position nomenclature.
[b] Plates are numbered from west to east within assemblies as positioned in the core.
[c] A bottom portion of the plate was attached to the top portion.
[d] Center of plate was melted.
[e] See Figure E-I

All samples were 3/4 inch in length and were examined in the unetched state using 50x magnification.

Examination of the composite photomicrograph (Figure H-1) for a sample taken at the ruptured edge of plate D-2321 reveals the melting of the meat and the cladding. The end is flared, indicating that it had been in a plastic state. Figure H-2, which is another photomicrograph of the same sample, but at a position further away from the ruptured edge, shows melting at the center and edge of the larger fuel particles, but no damage to the cladding. This sample is a longitudinal-type specimen, ie, the viewing surface is parallel to the long axis of the fuel plate. A transverse-type specimen (Figure H-3) from the rupture area shows some melting and change at the edges of the large fuel particles. This sample shows no indication of cladding damage.

Fig. H-1 Composite photomicrograph of ruptured end of fuel plate D-2321 (50x) (cross section).
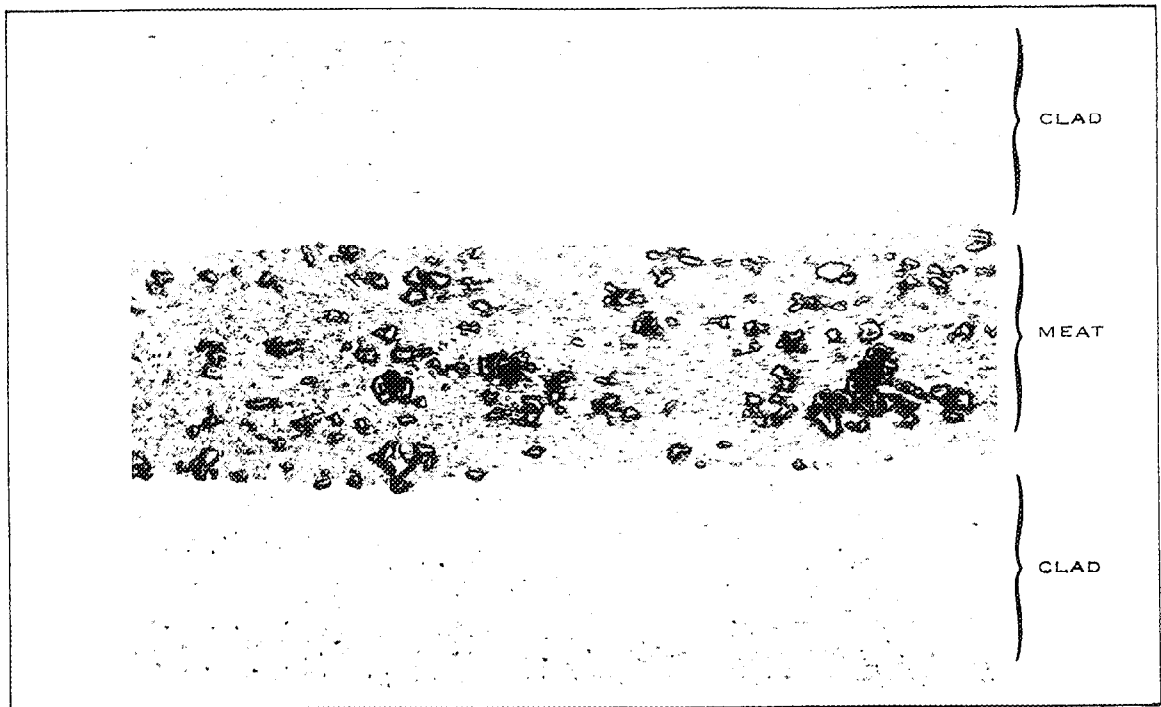
Fig. H-2 Photomicrograph of plate D-2321 away from ruptured edge (50x) (cross section).

Fig. H-3 Photomicrograph of transverse-type specimen from the rupture area of plate D-2321 (50x).

The photomicrographs obtained of plate D-2433 are quite similar to those of plate D-2321.

161
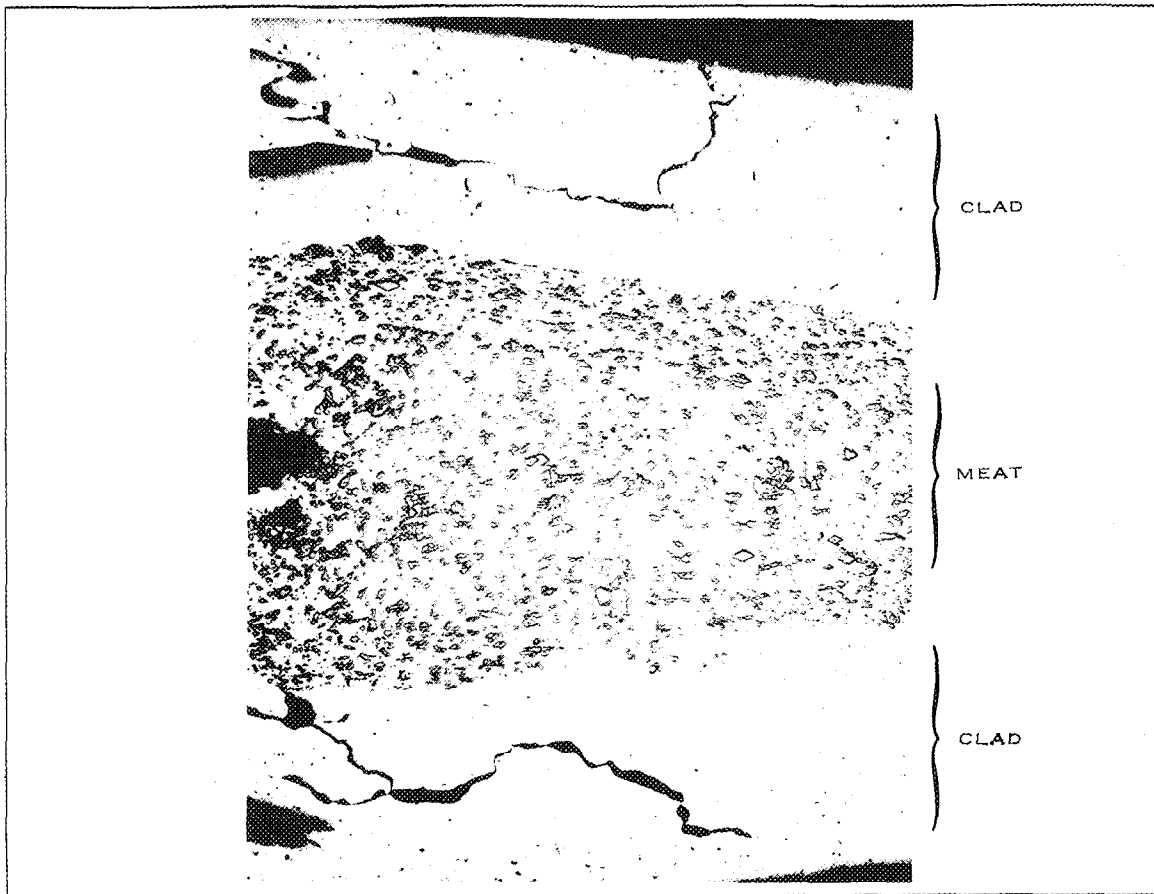
Fig. H-4 Photomicrograph of ruptured end of plate D-800 (50x) (cross section).

Photomicrographs of plate D-800 show the melting and mechanical damage of the fuel plate. Figure H-4 shows the ruptured edge of the fuel plate. The photomicrograph of Figure H-5 was taken immediately adjacent to that of Figure H-4 and shows the cladding damage. Figure H-6, which is an area about 3/8 inch away from the area shown in Figure H-5, is typical of undamaged fuel samples. A sample from the bottom portion of the D-800 fuel plate is shown in Figure H-7. The sample exhibits a melted area at the fuel centerline and no cladding damage. The sample split through the fuel before mounting and only one-half of the sample is shown in the figure.

Figure H-8 shows a sample of plate D-808 near the ruptured edge. In this case the cladding is severely cracked, and the meat shows some centerline fuel outlining. A sample which was taken two inches from the ruptured end shows no apparent melting.

Samples from plate numbers D-1930, D-1163, and D-365 exhibited characteristics similar to the samples from plate D-808.

Samples taken at 1/2, 10, 13-1/8, and 16-3/8 inches from the top of fuel plate D-2392 were examined. The 5-1/2- and 10-inch samples show typical areas with no melting. The 13-1/8- and 16-3/8-inch samples show no cladding damage and some outline melting of the larger fuel particles (Figure H-9).
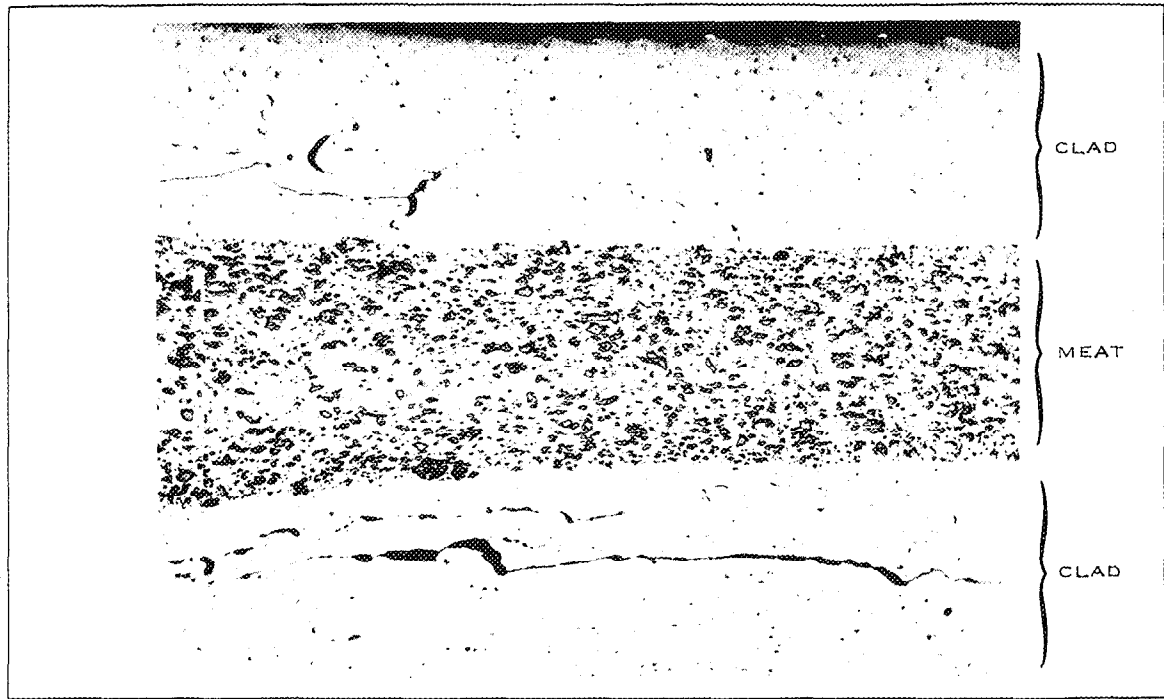
Fig. H-5 Photomicrograph of plate D-800. Sample taken immediately adjacent to that of Fig. 13 (50x) (cross section).
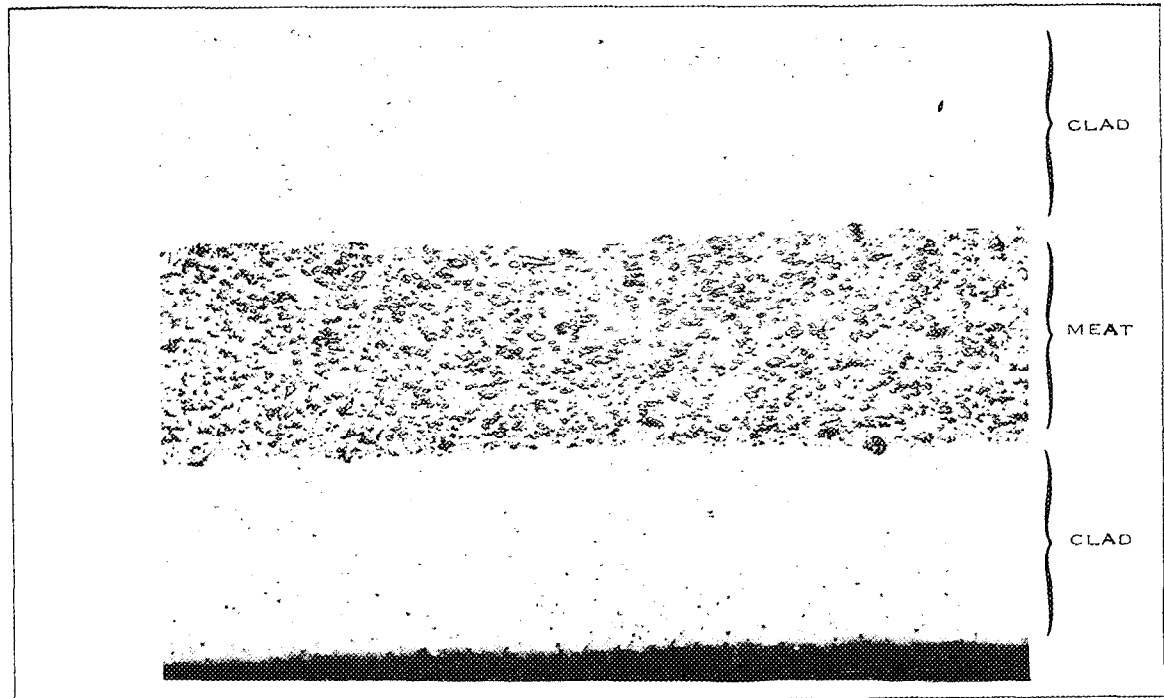
Fig. H-6 Photomicrograph of plate D-800. Sample taken about 3/8 inch from that of Fig. 14 (50x) (cross section).

Since the 13-1/8- and 13-3/8-inch samples were taken from the damaged area of the plate, it is somewhat surprising to see so little evidence of melting.

163
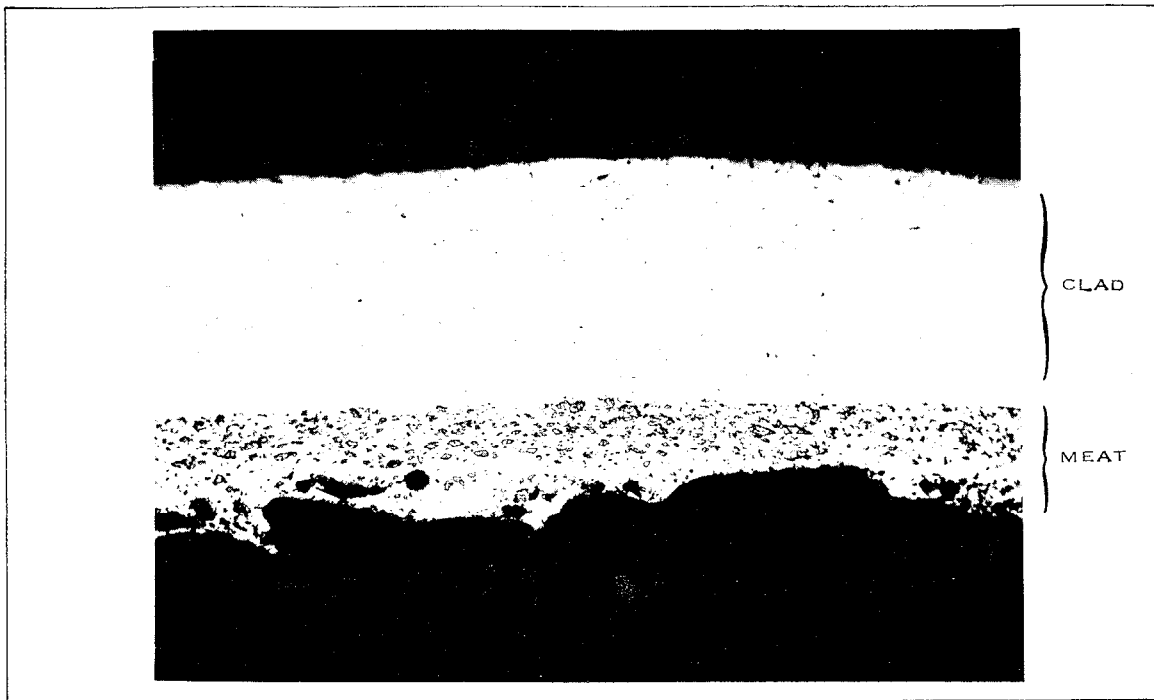
Fig. H-7 Photomicrograph of sample from bottom end of plate D-800. Only half of the sample is shown (50x) (cross section).
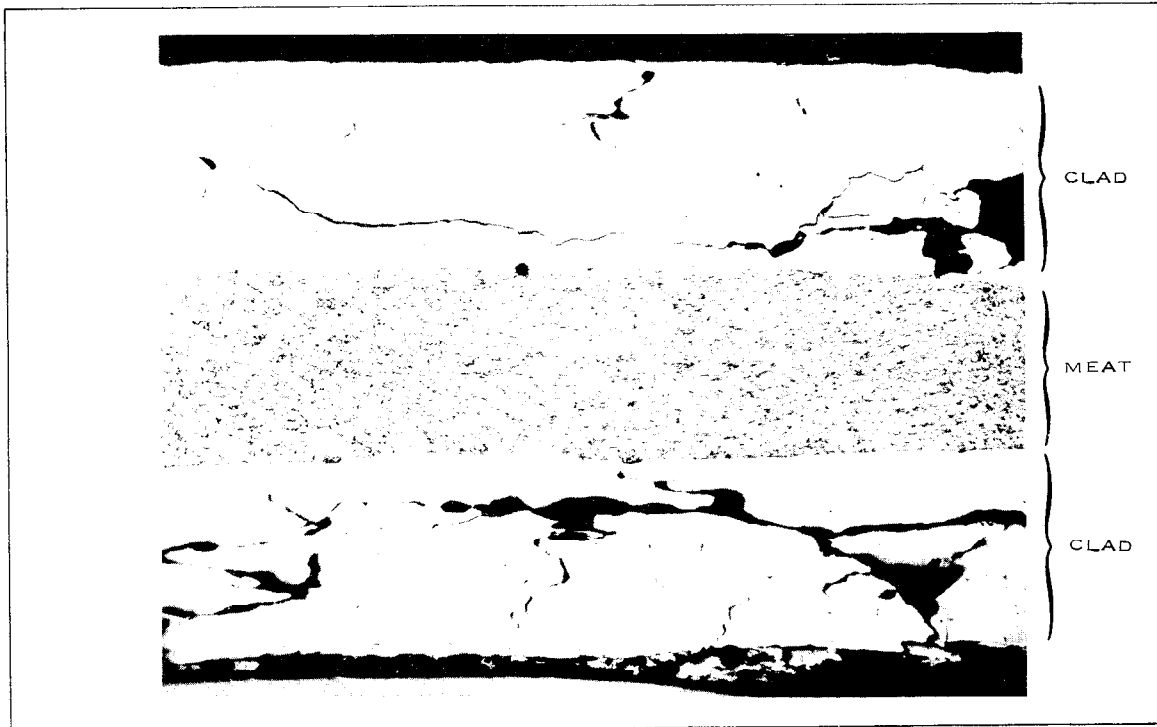
Fig. H-8 Photomicrograph of sample near the ruptured end of plate D-808 (50x).

In general, the melting of the fuel plates on the damaged ends extended into the plates about 1/8 inch. At about 3/8 inch from the ends, or in the middle of
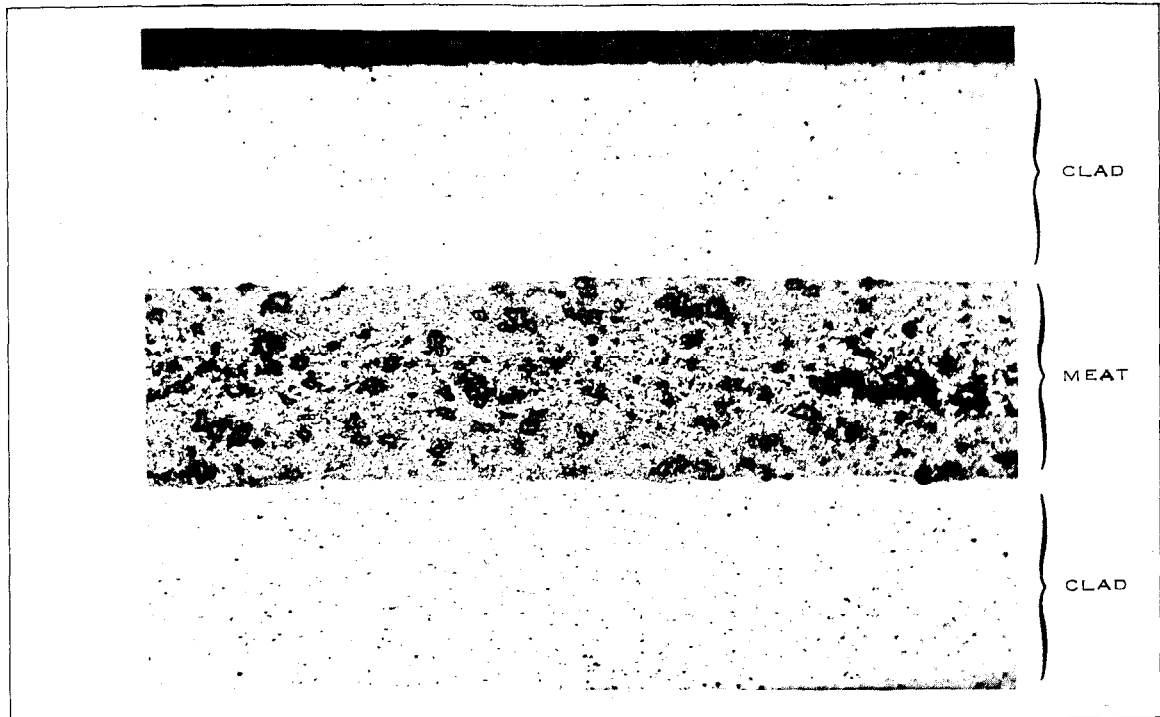
Fig. H-9 Photomicrograph of sample from plate D-2392 (50x) (cross section).

the specimens taken from the damaged ends, normal fuel plate structure was observed.

The failure of the fuel plates can be described as a combination of melting and mechanical damage. The observed intergranular cracking of the cladding and the melting of the meat near the ruptured ends shows that the plates must have reached a temperature of at least 640°C in this vicinity. Because of the absence of cladding and meat damage a short distance from the damaged end, it appears that the temperature gradient was large along the length of the plate. While this evidence, coupled with a temperature reading of 1230°C from the fuel-bearing capsule which was in the core, indicates that the temperature of the fuel plates was probably much higher than that recorded by surface thermocouples; there is no metallographic evidence that the maximum fuel temperatures approached the vaporization temperature of the alloy.

A more detailed presentation and discussion of metallographic data for the destructive test is contained in Reference 10.

APPENDIX I

RECOVERY AND CLEANUP OPERATIONS

APPENDIX I

RECOVERY AND CLEANUP OPERATIONS

Recovery and cleanup operations in the Spert I reactor vessel and surrounding area were initiated soon after the destructive test. For the first few days following the test, operations consisted primarily of the acquisition of information pertaining to the reactor condition and the recovery of radiation-sensitive items from the reactor area. These efforts included removal of motion picture cameras from their protective housing, removal of various activation samples, and a general documentation of the reactor condition by both motion pictures and still photography (see Figures 30-39). Upon the completion of these initial operations, it was necessary to recover those test components which had been ejected from the reactor tank and to make the necessary preparation for the more extensive core disassembly operations to follow. The items which had been expelled from the core, the majority of which were broken lights and light brackets, were noted as to location and identity, photographed, and removed to storage. After removal of certain items of equipment from the reactor building, such as the support stands for health physics experiments, the camera tables and tracks, some sand bags and blast shields for the cameras and electrical switch gear, several areas of the building were decontaminated to prevent the spread of the low-level contamination which was present; one of these areas was used as a clothing change area.

Systematic recovery of all items from the reactor vessel and the removal of the support bridges and the control rod drives was then initiated. The position and identity of each item was recorded and extensive written descriptions and photographic coverage was employed before it was removed to storage. All recovered fuel-bearing materials were weighed.

The majority of the recovery operations was accomplished with manually operated handling tools since most of the components were of small size. Large components were removed from the reactor tanks by using either long hook tools or ropes attached directly to the components. For the largest components, such as the lower support bridge, use was made of the building crane. During these operations the radiation level directly over the reactor tank was approximately 100 mr/hr. This relatively low direct radiation level and the low contamination levels present permitted the recovery operation to proceed rapidly with no unusual radiological problems.

Fifteen of the 25 fuel assembly cans in the core were found to be partially intact. Two of these assemblies were removed and transferred to a hot shop where they were cut open and photographed, using remote handling tools. The remaining 13 fuel assemblies were opened at the Spert I Terminal Building (Reference 1). The procedure used was to place a fuel assembly in a tank of water and to grind two of the edges from the fuel assembly permitting gradual opening. An electric motor was used to drive the grinding wheel through a flexible shaft. In this operation, the water served not only as a radiation shield but also to retain radioactive dust and chips resulting from the grinding operation. On completion of the grinding operation, the assembly was dried, using heat lamps, and then photographed. The fuel plates were then separated from the aluminum can and weighed, and the fuel and assembly parts removed to storage.

At frequent intervals during the recovery operation photographs were taken of the status of the reactor tank in order to document, in detail, the positions of various components. Samples of the metallic residue in the reactor vessel were taken periodically in order to obtain representative samples from all parts of the reactor vessel for subsequent analysis. Upon completion of the recovery operation, radiation levels in the reactor vessel were found to be near background and the facility was in such a condition as to allow restoration and repair to proceed for the next test program.

X-Sender: u075522@esh-mail.lanl.gov
X-Mailer: QUALCOMM Windows Eudora Pro Version 4.1
Date: Thu, 18 Mar 1999 10:31:26 -0700
To: "Richard K Mccardell" <RKM@inel.gov>
From: thomas mclaughlin <tpm@lanl.gov>
Subject: Re: Spert Reference Report

Thanks for your help.

Los Alamos National Laboratory
P. O. Box 1663
MS F-691
Los Alamos, NM 87545

                    Tom

At 09:50 AM 03/18/1999 -0700, you wrote:
>Hello Thomas,
>
>I will get you a hard copy of "Report of the SPERT-1 Destructive Test
>Program on an Aluminum, Plate-Type, Water Moderated Reactor" by R. W.
>Miller et.al., IDO-16883, June 1964. I need your street mailing address.
>
>
>
>
>
>Richard K. McCardell
>Consulting Enginer/Scientist
>Idaho National Engineering and
>Enviromental Laboratory
>
>